Vol. 50 ■ No. 3 ■ September 2022

JNMT
Journal of Nuclear Medicine Technology

Theranostics: The Future of Molecular Imaging and Therapy

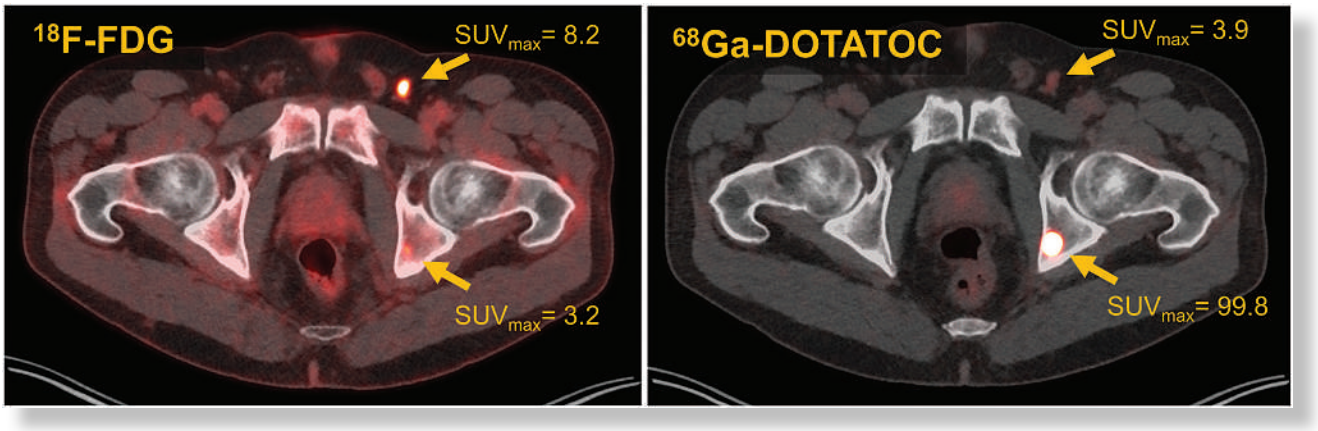

FEATURED IMAGE

Practical Considerations for Implementation of ^{177}Lu-DOTATATE Neuroendocrine Tumor Treatment Programs. Diane Soulek et al. See page 195.

SNMMI Value Initiative
SOCIETY OF NUCLEAR MEDICINE & MOLECULAR IMAGING

Streamlined. Simple. Accurate.

CRC® Dose Calibrator Family

Combine the speed and accuracy you need to measure and prepare doses with the performance and reliability that you've come to expect in one of the industry's finest packages.

CRC® - PC Smart Chamber
Network Ready with Remote Connectivity
The Most Advanced in Dose Calibration.

CRC®-55tPET Dose Calibrator (Touch Screen)
Speed and accuracy to measure
and prepare doses.

Driving Innovation... Together

Two leading brands of nuclear medicine products and technology, the **Capintec™** and **Biodex™** teams have joined forces under Mirion Medical.

CAPINTEC
A MIRION MEDICAL COMPANY

OPS-4421 - 08/22

Visit capintec.com to learn how we can support your unique requirements.

Pass the NMTCB CT Exam. We *GUARANTEE* It!

Because **MIC** is all about ***outcomes***.

Over 30 Years!

We guarantee you'll pass the NMTCB CT Exam or *your money back!*

- Technologists must complete 35 hours of didactic education related to CT during the 3 year period prior to applying for the CT Exam.
- NMTCB has approved **MIC**'s **CT Registry Review Program** along with **Sectional Anatomy & Imaging Strategies** to ***completely satisfy that 35-hour CT didactic requirement!***
- Excellent companion for technologists in hybrid imaging.

There's no better time to participate in

MIC's Self-Study CE

- Prepare for **CT certification**
- Satisfy NMTCB's **prerequisite**
- Ensure the **highest standards**

Ask for the CNMT discount when you enroll in both courses!

Technologists and their managers agree:
"MIC's courses really work!"

Sectional Anatomy & Imaging Strategies™

Learn the essentials of sectional imaging in a convenient self-study format!

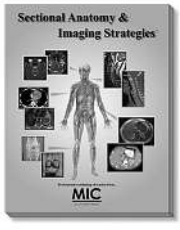

- Patient positioning, artifact reduction, image orientation, slice thickness, etc., for each clinical area.
- Explains sectional imaging with over 1,000 images and figures. The perfect companion to **The CT Registry Review Program**.
- 18 Credits
- 6 StudyModules

The CT Registry Review Program™

Pass the CT Exam after completing this course or we will refund your entire tuition!

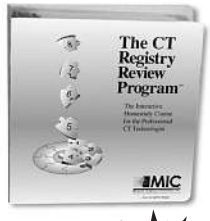

5th Ed!

- Learn **essential** and **advanced** topics on the NMTCB and ARRT CT Exam.
- Prior training in CT is recommended.
- Pass the NMTCB or ARRT Exam in CT or your money back!
- 22 Credits
- 8 StudyModules

A Proud Member of...
SNMMI

Call today for your
Free Info Kit
800-589-5685
or visit www.MIC*info*.com

MIC®
Medical Imaging Consultants, Inc.
1037 US Highway 46, Suite G2 • Clifton, NJ 07013 • 800-589-5685
...for *your* perfect image.

JNMT09/22

We Are Here for Him
So He Is There for Her

Patient Convenience. Targeted Detection

At **Jubilant Radiopharma**, our pharmacies are ready to dispense **PSMA-11 (gallium Ga68 gozetotide)** to your PET imaging center. If your department needs flexibility, reliability and confidence contact your local nuclear sales manager for more information by scanning the **QR code** or visiting **www.jubilantradiopharma.com**

Proudly Offering Both

Illuccix®
(kit for the preparation of gallium Ga68 gozetotide injection)

LOCAMETZ®
(kit for the preparation of gallium Ga68 gozetotide injection)

SNMMI Value Initiative
SOCIETY OF NUCLEAR MEDICINE & MOLECULAR IMAGING

Proud Leadership Circle Members of the SNMMI Value Initiative

Jubilant Radiopharma
790 Township Line Road, Yardley, PA 19067
Phone: 215.550.2810

JUBILANT RADIOPHARMA

JNMT

Volume 50, Number 3 • September 2022

JNMT Journal of NUCLEAR MEDICINE TECHNOLOGY

The Official Publication of **SNMMI-TS**

The *JOURNAL OF NUCLEAR MEDICINE TECHNOLOGY* (ISSN 0091-4916 [print]; ISSN 1535-5675 [online]) is published quarterly by the SNMMI, 1850 Samuel Morse Dr., Reston, VA 20190-5316; phone: (703) 708-9000; fax: (703) 708-9018. Periodicals postage paid at Reston, VA, and at additional mailing offi ces.

POSTMASTER: Send address changes to the *Journal of Nuclear Medicine Technology*, 1850 Samuel Morse Dr., Reston, VA 20190-5316.

EDITORIAL COMMUNICATIONS should be sent to the editor, Kathy S. Thomas, MHA, CNMT, PET, FSNMMI-TS, JNMT Office, SNMMI, 1850 Samuel Morse Dr., Reston, VA 20190-5316; phone: (703) 326-1185; fax: (703) 708-9018. To submit a manuscript, go to http://submit-tech.snmjournals.org.

BUSINESS COMMUNICATIONS concerning permission requests should be sent to the publisher, SNMMI, 1850 Samuel Morse Dr., Reston, VA 20190-5316; phone: (703) 708-9000; home page address: http://tech.snmjournals.org. Subscription requests, address changes, and missed issue claims should be sent to Membership Department, SNMMI, at the address above. Notify the Society of change of address and telephone number at least 30 days before date of issue by sending both the old and new addresses. Claims for copies lost in the mail are allowed within 90 days of the date of issue. Claims are not allowed for issues lost as a result of insufficient notice of change of address. For information on advertising, contact Team SNMMI (Kevin Dunn, Rich Devanna, and Charlie Meitner; (201) 767-4170; fax: (201) 767-8065; TeamSNMMI@cunnasso.com). Advertisements are subject to editorial approval and are restricted to products or services pertinent to nuclear medicine. Closing date is the 25th of the second month preceding the date of issue.

INDIVIDUAL SUBSCRIPTION RATES for the 2022 calendar year are $249 within the United States and Canada; $265 elsewhere. CPC IPM Sales Agreement No. 1415131. Sales of individual back copies are available for $58 at http://www.snmmi.org/subscribe (subscriptions@snmmi.org; fax: (703) 667-5134). Individual articles are available for sale online at http://tech.snmjournals.org.

MISSION: SNMMI-TS is dedicated to the advancement of molecular and nuclear medicine technologists by providing education, advocating for the profession, and supporting research to achieve clinical excellence and optimal patient outcomes. **VISION:** To be recognized as the leader in molecular imaging and therapy. To be dedicated to the advancement of the profession through adoption of emerging technologies.

JNMT Journal of NUCLEAR MEDICINE TECHNOLOGY

Building the Medical Puzzle—One Atom at a Time

Krystle W. Glasgow, MIS, CNMT, NMTCB(CT), NMAA, FSNMMI-TS

It has been a wild ride. After living several years with a pandemic that changed our lives dramatically, we are finally coming out on the other side. We managed to get back together in Vancouver, Canada, with a face-to-face meeting option for the first time since January 2020. The meeting was a success, and it was so good to see so many people outside of a small box on a computer screen. SNMMI-TS made it out of the pandemic unharmed, and we are thriving! This is largely due to our fantastic members, volunteers, and staff, who work tirelessly to get things done. For that, I would like to say congratulations and thank you!

It is an incredible honor and enormous responsibility to take over as president of the SNMMI-TS. I am humbled by the support from our community, and I take the president's responsibilities very seriously. We live in a rapidly changing world that is often as complicated as a 5,000 piece jigsaw puzzle. If the pieces are all placed perfectly, we end up with a beautiful picture—but the process is long and tedious, and often large blanks of uncertainty are present. Nuclear medicine is a very important piece of the puzzle of diagnostic and therapeutic medicine. I am thankful that I have been entrusted with its care and guidance, ensuring that nuclear medicine stays in its rightful place in the puzzle.

The SNMMI-TS mission is to improve human health by advancing technology and professionals in nuclear medicine and molecular imaging. Our vision is to ensure that nuclear medicine and molecular imaging are an integral part of the standard of care for patient diagnosis, treatment, and therapy.

In order to achieve our mission and vision, we must ensure that nuclear medicine stays at the forefront of therapeutics. As you know, the realm of radiopharmaceutical therapy has exploded with activity over the past few years. Whenever an area of medicine becomes popular, there are entities ready to step in and take over. We are seeing this with radiopharmaceutical therapy. Other areas of medicine are more than happy to take nuclear medicine technologists and physicians out of the equation; however, the joke is on them. Radiopharmaceutical therapy is ***ours***—it is in our DNA.

Nonetheless, there are challenges with keeping therapy under our umbrella. Radiopharmaceutical therapy is a big operation. It takes many skilled individuals to make therapies a success—especially when patient numbers are increasing dramatically. This brings us to one of the biggest issues facing nuclear medicine today: the shortage of nuclear medicine technologists and physicians.

Krystle W. Glasgow, MIS, CNMT, NMTCB(CT), NMAA, FSNMMI-TS

To help overcome this major issue, the SNMMI has launched a Workforce Pipeline initiative. The SNMMI-TS has a major place in the initiative, and we have a task force dedicated solely to the issue of the decreasing numbers of nuclear medicine technologists. The task force's goal is to figure out the root causes of the shortage and what the SNMMI-TS can do to combat those causes. This is my number one focus this year, and I am eagerly waiting to see what the task force accomplishes!

There is also a push to bring forth a new Nuclear Medicine Advanced Associate (NMAA) Program. The NMAA is a physician extender working under the supervision of a physician who is also an authorized user of radioactive materials. The goal is to enhance patient care in both the diagnostic realm and the radiopharmaceutical therapy environment. We have not had an active program for several years. A program that generates highly skilled NMAAs would be game-changing.

As the world of radiopharmaceutical therapy rapidly expands, there will be a need for mid-level providers to help fill the gaps. The NMAA has all the skills of a general physician assistant or nurse practitioner plus vast knowledge of radiation and its uses in medicine. I am excited to see how the NMAA can be used in the ever-changing arena of nuclear medicine.

Overall, this giant jigsaw puzzle seems daunting, but I am certain that the SNMMI and the nuclear medicine community will come out on top. We will keep our rightful place in the puzzle, and what is created in the end will be a masterpiece. Just hang on and hang in there, the SNMMI-TS is working for you.

Theranostics: The Future is Now!

Kathy S. Thomas, MHA, CNMT, PET, FSNMMI-TS

Editor, *JNMT*

Overall, in the past 50+ years, the diagnostic and therapeutic capabilities of nuclear medicine and molecular imaging have significantly advanced thanks to the constant improvement in imaging technology and continuous addition of new diagnostic and therapeutic radiopharmaceuticals. Looking back, we have seen numerous changes. From the early days of planar imaging and limited therapeutic procedures, to the explosive excitement of cardiac imaging in the early 1980s enhanced with SPECT, to the advent of PET radiopharmaceuticals and technology, followed quickly by hybrid technology (SPECT/CT, PET/CT, and PET/MR), and the many therapeutics along the way to treat thyroid disease, blood disorders, inflammatory joint disease, malignant effusions, bone metastasis, non-Hodgkin's lymphoma, and liver metastasis—yes, we've come a long way!

But today, excitement in nuclear medicine and molecular imaging lies in the new frontier of *theranostics* —a term comprising *therapeutics* and *diagnostics*. Theranostics is used to describe the ability to combine a radioactive drug tagged to a receptor found on a tumor cell membrane to image the tumor cell and a therapeutic radionuclide (e.g., ^{177}Lu or ^{90}Y) tagged to the same receptor to target and kill the tumor cell. To highlight the advancements of Theranostics, this issue of *JNMT* has been dedicated to innovations in this field.

Four continuing articles set the stage for understanding the application of theranostics in a clinical setting. The first article introduces the concept of basic biochemistry and molecular biology as it relates to today's radiopharmaceuticals (*1*). Next, Soulek describes the logistical considerations for implementing a ^{177}Lu-DOTATATE program to treat neuroendocrine tumors (*2*). ^{177}Lu-PSMA is an effective treatment for prostate cancer. Parent et al. highlight the treatment protocol's benefits and emphasize the need for close internal collaboration for streamlined patient care (*3*). The final continuing education article focuses on treating osteoblastic osseous metastatic disease for castration-resistant prostate cancer without visceral metastases and the technical issues to consider when implementing this therapeutic protocol (*4*). Three Practical Protocol Tips (^{177}Lu-DOTATATE, ^{177}Lu-PSMA, and ^{223}Ra-dichloride) follow each of their respective continuing education articles to provide a detailed protocol that can be clipped and incorporated into your procedure manual.

In an Invited Perspective, the Technologist Section's Advocacy Committee explores required training for the nuclear medicine technologist to successfully participate in current and future theranostic protocols and notes that "nuclear medicine technologists are well-positioned to take an active lead in theranostics growth and advancement" (*5*).

Kathy S. Thomas, MHA, CNMT, PET, FSNMMI-TS

Radioiodine is the first theranostic radionuclide used for imaging and therapy; however, the challenges associated with radioiodine therapy are patient-specific in terms of dosimetry and clinical limitations. Kumar et al. (*6*) summarize the considerations of radioiodine therapy for differentiated thyroid cancer with the clinical limitation of end-stage renal disease, and Oliveira et al. (*7*) describe the importance of residence time and dosimetry before radioiodine therapy.

When reading time is available, check out the additional topics associated with theranostics in radionuclide therapy, quality and practice management, imaging, radiation safety, and teaching case studies included in this issue.

As always, *JNMT* continues to look for new topics, clinical research, continuing educational articles, protocols, tips, and pointers. If you have ideas or suggestions or are considering writing but need some help getting started, please contact me at ksthomas0412@msn.com. Help is available!! If writing isn't your thing, but you're willing to share your expertise by becoming a reviewer for *JNMT*, please contact me!

REFERENCES

1. Glasgow KW, Dillard M, Hertenstein E, Justin A, George R, Brady A. Going nuclear with amino acids and proteins: basic biochemistry and molecular biology primer for the technologist. *J Nucl Med Technol.* 2022;50:186–194.
2. Soulek DK, Martin ME, Mastascusa NJ, Graves SA. Practical considerations for implementation of ^{177}Lu-DOTATATE neuroendocrine tumor treatment programs. *J Nucl Med Technol.* 2022;50:195–202.
3. Parent EE, Savir-Baruch B, Gayed IW, et al. ^{177}Lu-PSMA therapy. *J Nucl Med Technol.* 2022;50:205–212.
4. Grady E. Nuts and bolts of ^{223}Ra-dichloride therapy. *J Nucl Med Technol.* 2022;50: 215–221.
5. Beyder DD, Rickley CL, Peters TL, Iman JL, Arenas CM. The nuclear medicine technologist's role in theranostics: SNMMI-TS Advocacy's vision. *J Nucl Med Technol.* 2022;50: 224–227.
6. Kumar M, Subramanian K, Tanwar KS, et al. Radioiodine therapy in patient with differentiated thyroid cancer and end-stage renal disease on maintenance hemodialysis: case report with review of literature. *J Nucl Med Technol.* 2022; 50:228–232.
7. Oliveira CV, Camozzato TSC, Dorow PF, Pasqueta J. Analysis of residence time, effective half-life, and internal dosimetry before radioiodine therapy. *J Nucl Med Technol.* 2022;50:233–239.

Going Nuclear with Amino Acids and Proteins: Basic Biochemistry and Molecular Biology Primer for the Technologist

Krystle Glasgow[1], Mike Dillard[2], Eric Hertenstein[3], Allen Justin[4], Remo George[1], and Amy Brady[1]

[1]Nuclear Medicine and Molecular Imaging Sciences Program, Department of Clinical and Diagnostic Sciences, School of Health Professions, University of Alabama at Birmingham, Birmingham, Alabama; [2]Department of Nuclear Medicine, PET/CT, and Therapeutics, Inland Imaging, LLC, Spokane, Washington; [3]Nuclear Medicine Institute and Master of Science in Radiologic Sciences Graduate Program, Diagnostic Services Department, University of Findlay, Findlay, Ohio; and [4]Western Sierra Collegiate Academy, Rocklin, California

CE credit: For CE credit, you can access the test for this article, as well as additional *JNMT* CE tests, online at https://www.snmmilearningcenter.org. Complete the test online no later than September 2025. Your online test will be scored immediately. You may make 3 attempts to pass the test and must answer 75% of the questions correctly to receive Continuing Education Hour (CEH) credit. Credit amounts can be found in the SNMMI Learning Center Activity. SNMMI members will have their CEH credit added to their VOICE transcript automatically; nonmembers will be able to print out a CE certificate upon successfully completing the test. The online test is free to SNMMI members; nonmembers must pay $15.00 by credit card when logging onto the website to take the test.

In recent years, there has been an influx of new tracers into the field of nuclear medicine and molecular imaging. Most of those that have been Food and Drug Administration–approved for clinical imaging exploit various mechanisms of protein biochemistry and molecular biology to bring about their actions, such as amino acid metabolism, protein folding, receptor–ligand interactions, and surface transport mechanisms. In this review, we attempt to paint a clear picture of the basic biochemistry and molecular biology of protein structure, translation, transcription, posttranslational modifications, and protein targeting, in the context of the various radiopharmaceuticals currently used clinically, all in an easy-to-understand language for entry-level technologists in the field. Tracer characteristics, including indications, dosage, injection-to-imaging time, and the logic behind the normal and pathophysiologic biodistribution of these newer molecular tracers, are also discussed.

Key Words: proteins, biochemistry, molecular biology, molecular imaging, molecular therapy

J Nucl Med Technol 2022; 50:186–194
DOI: 10.2967/jnmt.122.263847

Proteins are the fundamental building blocks of every cell (*1*). They are made up of specific sequences of amino acids joined by peptide bonds and are arranged end to end in long chains called polypeptides. Two amino acids joined by a peptide bond is called a dipeptide, 3 amino acids linked by a peptide is a tripeptide, and so on, with an 8-amino-acid sequence making up an octapeptide as seen with the radiotracer ^{111}In-octreotide (*2*). The sequence of amino acids in proteins is determined by the genetic code of the DNA. The gene sequence in the DNA is transcribed into the messenger RNA (mRNA) in the nucleus by an enzyme called RNA polymerase, with the help of a host of assisting enzymes called transcription factors. The initial mRNA contains sequences that code for the protein (exon) along with noncoding regions (introns), which are processed (spliced) to obtain the final mRNA with the correct sequence coding for the given protein. One gene may code for multiple proteins, whereby the same gene sequence is spliced out in a variety of different patterns to yield function proteins of differing sequences (alternative splicing). This process increases the diversity and the coding capacity of the genes. However, aberrant splicing reactions can result in disease conditions such as β-thalassemia, which is a severe blood disorder characterized by abnormal formation of hemoglobin (*3*).

Once spliced, the processed mRNA is then exported from the nucleus into the cytoplasm. On reaching the cytoplasm, the ribosomes (protein-producing molecular machines) hop onto the mRNA in search of a specific 3-nucleotide sequence called the start codon, which will act as a cue for the ribosome to start building the polypeptide chain on the basis of the subsequent nucleotide sequences. In eukaryotes (organisms with an intact nucleus, which includes everything from amoebas, worms, birds, and plants to humans), the start codon usually codes for the amino acid methionine (*4*). In prokaryotes (unicellular organisms without a nucleus, in which the DNA is floating in the cytoplasm, including members such as bacteria and archaea), it is a modified version of methionine (formyl methionine) (*5*). The nucleotide sequence in the mRNA is read in triplets (codon), and each

Received Jan. 11, 2022; revision accepted Feb. 3, 2022.
For correspondence or reprints, contact Remo George (remogeorge@uab.edu).
Published online Feb. 23, 2022.

codon codes for an amino acid. However, one amino acid may be called on by different codons with differing nucleotide sequences (degeneracy of the codon), and this property of the genetic code makes it more fault-tolerant for point mutations. As the ribosomes move down the mRNA, reading the codons, the amino acids are brought to the ribosomes by specific transfer RNAs that carry the corresponding amino acid and have matching anticodon nucleotide sequences that can correctly base-pair (form a covalent bond) to the codon on which the ribosome sits at any given moment. The new amino acid is then added to the methionine (or to formyl methionine) in a condensation reaction in which a molecule of water is removed to form a peptide bond (-CONH-) between the terminal carbon atom of the methionine (C-terminal) and the amino terminal of the next amino acid (N-terminal) (Fig. 1) (*6*).

The previous transfer RNA (which brought in the methionine) is released, and the ribosome along with the new transfer RNA now carrying the 2 amino acids (dipeptide) then proceeds to the next codon. The process is repeated to generate a tripeptide, tetrapeptide, pentapeptide, and so on, until a long polypeptide protein chain is created as prescribed by the genetic code. Once the ribosome reaches the stop codon with a sequence that does not code for an amino acid and no transfer RNAs are recruited, the ribosomes recruit a release factor enzyme that causes hydrolysis of the final C-terminal group of the polypeptide and attaches it to the ribosome, thus resulting in release of the full-length polypeptide chain. There are multiple ribosomes hurtling down the mRNA doing the translation simultaneously, one behind the other, resulting in many polypeptides being synthesized from an mRNA and thereby increasing the yield of the protein product manyfold. Once the protein chain is translated, it must then be folded in precise 3-dimensional conformations for it to become functionally active. This folding process is done cotranslationally by special molecular chaperone proteins

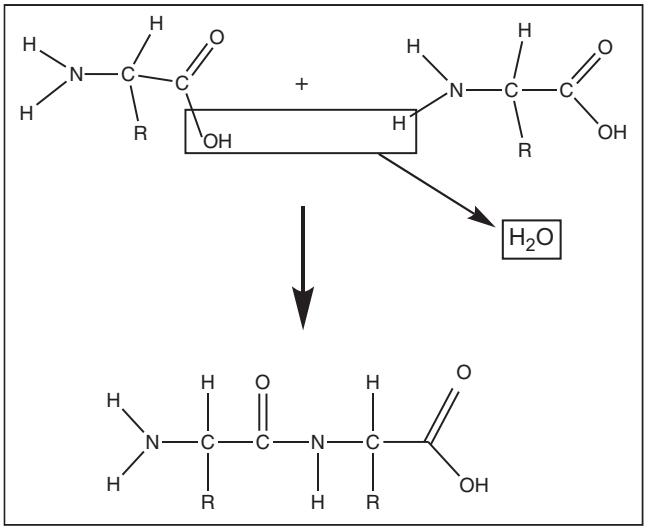

FIGURE 1. Condensation reaction. Two amino acids are joined together to form peptide bond with release of water molecule.

that guide the nascent polypeptide chain to fold into its secondary, tertiary, and quaternary structures (*7*). The precise folding of the long polypeptide chain is important for correct forming of the protein's active site where the catalyzing reaction occurs or for stable incorporation of the necessary ion or chemical group (cofactor) to achieve its designated biologic task (*8*). The secondary structure of the protein is formed by the meticulous folding of the peptide chain into a helix or a pleated sheet. This process is mediated by the specific ϕ- and ψ-torsion angles of the amino acids that would result in hydrogen bonding of the adjacent groups of the amino acids in the vicinity. The order of the amino acids specified by the genetic code dictates this folding process, which would result in an energetically favorable (less entropy) stable conformation (Fig. 2) (*9*).

The chain of helices and sheets is further folded in 3-dimensional space and stabilized by hydrogen bonds and ionic interactions between atoms within the chain and within the watery (aqueous) environment in the cytoplasm (Fig. 3).

Once the chain is correctly folded into its tertiary structure, it may then need to join cooperatively with one or more folded peptide chains to form the final functional quaternary structure (e.g., hemoglobin is made up of 4 folded polypeptide subunits with an iron group stabilized in the middle of each subunit) (Fig. 4) (*10,11*). Similarly, an antibody protein, such as the one used in the non-Hodgkin lymphoma radioimmunotherapy agent ^{90}Y-ibritumomab tiuxetan, is made up of 4 different polypeptide chains (primary structure) that are folded into β-barrels (secondary structures). This folding in turn makes it possible for those from the same and adjacent chains to form bonds with each other called disulfide bridges (tertiary structure), thus giving the antibody molecule its final 3-dimensional Y shape (quaternary structure) (*12*).

If the protein is not correctly folded, it may be destroyed by specialized enzymes called proteasomes (*13*). In some pathologic situations, this misfolding of proteins may result in aberrant protein aggregates such as those seen in Alzheimer disease, where the proteins amyloid β and tau are incorrectly folded, resulting in sticky tarlike plaques in the neuronal tissue of the brain and further leading to inflammation and associated pathology (*14*). These misfolded protein aggregates in the affected neurons of the brain are the

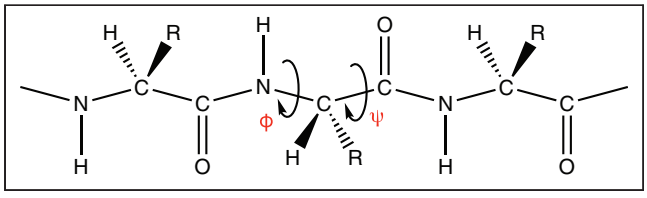

FIGURE 2. Protein secondary structure formation. Precise folding of polypeptide chain is achieved by rotational angles (φ, ψ) of backbone bonds flanking central α-carbon atom of each amino acid. These rotational angles are specific for each amino acid and are instrumental in shaping protein structure as prescribed by genetic code.

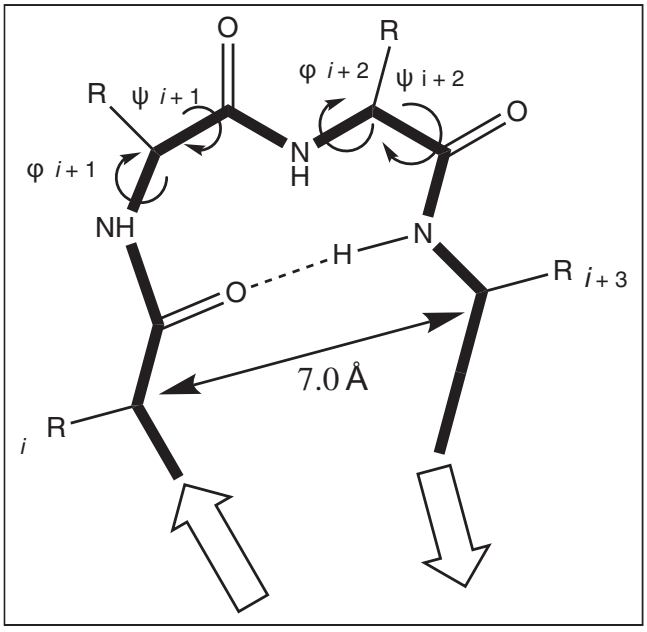

FIGURE 3. Protein tertiary structure: intra- and intermolecular bonds help form and stabilize precise 3-dimensional protein structure into helices and sheets.

targets of the Alzheimer detection agents ^{18}F-florbetaben, ^{18}F-florbetapir, and ^{18}F-flutemetamol, all of which detect amyloid β-plaques (*15*), and ^{18}F-flortaucipir, which detects misfolded tau protein tangles (Fig. 5) (*16*).

Once the protein is correctly folded, it either stays in the cytoplasm or is exported outside the cell to its correct destination in the body. This process is guided by the types of amino acid residues, called signal sequences, in the N-terminal region of the polypeptide chain (e.g., hormones such as insulin are produced by the pancreas and are secreted into the blood for blood sugar regulation, whereas digestive enzymes are secreted by stomach cells into the gut for the task of digestion) (*17*).

Some proteins are shunted to the cell surface to be part of the cell membrane to act as switches (also known as receptors) for transmitting a signal into the cell's nucleus. The signal starts a specific cellular function based on environmental cues or based on another specific outside protein, such as a hormone or neurotransmitter, binding to it (*18*). These receptors have extremely specialized functions, such as when cluster-of-differentiation (CD) receptor protein CD20 (detected by the tracer ^{90}Y-ibritumomab tiuxetan) on the surface of B lymphocytes helps to produce antibodies (*19*), or when the CD206 protein (bound by the lymphoscintigraphy mannose sugar tracer ^{99m}Tc-tilmanocept) on the surface of macrophages scavenges sugar molecules from pathogens (*20*). Sometimes a receptor is synthesized in many almost-identical forms (also known as subtypes) to achieve a variety of functions in different organs by the same activator ligand, as is the case with several subtypes of somatostatin receptor (SSTR): SSTR1, SSTR2 (bound by the neuroendocrine tumor theranostic agents ^{68}Ga/^{177}Lu/^{64}Cu-DOTATATE, ^{68}Ga/^{177}Lu/^{64}Cu-DOTATOC, and ^{111}In-octreotide), SSTR3 (bound by ^{111}In-octreotide), SSTR4, and SSTR5 (bound by ^{68}Ga/^{177}Lu/^{64}Cu-DOTATATE, ^{68}Ga/^{177}Lu/^{64}Cu-DOTATOC, and ^{111}In-octreotide), all of which, in response to somatostatin, inhibit a variety of cell growth and other activities from their cell surface locations depending on the organ (or cancer) in which they are present (*21*). Such versatile protein receptors are sometimes localized to the cytoplasm itself, such as the estrogen receptors (bound by the breast carcinoma estrogenlike synthetic tracer ^{18}F-fluoroestradiol), which would need the activating estradiol molecule (serving as a ligand) to cross the cell membrane and bind to the receptors. This causes the receptors to physically move into the nucleus and start the transcription of a multitude of genes regulating many important body functions, such as cell proliferation and bone health (*22*).

Not all surface proteins take up the role of being receptors for cell-signaling activities. Some function as carriers of other molecules across the cell membrane, such as when the dopamine active transporter helps to transport (reuptake) the secreted excitatory neurotransmitter dopamine back into the neuron (*23*). Also taken up into intact neurons in the brain is the Parkinson disease tracer ^{123}I-ioflupane, which is analogous to dopamine (*24*). Similarly, the uptake-1 transporter helps the reuptake of the neurotransmitter norepinephrine back into the neuron. This reaction also occurs with the neuroendocrine tumor theranostic agent $^{123/131}$I-*meta*-iodobenzylguanidine (MIBG), which is analogous to norepinephrine (*25,26*).

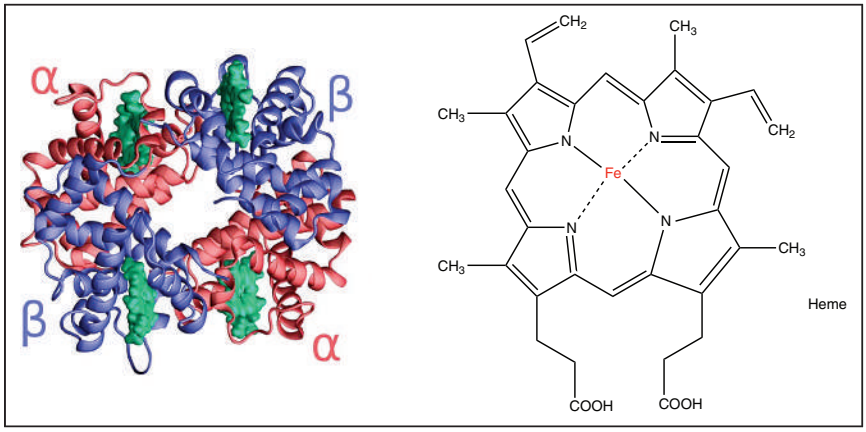

FIGURE 4. Protein quaternary structure: helices and pleated sheets of different polypeptide chains may further associate together to form quaternary structures as in case of hemoglobin molecule in red blood cells. Each hemoglobin molecule is composed of 4 polypeptide subunits (2 α-chains and 2 β-chains), each stabilized by ion group (heme) in center.

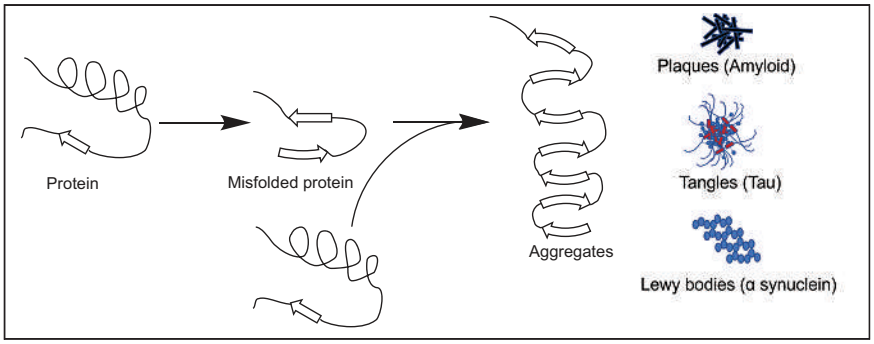

FIGURE 5. Protein misfolding can lead to pathology. Correct folding of protein into its proper 3-dimensional structure is important to function correctly. Incorrectly folded proteins either are destroyed by proteasomes or may form insoluble aggregates such as plaques, tangles, and Lewy bodies, which can lead to pathologic conditions as in Alzheimer disease.

Cell surface protein transporters act as transporters of not only neurotransmitters but also a variety of other biomolecules, including amino acids, which are needed for protein synthesis. In humans, there are 10 different types of amino acid transporters. Some of these, including L-type amino acid transporter and alanine-serine-cysteine transporter 2, in increased numbers are seen transporting large amounts of amino acids, such as leucine, into the cells for increased protein synthesis due to high demand in a cancerous state (*27*). A similar reaction occurs with the artificial nonmetabolizable amino acid leucin analog tracer ^{18}F-fluciclovine for prostate cancer imaging (*28*).

Some proteins, on the other hand, act as enzyme catalysts. A protein enzyme catalyzes a reaction by creating a conducive and protective environment in its active site that will produce an ideal condition for the chemical reaction to proceed (decrease of activation energy for starting the chemical reaction, resulting in the product's becoming more stable than the reactants) (Fig. 6) (*29*). These principles govern all the chemical reactions that take place in our body for the reactions to work in a complex chemical environment. An example of a cell surface transport protein that also acts as an enzyme is the prostate-specific membrane antigen (PSMA) seen on normal prostate cells, as well as on some other organs, including the kidneys, small intestine, and nervous system. PSMA enzymatically acts on dietary folic acid (vitamin B9) and on the neurotransmitter *N*-acetylaspartylglutamic acid to releases the amino acid glutamate, which helps mobilize calcium to support normal cell growth in the prostate and maintain neuronal functions in the brain (*30,31*). The increased presence of PSMA on prostate cancer cells is the target for the imaging agents ^{68}Ga-PSMA11 and ^{18}F-piflufolastat, which were approved by the Food and Drug Administration in 2020 and 2021, respectively.

MOLECULAR TRACER USING AMINO ACID METABOLISM (^{18}F-FLUCICLOVINE (AXUMIN; BLUE EARTH DIAGNOSTICS) (*32*))

^{18}F-fluciclovine is a synthetic amino acid that resembles leucine and is labeled with the radionuclide ^{18}F. It was approved by the Food and Drug Administration in 2016 for imaging of prostate cancer recurrence with increased blood levels of prostate-specific antigen. ^{18}F-fluciclovine is carried across the cancer cell's membrane by the L-type amino acid transporter and by alanine-serine-cysteine transporter 2, which are seen in higher amounts in cancer cells. The driving force for this tracer uptake, apart from the increased need of the cancer cells for amino acids for protein building, are the androgens (male sex hormone produced in the testicles), which in general are dangerous proponents of cancer growth. In one type of treatment for prostate cancer, biochemical castration, drugs are given that shut down production of this hormone in the male gonads. However, nature may eventually bypass this effect in some patients by producing androgen from sources outside the testicles or through DNA-changing mutations, eventually resulting in recurrence of prostate cancer and metastasis. This condition is clinically called metastatic castration-resistant prostate cancer. ^{18}F-fluciclovine, once transported into the prostate cancer cells, gets trapped in the cells. Being an artificial amino acid, it cannot be used for protein building by the cell's transfer RNAs and ribosomes (Table 1).

MOLECULAR TRACERS DETECTING PROTEIN FOLDING OR MISFOLDING

^{18}F-Florbetapir (Amyvid; Lilly), ^{18}F-Florbetaben (Neuraceq; Life Molecular Imaging), and ^{18}F-Flutemetamol (Vizamyl; GE Healthcare) (*33–35*)

^{18}F-florbetapir, ^{18}F-florbetaben, and ^{18}F-flutemetamol bind to the misfolded β-amyloid proteins forming plaques in the brain of Alzheimer disease patients, specifically plaques that appear in the gray matter of the outer cerebral cortex, where β-protein should not be present (Table 2).

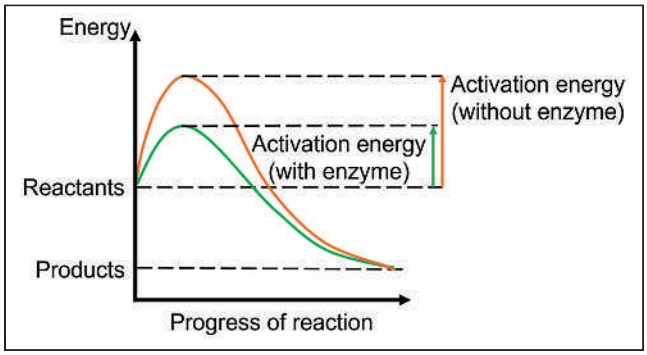

FIGURE 6. Enzyme as catalysts. Enzymes catalyze chemical reactions by lowering activation energy required for reactants to progress through steps of chemical reaction. This lowering of energy includes that of the high-energy transition state at the peak of the energy profile, which is lower when enzymes are present, hence making it easier for reaction to progress.

TABLE 1
Clinical Properties of Current Food and Drug Administration–Approved Molecular Tracer (^{18}F-Fluciclovine) Using Amino Acid Metabolism

Property	Description
Indication	Imaging in men with suspected prostate cancer recurrence based on elevated blood level of prostate-specific antigen after treatment
Administered dose for adults	370 MBq (10 mCi)
Injection route	Intravenous
Injection-to-imaging time	4–10 min
Normal biodistribution	Pancreas, liver, bone marrow, muscle

^{18}F-Flortaucipir (Tauvid; Lilly) (*36*)

^{18}F-flortaucipir binds to misfolded tau protein clumps called neurofibrillary tangles in the brain of Alzheimer disease patients (Table 2).

MOLECULAR TRACERS TARGETING CELL SURFACE PROTEIN RECEPTORS

^{18}F-Fluoroestradiol (Cerianna; Zionexa) (*37*)

^{18}F-fluoroestradiol is indicated for use in PET imaging for the detection of estrogen receptor–positive lesions in patients with recurrent or metastatic breast cancer. ^{18}F-fluoroestradiol is a synthetic estrogen analog that migrates to the estrogen receptor proteins in the cytoplasm of breast cancer cells (Table 3).

^{99m}Tc-Tilmanocept (Lymphoseek; Cardinal Health) (*38*)

^{99m}Tc-tilmanocept is indicated for use with or without scintigraphic imaging for lymphatic mapping using a handheld γ-probe to locate lymph nodes draining a primary solid-tumor site as a component of intraoperative management. It is also indicated with or without scintigraphic imaging for guiding a sentinel lymph node biopsy using a handheld γ-probe in patients with clinically node-negative squamous cell carcinoma of the oral cavity or with breast cancer or melanoma. ^{99m}Tc-tilmanocept is made up of many units of diethylenetriamine pentaacetic acid (kidney-imaging agent) and mannose (a type of sugar), linked together on a carbohydrate dextran backbone to form a giant molecule that is able to bind to the CD20 receptor protein on the surface of macrophages (a type of disease-fighting blood cell constantly

TABLE 2
Clinical Properties of Current Food and Drug Administration–Approved Molecular Tracers Detecting Protein Folding or Misfolding

Property	Description
Indication	
^{18}F-florbetapir	Imaging β-amyloid plaques in suspected AD patients
^{18}F-florbetaben	Imaging β-amyloid plaques in suspected AD patients
^{18}F-flutemetamol	Imaging β-amyloid plaques in suspected AD patients
^{18}F-flortaucipir	Imaging aggregated tau neurofibrillary tangles in suspected AD patients
Administered dose for adults	
^{18}F-florbetapir	370 MBq (10 mCi)
^{18}F-florbetaben	296 MBq (8 mCi)
^{18}F-flutemetamol	185 MBq (5 mCi)
^{18}F-flortaucipir	370 MBq (10 mCi)
Injection route	Intravenous
Injection-to-imaging time	
^{18}F-florbetapir	30–50 min
^{18}F-florbetaben	45–130 min
^{18}F-flutemetamol	80–100 min
^{18}F-flortaucipir	80–100 min
Normal biodistribution	
^{18}F-florbetapir	Inner white matter, from which blood clearance is slower
^{18}F-florbetaben	Inner white matter, from which blood clearance is slower
^{18}F-flutemetamol	Inner white matter, from which blood clearance is slower
^{18}F-flortaucipir	Some normal retention in choroid plexus, striatum, and brain stem nuclei

AD = Alzheimer disease.

TABLE 3
Clinical Properties of Current Food and Drug Administration–Approved Molecular Tracers Targeting Cell Surface Protein Receptors

Property	^{18}F-fluoroestradiol	^{99m}Tc-tilmanocept	^{68}Ga-DOTATATE, ^{68}Ga-DOTATOC, ^{177}Lu-DOTATATE, ^{64}Cu-DOTATATE, and ^{111}In-pentetreotide	^{90}Y-ibritumomab tiuxetan
Indication	Detecting estrogen receptor–positive lesions as adjunct to biopsy in patients with recurrent or metastatic breast cancer	Mapping lymph nodes draining from primary tumor site and guiding sentinel lymph node biopsy with intraoperative γ-probe	^{68}Ga-DOTATATE or ^{68}Ga-DOTATOC: locating SSTR-positive neuroendocrine tumors in adult and pediatric patients; ^{177}Lu/^{64}Cu-DOTATATE: treating SSTR-positive gastroenteropancreatic neuroendocrine tumors, including foregut, midgut, and hindgut neuroendocrine tumors in adults*	Evaluating relapsed or refractory, low-grade or follicular B-cell non-Hodgkin lymphoma
Administered dose for adults	111–222 MBq (3–6 mCi)	18.5 MBq (0.5 mCi)	^{68}Ga-DOTATATE: 2 MBq/kg (0.054 mCi/kg) up to 200 MBq (5.4 mCi); ^{68}Ga-DOTATOC: adult—148 MBq (4 mCi); pediatric—1.59 MBq/kg (0.043 mCi/kg) with range of 11.1 MBq (0.3 mCi) to 111 MBq (3 mCi); ^{177}Lu-DOTATATE: 7.4 GBq (200 mCi) every 8 wk for total of 4 doses; ^{64}Cu-DOTATATE: 148 MBq (4 mCi); ^{111}In-pentetreotide: 111–222 MBq (3–6 mCi)	14.8 MBq per kg (0.4 mCi/kg); dose adjustment needed if platelet counts are low
Injection route	Intravenous	Subcutaneous, intradermal, subareolar, or peritumoral injection in 1 mL or less	Intravenous	Intravenous
Injection-to-imaging time	80 min	10–15 min	^{68}Ga-DOTATATE: 40–90 min; ^{68}Ga-DOTATOC: 60 min†	Imaging not usually done
Normal biodistribution	Hepatobiliary system (excretion); intestines (excretion); heart, blood, uterus, kidney (excretion); and bladder (excretion)	Lymphatic channels draining injection site	Pituitary, thyroid, spleen, adrenals, kidney, pancreas, prostate, liver, and salivary glands	Significant marrow and splenic distribution without cold antibody pretreatment; pretreatment with rituximab cold anti-CD20 antibody blocks CD20 sites of normal circulating B-cells in spleen and bone marrow by binding to it, thereby allowing the following hot antibodies to reach tumor areas

*^{111}In-pentetreotide: detection of neuroendocrine tumors bearing somatostatin receptors.
†^{177}Lu-DOTATATE: not imaged; ^{64}Cu-DOTATATE: not imaged; ^{111}In-pentetreotide: 24–48 h.

patrolling the blood and lymph nodes). When injected under the skin, ^{99m}Tc-tilmanocept drains into the lymph and accumulates in the macrophages in the sentinel lymph node and beyond (Table 3).

^{68}Ga/^{177}Lu/^{64}Cu-DOTATATE (NETSPOT [Advanced Accelerator Applications]/LUTATHERA [Advanced Accelerator Applications]/Detectnet [Curium]), ^{68}Ga/^{177}Lu/^{64}Cu-DOTATOC, ^{68}Ga/^{177}Lu/^{64}Cu-DOTANOC, and ^{111}In-Octreotide (OctreoScan; Curium) (*39–42*)

The molecular agents ^{68}Ga/^{177}Lu/^{64}Cu-DOTATATE, ^{68}Ga/^{177}Lu/^{64}Cu-DOTATOC, ^{68}Ga/^{177}Lu/^{64}Cu-DOTANOC, and ^{111}In-octreotide bind to protein receptors on the surface of SSTR-containing neuroendocrine tumors. This binding is selective for the subtype of SSTR, with radiolabeled DOTATATE and DOTATOC binding to SSTR2 and SSTR5 whereas ^{111}In-octreotide binds to all 3 SSTR subtypes (SSTR2, SSTR3, and SSTR5). The radiolabeled DOTATATE fits the classic definition of a theranostic radiopharmaceutical, in that the same agent can be used for both diagnostic (^{68}Ga-DOTATATE) and therapeutic (^{177}Lu/^{64}Cu-DOTATATE) purposes (Table 3).

^{90}Y-Ibritumomab Tiuxetan (Zevalin; Acrotech Biopharma) (*43*)

The antibody radiopharmaceutical ^{90}Y-ibritumomab tiuxetan binds to CD20 receptor protein molecules on mature and malignant B lymphocytes, a type of disease-fighting cell in the blood, while sparing the immature and parent cells in the bone marrow. Although the function of the CD20 receptor on B cells is unknown, it is thought to play a role in calcium entry across the B-cell membrane and in maintenance of the required amounts of calcium inside the cell for activation in the disease-fighting process, including antibody production. The big advantage of anti-CD20 antibodies is that they attack only malignant B cells and not the precursor cells, thus preventing the patient from losing all B cells, avoiding even more negative outcomes. The β-radiation from the ^{90}Y isotope then destroys the cancerous B cells (Table 3).

MOLECULAR IMAGING TRACERS TARGETING CELL SURFACE PROTEIN TRANSPORTERS

^{123}I-Ioflupane (DaTscan; GE Healthcare) (*44*)

^{123}I-ioflupane binds to presynaptic dopamine transporters, seen in the striatal region of the brain. A defining feature of Parkinson disease is a marked reduction in the dopamine-secreting neurons in this portion of the brain. Dopamine, once secreted into the synaptic gap between the presynaptic and postsynaptic neurons (neurons sending and receiving the nerve signals, respectively), is reabsorbed back into the presynaptic neuron through the dopamine transporter proteins on the presynaptic neuron endings, thus preventing continuous excitation. The nerve signals are related to higher-order functions of the brain, including movement and coordination. In the absence or destruction of these neurons, movement disorders typical to those of Parkinson syndromes will

TABLE 4
Clinical Properties of Current Food and Drug Administration–Approved Molecular Tracers Targeting Cell Surface Protein Transporters

Property	^{123}I-ioflupane	^{123}I-iobenguane and ^{131}I-iobenguane	^{68}Ga-PSMA11 and ^{18}F-piflufolastat
Indication	Striatal dopamine transporter imaging to assist in evaluation of adults with suspected Parkinsonian syndromes	^{123}I-iobenguane: detection of primary or metastatic pheochromocytoma or neuroblastoma; ^{131}I-iobenguane: treatment of adults and children older than 12 y with iobenguane-positive, unresectable, locally advanced or metastatic pheochromocytoma or paraganglioma	PET of PSMA-positive lesions in prostate cancer patients who have suspected metastasis and are candidates for initial definitive therapy or who have suspected recurrence based on elevated serum prostate-specific antigen
Administered dose for adults	111–185 MBq (3–5 mCi)	^{123}I-iobenguane: 370 MBq (10 mCi); ^{131}I-iobenguane: 185–222 MBq (5–6 mCi) (dosimetric dose); 18,500 MBq (500 mCi) × 2 doses 90 d apart (therapeutic dose)	^{68}Ga-PSMA11: 111–259 MBq (3–7 mCi); ^{18}F-piflufolastat: 333 MBq (9 mCi) recommended; acceptable range, 8–296 to 370 MBq (10 mCi)
Injection route	Intravenous	Intravenous	Intravenous (bolus)
Injection-to-imaging time	3–6 h	24 ± 6 h	60 min
Normal biodistribution	Prominent comma-shaped striatal activity compared with surrounding brain tissue	Adrenals (not always visualized, but activity < liver), liver, heart (uptake inversely proportional to catecholamine levels), bowel (large intestine), salivary glands, lung, spleen, urinary bladder, and uterine/neck muscles	Kidneys, salivary glands, small intestine, tear glands, and spleen

result. By using a tracer that binds to the presynaptic dopamine transporters, one can obtain a quantitative measure and spatial distribution of these transporters and, hence, the dopamine secreting neurons (Table 4).

$^{123/131}$I-Iobenguane (AdreView [GE Healthcare]/Azedra; Progenics Pharmaceuticals) (*45*)

$^{123/131}$I-iobenguane, also known as MIBG, is structurally similar to the fight-or-flight hormone norepinephrine. Once secreted into the synapse between 2 neurons to facilitate neurotransmission, norepinephrine is taken back up into the presynaptic neurons through transporters called uptake 1. Uptake 1 is normally found in tissues but is overexpressed in certain neuroendocrine tumors, such as pheochromocytomas and neuroblastomas. Since MIBG resembles norepinephrine, it will be taken up in neuroendocrine tumor cells along with the neurotransporter in a higher amount. The radiolabeled MIBG is also a theranostic radiopharmaceutical; the same agent can be used for both diagnostic (^{123}I-MIBG) and therapeutic (^{131}I-MIBG) purposes (Table 4).

^{68}Ga-PSMA11 and ^{18}F-Piflufolastat (Pylarify; Lantheus) (*46,47*)

^{68}Ga-PSMA11 and ^{18}F-piflufolastat attach to the outer portion (extracellular domain) of the PSMA found in elevated levels (100- to 1,000-fold) on the surface of 95% of prostate cancer cells (*48*). PSMA is also normally seen at low levels in the kidneys, liver, tear glands, salivary glands, spleen, and nervous tissue. Once the radiotracer binds to the surface membrane protein, PSMA—along with the attached radiotracer—is transported into the cell, thus trapping the tracer within the cancer cell (Table 4) (*49*).

CONCLUSION

If past decades in nuclear medicine saw bold moves in physics and instrumentation, the future landscape is evolving to be the scintillating age of molecular and systems biology. The present and future growth of molecular imaging and therapy is based on using the intricate biologic and biochemical pathways of the human body. For the nuclear medicine technologist to appreciate the interactions of radiopharmaceuticals within the body and thus delineate the best information possible, a good understanding of the underlying mechanisms is required. This knowledge should be grounded in sound fundamentals of molecular processes in living systems, which will enable the technologist to integrate theory and processes into the realm of applied clinical practice. This ability will also engender a new generation of professionals who eagerly seek out cutting-edge knowledge and challenges that may elude the average health-care professional, leading the profession to the 21st century.

DISCLOSURE

No potential conflict of interest relevant to this article was reported.

REFERENCES

1. Whitford D. *Proteins: Structure and Function.* Wiley and Sons; 2005:528.
2. Bauer W, Briner U, Doepfner W, et al. SMS 201-995: a very potent and selective octapeptide analogue of somatostatin with prolonged action. *Life Sci.* 1982;31: 1133–1140.
3. Thalassemia major: molecular and clinical aspects. *Ann Intern Med.* 1979;91: 883–897.
4. Merrick WC. Overview: mechanism of translation initiation in eukaryotes. *Enzyme.* 1990;44:7–16.
5. Schmitt E, Guillon JM, Meinnel T, Mechulam Y, Dardel F, Blanquet S. Molecular recognition governing the initiation of translation in *Escherichia coli*: a review. *Biochimie.* 1996;78:543–554.
6. Forbes J, Krishnamurthy K. Biochemistry, peptide. StatPearls website. https://www.statpearls.com/ArticleLibrary/viewarticle/26914. Updated September 1, 2021. Accessed April 7, 2022.
7. Ellis RJ. The general concept of molecular chaperones. *Philos Trans R Soc Lond B Biol Sci.* 1993;339:257–261.
8. Hartley RW. Barnase and barstar: two small proteins to fold and fit together. *Trends Biochem Sci.* 1989;14:450–454.
9. Al Mughram MH, Herrington NB, Catalano C, Kellogg GE. Systematized analysis of secondary structure dependence of key structural features of residues in soluble and membrane-bound proteins. *J Struct Biol X.* 2021;5:100055.
10. Perutz MF, Rossmann MG, Cullis AF, Muirhead H, Will G, North AC. Structure of haemoglobin: a three-dimensional Fourier synthesis at 5.5-A. resolution, obtained by x-ray analysis. *Nature.* 1960;185:416–422.
11. Bringas M, Petruk AA, Estrin DA, Capece L, Marti MA. Tertiary and quaternary structural basis of oxygen affinity in human hemoglobin as revealed by multiscale simulations. *Sci Rep.* 2017;7:10926.
12. Davies DR, Padlan EA, Segal DM. Three-dimensional structure of immunoglobulins. *Annu Rev Biochem.* 1975;44:639–667.
13. Arrigo AP, Tanaka K, Goldberg AL, Welch WJ. Identity of the 19S 'prosome' particle with the large multifunctional protease complex of mammalian cells (the proteasome). *Nature.* 1988;331:192–194.
14. García-Morales V, Gonzalez-Acedo A, Melguizo-Rodriguez L, et al. Current understanding of the physiopathology, diagnosis and therapeutic approach to Alzheimer's disease. *Biomedicines.* 2021;9:1910.
15. Filippi L, Chiaravalloti A, Bagni O, Schillaci O. ^{18}F-labeled radiopharmaceuticals for the molecular neuroimaging of amyloid plaques in Alzheimer's disease. *Am J Nucl Med Mol Imaging.* 2018;8:268–281.
16. Wolters EE, Dodich A, Boccardi M, et al. Clinical validity of increased cortical uptake of [^{18}F]flortaucipir on PET as a biomarker for Alzheimer's disease in the context of a structured 5-phase biomarker development framework. *Eur J Nucl Med Mol Imaging.* 2021;48:2097–2109.
17. Lippincott-Schwartz J, Roberts TH, Hirschberg K. Secretory protein trafficking and organelle dynamics in living cells. *Annu Rev Cell Dev Biol.* 2000;16: 557–589.
18. Nair A, Chauhan P, Saha B, Kubatzky KF. Conceptual evolution of cell signaling. *Int J Mol Sci.* 2019;20:3292.
19. Rizzieri D. Zevalin® (ibritumomab tiuxetan): after more than a decade of treatment experience, what have we learned? *Crit Rev Oncol Hematol.* 2016;105:5–17.
20. Leong SP. Detection of melanoma, breast cancer and head and neck squamous cell cancer sentinel lymph nodes by Tc-99m tilmanocept (Lymphoseek®). *Clin Exp Metastasis.* 2022;39:39–50.
21. Pauwels E, Cleeren F, Bormans G, Deroose CM. Somatostatin receptor PET ligands: the next generation for clinical practice. *Am J Nucl Med Mol Imaging.* 2018;8:311–331.
22. Katzenellenbogen JA. The quest for improving the management of breast cancer by functional imaging: the discovery and development of 16α-[^{18}F]fluoroestradiol (FES), a PET radiotracer for the estrogen receptor, a historical review. *Nucl Med Biol.* 2021;92:24–37.
23. Bu M, Farrer MJ, Khoshbouei H. Dynamic control of the dopamine transporter in neurotransmission and homeostasis. *NPJ Parkinsons Dis.* 2021;7:22.
24. Tuma Santos CA, Wallace WD, Kim S, Vijayakumar V. Pitfalls and artifacts of ^{123}I-ioflupane SPECT in Parkinsonian syndromes: a quality improvement teaching tool. *J Nucl Med Technol.* 2021;49:114–119.
25. Shapiro B, Gross MD. Radiochemistry, biochemistry, and kinetics of ^{131}I-metaiodobenzylguanidine (MIBG) and ^{123}I-MIBG: clinical implications of the use of ^{123}I-MIBG. *Med Pediatr Oncol.* 1987;15:170–177.
26. Agrawal A, Rangarajan V, Shah S, Puranik A, Purandare N. MIBG (metaiodobenzylguanidine) theranostics in pediatric and adult malignancies. *Br J Radiol.* 2018; 91:20180103.
27. Broer S. Amino acid transporters as targets for cancer therapy: why, where, when, and how. *Int J Mol Sci.* 2020;21:6156.

28. Gusman M, Aminsharifi JA, Peacock JG, Anderson SB, Clemenshaw MN, Banks KP. Review of ^{18}F-fluciclovine PET for detection of recurrent prostate cancer. *Radiographics.* 2019;39:822–841.
29. Schowen RL. How an enzyme surmounts the activation energy barrier. *Proc Natl Acad Sci USA.* 2003;100:11931–11932.
30. O'Keefe DS, Bacich DJ, Huang SS, Heston WDW. A perspective on the evolving story of PSMA biology, PSMA-based imaging, and endoradiotherapeutic strategies. *J Nucl Med.* 2018;59:1007–1013.
31. Kaittanis C, Andreou C, Hieronymus H, et al. Prostate-specific membrane antigen cleavage of vitamin B9 stimulates oncogenic signaling through metabotropic glutamate receptors. *J Exp Med.* 2018;215:159–175.
32. Kogai T, Ohashi E, Jacobs MS, et al. Retinoic acid stimulation of the sodium/iodide symporter in MCF-7 breast cancer cells is mediated by the insulin growth factor-I/phosphatidylinositol 3-kinase and p38 mitogen-activated protein kinase signaling pathways. *J Clin Endocrinol Metab.* 2008;93:1884–1892.
33. Furuya F, Shimura H, Suzuki H, et al. Histone deacetylase inhibitors restore radioiodide uptake and retention in poorly differentiated and anaplastic thyroid cancer cells by expression of the sodium/iodide symporter thyroperoxidase and thyroglobulin. *Endocrinology.* 2004;145:2865–2875.
34. Kogai T, Kanamoto Y, Li AI, et al. Differential regulation of sodium/iodide symporter gene expression by nuclear receptor ligands in MCF-7 breast cancer cells. *Endocrinology.* 2005;146:3059–3069.
35. Dohán O, De la Vieja A, Carrasco N. Hydrocortisone and purinergic signaling stimulate sodium/iodide symporter (NIS)-mediated iodide transport in breast cancer cells. *Mol Endocrinol.* 2006;20:1121–1137.
36. Tanosaki S, Ikezoe T, Heaney A, et al. Effect of ligands of nuclear hormone receptors on sodium/iodide symporter expression and activity in breast cancer cells. *Breast Cancer Res Treat.* 2003;79:335–345.
37. Chai W, Yin X, Ren L, et al. Sodium/iodide symporter gene transfection increases radionuclide uptake in human cisplatin-resistant lung cancer cells. *Clin Transl Oncol.* 2015;17:795–802.
38. Guerrieri F, Piconese S, Lacoste C, et al. The sodium/iodide symporter NIS is a transcriptional target of the p53-family members in liver cancer cells. *Cell Death Dis.* 2013;4:e807.
39. Ohashi E, Kogai T, Kagechika H, Brent GA. Activation of the PI3 kinase pathway by retinoic acid mediates sodium/iodide symporter induction and iodide transport in MCF-7 breast cancer cells. *Cancer Res.* 2009;69:3443–3450.
40. Liu Z, Xing M. Induction of sodium/iodide symporter (NIS) expression and radioiodine uptake in non-thyroid cancer cells. *PLoS One.* 2012;7:e31729.
41. Kim HW, Kim JE, Hwang MH, et al. Enhancement of natural killer cell cytotoxicity by sodium/iodide symporter gene-mediated radioiodine pretreatment in breast cancer cells. *PLoS One.* 2013;8:e70194.
42. Unterholzner S, Willhauck MJ, Cengic N, et al. Dexamethasone stimulation of retinoic acid-induced sodium iodide symporter expression and cytotoxicity of 131-I in breast cancer cells. *J Clin Endocrinol Metab.* 2006;91:69–78.
43. Kogai T, Sajid-Crockett S, Newmarch LS, Liu YY, Brent GA. Phosphoinositide-3-kinase inhibition induces sodium/iodide symporter expression in rat thyroid cells and human papillary thyroid cancer cells. *J Endocrinol.* 2008;199:243–252.
44. Taki K, Kogai T, Kanamoto Y, Hershman JM, Brent GA. A thyroid-specific far-upstream enhancer in the human sodium/iodide symporter gene requires Pax-8 binding and cyclic adenosine 3′,5′-monophosphate response element-like sequence binding proteins for full activity and is differentially regulated in normal and thyroid cancer cells. *Mol Endocrinol.* 2002;16:2266–2282.
45. Schmutzler C, Winzer R, Meissner-Weigl J, Kohrle J. Retinoic acid increases sodium/iodide symporter mRNA levels in human thyroid cancer cell lines and suppresses expression of functional symporter in nontransformed FRTL-5 rat thyroid cells. *Biochem Biophys Res Commun.* 1997;240:832–838.
46. Bogazzi F, Bartalena L, Pinchera A, Martino E. Adjuvant effect of lithium on radioiodine treatment of hyperthyroidism. *Thyroid.* 2002;12:1153–1154.
47. Romão R, Rubio IG, Tomimori EK, Camargo RY, Knobel M, Medeiros-Neto G. High prevalence of side effects after recombinant human thyrotropin-stimulated radioiodine treatment with 30 mCi in patients with multinodular goiter and subclinical/clinical hyperthyroidism. *Thyroid.* 2009;19:945–951.
48. Silver DA, Pellicer I, Fair WR, Heston WD, Cordon-Cardo C. Prostate-specific membrane antigen expression in normal and malignant human tissues. *Clin Cancer Res.* 1997;3:81–85.
49. Rajasekaran SA, Anilkumar G, Oshima E, et al. A novel cytoplasmic tail MXXXL motif mediates the internalization of prostate-specific membrane antigen. *Mol Biol Cell.* 2003;14:4835–4845.

Practical Considerations for Implementation of ^{177}Lu-DOTATATE Neuroendocrine Tumor Treatment Programs

Diane K. Soulek, Molly E. Martin, Nic J. Mastascusa, and Stephen A. Graves

Department of Radiology, University of Iowa, Iowa City, Iowa

CE credit: For CE credit, you can access the test for this article, as well as additional *JNMT* CE tests, online at https://www.snmmilearningcenter.org. Complete the test online no later than September 2025. Your online test will be scored immediately. You may make 3 attempts to pass the test and must answer 75% of the questions correctly to receive Continuing Education Hour (CEH) credit. Credit amounts can be found in the SNMMI Learning Center Activity. SNMMI members will have their CEH credit added to their VOICE transcript automatically; nonmembers will be able to print out a CE certificate upon successfully completing the test. The online test is free to SNMMI members; nonmembers must pay $15.00 by credit card when logging onto the website to take the test.

The 2018 Food and Drug Administration approval of ^{177}Lu-DOTATATE for the treatment of somatostatin receptor–positive neuroendocrine tumors (NETs) represents a paradigm-shifting approach to cancer treatments around the globe. Gastroenteropancreatic NETs overexpress the somatostatin subtype receptor 2, which is now exploited for receptor-based imaging and therapy, thus generating significant progress in the diagnosis and treatment of this orphan disease. The recent Food and Drug Administration approval of receptor-based PET radiopharmaceuticals and a new peptide receptor radiopharmaceutical therapy, ^{177}Lu-DOTATATE, has dramatically impacted NET patient management. The focus of this paper is to review clinical considerations associated with implementing a ^{177}Lu-DOTATATE program. We review receptor-based NET radiopharmaceuticals; ^{177}Lu-DOTATATE patient selection criteria; administration methods; clinical, regulatory, and radiation safety considerations; technical factors; tissue dosimetry; and reimbursement guidelines.

Key Words: neuroendocrine tumor; ^{177}Lu-DOTATATE; somatostatin receptor; PRRT; dosimetry

J Nucl Med Technol 2022; 50:195–202
DOI: 10.2967/jnmt.122.263813

It is estimated that the annual incidence of neuroendocrine tumors (NETs) is 7 per 100,000 persons, resulting in approximately 23,000 new cases each year in the United States (*1*). NETs are slightly more common in women (52.7%), with 5-y overall survival depending strongly on the grade and stage of disease. At the time of diagnosis, approximately half of patients presents with localized disease whereas the other half has already progressed to regional disease or distant metastases. Localized disease is often well managed by surgery alone (*2*), with median overall survivals in the range of 4–30 y depending on site and grade (*1*).

NETs of gastroenteropancreatic origin often secrete serotonin and a variety of other peptide hormones that can cause characteristic symptoms known as carcinoid syndrome or other symptoms related to the tumor's site of origin. Shortly after the discovery of somatostatin receptors (SSTRs) in 1972 (*3*), it was observed that agents targeted to subtype 2 of the somatostatin receptor resulted in potent antisecretory effects in NETs, providing significant palliative benefit in patients with secreting gastroenteropancreatic NETs. These SSTR-targeted somatostatin analog (SSA) agents were initially available in short-acting immediate-release formulations (octreotide acetate, 1988) and were later made available in long-acting formulations (octreotide and lanreotide, 1998–2001) (*4*). In addition to the palliative therapeutic benefit of SSAs, these agents were found to exhibit antitumor effects (*5,6*), resulting in their clinical use as primary interventions for metastatic gastroenteropancreatic NETs regardless of hormone secretion status.

Expression of SSTR is observed in many cancer types, and this receptor is highly overexpressed in low-grade (grades 1 or 2) NETs (mitotic rate $\leq$ 20, Ki-67 index $\leq$ 20%) and to a lesser extent in high-grade (grade 3) NETs (mitotic rate $>$ 20, Ki-67 index $>$ 20%) (*7,8*). Based on the high degree of overexpression, as well as the known molecular structures with high-affinity binding to this receptor, research into the use of radiolabeled SSAs for imaging and therapy began in the early 1990s. The first proof-of-concept nuclear imaging studies used [^{123}I-Tyr3]-octreotide (*9,10*); shortly thereafter, use of ^{111}In-pentetreotide (an octreotide analog labeled with diethylenetriaminepentaacetic acid chelator for complexation of ^{111}In) gained traction for NET imaging, receiving Food and Drug Administration approval in 1994 (*11,12*). In subsequent years, SSAs with macrocycle chelators (DOTATOC, DOTANOC, DOTATATE) were developed and shown to have improved stability, biodistribution, and clearance for a variety of radiometal labels (*13,14*). Among these, ^{68}Ga-DOTATATE, ^{68}Ga-DOTATOC, and ^{64}Cu-DOTATATE have thus far received Food and Drug Administration approval and are in current

Received Jan. 10, 2022; revision accepted Jun. 8, 2022.
For correspondence or reprints, contact Diane Soulek (diane-soulek@uiowa.edu).
Published online Jun. 14, 2022.

clinical use, whereas ^{111}In-pentetreotide is being phased out in favor of the newer PET-based imaging agents.

Early success in the diagnostic imaging of gastroenteropancreatic NETs led to the development of SSTR-targeted radiotherapeutics, often referred to as peptide receptor radionuclide therapy (PRRT) in this context. The first therapeutic agent to be studied was ^{90}Y-DOTATOC, which was shown to have significant oncologic benefit in small animals and humans (*13,15,16*). Trials with ^{90}Y-DOTATOC demonstrated some renal and hematologic toxicity, and these off-target effects were found to be dose-limiting for this agent. Most recently, ^{177}Lu (half-life [$t_{1/2}$], 6.6 d)-labeled DOTATATE has been favored because of increased retention time in tumors, an apparent reduction in nephrotoxicity, as well as logistical considerations associated with these agents. In the phase 3 NETTER-1 trial, ^{177}Lu-DOTATATE was evaluated in patients with well-differentiated, unresectable or metastatic, progressive midgut NETs (*17*). In comparison to long-acting octreotide, ^{177}Lu-DOTATATE was associated with an improved response rate (18% vs. 3%, $P < 0.001$) and progression-free survival (65.2% vs. 10.8% at 20 mo). These data led to the Food and Drug Administration approval of ^{177}Lu-DOTATATE (Lutathera; Advanced Accelerator Applications USA Inc.) in 2018 for treatment of patients with SSTR-positive gastroenteropancreatic NETs. This therapeutic agent is now widely available and frequently used in the treatment of patients with NETs. As of 2021, Advanced Accelerator Applications reported that ^{177}Lu-DOTATATE is available at more than 230 treatment centers in the United States.

The purpose of this paper is to review the practical clinical considerations associated with ^{177}Lu-DOTATATE, with an emphasis on what the care team members (technologists, nurses, pharmacists, physicists) need to know for successful application of this newly approved PPRT agent.

PATIENT SELECTION

^{177}Lu-DOTATATE is not currently considered a first-line therapy for NET. Instead, patients with surgically unresectable, metastatic, or locally advanced midgut NET may be treated with first-line SSA therapy. If disease progresses during SSA therapy and SSTR positivity is confirmed with functional imaging, the patient may be considered for ^{177}Lu-DOTATATE therapy (*18*). A multidisciplinary team (nuclear medicine, medical oncology, endocrinology, surgical oncology, interventional radiology, radiation oncology) should evaluate the patient's performance status, clinical and imaging data, potential alternative treatments, and PRRT contraindications before deciding to proceed with PRRT. Adequate bone, liver, and renal function should be verified with the European Neuroendocrine Tumor Society exclusion criteria detailed in Table 1, and the patient's Karnofsky performance, a measure of health status, should be at least 60% (*19*).

TABLE 1
PRRT Exclusion Criteria Considerations (*19*)

Parameter	Exclusion criterion
Serum creatinine	>150 μmol/L (>1.7 mg/dL) or creatinine clearance < 50 mL/min
Hemoglobin	<5.0 mmol/L (<8.0 g/dL)
White-cell count	<2,000/mm^3 (2 × 10^9/L)
Platelet count	<75,000/mm^3 (75 × 10^9/L)
Total bilirubin	>3 times upper limit of reference range
Serum albumin	<25 g/L and prothrombin time increased 1.5 times upper limit of reference range*

*Indicates biosynthetic liver failure.

Fundamental to patient selection is the clinical behavior of the gastroenteropancreatic NET, often determined by the tumor's primary site, grade, and differentiation. NET grade reflects the proliferative activity of cells, measured by mitotic rate or Ki-67 index, and differentiation describes the extent to which tumor cells resemble their healthy endogenous cell line (*20*). Gastroenteropancreatic neuroendocrine neoplasms were recently subdivided in the 2019 World Health Organization classification system (*21*) and are summarized in Table 2. NET tumor grade inversely correlates with SSTR density and prognosis; in general, the lower the grade, the higher the SSTR density. A high SSTR density thus correlates with an improved response to PRRT and better prognosis (*20*). Because of weak or absent SSTR expression, as well as being generally more aggressive, higher-grade NETs and poorly differentiated neuroendocrine cancers have a worse prognosis (*22*). SSTR positivity for all lesions should be confirmed with SSTR imaging before ^{177}Lu-DOTATATE therapy; PET-based SSTR imaging (DOTATATE, DOTATOC, DOTANOC) has become the standard of care and is preferred over ^{111}In-pentetreotide scintigraphy because of the higher spatial resolution and dramatically improved lesion detectability of these agents (*23*). Lesions with uptake more intense than normal liver activity are deemed SSTR-positive and thus better candidates for PRRT (*24*).

Because of the frequent lack of SSTR expression in higher grade (grades 2 or 3) and poorly differentiated NETs, these tumors are often examined with ^{18}F-FDG PET imaging in lieu of, or in addition to, SSTR PET imaging. PRRT administration has historically been contraindicated in patients with sites of discordant or mismatched lesions (lesions with positive ^{18}F-FDG uptake, positive contrast enhancement on CT or MRI, and negative SSTR expression). ^{18}F-FDG–positive lesions are known to be associated with a reduced likelihood of response to PRRT. In this patient population, multidisciplinary teams may consider the addition of concomitant chemotherapy to a PRRT regimen. Higher-grade NETs (grades 2 or 3) are currently being evaluated in the phase III NETTER-2 trial, which is investigating PRRT as first-line therapy when used in combination with long-acting, high-dose octreotide (*22*). The phase III COMPETE trial is currently comparing 4 cycles of

TABLE 2
Classification and Grading Criteria for Neuroendocrine Neoplasms of Gastrointestinal Tract and Hepatopancreatobiliary Organs (*21*)

Terminology	Differentiation	Grade	Mitotic rate	Ki-67 index
NET, grade 1	Well differentiated	Low	<2	<3%
NET, grade 2	Well differentiated	Intermediate	2–20	3%–20%
NET, grade 3	Well differentiated	High	>20	>20%
NEC, small-cell type	Poorly differentiated	High*	>20	>20%
NEC, large-cell type	Poorly differentiated	High*	>20	>20%
MiNEN	Well or poorly differentiated	Variable†	Variable†	Variable†

*Poorly differentiated neuroendocrine carcinomas are not formally graded but are considered high-grade.

†In most mixed neuroendocrine–nonneuroendocrine neoplasms, both neuroendocrine and nonneuroendocrine components are poorly differentiated, and neuroendocrine component has proliferation indices in same range as other neuroendocrine carcinomas, but this conceptual category allows for possibility that one or both components may be well differentiated; when feasible, each component should therefore be graded separately.

MiNEN = mixed neuroendocrine–nonneuroendocrine neoplasm; NEC = neuroendocrine carcinoma.

Mitotic rates are number of mitoses/2 mm^2 as determined by counting 50 fields of 0.2 mm^2 (i.e., in total area of 10 mm^2); Ki-67 proliferation index value is determined by counting at least 500 cells in regions of highest labeling (hot spots), which are identified at scanning magnification; final grade is based on whichever of 2 proliferation indices places neoplasm in higher-grade category.

7.4 GBq (200 mCi) of ^{177}Lu-DOTATOC with daily everolimus administration in patients with SSTR-positive disease (*25*). Further studies of ^{177}Lu-DOTATATE are being conducted on pediatric patient populations, including the NETTER-P study, as well as investigator-initiated studies (*26*).

CLINICAL CONSIDERATIONS

Patient preparation is a component critical to the success of PRRT. Many NET patients receive SSAs for symptomatic control of their disease, and the SSAs elicit their therapeutic effect by binding to SSTRs. ^{177}Lu-DOTATATE also works by targeting SSTRs, and administration of SSAs should be carefully planned during ^{177}Lu-DOTATATE treatment to prevent receptor saturation, which can interfere with the efficacy of PRRT (*24,27*). Long-acting SSAs should be discontinued at least 4 wk before each ^{177}Lu-DOTATATE dose; short-acting SSAs may be used as needed up to 24 h before each treatment. SSAs may be resumed 4 h after administration of ^{177}Lu-DOTATATE for symptomatic management between therapeutic cycles and after completion of treatment (*24*).

During ^{177}Lu-DOTATATE administration, patients should be monitored for potential reactions to the infusion (*24,27*). Although infrequent, extravasation of the radiopharmaceutical may occur if the intravenous line becomes obstructed; patency of the line should be verified before the start of the infusion and monitored throughout the administration. Signs of extravasation, such as pain and swelling, should be immediately addressed to increase the clearance of the radiopharmaceutical from the infusion site. Steps to be taken include image acquisition to confirm and quantify the amount of extravasated radiopharmaceutical (whole-body planar scintigraphy and SPECT/CT of the affected area), elevation and exercise of the affected arm as much as possible for 24 h, and application of a compression bandage with heated gel pads for 20 min every 6 h to facilitate redistribution of the radiopharmaceutical. After the initial 24 h, imaging should be repeated. A qualified medical physicist should be consulted regarding the radiation dosimetry of this event, and referral to plastic surgery should be considered on the basis of the dosimetry results. Additional information can be found in literature case reports and reviews (*28,29*).

In addition to the risk of extravasation, patients may experience a neuroendocrine hormonal crisis during ^{177}Lu-DOTATATE administration due to excessive hormone released by the tumor (*30*). Symptoms include cutaneous flushing, diarrhea, bronchospasm, and hypotension and generally occur during or within 24 h of the initial ^{177}Lu-DOTATATE dose. A hormonal crisis can be treated by intravenous administration of SSAs and fluids, corticosteroids, and correction of electrolyte imbalances (*24,30*). ^{177}Lu-DOTATATE may be administered in an outpatient setting not immediately equipped to deal with a carcinoid crisis. Institutional policies describing how to obtain additional medical support or transport the patient to an emergency clinic, if needed, should be in place.

Since the kidneys receive a significant radiation dose, amino acids should be given simultaneously with each cycle of ^{177}Lu-DOTATATE to decrease absorption through the proximal tubules, thus reducing the radiation dose to the kidneys (*27,31,32*). The amino acid solution must be infused over 4 h and should contain 18–25 g each of L-lysine HCl and L-arginine HCl in a total volume of 1–2 L. Several commercial amino acid solutions are available that contain the required amounts of lysine and arginine. However, the presence of additional amino acids in these products may cause significant nausea and vomiting for the patient. Alternatively, a 2-amino-acid solution containing only lysine and arginine may be compounded by the hospital or local pharmacy to improve

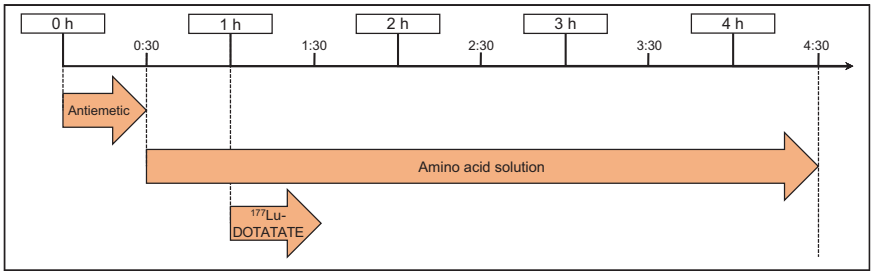

FIGURE 1. ^{177}Lu-DOTATATE PRRT administration time line.

patient tolerability (*33,34*). Figure 1 illustrates the time line for administration of ^{177}Lu-DOTATATE PRRT. Antiemetics are administered first, followed by the start of the amino acid infusion 30 min later. The amino acid infusion should run at a rate that allows for the entire volume to be infused over a total of 4 h. Administration of ^{177}Lu-DOTATATE begins 30 min after the start of the amino acid infusion. If the ^{177}Lu-DOTATATE prescribed activity is decreased, the amount of amino acids administered is not altered (*24*).

Long-term radiation effects of ^{177}Lu-DOTATATE treatment may occur and can include myelosuppression and renal toxicity (*24,27,31*). Laboratory values, including complete blood count and renal function tests, should be monitored throughout the treatment cycle and after the completion of PRRT to assess for toxicity. On the basis of acute changes, typically myelosuppression, the prescribed ^{177}Lu-DOTATATE activity can be reduced, withheld, or permanently discontinued (*24*).

The use of ^{177}Lu-DOTATATE in specific populations may require additional clinical considerations. Pregnancy status should be verified in patients with reproductive potential before initiation of therapy, as ^{177}Lu-DOTATATE can harm the fetus. All patients should be counseled on the use of effective contraception during and after treatment and advised of the potential for infertility. Patients who are lactating should be advised not to breastfeed during the treatment cycle and for 2.5 mo after the conclusion of therapy.

Dose adjustment is not automatically necessary for mild to moderate renal impairment; however, renal function should be monitored more frequently in these patients. Decreased renal function can lead to a longer residence time in the kidneys and higher exposure rates and may require dose adjustment for subsequent cycles. Limited data are available on the safety of ^{177}Lu-DOTATATE in patients with severe renal impairment or end-stage renal disease (*35*), but it is not a contraindication for treatment.

Caution should be exercised when considering PRRT in patients with extensive peritoneal carcinomatosis because of the risk of radiation-induced bowel obstruction. Spontaneous urinary incontinence may make the safe administration of PRRT impossible. Additional PRRT clinical considerations can be found in consensus guidelines by Hicks et al. (*19*). Because special situations can vary in complexity, the multidisciplinary team should communicate and tailor the treatment plan to each patient's individual needs.

REGULATORY AND RADIATION SAFETY CONSIDERATIONS

Before initiating a PRRT program, sites will need to ensure that their radioactive materials license includes the possession and use of ^{177}Lu in sufficient quantities to cover ordered doses as well as residual waste material (*36*). It is also important to review the waste disposal policy with the site radiation safety officer. Although the $t_{1/2}$ of ^{177}Lu is relatively short (6.6 d), ^{177}Lu-DOTATATE may contain small amounts (~0.1%) of the long-lived contaminant ^{177m}Lu ($t_{1/2}$, 161 d). This contaminant can make it difficult to comply with the waste storage and disposal requirement (<120-d $t_{1/2}$) outlined in Nuclear Regulatory Commission title 10 of *Code of Federal Regulations,* part 35, section 35.92. If decay in storage is not a viable option, the radiation safety officer or nuclear pharmacist can coordinate pickup and disposal with the local radiopharmacy or a third-party vendor (*36,37*).

The Nuclear Regulatory Commission requires the authorized user physician to date and sign a directive containing the patient's name, radiopharmaceutical, prescribed administered activity, and route of administration before the ^{177}Lu-DOTATATE is administered. The nuclear medicine staff should follow the site's procedure for administration of therapeutic radiopharmaceuticals, including verifying patient identity, verifying activity to be administered, and administering the drug per the written directive (*36*).

Care should be taken when handling and administering ^{177}Lu-DOTATATE to keep radiation exposure as low as reasonably achievable for the staff and general public (*37*). Appropriate personal protective equipment should be worn, and shielding and tongs should be used for manipulation of the ^{177}Lu-DOTATATE vial. ^{177}Lu-DOTATATE is shipped by Advanced Accelerator Applications or Novartis directly to the end-user site as a 7.4-GBq (200 mCi) quantity in a shielded vial. A variety of methods have been developed for direct infusion from the vial, or the activity may be drawn up into a shielded syringe for use in a syringe pump (*24*). For patients requiring a reduced 3.7-GBq (100 mCi) administration, the site can use an infusion pump to administer the correct volume of ^{177}Lu-DOTATATE from the unit dose vial. Alternatively, the vial can be adjusted by aseptically withdrawing the excess volume of ^{177}Lu-DOTATATE using a shielded syringe; the residual volume of ^{177}Lu-DOTATATE should be properly disposed of according to the site's waste disposal policy.

Except in the case of medical events, only the patient and nuclear medicine staff should be in the treatment room from the start of the infusion until the patient has been released. The patient should also have access to a single-user restroom during the visit because urine will be radioactive after infusion. If a medical event does occur, all steps should be taken

to ensure the medical safety of the patient without regard for personnel radiation exposure. After the medical intervention, the qualified medical physicist or radiation safety officer may provide radiation dose estimates for unbadged personnel who participated in patient care. The patient may be released after therapy, provided the radiation dose to the maximally exposed member of the public is expected to be less than 5 mSv (0.5 rem). The patient must be provided with written instructions on how to follow as-low-as-reasonably-achievable principles, including interruption or discontinuation of breastfeeding, if applicable; restroom use; interaction with household family members; and other considerations deemed relevant by the authorized user or radiation safety officer (*38*). ^{177}Lu-DOTATATE is usually administered as an outpatient procedure, as exposure to the general public after the infusion is unlikely to exceed Nuclear Regulatory Commission limits (*39*).

PROTOCOL AND TECHNICAL CONSIDERATIONS

After a patient has been approved for treatment, the product is ordered through the manufacturer's Web-based ordering system. The manufacturer confirms via email, unless the desired treatment date is within 3 d, in which case the ordering facility must call the manufacturer to verify material availability. The manufacturer recommends that subsequent treatments be scheduled when the first treatment is scheduled. After production, the manufacturer ships the radiopharmaceutical to the end user under quarantine; the ^{177}Lu-DOTATATE cannot be infused into the patient until the batch-release document from the manufacturer is received via email, thus releasing the lot from quarantine. The radiopharmaceutical is supplied in a 30-mL unit dose vial containing 7.4 GBq (200 mCi) ± 10% of ^{177}Lu-DOTATATE in 20.5–25 mL at a concentration of 370 MBq/mL (10 mCi/mL) calibrated to the time of infusion. The default ^{177}Lu dose calibrator setting may be used for measuring ^{177}Lu-DOTATATE, but it is recommended that end users obtain an annual calibration source from Advanced Accelerator Applications or Novartis to determine a more precise dial setting. Currently, approved labeling for ^{177}Lu-DOTATATE describes only a 3.7 or 7.4 GBq (100 or 200 mCi) administration, and there appears to be minimal dose calibrator geometry effect (*40,41*) for volume modification between these levels.

Several different radiopharmaceutical administration methods have been reported (*27,42*). The gravity method arose from the NETTER-1 clinical trial experience. This method involves hanging a normal saline bag and connecting it via an intravenous line to an upright shielded ^{177}Lu-DOTATATE vial with the needle tip above the level of the contents. A longer needle is inserted into and touches the bottom of the ^{177}Lu DOTATATE vial, which is connected to the patient administration intravenous line. The saline entering the closed system at the top of the vial pushes the radiopharmaceutical out through the elongated needle placed at the bottom of the vial and into the patient. Further reading regarding the gravity infusion method is included in Hope et al. (*27*) and the manufacturer's package insert (*24*). There have been issues reported with this technique (*43*), including loss of pressure in the vial to the room air from improper needle placement through the vial septum. Because U.S. Pharmacopeia general chapter <825> radiopharmaceutical guidelines were published in February 2021 (*44*) and have already been adopted in some areas, it is imperative to follow these guidelines for beyond-use times after puncturing a vial septum to ensure patient safety.

Our institution uses a ^{177}Lu-DOTATATE secondary pump infusion method (*45*) similar to the Rotterdam method (Fig. 2). For this method, the ^{177}Lu-DOTATATE vial is placed into a shield, spiked with a vial spike administration set, inverted, and infused with an intravenous pump. Using this simple and easily reproducible method, we have observed very little residual activity in the administration vial, essentially no contamination, and marginal additional exposure to the technical staff (*46*). Alternatively, the activity may be drawn up into a shielded syringe for administration via a syringe pump (*47*). Regardless of the ^{177}Lu-DOTATATE administration method used, the timing of antiemetics and amino acid infusion before and immediately after the ^{177}Lu-DOTATATE administration should not be modified with any alternative administration technique.

DOSIMETRY AND IMAGING

Imaging plays a major role in the management of patients with NETs. During workup, patients undergo a PET/CT study

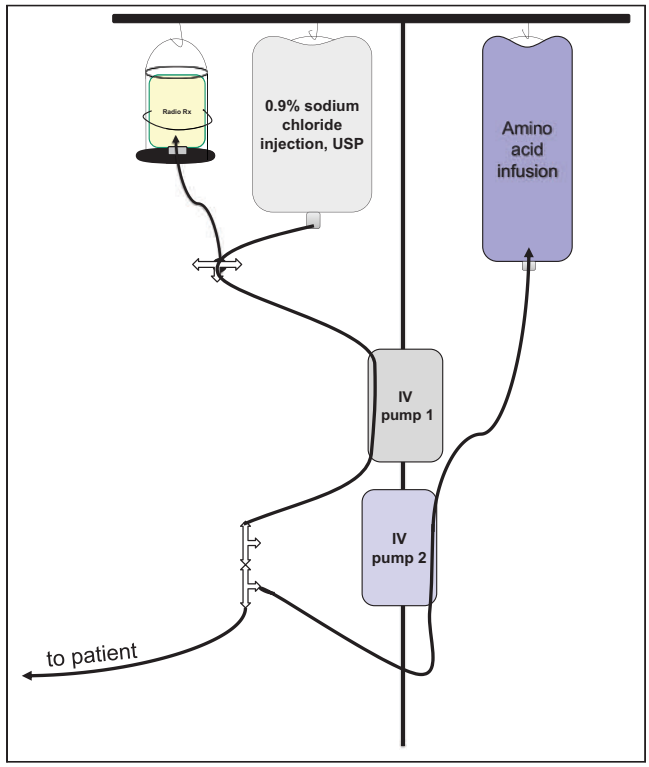

FIGURE 2. ^{177}Lu-DOTATATE Rotterdam secondary pump infusion method. IV = intravenous; Radio Rx = ^{177}Lu-DOTATATE; USP = U.S. Pharmacopeia.

(^{68}Ga-DOTATATE, ^{68}Ga-DOTATOC, or ^{64}Cu-DOTATATE) to assess for SSTR receptor positivity. Patients with low uptake of the SSTR-targeted radiotracer, in comparison to the liver or spleen, should not be considered eligible for treatment with ^{177}Lu-DOTATATE. In some cases, it can be helpful to also obtain a ^{18}F-FDG PET/CT study to identify lesions with increased metabolic rates. Determining lesion ^{18}F-FDG positivity, as well as discordant tracer uptake (^{18}F-FDG–positive and DOTATATE/TOC–negative), provides prognostic value beyond what standard histopathologic grading can provide (*48*). An example of ^{18}F-FDG and ^{68}Ga-DOTATOC discordance is shown in Figure 3. Although tumor uptake on pretreatment SSTR PET imaging weakly correlates with absorbed dose from ^{177}Lu-DOTATATE therapy and likelihood of response, it is not possible to accurately predict absorbed dose to tumors and normal organs from pretreatment PET imaging. This impossibility is due to the short $t_{1/2}$ of ^{68}Ga (68 min), typically conducive to imaging at about 1 h after radiopharmaceutical administration. Tumor uptake of DOTATATE/TOC typically peaks several hours after administration, and the clearance kinetics must be characterized for accurate absorbed dose determination. The $t_{1/2}$ of ^{64}Cu (12.7 h) may be sufficient to obtain quantitative information at later PET imaging time points (2–3 d) (*49*), but this sufficiency has yet to be demonstrated conclusively in the literature. For these reasons, it is most common to perform dosimetry by SPECT/CT or planar γ-imaging after administration of the therapeutic quantity of ^{177}Lu-DOTATATE. An example of DOTATATE imaging, both pretreatment PET/CT and posttreatment SPECT/CT, from our own institution is shown in Figure 4. In addition to providing quantitative information for dosimetry, posttreatment imaging is useful for rapid evaluation of whether any extravasation has occurred during infusion of the ^{177}Lu-DOTATATE. Although rare, extravasation can require immediate medical intervention to prevent excess radiation exposure at the site of injection.

^{177}Lu emits 2 photons that can be used for imaging: 113 keV in 6.2% of decays and 208 keV in 10.4% of decays. Details regarding quantitative SPECT imaging of ^{177}Lu can be found in MIRD pamphlet no. 26 (*50*). Typical acquisition parameters include the use of a medium-energy collimator, an auto-contouring orbit, at least 60 views per head, 15–30 s/view, a 128 × 128 or higher matrix size, a 15%–20% energy window on the 208-keV photopeak, and 5%–10% scatter windows above and below the 208-keV photopeak. Images are typically reconstructed using iterative techniques with CT-based attenuation correction, triple-energy-window scatter correction, collimator detector response modeling, iterative updates adequate to achieve activity recovery convergence (e.g., 12i8s for typical 3-dimensional ordered-subsets expectation maximization), and minimal or no pre- or postreconstruction filtering. In addition to these acquisition and reconstruction parameters, system sensitivity should be assessed via an

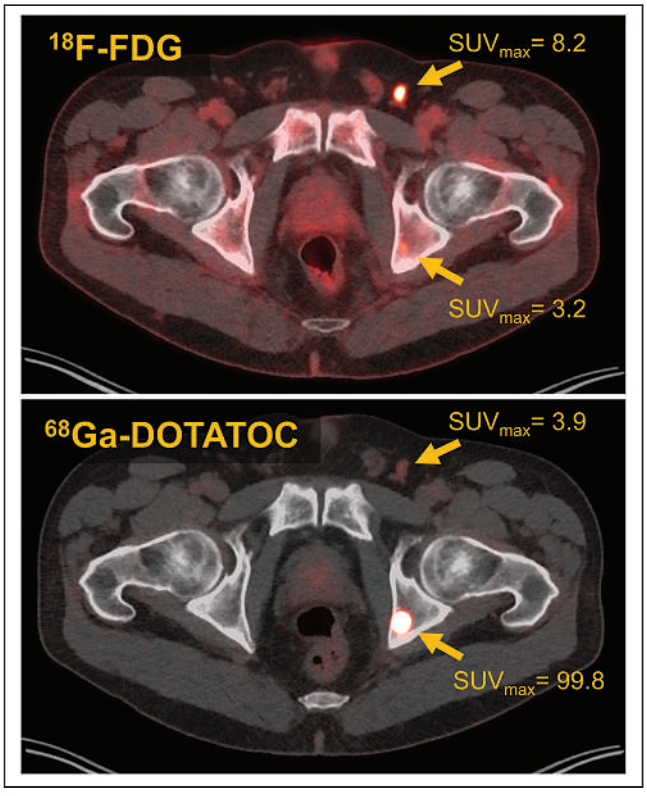

FIGURE 3. Example of discordant uptake on ^{18}F-FDG and ^{68}Ga-DOTATOC imaging. Two lesions are visualized: left inguinal node (^{18}F-FDG–positive, minimal ^{68}Ga-DOTATOC uptake) and left ischium bone lesion (^{68}Ga-DOTATOC–positive, ^{18}F-FDG–negative).

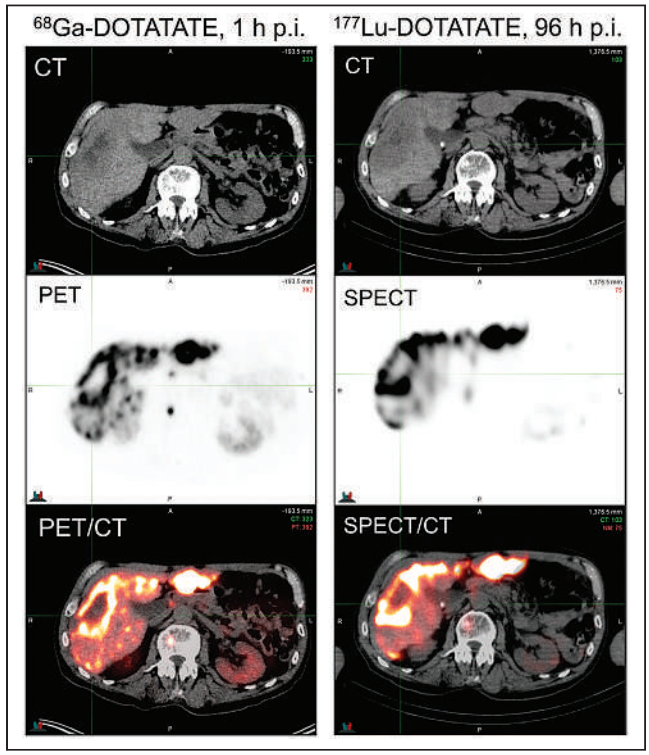

FIGURE 4. PET/CT imaging 1 h after injection of ^{68}Ga-DOTATATE, and SPECT/CT imaging 96 h after injection of ^{177}Lu-DOTATATE. p.i. = after injection.

appropriate phantom experiment (*51*), and dead time should be estimated from measured patient count rates during imaging (*52*).

Fully calibrated and corrected images can then be used to assess patient-specific dosimetry. Methods for determination of patient-specific absorbed dose vary in complexity and accuracy; there are an increasing number of software tools to facilitate dose calculation from radiopharmaceuticals (*53*). The interested reader can find pertinent dosimetry details in the papers by Graves et al., Bolch et al., and Siegel et al., as well as from the *MIRD Primer for Absorbed Dose Calculations, Revised* (published in 1991, new edition expected in early 2022) (*54–57*). Tissues of relevance in dosimetry calculations for ^{177}Lu-DOTATATE often include bone marrow, kidneys, and occasionally liver in cases of prior or planned liver-directed therapy or extensive hepatic tumor burden. Details of normal-tissue dose limits for radiopharmaceuticals can be found in the recent article by Wahl et al. (*58*).

BILLING AND CODING

On January 1, 2019, the Centers for Medicare and Medicaid Services issued a Healthcare Common Procedure Coding System code of A9513 to ^{177}Lu-DOTATATE. The A9513 code descriptor specifies billing as per 1 mCi, and it is important to ensure that the administered millicurie amount for the therapy is accurately documented and submitted (*59*). If a portion of the ^{177}Lu-DOTATATE activity is wasted because of personalized dosimetry or other reasons, a JW modifier should be used. The JW modifier is used to report discarded drug amounts still eligible for payment under Medicare's discarded drug policy (*60*). The Healthcare Common Procedure Coding System codes for antiemetics and amino acids will vary with physician drug choice and amino acid procurement location. Current Procedural Terminology codes are also used for ^{177}Lu-DOTATATE treatment. Current Procedural Terminology code 79101 (radiopharmaceutical therapy, intravenous administration) can be used for ^{177}Lu-DOTATATE administration. The first hour of intravenous amino acid administration can be coded with 96365, and subsequent hours can be coded with 96366. Coding for antiemetic premedication will vary with drug type and route of administration (*59*).

Medical billing and coding guidelines can vary by practice and region, and readers are encouraged to consult the SNMMI's coding and reimbursement Web pages, manufacturer's reimbursement guide, and internal institutional reimbursement specialists. The accurate coding and classification of a patient's diagnosis and treatment are essential, and billing modifiers may be required. Billing codes and reimbursement rates are subject to change based on payer, date of service, and billing setting, and the information shared at the time of this publication is no guarantee of reimbursement. Billing and coding guidelines will continue to evolve with the growth of PRRT. Additionally, reimbursement approaches to dosimetry-guided radiopharmaceutical therapy are emerging, as detailed by Graves et al. (*61*).

CONCLUSION

^{177}Lu-DOTATATE currently serves as a second-line treatment option for patients with surgically unresectable, metastatic, or locally advanced midgut NETs that have failed first-line SSA therapy and is a paradigm-shifting approach to cancer treatment. ^{177}Lu-DOTATATE is paving the way to the future of receptor-based therapy and personalized cancer treatment; this PRRT agent has yielded significant treatment progress for NETs and dramatically impacted patient management. Before offering a patient ^{177}Lu-DOTATATE therapy, a multidisciplinary team should evaluate patient-specific clinical considerations, and SSTR positivity should be confirmed with functional imaging. Sites wanting to implement a ^{177}Lu-DOTATATE program are encouraged to consider the patient selection criteria; PRRT administration methods; clinical, regulatory, and radiation safety considerations; technical factors; tissue dosimetry; and reimbursement practices required with this newly approved PRRT agent.

DISCLOSURE

Nic Mastascusa has served as a consultant for Novartis Inc., and Stephen Graves has a research proposal being reviewed by Novartis Inc. relating to ^{177}Lu-DOTATATE. No other potential conflict of interest relevant to this article was reported.

ACKNOWLEDGMENTS

We thank our respective families and colleagues for their ongoing support.

REFERENCES

1. Dasari A, Shen C, Halperin D, et al. Trends in the incidence, prevalence, and survival outcomes in patients with neuroendocrine tumors in the United States. *JAMA Oncol.* 2017;3:1335–1342.
2. Shah MH, Goldner WS, Benson AB, et al. Neuroendocrine and adrenal tumors, version 2.2021, NCCN clinical practice guidelines in oncology. *J Natl Compr Canc Netw.* 2021;19:839–868.
3. Brazeau P, Vale W, Burgus R, et al. Hypothalamic polypeptide that inhibits the secretion of immunoreactive pituitary growth hormone. *Science.* 1973;179:77–79.
4. Öberg K, Lamberts SW. Somatostatin analogues in acromegaly and gastroenteropancreatic neuroendocrine tumours: past, present and future. *Endocr Relat Cancer.* 2016;23:R551–R566.
5. Rinke A, Wittenberg M, Schade-Brittinger C, et al. Placebo-controlled, double-blind, prospective, randomized study on the effect of octreotide LAR in the control of tumor growth in patients with metastatic neuroendocrine midgut tumors (PROMID): results of long-term survival. *Neuroendocrinology.* 2017;104:26–32.
6. Halfdanarson TR, Rabe K, Rubin J, Petersen G. Pancreatic neuroendocrine tumors (PNETs): incidence, prognosis and recent trend toward improved survival. *Ann Oncol.* 2008;19:1727–1733.
7. Reubi JC, Waser B, Schaer J-C, Laissue JA. Somatostatin receptor sst1–sst5 expression in normal and neoplastic human tissues using receptor autoradiography with subtype-selective ligands. *Eur J Nucl Med.* 2001;28:836–846.
8. Wang Y, Wang W, Jin K, et al. Somatostatin receptor expression indicates improved prognosis in gastroenteropancreatic neuroendocrine neoplasm, and octreotide long-acting release is effective and safe in Chinese patients with advanced gastroenteropancreatic neuroendocrine tumors. *Oncol Lett.* 2017;13:1165–1174.

9. Lamberts SW, Barker W, Reubi J-C, Krenning E. Somatostatin-receptor imaging in the localization of endocrine tumors. *N Engl J Med.* 1990;323:1246–1249.
10. Bakker WH, Krenning EP, Breeman WA, et al. In vivo use of a radioiodinated somatostatin analogue: dynamics, metabolism, and binding to somatostatin receptor-positive tumors in man. *J Nucl Med.* 1991;32:1184–1189.
11. Bakker WH, Albert R, Bruns C, et al. [^{111}In-DTPA-D-Phe1]-octreotide, a potential radiopharmaceutical for imaging of somatostatin receptor-positive tumors: synthesis, radiolabeling and in vitro validation. *Life Sci.* 1991;49:1583–1591.
12. Krenning EP, Bakker W, Kooij P, et al. Somatostatin receptor scintigraphy with indium-111-DTPA-D-Phe-1-octreotide in man: metabolism, dosimetry and comparison with iodine-123-Tyr-3-octreotide. *J Nucl Med.* 1992;33:652–658.
13. Otte A, Jermann E, Behe M, et al. DOTATOC: a powerful new tool for receptor-mediated radionuclide therapy. *Eur J Nucl Med.* 1997;24:792–795.
14. Forrer F, Uusijärvi H, Waldherr C, et al. A comparison of 111 In-DOTATOC and 111 In-DOTATATE: biodistribution and dosimetry in the same patients with metastatic neuroendocrine tumours. *Eur J Nucl Med Mol Imaging.* 2004;31:1257–1262.
15. Otte A, Mueller-Brand J, Dellas S, Nitzsche E, Herrmann R. Yttrium-90-labelled somatostatin analogue for cancer treatment. *Lancet.* 1998;351:417–418.
16. Otte A, Herrmann R, Heppeler A, et al. Yttrium-90 DOTATOC: first clinical results. *Eur J Nucl Med.* 1999;26:1439–1447.
17. Strosberg J, El-Haddad G, Wolin E, et al. Phase 3 trial of ^{177}Lu-Dotatate for midgut neuroendocrine tumors. *N Engl J Med.* 2017;376:125–135.
18. Hope TA, Bodei L, Chan JA, et al. NANETS/SNMMI consensus statement on patient selection and appropriate use of ^{177}Lu-DOTATATE peptide receptor radionuclide therapy. *J Nucl Med.* 2020;61:222–227.
19. Hicks RJ, Kwekkeboom DJ, Krenning E, et al. ENETS consensus guidelines for the standards of care in neuroendocrine neoplasms: peptide receptor radionuclide therapy with radiolabelled somatostatin analogues. *Neuroendocrinology.* 2017;105:295–309.
20. Cives M, Strosberg JR. Gastroenteropancreatic neuroendocrine tumors. *CA Cancer J Clin.* 2018;68:471–487.
21. Nagtegaal ID, Odze RD, Klimstra D, et al. The 2019 WHO classification of tumours of the digestive system. *Histopathology.* 2020;76:182–188.
22. Telo S, Filice A, Versari A, et al. Peptide receptor radionuclide therapy for GEP-NET: consolidated knowledge and innovative applications. *Clin Transl Imaging.* 2021;9:423–438.
23. Bodei L, Ambrosini V, Herrmann K, Modlin I. Current concepts in ^{68}Ga-DOTATATE imaging of neuroendocrine neoplasms: interpretation, biodistribution, dosimetry, and molecular strategies. *J Nucl Med.* 2017;58:1718–1726.
24. LUTATHERA® [prescribing information]. Advanced Accelerator Applications USA, Inc.; 2021.
25. Buscombe JR. Evidence base for the use of PRRT. *Semin Nucl Med.* 2020;50:399–404.
26. McElroy KM, Binkovitz LA, Trout AT, Czachowski MR, Seghers VJ, Lteif AN. Pediatric applications of Dotatate: early diagnostic and therapeutic experience. *Pediatr Radiol.* 2020;50:882–897.
27. Hope TA, Abbott A, Colucci K, et al. NANETS/SNMMI procedure standard for somatostatin receptor–based peptide receptor radionuclide therapy with ^{177}Lu-DOTATATE. *J Nucl Med.* 2019;60:937–943.
28. Arveschoug AK, Bekker AC, Iversen P, Bluhme H, Villadsen GE, Staanum PF. Extravasation of [^{177}Lu] Lu-DOTATOC: case report and discussion. *EJNMMI Res.* 2020;10:68.
29. van der Pol J, Vöö S, Bucerius J, Mottaghy FM. Consequences of radiopharmaceutical extravasation and therapeutic interventions: a systematic review. *Eur J Nucl Med Mol Imaging.* 2017;44:1234–1243.
30. Zandee WT, Brabander T, Blažević A, et al. Symptomatic and radiological response to ^{177}Lu-DOTATATE for the treatment of functioning pancreatic neuroendocrine tumors. *J Clin Endocrinol Metab.* 2019;104:1336–1344.
31. Löser A, Schwarzenböck SM, Heuschkel M, Willenberg HS, Krause BJ, Kurth J. Peptide receptor radionuclide therapy with ^{177}Lu-DOTA-octreotate: dosimetry, nephrotoxicity, and the effect of hematological toxicity on survival. *Nucl Med Commun.* 2018;39:236–246.
32. Hennrich U, Kopka K. Lutathera®: the first FDA- and EMA-approved radiopharmaceutical for peptide receptor radionuclide therapy. *Pharmaceuticals (Basel).* 2019;12:114.
33. Rolleman EJ, Valkema R, de Jong M, Kooij PP, Krenning EP. Safe and effective inhibition of renal uptake of radiolabelled octreotide by a combination of lysine and arginine. *Eur J Nucl Med Mol Imaging.* 2003;30:9–15.
34. Lyashchenko S, DeNoble P, Brown A, Lewis J. A better alternative: an amino acid solution for renal protection during ^{177}Lu peptide therapy [abstract]. *J Nucl Med.* 2016;57(suppl 2):1120.
35. Dierickx LO, Séverine B, Fatima M, Amel B, Rosine G. Successful and safe treatment with ^{177}Lu-DOTATATE (Lutathera) of progressive metastatic pancreatic neuroendocrine tumor under hemodialysis. *Clin Nucl Med.* 2020;45:e400–e402.
36. Medical Use of Byproduct Material. 10 CFR 35 (2014).
37. Standards for Protection Against Radiation. 10 CFR 20 (2016).
38. *Regulatory Guide 8.39 Revision 1: Release of Patients Administered Radioactive Material*. U.S. Nuclear Regulatory Commission; 2020:1–22.
39. Underwood J, Sturchio G, Arnold S. Patient release and instructions for lutetium dotatate radiopharmaceutical therapy. *Health Phys.* 2021;121:160–165.
40. Talukdar M, Dewhirst H, Paulsen A. Assaying lutetium 177 in a dose calibrator [abstract]. *J Nucl Med.* 2019;60(suppl 1):2080.
41. Sharma S, Singh B, Koul A, Mittal BR. Deviation in the predefined calibration factors of the dose calibrators and the associated inaccuracy in the radioactivity measurements of beta-gamma emitters. *Indian J Nucl Med.* 2015;30:122–127.
42. Abbott A, Jacene HA. ^{177}Lu-DOTATATE peptide receptor radionuclide therapy. *J Nucl Med Technol.* 2018;46:245–246.
43. Davis AB, Pietryka MH, Passalaqua S. Technical aspects and administration methods of ^{177}Lu-DOTATATE for nuclear medicine technologists. *J Nucl Med Technol.* 2019;47:288–291.
44. *USP General Chapter <825> Radiopharmaceuticals: Preparation, Compounding, Dispensing, and Repackaging*. U.S. Pharmacopeial Convention; 2018:4–18.
45. Ponto JSJ, Bricker J. Modified method for administration of Lu-177 peptide [abstract]. *J Am Pharm Assoc.* 2014;54:148.
46. Mastascusa NPJ. Retention of Lu-177 peptide in dose vial and administration tubing [abstract]. *J Am Pharm Assoc.* 2020;60:150.
47. LUTATHERA [package insert]. Advanced Accelerator Applications USA, Inc.; 2021.
48. Karfis I, Marin G, Levillain H, et al. Prognostic value of a three-scale grading system based on combining molecular imaging with ^{68}Ga-DOTATATE and ^{18}F-FDG PET/CT in patients with metastatic gastroenteropancreatic neuroendocrine neoplasias. *Oncotarget.* 2020;11:589–599.
49. Merrick M, Dunnwald L, Tiwari A, Sunderland J, Graves S. Longitudinal PET/CT imaging of ^{64}Cu for radiopharmaceutical therapy dosimetry [abstract]. Presented at: AAPM 63rd Annual Meeting and Exhibition [virtual]; July 25, 2021.
50. Ljungberg M, Celler A, Konijnenberg MW, Eckerman KF, Dewaraja YK, Sjögreen-Gleisner K. MIRD pamphlet no. 26: joint EANM/MIRD guidelines for quantitative ^{177}Lu SPECT applied for dosimetry of radiopharmaceutical therapy. *J Nucl Med.* 2016;57:151–162.
51. Graves S, Merrick M, Tiwari A, Sunderland J. Evaluation of a scalable qSPECT calibration method for radiopharmaceutical dosimetry [abstract]. *J Nucl Med.* 2021;62(suppl 1):1433.
52. Uribe CF, Esquinas PL, Gonzalez M, Zhao W, Tanguay J, Celler A. Deadtime effects in quantification of ^{177}Lu activity for radionuclide therapy. *EJNMMI Phys.* 2018;5:2.
53. Capala J, Graves SA, Scott A, et al. Dosimetry for radiopharmaceutical therapy: current practices and commercial resources. *J Nucl Med.* 2021;62(suppl 3):3S–11S.
54. Graves SA, Hobbs RF. Dosimetry for optimized, personalized radiopharmaceutical therapy. *Semin Radiat Oncol.* 2021;31:37–44.
55. Bolch WE, Eckerman KF, Sgouros G, Thomas SR. MIRD pamphlet no. 21: a generalized schema for radiopharmaceutical dosimetry—standardization of nomenclature. *J Nucl Med.* 2009;50:477–484.
56. Siegel JA, Thomas SR, Stubbs JB, et al. MIRD pamphlet no. 16: techniques for quantitative radiopharmaceutical biodistribution data acquisition and analysis for use in human radiation dose estimates. *J Nucl Med.* 1999;40:37S–61S.
57. Loevinger R, Budinger T, Watson E. *MIRD Primer for Absorbed Dose Calculations, Revised.* Society of Nuclear Medicine and Molecular Imaging; 1991.
58. Wahl RL, Sgouros G, Iravani A, et al. Normal-tissue tolerance to radiopharmaceutical therapies, the knowns and the unknowns. *J Nucl Med.* 2021;62(suppl 3):23S–35S.
59. LUTATHERA® [reimbursement guide]. Advanced Accelerator Applications USA, Inc.; July 2020.
60. Medicare program: JW modifier—drug/biological amount discarded/not administered to any patient: frequently asked questions. https://www.cms.gov/Medicare/Medicare-Fee-for-Service-Payment/HospitalOutpatientPPS/Downloads/JW-Modifier-FAQs.pdf. Published August 26, 2016. Accessed July 25, 2021.
61. Graves SA, Bageac A, Crowley JR, Merlino DA. Reimbursement approaches for radiopharmaceutical dosimetry: current status and future opportunities. *J Nucl Med.* 2021;62(suppl 3):48S–59S.

Reprinted from the September 2018 *Journal of Nuclear Medicine Technology*

^{177}Lu-DOTATATE Peptide Receptor Radionuclide Therapy

Amanda Abbott and Heather Jacene

The peptide receptor radionuclide therapy (PRRT) ^{177}Lu-DOTATATE binds to somatostatin receptors (*1*). A multidisciplinary team should be involved when treating patients with ^{177}Lu-DOTATATE PRRT, including medical oncologists, nuclear medicine physicians and technologists, nurses, radiation safety professionals, and pharmacists (*2*).

Clinical Indications

Somatostatin receptor–positive gastroenteropancreatic neuroendocrine tumors in adults (*1*).

Contraindications

None (*1*).

Treatment Plan (*1*)

- 7.4 GBq (200 mCi) of ^{177}Lu-DOTATATE PRRT intravenously every 8 weeks (wk) for a total of 4 administrations.
- Concomitant amino acid infusion to reduce the radiation dose to the kidneys.
- Antiemetic medication(s) to reduce nausea and vomiting caused by amino acids.

Patient Preparation/Education

Patient education should include a detailed description of the treatment day and posttreatment care, including possible side effects, instructions about radiation safety to reduce exposure to others, fertility and precautions during sex, and the safe handling of body waste at home.

Before ^{177}Lu-DOTATATE PRRT, the patient should:

- Discontinue long-acting somatostatin analogs (long-acting-release octreotide [Sandostatin LAR Depot; Novartis] or Lanreotide Autogel [Somatuline Depot; Ipsen]) for at least 4 wk or short-acting somatostatin analogs (subcutaneous octreotide) for at least 24 hours (h) (*1*).
- Consider changing into scrubs for the day (*2*).

During ^{177}Lu-DOTATATE PRRT, the patient should tell the care team if any dizziness, flushing, loose stools, trouble breathing, or tightness of the throat occurs.

After ^{177}Lu-DOTATATE PRRT, the patient should:

- Empty his or her bladder as frequently as possible until the end of the third day after the treatment.
- Tell the care team if loose stools last more than 24 h after the treatment.
- Tell the care team if any trouble breathing, fatigue, fever, chills, cough, bleeding, or bruising occurs (*2*) (and seek immediate medical attention if, within 24 h of the treatment, dizziness, flushing, loose stools, trouble breathing, or tightness of throat occurs).
- Keep all lab appointments.

Treatment Instructions

- Check laboratory values, including creatinine, glomerular filtration rate, and complete blood count, before each treatment. Whether to proceed is a clinical decision (*2*).
- Give antiemetic medication 30 minutes (min) before starting the amino acid infusion and then as needed.
- Infuse at least 1/8 of the total volume of amino acids at least 30 min before the ^{177}Lu-DOTATATE PRRT infusion, and continue the amino acid infusion for at least 4 h and up to 6–7 h, depending on the rate. A slower rate may help reduce nausea and vomiting (*2*).
- Infuse the ^{177}Lu-DOTATATE PRRT for approximately 30 min. If a neuroendocrine hormonal crisis occurs (dizziness, flushing, loose stools, trouble breathing, or tightness of throat), report it immediately.
- Continue infusing amino acids until the entire volume has been given.
- If needed, administer a long-acting somatostatin analog 4–24 h after the end of the ^{177}Lu-DOTATATE PRRT (*1*).

Therapeutic Dose Calculations

- Give the standard adult dose of 7.4 GBq (200 mCi) every 8 wk for 4 total administrations (*1*).

TABLE 1
Radiopharmaceutical Identity, Dose, Route of Administration, Infusion Time, and Infusion Duration

Radiopharmaceutical	Dose	Administration route	Infusion start time	Infusion duration
^{177}Lu-DOTATATE	7.4 GBq (200 mCi)	Intravenous	At least 30 min (or 1/8 of total volume) after initiation of amino acid infusion	~30 min

DOI: 10.2967/jnmt.118.217844

TABLE 2
Pharmaceutical Identity, Dose, Route of Administration, and Administration Requirements

Pharmaceutical	Dose	Administration route	Administration requirements
Antiemetic	As prescribed	Oral or intravenous	30 min before starting amino acid infusion and as needed
Amino acids	18–24 g lysine and 18–24 g arginine	Intravenous	≥30 min (at least 1/8 of total volume) before starting ^{177}Lu-DOTATATE infusion until total volume is given (≥4 h total)

- If adverse events occur, reduce the dose by half and delay up to 16 wk as described in the prescribing information (*1*).

Warnings/Precautions

^{177}Lu-DOTATATE PRRT is a radioactive therapy, and appropriate radiation safety practices should be used (*1*).

REFERENCES

1. LUTATHERA® (lutetium Lu 177 dotatate) injection, for intravenous use [package insert]. Colleretto Giacosa (TO), Italy: Advanced Accelerator Applications S.r.l.; 2018.
2. Abbott A, Sakellis C, Andersen E, et al. Guidance on ^{177}Lu-DOTATATE peptide receptor radionuclide therapy from the experience of a single nuclear medicine division. *J Nucl Med Technol*. 2018;59:237–244.

^{177}Lu-PSMA Therapy

Ephraim E. Parent[1], Bital Savir-Baruch, FACNM[2], Isis W. Gayed[3], Frankis Almaguel[4], Bennett B. Chin[5], Austin R. Pantel, MSTR[6], Evan Armstrong, NMR, CT[7], Amanda Morley[7], Robin C. Ippisch[7], and Robert R. Flavell[7]

[1]Department of Radiology, Mayo Clinic, Jacksonville, Florida; [2]Department of Medical Imaging, University of Arizona, Tucson, Arizona; [3]Department of Diagnostic and Interventional Imaging, McGovern Medical School, Houston, Texas; [4]Loma Linda University, Loma Linda, California; [5]University of Colorado, Aurora, Colorado; [6]Department of Radiology, University of Pennsylvania, Philadelphia, Pennsylvania; and [7]Department of Radiology and Biomedical Imaging, University of California, San Francisco, San Francisco, California

CE credit: For CE credit, you can access the test for this article, as well as additional *JNMT* CE tests, online at https://www.snmmilearningcenter.org. Complete the test online no later than September 2025. Your online test will be scored immediately. You may make 3 attempts to pass the test and must answer 75% of the questions correctly to receive Continuing Education Hour (CEH) credit. Credit amounts can be found in the SNMMI Learning Center Activity. SNMMI members will have their CEH credit added to their VOICE transcript automatically; nonmembers will be able to print out a CE certificate upon successfully completing the test. The online test is free to SNMMI members; nonmembers must pay $15.00 by credit card when logging onto the website to take the test.

Radiopharmaceutical therapy using ^{177}Lu-prostate-specific membrane antigen (PSMA) is an effective prostate cancer treatment that was recently approved by the U.S. Food and Drug Administration. This method leverages the success of PSMA-targeted PET imaging, enabling delivery of targeted radiopharmaceutical therapy; has demonstrated a clear benefit in large prospective clinical trials; and promises to become part of the standard armamentarium of treatment for patients with prostate cancer. This review highlights the evidence supporting the use of this agent, along with important areas under investigation. Practical information on technology aspects, dose administration, nursing, and the role of the treating physician is highlighted. Overall, ^{177}Lu-PSMA treatment requires close collaboration among referring physicians, nuclear medicine technologists, radiopharmacists, and nurses to streamline patient care.

Key Words: genitourinary; radiation safety; radionuclide therapy; prostate; radiopharmaceutical therapy; technology

J Nucl Med Technol 2022; 50:205–212
DOI: 10.2967/jnmt.122.263814

Aside from nonmelanoma skin cancer, prostate cancer is the most common cancer among men in the United States, with 1 of 8 men diagnosed during their lifetime (*1*). Although prostate cancer is highly treatable, up to 30% of patients will develop metastatic castration-resistant prostate cancer (mCRPC) (*2*). Treatment for mCRPC commonly includes immunotherapy, radionuclide therapy with ^{223}Ra, cytotoxic agents, and androgen deprivation therapy. These treatments have improved overall survival (OS); however, despite advances in systemic therapies, mCRPC remains incurable (*3*).

Prostate-specific membrane antigen (PSMA) has emerged as a valuable target in mCRPC for both diagnosis and therapy. PSMA is highly overexpressed in more than 90% of prostate cancer metastatic lesions and demonstrates higher expression with greater Gleason grades (*4,5*). Furthermore, PSMA PET/CT has been demonstrated to outperform other conventional imaging modalities in the sensitivity and specificity of detecting prostate cancer recurrence and metastasis (*6*). Given the differential expression of PSMA between prostate cancer and normal tissue, small-molecule PSMA inhibitors have been developed, such as ^{177}Lu-PSMA-617 (^{177}Lu-vipivotide tetraxetan; Pluvicto [Novartis]) and ^{177}Lu-PSMA I&T, for therapy of mCRPC. The benefit of this targeted molecular therapy is based on the binding, internalization, and retention of the PSMA ligands within tumor cells (*7*).

Labeling PSMA molecules with a variety of radioisotopes (including ^{18}F, ^{68}Ga, ^{99m}Tc, ^{177}Lu, ^{225}Ac, ^{111}In, and ^{90}Y, among others) allows for PET or SPECT imaging as well as radioligand therapy (RLT) with β^- or α emitters. Over the last decade, significant knowledge about the efficacy of PSMA RLT has been gained. ^{177}Lu-PSMA-617 has now achieved widespread acceptance as a viable targeted treatment for mCRPC, with U.S. Food and Drug Administration (FDA) approval granted on March 23, 2022, for adults who have PSMA-positive mCRPC and have been treated with androgen receptor pathway inhibition and taxane-based chemotherapy (*8*). This continuing education article will cover patient selection, clinical considerations, technical considerations, treatment protocols, imaging, response to therapy, dosimetry, future developments, and radiation safety. However, billing and coding, payer reimbursement, and regulatory considerations for ^{177}Lu-PSMA-617 have not yet been determined as of the time of publication and are not discussed here.

Received Mar. 31, 2022; revision accepted Jul. 13, 2022.
For correspondence or reprints, contact Robert R. Flavell (robert.flavell@ucsf.edu).
Published online Jul. 26, 2022.

PATIENT SELECTION

Given a shared target, PSMA PET has been used to assess patients eligible for PSMA-targeted RLT such as ^{177}Lu-PSMA or ^{225}Ac-PSMA (*9,10*). PSMA PET is essential for mCRPC patients being considered for PSMA RLT to help stage and identify PSMA-positive lesions that will respond to PSMA RLT (*11*). The FDA package insert for ^{177}Lu-PSMA-617 (^{177}Lu-vipivotide tetraxetan) specifies that patients to be selected for treatment must use the FDA-approved PSMA PET radiopharmaceutical ^{68}Ga-PSMA-11 (^{68}Ga-gozetotide; Illuccix [Telix Pharmaceuticals] or Locametz [Advanced Accelerator Applications]) (*8*). There are currently 2 FDA-approved PSMA PET radiopharmaceuticals for initial staging and biochemically recurrent mCRPC: ^{68}Ga PSMA-11 (^{68}Ga-gozezotide) and ^{18}F-DCFPyL (^{18}F-piflufolastat; Pylarify [Progenics Pharmaceuticals]).

Many clinical trials have shown the utility of using PSMA PET to identify mCRPC patients who will benefit from PSMA RLT and to exclude those who are most likely to be nonresponders. Two major multicenter clinical trials, VISION (United States and Canada) and TheraP (Australia), investigated the outcome of patients with mCRPC after ablation with ^{177}Lu-PSMA-617 RLT (*12,13*). The phase III VISION trial evaluated ^{177}Lu-PSMA-617 RLT in 831 patients with mCRPC and was the principal justification for FDA approval of ^{177}Lu-PSMA-617 RLT. Primary outcomes measured imaging-based progression-free survival and OS between ^{177}Lu-PSMA-617 RLT plus standard of care (SOC) versus SOC alone. ^{177}Lu-PSMA-617 plus SOC significantly prolonged both imaging-based progression-free survival (median, 8.7 vs. 3.4 mo) and OS (median, 15.3 vs. 11.3 mo), compared with SOC. Additionally, whereas the incidence of adverse events (AEs), grade 3 or above, was higher in the ^{177}Lu-PSMA-617 arm (52.7% vs. 38.0%), quality-of-life measures were not significantly impacted.

The phase II TheraP trial compared ^{177}Lu-PSMA-617 RLT with SOC cabazitaxel in 200 men with mCRPC. The primary endpoint was prostate-specific antigen (PSA) response defined by a reduction in PSA by at least 50% from baseline. In contrast to VISION, TheraP set requirements of at least 1 lesion on ^{68}Ga-PSMA-11 PET with an SUV_{max} of more than 20, the remaining metastatic lesions with an SUV_{max} of more than 10, and no discordant hypermetabolic disease. PSA responses were more frequent in the ^{177}Lu-PSMA-617 RLT group than the cabazitaxel group (66% vs. 37%, respectively). Grade 3–4 AEs occurred in 33% of the ^{177}Lu-PSMA-617 RLT group versus 53% of the cabazitaxel group. It is yet to be determined whether stratifying by SUV_{max} can improve patient outcomes, and the OS of the TheraP trial has yet to be reported.

Although both trials reported better outcomes for patients who received ^{177}Lu-PSMA-617 RLT than for those who received SOC chemotherapy, the TheraP outcome is considered superior to the VISION outcome. The better outcome is believed to result from more strict criteria that excluded mCRPC patients with discordant hypermetabolic lesions. The main criteria for both VISION and TheraP included patients with PSMA-positive metastatic lesions on ^{68}Ga-PSMA-11 PET/CT and excluded patients without PSMA uptake on ^{68}Ga-PSMA-11 PET/CT. Although VISION used conventional imaging to exclude patients with discordant lesions (lesions positive on CT and negative on PSMA PET), TheraP used functional techniques including ^{18}F-FDG PET/CT in conjunction with PSMA PET/CT, and patients with at least 1 discordant hypermetabolic lesion (PSMA-negative or ^{18}F-FDG–positive) were excluded. Many studies using PSMA PET on patients with mCRPC have consistently shown that a sizable minority has at least 1 discordant hypermetabolic lesion and that these patients have worse outcomes. For example, Chen et al., in a study of 56 patients, found that 23.2% had at least 1 discordant lesion and that prostate serum antigen (PSA) and Gleason score were both higher in these patients (Fig. 1) (*14*).

A subanalysis of a single-center phase 2 trial of ^{177}Lu-PSMA-617 RLT similarly found that 16 of 50 patients had at least 1 discordant lesion and were deemed ineligible for ^{177}Lu-PSMA-617 therapy. The OS of these patients was 2.6 mo (compared with 13.5 mo for patients who received ^{177}Lu-PSMA-617) (*15*).

Until recently, it was unknown whether the inclusion and exclusion criteria of VISION and TheraP were appropriate or whether all patients with mCRPC would benefit from ^{177}Lu-PSMA RLT regardless of PSMA PET findings. A recent retrospective analysis compared the outcomes of patients who were treated with ^{177}Lu-PSMA-617 RLT and who would have failed the VISION inclusion criteria (positive metastatic lesions on CT and with low or no PSMA uptake) versus patients who received ^{177}Lu-PSMA-617 RLT

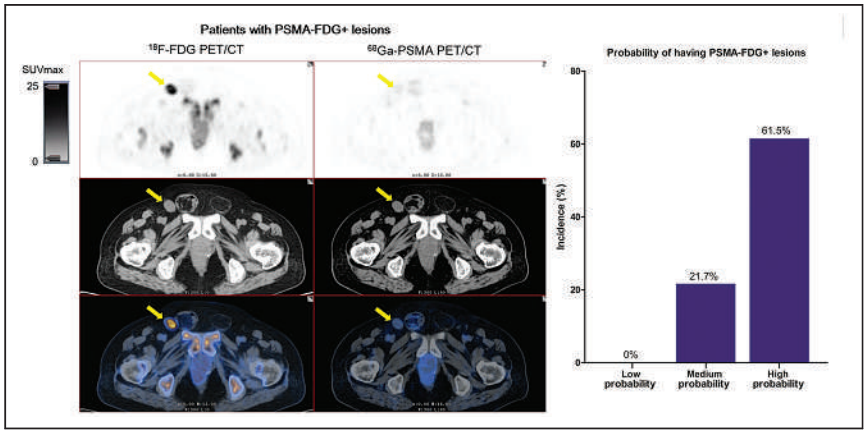

FIGURE 1. Previously published image demonstrating discordant hypermetabolic right inguinal metastatic deposit with high ^{18}F-FDG PET uptake and little to no PSMA accumulation. (Reprinted from (*13*).)

and met the VISION eligibility criteria. The outcome for the VISION-noneligible group was significantly worse than that of patients who met the VISION inclusion criteria, with a PSA response rate of 21% versus 50% ($P = 0.005$), PSA progression-free survival of 2.1 versus 4.1 mo ($P = 0.023$), and a trend toward a shorter OS of 9.6 mo versus 14.2 mo ($P = 0.16$), respectively (*16*). Several additional similar trials have also found significant differences in ^{177}LuPSMA RLT outcome between patients with discordant hypermetabolic disease and those with PSMA-matched or ^{18}F-FDG–negative disease. For example, Michalski et al. demonstrated that in a study with 54 patients who received ^{177}Lu-PSMA RLT and included patients both with and without discordant hypermetabolic disease, patients with discordant hypermetabolic disease had an OS of 6.0, versus 16.0 mo for those without discordant disease (*17*). Although that study showed that patients can develop discordant hypermetabolic disease after ^{177}Lu-PSMA RLT, these patients do not appear to have outcomes different from patients with ^{18}F-FDG–concordant disease (*18*). Despite the seemingly clear and consistent evidence that PSMA PET is needed for patient stratification before ^{177}Lu-PSMA RLT, there remains debate from both industry and the medical community about the need for pretherapy PSMA PET/CT. To address this concern, a recent review article summarized the community's hope that "the prostate cancer medical community will stand up for precision medicine, including by ordering PSMA (and ^{18}F-FDG) PET before treating a patient with ^{177}Lu-PSMA-617," adding, "PSMA RLT for prostate cancer without PSMA PET should not be accepted" (*19*).

According to the Centers for Medicare and Medicaid Services, the use of ^{18}F-FDG PET/CT in the evaluation of patients with prostate cancer is not approved for billing in the United States. Therefore, using ^{18}F-FDG PET/CT as an adjunct to PSMA PET to optimize patient selection for ^{177}Lu-PSMA RLT may be challenging. Alternative PET agents that are approved for biochemically recurrent prostate cancer, such as ^{18}F-fluciclovine (*20*) and ^{11}C-choline, may potentially be used in the future as an adjunct to optimize patient selection and improve outcomes. However, this possibility should be evaluated in clinical trials.

CLINICAL CONSIDERATIONS

With the recent FDA approval of ^{177}Lu-PSMA-617 (^{177}Lu-vipivotide tetraxetan), the field of PSMA RLT is expected to evolve rapidly. The European Association of Nuclear Medicine has published procedure guidelines for ^{177}Lu-PSMA radiotherapies (*21*), and procedure standards from the Society of Nuclear Medicine and Molecular Imaging are under development. The European Association of Nuclear Medicine guidelines promote the use of ^{177}Lu-PSMA radiotherapy for patients with mCRPC "who have exhausted or are ineligible for approved alternative options and with adequate uptake of PSMA ligands on the basis of a pre-therapy imaging." However, the decision on whether alternative therapies have been exhausted is often beyond the scope of a nuclear medicine or radiology physician. Therefore, the involvement of a multidisciplinary tumor board comprising a nuclear medicine or radiology physician, a medical oncologist, a radiation oncologist, and/or a urologist is strongly encouraged. A full discussion of the benefits and risks of alternative therapies (including androgen deprivation therapy, antiandrogens, secondary hormone agents [e.g., abiraterone, enzalutamide], chemotherapy, and other targeted radionuclide therapies [e.g., $^{223}RaCl_2$]) is beyond the scope of this article.

Although the FDA package insert for ^{177}Lu-PSMA-617 does not specify any contraindications, the European Association of Nuclear Medicine guidelines have published contraindications for PSMA RLT. For the most part, these guidelines have mirrored the inclusion and exclusion criteria of large phase II or III trials such as VISION (*12*) and TheraP (*13*), with some minor variations. These contraindications include a life expectancy of less than 6 mo, an Eastern Cooperative Oncology Group performance status of more than 2, an unacceptable medical or radiation safety risk, an unmanageable urinary tract obstruction or hydronephrosis, inadequate organ function (glomerular filtration rate < 30 mL/min or creatinine $>$ 2-fold the upper limit of normal; liver enzymes $>$ 5-fold the upper limit of normal), inadequate marrow function (total white cell count $< 2.5 \times 10^9$/L and platelet count $< 75 \times 10^9$/L), and conditions that require timely interventions (radiation therapy, surgery). For example, for spinal cord compression and unstable fractures, PSMA RLT might be performed afterward depending on the patient's condition.

^{177}Lu-PSMA RLT has been shown to have a low rate of AEs in several clinical studies. There are, though, some observed risks that the nuclear medicine physician and patient should know about. In the phase III VISION study, 52.7% of patients experienced grade 3 or higher AEs, greater than the 38.0% of patients with similar events in the control group. Anemia was the most common AE of grade 3 or higher, observed in 12.9% of subjects. This finding is somewhat surprising given the relatively low uptake in bone marrow. This anemia is considered a real effect, as a recently published metaanalysis of 250 studies with a total of 1,192 patients similarly found that although grade 3 and 4 toxicities were uncommon, anemia was the highest reported AE for both ^{177}Lu-PSMA-617 and ^{177}Lu-PSMA I&T (*22*). Other notable AEs include the 7.9% and 2.5% of patients in VISION who experienced thrombocytopenia and leukopenia, respectively. An elevated transaminase level is often seen; this is somewhat expected, given the moderate amount of ^{177}Lu-PSMA uptake in the liver. Greater than 35% of patients in the treatment group of VISION experienced fatigue, xerostomia (dry mouth), or nausea, though almost all were grade 2 or less (*12*). The AE incidence was similar to that in smaller early-phase studies that preceded VISION (*13,23–25*). Quality of life was not adversely affected in VISION, supporting its inclusion in a treatment plan, with the ^{177}Lu-

PSMA-617 arm reporting a favorable pain intensity score on the short form of the Brief Pain Inventory, as well as a favorable time to deterioration in the Functional Assessment of Cancer Therapy–Prostate questionnaire (*12*). Additionally, the reported mean global health status was similar between the ^{177}Lu-PSMA-617 arm and the SOC arm in TheraP.

TECHNICAL CONSIDERATIONS

The production and quality control recommendations of the joint International Atomic Energy Agency, European Association of Nuclear Medicine, and Society of Nuclear Medicine and Molecular Imaging on peptide receptor radionuclide therapy for neuroendocrine tumors are applicable to ^{177}Lu-PSMA RLT (*26*). ^{177}Lu-PSMA consists of a pharmacophore (PSMA) conjugated with a chelating moiety (DOTA) to bind to the ^{177}Lu radiometal (*27*). The DOTA–PSMA precursor is typically produced under good-manufacturing-practice conditions by a commercial supplier such as ABX. The ^{177}Lu is supplied as $^{177}LuCl_3$ and is also produced under good-manufacturing-practice conditions. This radiosynthesis has previously been described in detail (*28*), consisting of a radiolabeling step followed by purification. The radiolabeling is typically performed in ascorbate buffer, which is used to control the pH of the reaction and to stabilize the radiolysis. The reaction is heated and then purified using a series of solid-phase extraction cartridges. Purification consists of passing a diluted reaction solution through a C18 cartridge, which retains the radiolabeled ^{177}Lu-PSMA and allows any unreacted $^{177}LuCl_3$ to pass through to waste. The C18 is rinsed and eluted with an ethanol–water solution and then diluted with saline containing ascorbic acid. The solution is then passed through a cation-exchange cartridge containing diethylenetriamine pentaacetate and is finally passed over a 0.22-μm sterilizing filter. A small aliquot (<1 mL) is taken for quality control analysis.

Quality control testing typically consists of tests for radiochemical purity, radiochemical identity, appearance, pH, endotoxin content, filter integrity, and sterility. Radiochemical purity and identity are analyzed by high-performance liquid chromatography; appearance, by visual inspection; pH, by pH paper strips; endotoxin content, by a PTS Endosafe (Charles River Laboratories) system according to U.S. Pharmacopeia <85>; filter integrity, by a bubble-point test; and sterility, by direct inoculation of trypticase soy broth and fluid thioglycollate medium according to U.S. Pharmacopeia <71>. Typical specifications are shown in Table 1.

TABLE 1
Typical Specifications for Quality Control Tests

Test	Specification
Radiochemical purity (HPLC)	>95%
Radiochemical identity (HPLC)	t_R ± 5% reference standard
Appearance (visual inspection)	Clear, colorless, particulate-free
pH	4.0–7.0
Endotoxin content (USP <85>)	<175 EU/injected dose
Filter integrity (bubble point)	According to filter manufacturer
Sterility	Sterile after 14 d

EU = endotoxin units; HPLC = high-performance liquid chromatography; t_R = retention time; USP = U.S. Pharmacopeia.

ADMINISTRATION PROTOCOL

Clinical administration of ^{177}Lu-PSMA requires close collaboration between nuclear medicine physicians, nurses, radiopharmacists, and technologists. Although the specific roles and responsibilities of each team member may vary depending on the established hospital protocols, the following section can be considered a guide.

The FDA package insert for ^{177}Lu-PSMA-617 specifies that each patient be treated with up to 6 cycles of 7.4 GBq (200 mCi) every 6 wk, with the dose being interrupted, reduced, or permanently discontinued if there are adverse reactions. VISION provided for a ±1-wk allowance of treatment dates. On the day of therapy, the patient may work with providers such as a nurse, a nuclear medicine physician, and a nuclear medicine technologist.

Baseline laboratory tests are typically performed before therapy. These usually include a complete blood count and testing of albumin, creatinine, aspartate aminotransferase, alanine aminotransferase, total bilirubin, alkaline phosphatase, and PSA levels. When patients arrive, the nurse orients them to the therapy room, explains radiation safety guidelines, obtains a set of vital-sign measurements, and reviews with the patient the discharge paperwork, including expected side effects; unexpected mild, moderate, and severe side effects and what to do if they occur; and the dates of future appointments. If patients have been prescribed a methylprednisolone dose pack to offset any expected increase in bone pain, they are asked to bring the medication to the appointment. The nursing team goes over the instructions with patients and encourages them to take their first dose before leaving.

The nuclear medicine physician obtains the patient's consent to undergo the procedure and instructs the patient on radiation safety measures, according to the institutional radiation safety guidelines. The patient is typically given a copy of these instructions and told to bring them along on any air travel during the next 2 mo in case of causing radiation detection alarms. Typical recommendations include minimizing exposure of others to radiation by limiting close contact (<91 cm [3 ft]) for 2 d and limiting sexual activity for 7 d. Patients are also advised to sleep in a separate bedroom for 3 d, increasing this to 7 d if there are children in the household or 15 d if there are pregnant women (*8*).

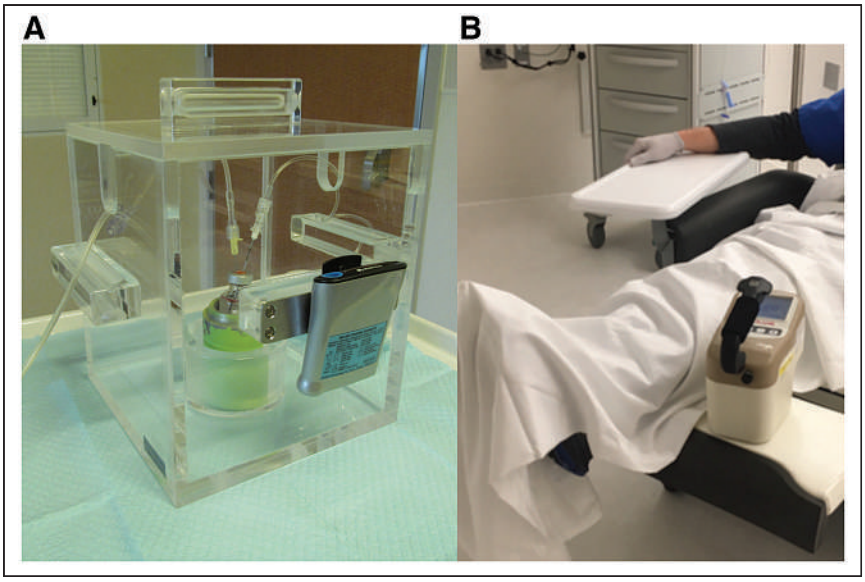

FIGURE 2. Gravity-method ^{177}Lu-PSMA-617 delivery system with inflow and outflow needles (A) and acrylic glass shielding to reduce radiation dose to nuclear technologist while maintaining validation of adequate flow. Radiation survey meter is used during ^{177}Lu-PSMA-617 infusion to verify systemic administration (B).

Patients are encouraged to drink fluids during the procedure and to void as often as feasible to reduce bladder radiation. The nurse establishes an intravenous line or accesses an existing port, collects a preinfusion blood sample for PSA measurement, and starts a saline drip, with a minimum of 10 mL as recommended by the prescribing information. After the saline infusion is complete, the nuclear medicine technologist infuses the ^{177}Lu-PSMA-617 via the syringe method (a disposable syringe fitted with a syringe shield), vial method (with a peristaltic infusion pump), or gravity method (with or without an infusion pump) (*29*) (Fig. 2). It is important that the infusion method be able to transfer the radiopharmaceutical to the patient safely and with the least manipulation to decrease exposure of the technologist to radiation, lower the chances of contamination, and ensure sterility. The radiopharmaceutical is typically provided by a radiopharmacy in a vial.

Syringe Method

The manual-push syringe technique is the most common transfer method in nuclear medicine, is the same technique as used for other liquid radiopharmaceuticals in a syringe, and has the lowest learning curve for the technologist, making it the easiest technique to adopt. The syringe is Luer-locked to the intravenous line of the patient. The main pitfalls of the manual push are an inconsistent rate of infusion and the highest exposure of the technologist to radiation.

Vial Method

Another method using a syringe—the vial method with a peristaltic infusion pump—has multiple steps. Pumps are common in hospitals and are frequently used by anesthesia staff. This method decreases exposure of the technologist, with most of the exposure coming from setting up the pump. The infusion rate is consistent, and risk for contamination is low.

Gravity Method

The gravity method uses a 250-mL saline bag punctured by a line with long and short needles to rinse the vial and a second line to the patient. There are several potential pitfalls to this method. The probability of contamination increases because of multiple punctures to the vial, leading to fluid overfilling the vial. Additionally, the residual is difficult to determine because of the length of the tubing and shielding. The technologist will have to constantly monitor the vial for fluid overfills to prevent contamination. If a reduced dose of ^{177}Lu-PSMA-617 is to be administered, the syringe method or vial method should be used because the gravity method may result in an incorrect volume. Medication pumps may include air sensors, pressure sensors, and microtubing allowing a safe transfer of the radiopharmaceutical to the patient while the patient is being monitored from a distance. This method greatly reduces the risk of infiltration, contamination, and exposure. The downside is the learning curve, and supplies can be costly.

When technologists are performing each infusion technique, they must follow as-low-as-reasonably-achievable principles to decrease radiation exposure; all methods discussed here can be applied behind an L-block or acrylic glass shielding.

The patient is kept for observation for 1 h. During observation, the nursing staff and nuclear medicine technologist check for any AEs from treatment. After administration of the ^{177}Lu-PSMA-617 the patient may—depending on the institutional protocols—undergo whole-body imaging with SPECT (with or without CT) to document radiotracer accumulation within the PSMA-avid disease and to allow for dosimetry. SPECT is not considered essential for successful administration of ^{177}Lu-PSMA-617. If used, SPECT may be performed 24 h or later after administration of ^{177}Lu-PSMA-617. The visit for the posttherapy scan is a good opportunity to again review potential side effects, such as increased fatigue, increased bone pain lasting approximately 5 d, and xerostomia. Three weeks after treatment, a complete blood count will typically be obtained, along with measurement of albumin, creatinine, aspartate aminotransferase, alanine aminotransferase, total bilirubin, alkaline phosphatase, and PSA levels. The laboratory and SPECT results are reviewed, and the next cycle of PSMA is confirmed. If there are abnormalities in the laboratory test results or clinical outcome, the dose may be reduced or discontinued in some cases.

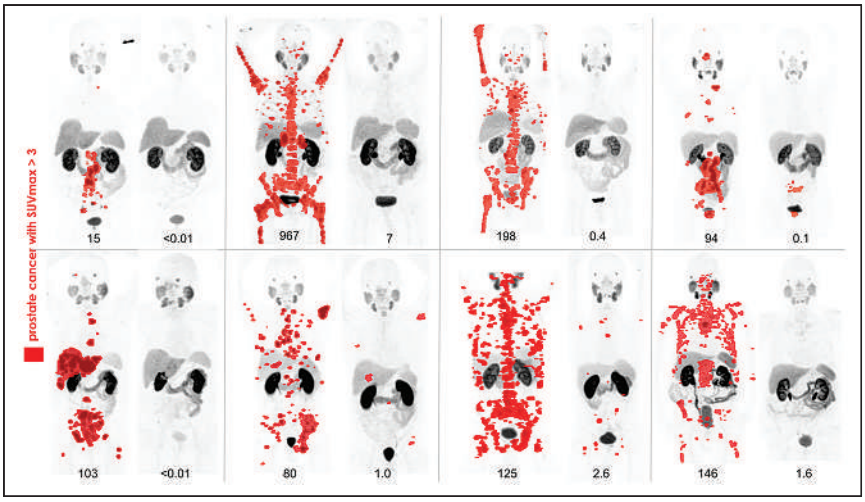

FIGURE 3. Previously published data showing 6 individual subjects with good serum PSA response. Paired ^{68}Ga PSMA-11 PET maximum-intensity projections are shown before (left) and 3 mo after (right) ^{177}Lu-PSMA therapy. Highlighted in red are lesions that have SUV_{max} over 3. Serum PSA values before and after ^{177}Lu-PSMA therapy serum are shown below each image and demonstrate good response to treatment. (Reprinted from (*29*).)

IMAGING AND RESPONSE TO THERAPY

In clinical trials, the most commonly accepted primary metrics of response to therapy include serum PSA response (*12,13,24*), radiographic progression-free survival by RECIST 1.1, and OS (*12,13*). A PSA response in clinical trials is commonly defined as a decrease in serum PSA of 50% or greater compared with baseline. Although quantification of disease burden by PSMA PET imaging response criteria has not been uniformly established, some academic groups use a semiquantitative threshold of residual disease to demonstrate therapeutic effects (Fig. 3) (*30*). Posttherapy SPECT imaging may also be used for this purpose. Standardized quality-of-life and symptom metrics, such as pain scores, may also be used to assess clinical benefit (*12,13,24*). TheraP demonstrated that PSA responses were more frequent in the ^{177}Lu-PSMA-617 arm (65%) than in the cabazitaxel arm (37%) (*13*). A metaanalysis of 1,192 patients found that approximately 46% patients with mCRPC treated with at least 1 cycle of ^{177}Lu-PSMA had PSA reductions of at least 50% (*22*).

In clinical practice, physicians and patients typically make treatment decisions based on the currently available clinical data. Because PSA response in clinical trials frequently correlates with radiographic progression-free survival outcomes, PSA response provides a practical metric of disease response. Overall, the serum PSA level is typically a sensitive and early biomarker of disease recurrence or progression. Imaging-based assessments commonly include CT and bone scanning. Other potential tests include PSMA or ^{18}F-FDG PET/CT. The FDG PET/CT may identify more glycolytically active, clinically aggressive disease and support the rationale to change therapy or perform a biopsy.

DOSIMETRY AND FUTURE DEVELOPMENTS

Using dosimetry to tailor dosing to a patient's particular biology has potential to advance ^{177}Lu-PSMA-617 RLT. Although the large TheraP (*13*) and VISION (*12*) trials used a fixed dose of 7.4 GBq (200 mCi), a small study demonstrated the safety of up to a 9.3-GBq (250 mCi) dose in selected cohorts (*31*). In principle, a more patient-centered dosing scheme could be applied, using dosimetry to calculate the safe dose to the organs at risk (maximum tolerated activity) or to deliver predictable radiation doses to tumors (lesional dosimetry) (*32,33*). One piece of evidence supporting a lesional dosimetry-based approach is the study of Violet et al. (*34*), which demonstrated that patients receiving less than 10 Gy to tumors were unlikely to achieve a PSA response, defined as more than a 50% decline in pretreatment PSA level after therapy. Moreover, recent studies have demonstrated a tumor sink effect, in which patients with a particularly high tumor burden demonstrated reduced delivery of ^{68}Ga-PSMA-11 (*35*) or ^{177}Lu-PSMA-617 (*36*) to organs at risk (Fig. 4). Taken together, these studies suggest a dosimetry-guided strategy for ^{177}Lu-PSMA-617 in which either pretherapy PSMA PET or intercycle ^{177}Lu-PSMA-617 SPECT might be used to select a more patient-centered dose.

Optimal dosimetry requirements and recommendations for ^{177}Lu-PSMA have recently been reported, and a full description is beyond the scope of this review (*37*). Optimal dosimetry includes imaging over several time points using

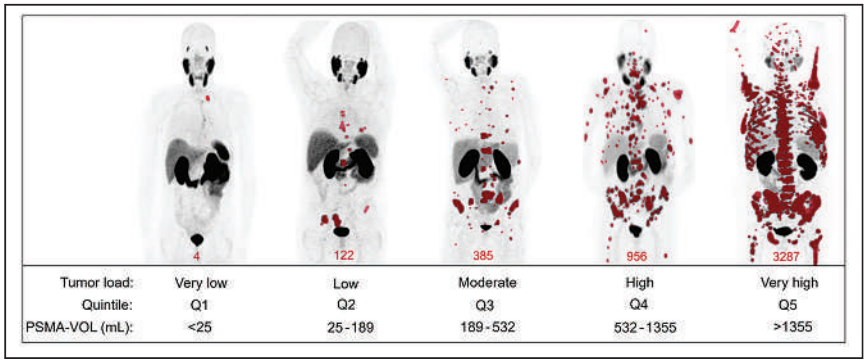

FIGURE 4. Previously published image providing examples of maximum-intensity projections of PSMA PET for each tumor load group. PSMA-positive tumor segmentation is highlighted in red. (Reprinted from (*34*).)

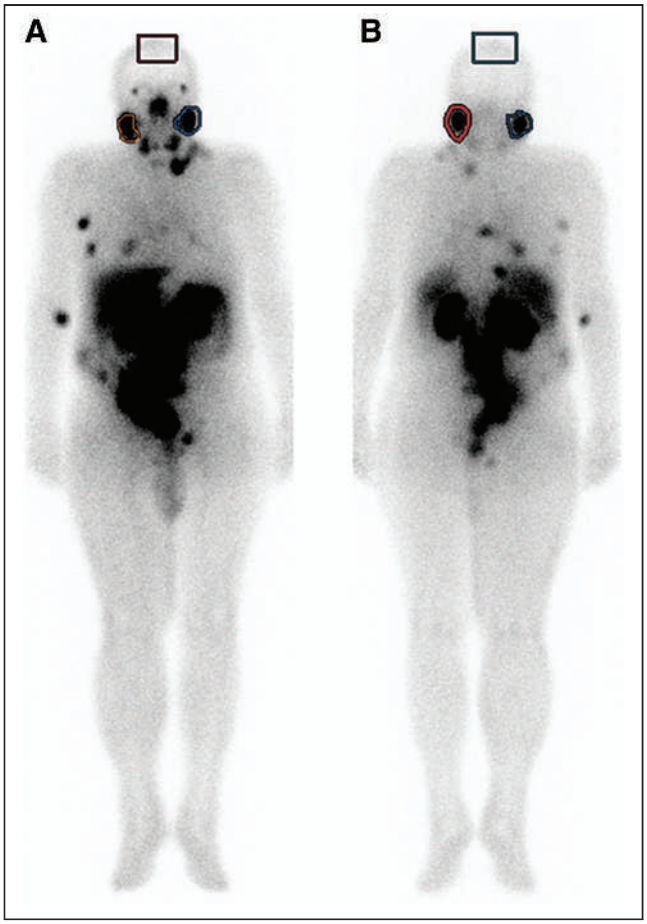

FIGURE 5. Previously published region-of-interest measurements on ^{177}Lu-PSMA-617 uptake (anterior [A]; posterior [B]) in both parotid glands and cranium in patient on whom right-sided ice pack was used during posttreatment SPECT/CT. No differences in radioligand uptake were observed between cooled (right) and noncooled (left) sides, with region of interest or volume of interest on images shown. (Reprinted from (*44*).)

quantitative 3-dimensional techniques such as SPECT/CT. However, outside of clinical trials, this recommendation may be difficult to achieve for routine patient care. Delayed imaging is the most accurate determinant of the absorbed doses to organs or tumors, with the ideal timing being approximately 4–7 d after ^{177}Lu-PSMA RLT.

Although strong evidence has emerged to support the use of ^{177}Lu-PSMA in men with mCRPC, there are several open questions and innovations that promise to further extend the role of theranostics in prostate cancer. For example, the synergistic effects from combination therapies, as well as appropriate sequencing of the treatment in the disease course, remain uncertain. Both VISION and TheraP were deployed late in mCRPC disease, when patients have limited therapy options remaining. Both trials demonstrated ^{177}Lu-PSMA-617 RLT to be effective at improving clinical outcomes, but ^{177}Lu-PSMA may have more significant benefits if used earlier in the disease evolution. Several trials are under way in hopes of answering this question. The UpFrontPSMA and PSMAddition trials seek to determine the efficacy and safety of ^{177}Lu-PSMA-617 in men with metastatic hormone-sensitive prostate cancer. Other trials are assessing ^{177}Lu-PSMA-617 as first-line therapy for mCRPC. In addition, ^{177}Lu-PSMA-617 is being tested as neoadjuvant therapy for localized prostate cancer.

Another area of emerging interest is the use of α-emitting isotopes such as ^{225}Ac for therapy. Kratochwil et al. (*21*) reported 2 patients who had a complete response to ^{225}Ac-PSMA-617, including one who had previously progressed after ^{177}Lu-PSMA-617 treatment. This initial report has been confirmed in several small case series (*38,39*). Pooling 10 small studies together, a recent metaanalysis found a 62.8% response rate for a PSA decline of more than 50% (*40*). Although the efficacy of ^{225}Ac-PSMA is likely greater than that of ^{177}Lu-PSMA, the side effect profile also appears to be more significant, including a greater incidence of xerostomia. In recognition of these effects, small trials of a tandem therapy strategy incorporating small doses of ^{225}Ac-PSMA together with ^{177}Lu-PSMA have been reported, with promising results (*41*). However, an additional major current challenge in the clinical use of ^{225}Ac-PSMA is the limited availability of the isotope itself. Nevertheless, the clinical future for ^{225}Ac-PSMA appears highly promising.

RADIATION SAFETY

General radiation safety precautions should be followed with ^{177}Lu-PSMA, with local and national guidelines dictating specific clinical practice. Radiation safety precautions may be modeled after ^{177}Lu-DOTATATE therapy for neuroendocrine tumors given a shared radionuclide (*9,42*). A recent metaanalysis of ^{177}Lu-PSMA-617 dosimetry found that the lacrimal and salivary glands are the critical organs, with the kidneys also receiving a significant radiation dose (*43*). The calculated absorbed radiation doses to the lacrimal and salivary glands after 4 cycles of ^{177}Lu-PSMA-617 are near the tolerated dose limit, whereas the dose to the kidneys is far below the dose tolerance limit. The use of polyglutamate or external cooling through ice packs has been described as reducing salivary gland uptake, with the studies reporting a reduction in salivary gland uptake induced by polyglutamate uptake, but no change in salivary gland uptake induced by cooling (Fig. 5) (*44,45*). The liver, spleen, and bone marrow received a relatively lower amount of radiation, but the authors of those studies noted that dosimetry may underestimate the bone marrow dose in mCRPC patients with extensive bone metastases.

CONCLUSION

With the recent FDA approval of ^{177}Lu-PSMA-617, and the emerging promising data on the use of other PSMA RLT agents, radiopharmaceutical therapy is expected to become part of the SOC for treatment of prostate cancer. Routine incorporation of this treatment in nuclear medicine departments will require collaboration between referring

physicians, nuclear medicine physicians, nurses, and nuclear medicine technologists.

DISCLOSURE

No potential conflict of interest relevant to this article was reported.

REFERENCES

1. Siegel RL, Miller KD, Fuchs HE, Jemal A. Cancer statistics, 2022. *CA Cancer J Clin.* 2022;72:7–33.
2. Sung H, Ferlay J, Siegel RL, et al. Global cancer statistics 2020: GLOBOCAN estimates of incidence and mortality worldwide for 36 cancers in 185 countries. *CA Cancer J Clin.* 2021;71:209–249.
3. Thompson IM Jr, Goodman PJ, Tangen CM, et al. Long-term survival of participants in the prostate cancer prevention trial. *N Engl J Med.* 2013;369:603–610.
4. Sonni I, Eiber M, Fendler WP, et al. Impact of ^{68}Ga-PSMA-11 PET/CT on staging and management of prostate cancer patients in various clinical settings: a prospective single-center study. *J Nucl Med.* 2020;61:1153–1160.
5. Tateishi U. Prostate-specific membrane antigen (PSMA)-ligand positron emission tomography and radioligand therapy (RLT) of prostate cancer. *Jpn J Clin Oncol.* 2020;50:349–356.
6. Zhou J, Gou Z, Wu R, Yuan Y, Yu G, Zhao Y. Comparison of PSMA-PET/CT, choline-PET/CT, NaF-PET/CT, MRI, and bone scintigraphy in the diagnosis of bone metastases in patients with prostate cancer: a systematic review and meta-analysis. *Skeletal Radiol.* 2019;48:1915–1924.
7. Weineisen M, Schottelius M, Simecek J, et al. ^{68}Ga- and ^{177}Lu-labeled PSMA I&T: optimization of a PSMA-targeted theranostic concept and first proof-of-concept human studies. *J Nucl Med.* 2015;56:1169–1176.
8. Pluvicto™ (lutetium Lu 177 vipivotide tetraxetan) injection, for intravenous use. Food and Drug Administration website. https://www.accessdata.fda.gov/drugsatfda_docs/label/2022/215833s000lbl.pdf. Published 2022. Revised March 2022. Accessed July 28, 2022
9. Kratochwil C, Fendler WP, Eiber M, et al. EANM procedure guidelines for radionuclide therapy with ^{177}Lu-labelled PSMA-ligands (^{177}Lu-PSMA-RLT). *Eur J Nucl Med Mol Imaging.* 2019;46:2536–2544.
10. Ferdinandus J, Violet J, Sandhu S, Hofman MS. Prostate-specific membrane antigen theranostics: therapy with lutetium-177. *Curr Opin Urol.* 2018;28:197–204.
11. Mokoala K, Lawal I, Lengana T, et al. PSMA theranostics: science and practice. *Cancers (Basel).* 2021;13:3904.
12. Sartor O, de Bono J, Chi KN, et al. Lutetium-177-PSMA-617 for metastatic castration-resistant prostate cancer. *N Engl J Med.* 2021;385:1091–1103.
13. Hofman MS, Emmett L, Sandhu S, et al. [^{177}Lu]Lu-PSMA-617 versus cabazitaxel in patients with metastatic castration-resistant prostate cancer (TheraP): a randomised, open-label, phase 2 trial. *Lancet.* 2021;397:797–804.
14. Chen R, Wang Y, Zhu Y, et al. The added value of ^{18}F-FDG PET/CT compared with ^{68}Ga-PSMA PET/CT in patients with castration-resistant prostate cancer. *J Nucl Med.* 2022;63:69–75.
15. Thang SP, Violet J, Sandhu S, et al. Poor outcomes for patients with metastatic castration-resistant prostate cancer with low prostate-specific membrane antigen (PSMA) expression deemed ineligible for ^{177}Lu-labelled PSMA radioligand therapy. *Eur Urol Oncol.* 2019;2:670–676.
16. Hotta M, Gafita A, Czernin J, Calais J. Outcome of patients with PSMA-PET/CT screen failure by VISION criteria and treated with ^{177}Lu-PSMA therapy: a multicenter retrospective analysis. *J Nucl Med.* March 10, 2022 [Epub ahead of print].
17. Michalski K, Ruf J, Goetz C, et al. Prognostic implications of dual tracer PET/CT: PSMA ligand and [^{18}F]FDG PET/CT in patients undergoing [^{177}Lu]PSMA radioligand therapy. *Eur J Nucl Med Mol Imaging.* 2021;48:2024–2030.
18. Hartrampf PE, Lapa C, Serfling SE, et al. Development of discordant hypermetabolic prostate cancer lesions in the course of [^{177}Lu]PSMA radioligand therapy and their possible influence on patient outcome. *Cancers (Basel).* 2021;13:4270.
19. Srinivas S, Iagaru A. To scan or not to scan: an unnecessary dilemma for PSMA radioligand therapy. *J Nucl Med.* 2021;62:1487–1488.
20. Parent EE, Schuster DM. Update on ^{18}F-fluciclovine PET for prostate cancer imaging. *J Nucl Med.* 2018;59:733–739.
21. Kratochwil C, Fendler WP, Eiber M, et al. EANM procedure guidelines for radionuclide therapy with 177Lu-labelled PSMA-ligands (^{177}Lu-PSMA-RLT). *Eur J Nucl Med Mol Imaging.* 2019; 46:2536–2544.
22. Sadaghiani MS, Sheikhbahaei S, Werner RA, et al. A systematic review and meta-analysis of the effectiveness and toxicities of lutetium-177-labeled prostate-specific membrane antigen-targeted radioligand therapy in metastatic castration-resistant prostate cancer. *Eur Urol.* 2021;80:82–94.
23. Rahbar K, Ahmadzadehfar H, Kratochwil C, et al. German multicenter study investigating ^{177}Lu-PSMA-617 radioligand therapy in advanced prostate cancer patients. *J Nucl Med.* 2017;58:85–90.
24. Hofman MS, Violet J, Hicks RJ, et al. [^{177}Lu]-PSMA-617 radionuclide treatment in patients with metastatic castration-resistant prostate cancer (LuPSMA trial): a single-centre, single-arm, phase 2 study. *Lancet Oncol.* 2018;19:825–833.
25. Violet J, Sandhu S, Iravani A, et al. Long-term follow-up and outcomes of retreatment in an expanded 50-patient single-center phase II prospective trial of ^{177}Lu-PSMA-617 theranostics in metastatic castration-resistant prostate cancer. *J Nucl Med.* 2020;61:857–865.
26. Bodei L, Mueller-Brand J, Baum RP, et al. The joint IAEA, EANM, and SNMMI practical guidance on peptide receptor radionuclide therapy (PRRNT) in neuroendocrine tumours. *Eur J Nucl Med Mol Imaging.* 2013;40:800–816.
27. Chakraborty A, Mitra A, Tawate M, et al. Therapeutic multidose preparation of a ready-to-use ^{177}Lu-PSMA-617 using carrier added lutetium-177 in a hospital radiopharmacy and its clinical efficacy. *Cancer Biother Radiopharm.* 2021;36:682–692.
28. Martin S, Tonnesmann R, Hierlmeier I, et al. Identification, characterization, and suppression of side products formed during the synthesis of [^{177}Lu]Lu-PSMA-617. *J Med Chem.* 2021;64:4960–4971.
29. Ebbers SC, Barentsz MW, de Keizer B, Krijger GC, Lam M, Braat A. A rapid and safe infusion protocol for ^{177}Lu peptide receptor radionuclide therapy. *J Nucl Med.* 2021;62:816–822.
30. Hofman MVJ, Sandhu S, Ferdinandus J, et al. High activity, pain reduction and low toxicity with lutetium-177 PSMA617 theranostics in metastatic castrate-resistant prostate cancer (mCRPC): results of a phase II prospective trial [abstract]. *J Nucl Med.* 2018;59(suppl 1):531.
31. Rathke H, Giesel FL, Flechsig P, et al. Repeated ^{177}Lu-labeled PSMA-617 radioligand therapy using treatment activities of up to 9.3 GBq. *J Nucl Med.* 2018;59: 459–465.
32. Jackson P, Hofman M, McIntosh L, Buteau JP, Ravi Kumar A. Radiation dosimetry in ^{177}Lu-PSMA-617 therapy. *Semin Nucl Med.* 2022;52:243–254.
33. Lawhn-Heath C, Hope TA, Martinez J, et al. Dosimetry in radionuclide therapy: the clinical role of measuring radiation dose. *Lancet Oncol.* 2022;23:e75–e87.
34. Violet J, Jackson P, Ferdinandus J, et al. Dosimetry of ^{177}Lu-PSMA-617 in metastatic castration-resistant prostate cancer: correlations between pretherapeutic imaging and whole-body tumor dosimetry with treatment outcomes. *J Nucl Med.* 2019;60:517–523.
35. Gafita A, Wang H, Robertson A, et al. Tumor sink effect in ^{68}Ga-PSMA-11 PET: myth or reality? *J Nucl Med.* 2022;63:226–232.
36. Filss C, Heinzel A, Miiller B, Vogg ATJ, Langen KJ, Mottaghy FM. Relevant tumor sink effect in prostate cancer patients receiving ^{177}Lu-PSMA-617 radioligand therapy. *Nuklearmedizin.* 2018;57:19–25.
37. Sjögreen Gleisner K, Chouin N, Gabina PM, et al. EANM dosimetry committee recommendations for dosimetry of ^{177}Lu-labelled somatostatin-receptor- and PSMA-targeting ligands. *Eur J Nucl Med Mol Imaging.* 2022;49:1778–1809.
38. van der Doelen MJ, Mehra N, van Oort IM, et al. Clinical outcomes and molecular profiling of advanced metastatic castration-resistant prostate cancer patients treated with ^{225}Ac-PSMA-617 targeted alpha-radiation therapy. *Urol Oncol.* 2021;39: 729.e7–729.e16.
39. Sathekge M, Bruchertseifer F, Knoesen O, et al. ^{225}Ac-PSMA-617 in chemotherapy-naive patients with advanced prostate cancer: a pilot study. *Eur J Nucl Med Mol Imaging.* 2019;46:129–138.
40. Satapathy S, Sood A, Das CK, Mittal BR. Evolving role of ^{225}Ac-PSMA radioligand therapy in metastatic castration-resistant prostate cancer: a systematic review and meta-analysis. *Prostate Cancer Prostatic Dis.* 2021;24:880–890.
41. Khreish F, Ebert N, Ries M, et al. ^{225}Ac-PSMA-617/^{177}Lu-PSMA-617 tandem therapy of metastatic castration-resistant prostate cancer: pilot experience. *Eur J Nucl Med Mol Imaging.* 2020;47:721–728.
42. Hope TA, Abbott A, Colucci K, et al. NANETS/SNMMI procedure standard for somatostatin receptor-based peptide receptor radionuclide therapy with ^{177}Lu-DOTATATE. *J Nucl Med.* 2019;60:937–943.
43. Nautiyal A, Jha AK, Mithun S, Rangarajan V. Dosimetry in Lu-177-PSMA-617 prostate-specific membrane antigen targeted radioligand therapy: a systematic review. *Nucl Med Commun.* 2022;43:369–377.
44. Paganelli G, Sarnelli A, Severi S, et al. Dosimetry and safety of ^{177}Lu PSMA-617 along with polyglutamate parotid gland protector: preliminary results in metastatic castration-resistant prostate cancer patients. *Eur J Nucl Med Mol Imaging.* 2020; 47:3008–3017.
45. Yilmaz B, Nisli S, Ergul N, Gursu RU, Acikgoz O, Cermik TF. Effect of external cooling on ^{177}Lu-PSMA uptake by the parotid glands. *J Nucl Med.* 2019;60:1388–1393.

^{177}Lu-Vipivotide Tetraxetan (^{177}Lu-PSMA-617, Pluvicto) Therapy

Sarah Clements, CNMT, Daniel Tempesta, CNMT, and Heather Jacene, MD

^{177}Lu-vipivotide tetraxetan is a radioligand therapeutic agent for the treatment of prostate cancer (*1*). It binds to prostate-specific membrane antigen (PSMA), which is overexpressed on prostate cancer cells, and the β-radiations emitted by ^{177}Lu result in DNA damage to the tumor cells and surrounding tissue (*2*). An integrative approach with physicians, nurses, technologists, radiation safety officers, and pharmacists is required to ensure the best patient outcomes.

CLINICAL INDICATIONS (*1*)

- ^{177}Lu-vipivotide tetraxetan is used for the treatment of metastatic castration-resistant prostate cancer in adults who have PSMA-positive tumors.

PATIENT SELECTION

Patients undergoing ^{177}Lu-vipivotide tetraxetan treatment should meet all the following criteria:

- Have metastatic castration-resistant prostate cancer (mCRPC) (*1*).
- Been previously treated with androgen receptor pathway inhibition and taxane-based chemotherapy (*1*).
- Have PSMA-positive tumor as determined by PSMA PET/CT imaging (*1*).
  - ^{68}Ga-PSMA-11 and ^{18}F-DCFPyL PET agents are considered equivalent for use in selecting patients for therapy with ^{177}Lu-vipivotide tetraxetan (*3,4*).

CONTRAINDICATIONS

- None (*1*).

TREATMENT PLAN (*1*)

- Intravenously administer 7.4 GBq (200 mCi) of ^{177}Lu-vipivotide tetraxetan every 6 wk for up to 6 administrations.

PATIENT PREPARATION/EDUCATION (*1*)

- Patients should increase their oral fluid intake and are encouraged to increase voiding as frequently as possible to reduce deleterious effects on the kidneys and bladder.
- Patients should be educated on radiation safety precautions before and after the administration of ^{177}Lu-vipivotide tetraxetan. Radiation safety precautions include but are not limited to:
  - Limit contact less than 3 feet from other household members for 2 d and children and pregnant individuals for 7 d. Precautionary measures should include sleeping in a separate bedroom for the aforementioned number of days for each household population.
  - Patients should not participate in sexual activity for 7 d after treatment. For the duration of their treatment course and for 14 wk after their final dose, sexual partners of reproductive potential should use effective contraception.

TREATMENT INSTRUCTIONS (*1*)

- Verify that the patient's complete blood counts, kidney function, and liver function are sufficient to proceed with treatment. Whether or not to procced with treatment is a clinical decision.
- ^{177}Lu-vipivotide tetraxetan is given intravenously over 1–10 min.
  - Methods of administration include injection via disposable syringe, an infusion using the gravity method, and the vial method using a pump.
- Before initiating the treatment and after its completion, the intravenous line used for ^{177}Lu-vipivotide tetraxetan must be flushed with at least 10 mL of 0.9% sterile sodium chloride solution.

THERAPEUTIC DOSE CALCULATIONS (TABLE 1) (*1*)

- The standard dose of ^{177}Lu-vipivotide tetraxetan is 7.4 GBq (200 mCi) every 6 wk for 6 administrations.

TABLE 1
Radiopharmaceutical, Dose, Administration Route, and Infusion Duration of ^{177}Lu-Vipivotide Tetraxetan (*1*)

Radiopharmaceutical	Dose	Administration route	Infusion duration
^{177}Lu-vipivotide tetraxetan (Pluvicto, ^{177}Lu-PSMA-617)	7.4 GBq (200 mCi)	Intravenous	1–10 min

DOI: 10.2967/jnmt.122.264731

Treatment may be delayed or the administered radioactivity can be reduced to 5.9 GBq (160 mCi) in the setting of adverse reactions as described in the prescribing information.

- If patients require more than a 10-wk gap between doses, or an adverse reaction persists for greater than 4 wk, or they require a dose less than 5.9 GBq (160 mCi), treatment discontinuation should be considered.

PRECAUTIONS (*1*)

- Patients should be monitored closely for adverse events, including but not limited to myelosuppression and renal toxicity. Patients should be told to notify their clinician if they exhibit any clinical signs of either of these conditions, such as decreased urination frequency, bruising more easily, or excessive tiredness.
- Because ^{177}Lu-vipivotide tetraxetan is a radioactive therapy agent, extra care should be taken to educate patients, their household members, and administering health-care personnel about appropriate radiation safety precautions.

REFERENCES

1. PLUVICTO™ (lutetium Lu 177 vipivotide tetraxetan) injection, for intravenous use [package insert]. Novartis website. https://www.novartis.com/us-en/sites/novartis_us/files/pluvicto_0.pdf. Approved 2022. Accessed August 1, 2022.
2. Sartor O, de Bono J, Chi KN, et al. Lutetium-177-PSMA-617 for metastatic castration-resistant prostate cancer. *N Engl J Med.* 2021;385:1091–1103.
3. Hope TA, Jadvar H. Updates to appropriate use criteria for PSMA PET. *J Nucl Med.* 2022;63:14N.
4. NCCN Clinical Practice Guidelines in Oncology. (NCCN Guidelines®) for prostate cancer, version 4.2002, May 10, 2022. https://www.nccn.org/professionals/physician_gls/pdf/prostate.pdf

Nuts and Bolts of ^{223}Ra-Dichloride Therapy

Erin Grady

Division of Nuclear Medicine and Molecular Imaging, Department of Radiology, Stanford University, Stanford, California

CE credit: For CE credit, you can access the test for this article, as well as additional *JNMT* CE tests, online at https://www.snmmilearningcenter.org. Complete the test online no later than September 2025. Your online test will be scored immediately. You may make 3 attempts to pass the test and must answer 75% of the questions correctly to receive Continuing Education Hour (CEH) credit. Credit amounts can be found in the SNMMI Learning Center Activity. SNMMI members will have their CEH credit added to their VOICE transcript automatically; nonmembers will be able to print out a CE certificate upon successfully completing the test. The online test is free to SNMMI members; nonmembers must pay $15.00 by credit card when logging onto the website to take the test.

Radionuclide therapy with ^{223}Ra-dichloride can be helpful for patients with osteoblastic osseous metastatic disease in the setting of castration-resistant prostate cancer without visceral metastases. This article reviews the indications, proper use and handling, patient work-up before therapy, and many of the technical considerations, including a discussion of coding and billing, along with pitfalls that have been identified.

Key Words: ^{223}Ra-dichloride; radium; radionuclide therapy; CRPC; osseous metastases

J Nucl Med Technol 2022; 50:215–221
DOI: 10.2967/jnmt.122.263812

Early after its discovery in the early 1900s, ^{223}Ra was known as actinium X or radio-actinium (*1–6*). Much has been learned about this radionuclide since that time. ^{223}Ra-dichloride (Xofigo; Bayer HealthCare), a bone-seeking calcium mimetic, works as an α-particle therapy that binds to areas of increased bony turnover in osseous metastases within the hydroxyapatite matrix, such as ^{99m}Tc-methlyene diphosphonate, ^{99m}Tc-hydroxydiphosphonate, or ^{18}F-sodium fluoride. Once localized, the α-particle deposits its energy in a highly localized manner, within a range of 100 μm (*7*), or on the order of a few cells apart from the site of disease. The α-particles deposit high levels of energy that cause predominantly double-stranded DNA breaks in the treatment region, leading to highly localized cell death (*8,9*) and sparing adjacent normal tissues (*10,11*). More than a century after the discovery of ^{223}Ra, it was studied to treat osseous metastases in the setting of prostate cancer and found to demonstrate a survival benefit in the landmark Alpharadin in Symptomatic Prostate Cancer Patients (ALSYMPCA) study (*12*). It was subsequently approved by the Food and Drug Administration on May 15, 2013 (*13*), for the treatment of patients with castration-resistant prostate cancer, symptomatic bone metastases, and no known visceral metastatic disease (*14*). ALSYMPCA demonstrated not only a survival benefit but also favorable effects on patient quality of life and a favorable safety profile (*12*).

After lung cancer, prostate cancer is the most common cancer in men in the United States. It affects 1 in 8 men and is the cause of death in 1 in 41 men (*15*). Osseous metastatic disease in the setting of prostate cancer occurs in 70%–90% of patients (*16,17*). Prostate cancer patients with osseous metastatic disease are known to have a lower quality of life, an increased cost of care, and higher mortality (*17,18*). Therefore, radium therapy can have a clear impact on these patients. The ALSYMPCA trial demonstrated a survival benefit of 14.9 mo in the treated group versus 11.3 mo in the untreated group, which received the best standard of care plus a placebo (*12*). Though this seems a short time, it does amount to a 30% longer time frame than in patients who did not receive ^{223}Ra-dichloride.

PATIENT SELECTION, CLINICAL CONSIDERATIONS, AND PROTOCOL

The Food and Drug Administration approved use of ^{223}Ra-dichloride for treatment of patients with castration-resistant prostate cancer, symptomatic bone metastases, and no known visceral metastatic disease. Castration-resistant cancer is cancer that continues to grow even when the testosterone levels are at or below the castrate level; it is also known as hormone-refractory or hormone-resistant prostate cancer (*19*). Careful screening of prior imaging for visceral metastatic disease in organs and lymph nodes is helpful; the package insert advises an upper limit of 3 cm for lymph nodes (*14*). Clinical guidelines indicate that patients should undergo CT of the chest, abdomen, and pelvis (if not already performed) before therapy to assess for visceral metastatic disease (*20*). Prostate bed disease or localized involvement of the urinary bladder is not considered visceral disease (*20*). Hematologic analysis must also be performed if the patient does not have visceral metastases and is being considered for therapy. Per the package insert, before the first treatment the absolute neutrophil count should be at least 1.5×10^9/L, the platelet count at least 100×10^9/L, and the hemoglobin at

Received Apr. 1, 2022; revision accepted Jul. 13, 2022.
For correspondence or reprints, contact Erin Grady (egrady@stanford.edu).
Published online Jul. 26, 2022.

least 10 g/dL (*14*). Blood work should be done within at least 30 d of the initial therapy (*20*). There is some expected impact on bone marrow, and the patient will need follow-up blood count analysis before additional therapies. For subsequent administration of the radionuclide therapy, the patient should have an absolute neutrophil count of 1×10^9/L and a platelet count of 50×10^9/L; no hemoglobin limit is required for subsequent therapies (Table 1) (*14*).

Because this therapy localizes to regions of bony turnover, it is imperative that a patient undergo bone scanning before being considered for therapy. If the osseous metastases do not take up tracer, the patient will not benefit from this therapy and should not receive it. Pretherapy bone scans can be done with SPECT or PET bone scanning agents. Clinical guidelines indicate that there should be at least 2 osseous metastatic lesions (*20*). PET agents such as prostate-specific membrane antigen and fluciclovine are not a substitute for bone-seeking tracers in this setting (*21*).

Increasingly, nuclear medicine professionals are seeing patients in consultation before therapies and are using evaluation and management codes. This change is beneficial for patients, as they are not seen only on the day of therapy but rather have time to prepare for potentially unexpected radiation safety instructions. Consultations also allow patients or caregivers to ask questions and may ease patient concerns about the therapy and its side effects. Nuclear medicine professionals also benefit by having time to review the patient's history; coordinate with the urologist, oncologist, or other clinical colleagues who referred the patient; and obtain insurance preauthorization. During the consultation process, needed items can be identified, such as a bone scan or blood work, which can then be obtained in a timelier manner so as not to delay care or result in a wasted therapy dose.

TABLE 1
Clinical Eligibility Criteria for Therapy (*14*)

Clinical metric	Requirement
Castration-resistant prostate cancer metastatic to bone	Symptomatic
	No visceral metastatic disease
	Whole-body bone scan with at least 2 lesions
Complete blood count with differential	Before first treatment:
	Absolute neutrophil count $\geq 1.5 \times 10^9$/L
	Platelet count $\geq 100 \times 10^9$/L
	Hemoglobin $\geq$ 10 g/dL
	Before subsequent administration:
	Absolute neutrophil count = 1×10^9/L
	Platelet count = 50×10^9/L
	No hemoglobin requirement

Understanding prior therapies the patient has had is also important. ^{223}Ra-dichloride when given in conjunction with abiraterone therapy + prednisone or prednisolone has been associated with an increased frequency of fractures, compared with patients who did not receive the ^{223}Ra-dichloride (*22*). This association has caused the European Medicines Agency to recommend a contraindication in this setting. This recommendation is not reflected in the Food and Drug Administration's package insert at this time, but nonetheless, current guidelines discourage this practice (*20*). Other myelosuppressive therapies the patient may have had in the 4 wk before therapy may also set the patient up for more profound myelosuppression. Likewise, if patients have had external-beam hemibody radiation or other systemic radionuclides within 24 wk of therapy, careful consideration of the risk-to-benefit ratio of therapy is recommended (*20*). If patients have epidural tumor or spinal cord compression, they should be treated preferentially with external-beam radiation therapy before ^{223}Ra-dichloride (*20*). Working together with clinical colleagues to settle on an appropriate time for ^{223}Ra-dichloride therapy is important.

Assessing performance status is recommended. This assessment can be done with the Eastern Cooperative Oncology Group or Zubrod performance status criteria (*23*). Guidelines suggest that life expectancy should be at least greater than 6 mo, and an Eastern Cooperative Oncology Group performance status of 0 to 2 is preferred (*20*). Guidelines also recommend documentation of pain and patient-related symptoms before and during therapy to evaluate the patient's quality of life (*20,22*).

Because of the complexity of tracking the many elements of therapy, it can be helpful to use a checklist for each patient. Example items to keep on such a checklist are in Table 2.

Provided the patient meets the laboratory parameters and functional status requirements, therapy is given intravenously every 4 wk for a total of 6 therapies. If there is evidence of myelosuppression after a therapy, the next therapy can be delayed for to up to 6–8 wk. If blood counts do not improve despite supportive care, no further treatment is given (*14*). Table 3 reviews important clinical metrics to evaluate before therapy. Figure 1 illustrates the therapy procedure at a glance.

RADIOPHARMACEUTICAL THERAPY PROPERTIES AND DOSIMETRY

^{223}Ra is an α-particle and has a half-life of 11.43 d. Most of the therapy (95.6% abundance) is α-particles, which deposit high energy with a very short pathlength. β-particles make up 3.6% of the decay, and γ-photons make up 1.1% (*14*). These γ-photons allow for easy measurement on standard dose calibrators and survey meters. The full decay schema is described in Figure 2, and the dosimetry is detailed in Table 4 (*24*). Given the dosimetric data, one can understand why gastrointestinal symptoms may occur, as the radiopharmaceutical is excreted predominantly via the gastrointestinal tract in healthy individuals.

TABLE 2
Items to Include in ^{223}Ra-Dichloride Therapy Checklist and Consultation Note

Item	Reason
Documentation of bone scan demonstrating uptake in osseous metastatic disease	Required by package insert; if there is no uptake on bone scan, therapeutic radionuclide will not localize in suspected areas of metastatic disease
Documentation of no visceral metastatic disease	Required by package insert; therapeutic radionuclide treats not visceral metastatic disease but osseous metastatic disease, given its mechanism of localization (guidelines suggest CT of chest, abdomen, and pelvis before therapy)
Documentation of complete blood count with differential counts	Required by package insert and serves as baseline before other therapies, given potential myelosuppression of this therapy
Plan or order for follow-up laboratory analysis before planned upcoming therapies	Required by package insert; some lab tests may be organized by clinician who refers patient, but where to find this information should be known before upcoming doses are ordered (these lab tests are needed at least 1 wk before each planned treatment)
Documentation of Eastern Cooperative Oncology Group or Zubrod performance status	Helpful for future reference before starting therapy
Review of patient continence of urine and stool	Helpful when giving directed radiation safety instructions (therapy excreted mostly via gastrointestinal tract and, to lesser degree, urinary tract)
Review of such factors as home situation, travel, and occupational considerations	Helpful when giving directed radiation safety instructions
Review of side effects, with recommendation for relevant as-needed medications	Should be done for any medical therapy as part of consent
Plan for follow-up weight measurements and documentation of patient weight	Helpful to know ahead of time because doses are weight-based and patient weight may vary because of a variety of circumstances during therapy
Signed consent form	Should be done for any medical therapy as part of consent and understanding of potential risks and benefits
Radiation safety instructions	Should be done for any radionuclide therapy
Completed written directive for sixth therapy	Should be done for any medical therapy (ensure updated weight is used for calculation)

RADIATION SAFETY PRECAUTIONS, PATIENT CONSENT, AND AS-NEEDED MEDICATIONS

According to the Nuclear Regulatory Commission, all radionuclide therapies should be given under the auspices of a quality management program (*20*). A written directive is required for each ^{223}Ra-dichloride therapy for each individual (i.e., 6 written directives for an individual patient for the entire course of therapy). Written directives include the administered activity, which in this case is weight-based (55.13 kBq [1.49 μCi]/kg), and an updated weight will be necessary for ordering doses a week before therapy. Once again, assessment of the complete blood count with differential will be necessary to determine whether the patient is experiencing myelosuppression and needs a pause or discontinuation of therapy.

During the clinical consultation, there should be careful discussion of the radiation safety precautions, side effects,

TABLE 3
Elements to Review Before Treatment on Day of Therapy

Element	Reason
Review consultation	To better understand new patient or refresh memory of previous patient
Review complete blood count with differential	To ensure parameters are within appropriate range for therapy
Confirm weight and accuracy of administered activity calculation	To ensure correct dose
Verify patient identity per institutional protocol	To ensure correct patient receives therapy
Confirm that pretherapy and posttherapy medications have been given as needed	To ensure patient comfort in event of side effects
Provide radiation safety instructions	To ensure patient has instructions and opportunity to ask questions
Provide as-needed medications	To ensure patient has as-needed medication and instructions on when to use
Determine how well patient tolerated previous therapies	To review symptoms and needs for pain medication and to preview current therapy (e.g., if patient is no longer constipated because less pain medication is needed than previously, there could be higher risk of soft stools or diarrhea during current therapy)

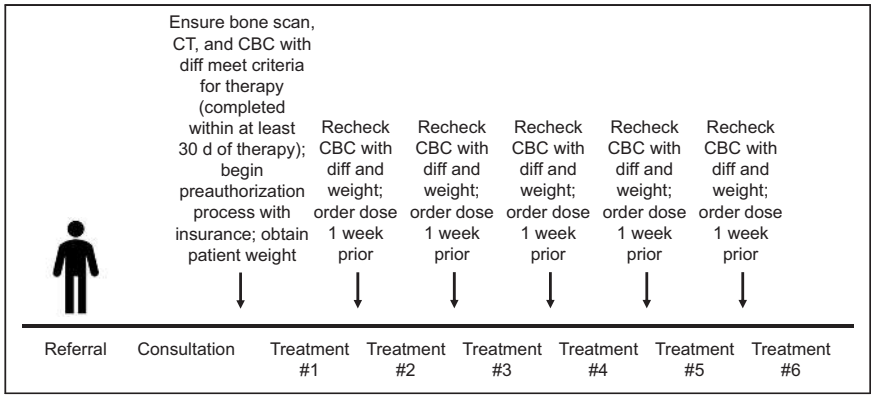

FIGURE 1. Therapy process. CBC = complete blood count; diff = differential.

and complications. When discussing precautions to take after the therapy, nuclear medicine professionals should primarily focus on stool and body fluids. Patients should be told to sit while urinating to minimize splatter and that careful handwashing after using the restroom is imperative. If there is a urinary catheter, patients should be told to use disposable gloves when manipulating or changing it. Instructions are also recommended on disposal of any materials that could contain body products. As part of consenting to the therapy, the patient should understand the potential side effects. The most common are myelosuppression, diarrhea, nausea, and peripheral edema. As-needed medications for nausea and diarrhea may be prescribed, or over-the-counter versions can be recommended. Patients should also be made aware of the potential for a transient increase in bone pain, often referred to as the flare phenomenon (*20*). Because of this potential, and because a patient may already have pain at baseline, the clinician who treats that pain should be told of the possible need for an increase in medication, so it can be arranged for in advance.

Complications that have been reported from ALSYMPCA are myelosuppression (13%), neutropenia (2%), thrombocytopenia (7%), and grade 5 treatment-emergent adverse events (13%). Long-term follow-up of patients from the trial yielded no suggestion of myelodysplastic syndrome, acute myelogenous leukemia, or new primary bone cancer. Secondary non–treatment-related malignancies occurred in 4 patients treated with ^{223}Ra-dichloride, whereas 3 occurred in placebo patients. One patient experienced aplastic anemia 16 mo after the last injection (*12*).

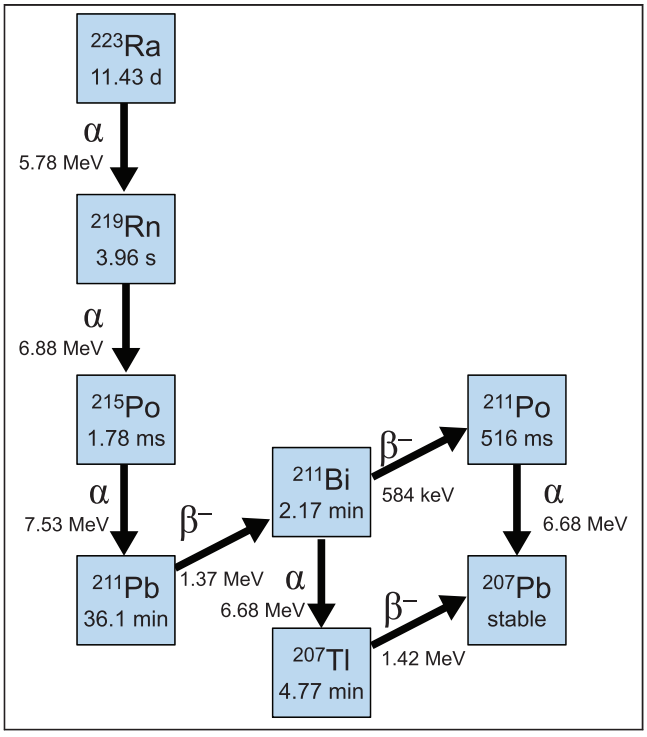

FIGURE 2. Decay schema for ^{223}Ra-dichloride.

DAY-OF-THERAPY TECHNICAL CONSIDERATIONS

Although external radiation exposure from ^{223}Ra-dichloride is quite low compared with other therapies, care in administration is key. Care should be taken to avoid internal radiation contamination through injection, inhalation, or skin absorption. Because α-particles deposit their energy in a highly localized range, greater damage can occur than with β-particles or γ-photons. Because of the long half-life, spills should be avoided but can be identified with standard survey equipment because of the γ-photons. Contamination can be cleaned up with a dilute aqueous ethylenediaminetetraacetic acid solution, and areas can be resurveyed to ensure that they are decontaminated.

Before administration, the therapeutic dose should be measured, absorbent shielding should be placed under the patient's arm to prevent spillage, and the intravenous catheter should be checked for patency. The therapy is often given with a 3-way stopcock with a saline flush to ensure maximal delivery; all intravenous lines and connections should be secure. Because this is an α-particle therapy, more localized damage may occur in the event of extravasation. A shield is recommended to keep the dose to the individual delivering the therapy as low as reasonably achievable. Dose rates are surprisingly high near the point source itself (Table 5). Some institutions choose to use a test dose of a small amount of ^{99m}Tc-pertechnetate and acquire dynamic images to ensure a patent intravenous catheter. A slow intravenous injection over 1 min is used. After injection, flushing with isotonic saline is recommended (*20*).

CREATING A SUCCESSFUL RADIONUCLIDE THERAPY PROGRAM WITH ^{223}RA-DICHLORIDE

According to the manufacturer, Bayer HealthCare, technical prerequisites for site initiation include obtaining a radioactive

TABLE 4
^{223}Ra-Dichloride Dosimetry (*24*)

Organ	Absorbed dose (Gy/Bq) α-particles (high LET)	Absorbed dose (Gy/Bq) β/γ dose (low LET)	Dose coefficient (Gy/Bq)	Contribution of β/γ dose to total dose (%)
Adrenals	3.2E–09	2.4E–10	1.6E–08	7
Bladder wall	3.3E–09	4.1E–10	1.7E–08	11
Bone endosteum	3.3E–09	1.1E–10	3.8E–06	1
Brain	3.2E–09	1.8E–10	1.6E–08	5
Breast	3.2E–09	1.6–10	1.6E–08	5
Gastrointestinal tract				
Esophagus	3.2E–09	1.7E–10	1.6E–08	5
Stomach wall	3.2E–09	3.9E–10	1.6E–08	6
Small intestine wall	3.2E–09	3.9E–10	1.7E–08	11
Upper large intestine wall	6.8E–09	1.4E–08	4.8E–08	67
Lower large intestine wall	1.3E–08	4.0E–08	1.1E–07	75
Colon	9.5E–09	2.5E–08	7.3E–08	72
Kidneys	3.4E–09	2.4E–10	1.7E–08	7
Liver	3.6E–09	1.5E–10	1.8E–08	4
Muscle	3.2E–09	2.0E–10	1.6E–08	6
Pancreas	3.2E–09	2.2E–10	1.6E–08	6
Red marrow	7.2E–08	5.5E–09	3.7E–07	7
Respiratory tract				
Airways	3.2E–09	1.7E–10	1.6E–08	5
Lungs	3.2E–09	1.9E–10	1.6E–08	6
Skin	3.2E–09	1.6E–10	1.6E–08	5
Spleen	3.2E–09	1.9E–10	1.6E–08	6
Testes	3.2E–09	1.8E–10	1.6E–08	5
Thymus	3.2E–09	1.7E–10	1.6E–08	5
Thyroid	3.2E–09	1.7E–10	1.6E–08	8

LET = linear energy transfer.

materials license approved for medical use of ^{223}Ra-dichloride, creating an authorized-user list for medical application of ^{223}Ra-dichloride, providing documentation regarding training on handling and use of ^{223}Ra-dichloride, and verifying the accuracy of dose calibrators to measure ^{223}Ra-dichloride activity. Dose calibrator testing with a National Institute of Standards and Technology–traceable ^{223}Ra standard is provided by Cardinal Health. Additional prerequisites, which may already be established in a nuclear medicine area, include monitoring occupational doses and securing areas for storage, waste disposal, and inventory management (*25*).

Some studies have established data that ^{223}Ra-dichloride is cost-competitive as compared with other prostate cancer therapies. In addition, ^{223}Ra-dichloride therapy has been found to result in fewer skeleton-related events than other therapies, and other groups have demonstrated a slower decline of quality of life over time, with meaningful improvement, in patients who receive this therapy than in those who receive placebo (*12,26*).

TABLE 5
Dose Rates Comparing ^{99m}Tc Vs. ^{223}Ra Derived from Exposure Rate Constants (μSv/h per MBq) (*31*)

Distance from point source	^{99m}Tc	^{223}Ra	^{223}Ra + progeny
1 m	0.02	~0.02	0.047
10 cm	2	~2	4.7
1 cm	200	~200	470

After a site has been initiated, understanding the codes involved in billing is important (Table 6). If the therapy is administered in a hospital setting, working closely with the hospital billing office is important, as is staying attuned to potential annual changes in Centers for Medicare and Medicaid Services coding practices. Both inside and outside the hospital, Xofigo Access Services offers guidance on coding (*25*). Before therapy is administered, it is recommended that insurance companies be queried on the need for prior authorization. The time needed for prior authorization is quite variable among different insurance providers, but 15 or more business days may be needed. Failure to use codes can result in denial. In addition, failure to allow enough time for preauthorization or for managing clinician and patient expectations can also be problematic. To ensure that patients do not have an out-of-pocket burden, close work with institutional billing offices or Xofigo Access Services should allow them to provide guidance on issues encountered in coding and billing. In addition, the Society of Nuclear Medicine and Molecular Imaging website has a "Coding and Reimbursement Q&A" section with resources available to members (*27*).

TABLE 6
Current Codes in ^{223}Ra-Dichloride Therapy (*27*)

Code	Purpose
CPT code 99242 (new, outpatient, problem-focused, 30 min)	Code for evaluation and management (dependent on type and length of consultation)
CPT code 79101	Code for radiopharmaceutical therapy by intravenous administration
Radiopharmaceutical code A9606	Code for therapeutic ^{223}Ra-dichloride, per microcurie
JW modifier	Code to report wasted product and ensure ability to report full cost of ordered dose*
ICD-10-CM codes (C61: malignant neoplasm of prostate; C79.51: secondary malignant neoplasm of bone)	Codes to support the above codes and ensure correct indication

*Given long half-life, may not be needed, but Society of Nuclear Medicine and Molecular Imaging supports use of this modifier.
CPT = Current Procedural Terminology; JW modifier = Healthcare Common Procedure Coding System (HCPCS) Level II modifier used on Medicare Part B drug claim to report amount of drug or biological that is discarded and eligible for payment under the discarded drug policy (*32*); ICD-10-CM = International Classification of Diseases, tenth revision, clinical modification.

In addition to these items, it is imperative to provide patients with multidisciplinary care and identify clinicians of various backgrounds who will be involved in therapy referral and follow-up. Follow-up practices may differ on the basis of institutional protocols. Some practices include mid-therapy evaluation with laboratory biomarkers or imaging; however, no well-defined guidelines exist yet.

LOOKING AHEAD

The use of ^{223}Ra-dichloride is likely to evolve, considering the recent Food and Drug Administration approval of ^{177}Lu-vipvotide tetraxetan (also known as ^{177}Lu-PSMA-617) (*28*). ^{223}Ra-dichloride is a bone-based therapy, whereas ^{177}Lu-vipvotide tetraxetan is a therapy that can also target soft-tissue lesions. Holistic evaluation and the tracer uptake profile of the patient may be needed to assess which agent would be of most benefit.

Another area of interest may be repeat ^{223}Ra-dichloride therapy. Some research has already been done in this area, and the findings suggest that the therapy is well tolerated and provides additional control of osseous metastatic disease (*29,30*). Longer-term follow-up may be helpful to evaluate for continued long-term safety.

EDUCATION AND RECOMMENDED READING

There is a good deal of helpful information available to those starting a ^{223}Ra-dichloride therapy program. Some of the higher-yield materials include the ^{223}Ra practice parameters of the American College of Radiology, American College of Nuclear Medicine, American Society for Radiation Oncology, and Society of Nuclear Medicine and Molecular Imaging (*20*); the ALSYMPCA trial (*12*); and Xofigo access services (*25*).

CONCLUSION

^{223}Ra-dichloride remains an effective therapy that improves survival for patients with osseous metastatic disease related to castration-resistant prostate cancer in the absence of visceral metastatic disease.

DISCLOSURE

No potential conflict of interest relevant to this article was reported.

REFERENCES

1. Godlewski T. A new radio-active product from actinium. *Nature.* 1905;71:294–295.
2. Hahn O. A new product of actinium. *Nature.* 1906;73:559–560.
3. Allen HS. Radium, actinium and helium [letter]. *Nature.* 1906;75:126.
4. Rutherford E. Production of radium from actinium [letter]. *Nature.* 1907;270–271.
5. McClennan JC. On the relation of "recoil" phenomena to the final radio-active product of radium. *Nature.* 1909;80:490–491.
6. Marsden E, Wilson RH. Branch product in actinium C [letter]. *Nature.* 1913;92:29.
7. Bruland ØS, Nilsson S, Fisher DR, et al. High-linear energy transfer irradiation targeted to skeletal metastases by the alpha-emitter ^{223}Ra: adjuvant or alternative to conventional modalities? *Clin Cancer Res.* 2006;12:6250s–6257s.
8. Lewington VJ. Bone-seeking radiopharmaceuticals in bone-metastatic prostate cancer. *J Nucl Med.* 2005;46(suppl 1):38S–47S.
9. Liepe K. Alpharadin, a ^{223}Ra-based alpha-particle-emitting pharmaceutical for the treatment of bone metastases in patients with cancer. *Curr Opin Investig Drugs.* 2009;10:1346–1358.
10. Kerr C. ^{223}Ra targets skeletal metastases and spares normal tissue. *Lancet Oncol.* 2002;3:453.
11. Li Y, Russell PJ, Allen BJ. Targeted alpha-therapy for control of micrometastatic prostate cancer. *Expert Rev Anticancer Ther.* 2004;4:459–468.
12. Parker C, Nilsson S, Heinrich D, et al. Alpha emitter radium-223 and survival in metastatic prostate cancer. *N Engl J Med.* 2013;369:213–223.
13. Xofigo FDA approval history. Drugs.com website. https://www.drugs.com/history/xofigo.html. Updated January 27, 2021. Accessed July 28, 2022.
14. Xofigo (radium Ra 223 dichloride) injection, for intravenous use. Food and Drug Administration website. https://www.accessdata.fda.gov/drugsatfda_docs/label/2013/203971lbl.pdf. Published 2013. Revised May 2013. Accessed July 28, 2022.
15. Key statistics for prostate cancer. American Cancer Society website. https://www.cancer.org/cancer/prostate-cancer/about/key-statistics.html. Revised January 12, 2022. Accessed July 28, 2022.
16. Roodman GD. Mechanisms of bone metastasis. *N Engl J Med.* 2004;350:1655–1664.
17. Lin SC, Yu-Lee LY, Lin SH. Osteoblastic factors in prostate cancer bone metastasis. *Curr Osteoporos Rep.* 2018;16:642–647.
18. Lange PH, Vessella RL. Mechanisms, hypotheses and questions regarding prostate cancer micrometastases to bone. *Cancer Metastasis Rev.* 1998–1999;17:331–336.

19. Castrate-resistant prostate cancer. NCI website. https://www.cancer.gov/publications/dictionaries/cancer-terms/def/castrate-resistant-prostate-cancer. Accessed July 28, 2022.
20. Hurwitz M, Buscombe JR, Jacene HA, et al. ACR-ACNM-ASTRO-SNMMI practice parameter for the performance of therapy with radium-223. *Am J Clin Oncol.* 2020;43:539–544.
21. Brito AE, Etchebehere E. Radium-223 as an approved modality for treatment of bone metastases. *Semin Nucl Med.* 2020;50:177–192.
22. van der Poel H. Re: addition of radium-223 to abiraterone acetate and prednisone or prednisolone in patients with castration-resistant prostate cancer and bone metastases (ERA223): a randomised, double-blind, placebo-controlled phase 3 trial. *Eur Urol.* 2019;76:705–706.
23. Oken MM, Creech RH, Tormey DC, et al. Toxicity and response criteria of the Eastern Cooperative Oncology Group. *Am J Clin Oncol.* 1982;5:649–655.
24. Lassmann M, Nosske D. Dosimetry of ^{223}Ra-chloride: dose to normal organs and tissues. *Eur J Nucl Med Mol Imaging.* 2013;40:207–212.
25. Successfully integrating Xofigo into a community practice. Xofigo website. https://www.xofigohcp.com/access/community-practice-integration. Accessed August 8, 2022.
26. Peters ML, de Meijer C, Wyndaele D, et al. Dutch economic value of radium-223 in metastatic castration-resistant prostate cancer. *Appl Health Econ Health Policy.* 2018;16:133–143.
27. Xofigo® (radium Ra 223 dichloride). SNMMI website. https://www.snmmi.org/IssuesAdvocacy/QandADetail.aspx?ItemNumber=1895&navItemNumber=24950. Accessed July 28, 2022.
28. Pluvicto™ (lutetium Lu 177 vipivotide tetraxetan) injection, for intravenous use. Novartis website. https://www.novartis.us/sites/www.novartis.us/files/pluvicto.pdf. Published 2022. Revised March 2022. Accessed July 28, 2022.
29. Radium-223 (Ra-223) re-treatment (re-tx): first experience from an international, multicenter, prospective study in patients (pts) with castration-resistant prostate cancer and bone metastases (mCRPC). *Clin Adv Hematol Oncol.* 2016;14(suppl 5):10–11.
30. Sartor O, Heinrich D, Mariados N, et al. Re-treatment with radium-223: 2-year follow-up from an international, open-label, phase 1/2 study in patients with castration-resistant prostate cancer and bone metastases. *Prostate.* 2019;79:1683–1691.
31. Smith DS, Stabin MG. Exposure rate constants and lead shielding values for over 1,100 radionuclides. *Health Phys.* 2012;102:271–291.
32. Medicare Program: JW Modifier—Drug/Biological Amount Discarded/Not Administered To Any Patient. Centers for Medicare & Medicaid Services website. https://www.cms.gov/medicare/medicare-fee-for-service-payment/hospitaloutpatientpps/downloads/jw-modifier-faqs.pdf. August 26, 2016. Accessed August 8, 2022.

^{223}Ra-Dichloride Therapy

Sarah Clements, CNMT, Daniel Tempesta, CNMT, and Matthew Robertson, MD

SUMMARY

^{223}Ra-dichloride (Xofigo; Bayer) is an α-emitting radioactive agent used to treat symptomatic bone metastases in patients with castration-resistant prostate cancer in the absence of visceral metastases (*1*). It functions as a calcium analog and causes double-strand DNA breaks in tissue, resulting in the death of tumor cells (*2*).

CLINICAL INDICATIONS (*1*)

- ^{223}Ra-dichloride is indicated for treatment of symptomatic bone metastasis in patients who have castration-resistant prostate cancer with no known visceral metastasis.

PATIENT SELECTION (*1*)

- To be eligible for treatment, patients must have all of the following:
  - Castration-resistant prostate cancer.
  - Symptomatic bone metastasis.
  - No known visceral metastasis.
- Once deemed eligible, patients must meet the following hematologic criteria before their first treatment:
  - Absolute neutrophil count $\geq 1.5 \times 10^9$/L.
  - Platelet count $\geq 100 \times 10^9$/L.
  - Hemoglobin ≥ 10 g/dL.
- For all subsequent treatments, the patient's hematologic values must be as follows:
  - Absolute neutrophil count $\geq 1 \times 10^9$/L.
  - Platelet count $\geq 50 \times 10^9$/L.

CONTRAINDICATIONS (*1*)

- There are no contraindications to use of ^{223}Ra-dichloride.

TREATMENT PLAN (*1*)

- 55 kBq (1.49 μCi) of ^{223}Ra-dichloride is given per kilogram of body weight every 4 weeks for a total of 6 treatments.
  - Volume (mL) to inject, in kBq/kg:
    $$\frac{\text{body weight in kg} \times 55 \text{ kBq/kg body weight}}{\text{decay factor} \times 1{,}100 \text{ kBq/mL}}$$
  - Volume (mL) to inject, in μCi/kg:
    $$\frac{\text{body weight in kg} \times 1.49 \text{ uCi/kg body weight}}{\text{decay factor} \times 30 \text{ uCi/mL}}$$
- Prescribing information provides up-to-date dose calculations.

PATIENT PREPARATION/EDUCATION (*1*)

- The most common side effects of ^{223}Ra-dichloride are myelosuppression, nausea, vomiting, diarrhea, and peripheral edema.
- Patients should be given information on radiation safety precautions before administration of ^{223}Ra-dichloride to reduce exposure to others. For example:
  - Flushing the toilet multiple times after each use.
  - Washing clothing soiled with ^{223}Ra-dichloride, feces, or urine quickly after they become contaminated. This should be done separately from other clothing or items.
  - Using gloves and frequently washing the hands when anyone handles patient clothing and bodily fluids.
  - Using condoms for the duration of treatments and 6 months afterward. Partners of reproductive capability should also use effective forms of contraception for the length of treatment and 6 months afterward.
- Other than the sexual activity restrictions, the prescribing information does not specify any distance or length of time that patients must restrict contact with household members.

TREATMENT INSTRUCTIONS

- The patient's blood counts must be obtained and confirmed to be in the desired range before treatment (*1*). The decision to delay treatment, reduce the dose given, or make any other alterations to the standard treatment plan is ultimately a clinical decision (*2*).
- A 55-kBq (1.49 μCi) dose of ^{223}Ra-dichloride per kilogram of body weight is administered intravenously over 1 min (*1*). For dose accuracy, the patient's body weight should be measured on the day of treatment.
- Before and after administration of ^{223}Ra-dichloride, the intravenous line should be flushed with isotonic saline (*1*).
- Roughly 1% of the emissions from ^{223}Ra-dichloride are γ-radiation, which allows surfaces and personnel to be surveyed for contamination with standard instruments (*1*).

DOI: 10.2967/jnmt.122.264765

TABLE 1
Dose, Administration Route, and Infusion Duration for ^{223}Ra-Dichloride (*1*)

Dose	Administration route	Infusion duration
55 kBq (1.49 μCi)/kg of body weight	Intravenous	1 min

THERAPEUTIC DOSE CALCULATIONS (*1*)

- The therapeutic dose is 55 kBq (1.49 μCi) per kilogram of body weight.
- Discontinuation of treatment should be considered if the patient's laboratory values do not recover within 6–8 weeks of the last treatment received.

WARNINGS/PRECAUTIONS

- Bone marrow suppression is a possible side effect of ^{223}Ra-dichloride, and patients should be closely monitored for signs of bone marrow failure (*1*). Patients should be instructed to inform their care team if they have any signs of bleeding or symptoms of infection.
- ^{223}Ra-dichloride is not recommended in combination with abiraterone acetate plus prednisone or prednisolone as it increases the risk of fractures and mortality (*1*).
- ^{223}Ra-dichloride has the potential to cause fetal harm. Patients should use condoms, and patients' partners of reproductive capability should use effective contraception for the length of treatment and 6 months afterward (*1*).
- Receiving docetaxel or any other form of systemic therapy except for androgen deprivation therapy while undergoing treatment with ^{223}Ra-dichloride is not recommended. ^{223}Ra-dichloride is also not intended to be used in conjunction with chemotherapy, as this increases the risk and burden of myelosuppression (*3*).

REFERENCES

1. Xofigo® (radium Ra 223 dichloride) injection, for intravenous use [package insert]. Bayer Aktiengesellschaft; 2013.
2. Deshayes E, Roumiguie M, Thibault C, et al. Radium 223 dichloride for prostate cancer treatment. *Drug Des Devel Ther*. 2017;11:2643–2651.
3. NCCN clinical practice guidelines in oncology (NCCN Guidelines®): prostate cancer. National Comprehensive Cancer Network website. https://www.nccn.org/professionals/physician_gls/pdf/prostate.pdf. Published May 10, 2022. Accessed August 8, 2022.

The Nuclear Medicine Technologist's Role in Theranostics: SNMMI-TS Advocacy's Vision

Dmitry D. Beyder, MPA, CNMT[1], Cheryl L. Rickley, CNMT, FSNMMI-TS[2], Tricia L. Peters, CNMT, PET, RT(CT)[3], Jeremy L. Iman, CNMT, PET CRA, CT[4], and Christina M. Arenas, JD, MPH[5]

[1]*Barnes-Jewish Hospital/Mallinckrodt Institute of Radiology, St. Louis, Missouri;* [2]*TTG Imaging Solutions, Pittsburgh, Pennsylvania;* [3]*Ridley-Tree Cancer Center at Sansum Clinic, Santa Barbara, California;* [4]*UNC REX Healthcare, Raleigh, North Carolina; and* [5]*Society of Nuclear Medicine and Molecular Imaging, Reston, Virginia*

With the approval of ^{177}Lu PSMA-617, theranostics' presence in nuclear medicine is expanding beyond thyroid cancer and neuroendocrine tumors to higher-incidence diseases. This April (2022), *The Journal of Nuclear Medicine* published an ahead-of-print article, "Joint EANM, SNMMI and IAEA Enabling Guide: How to Set Up a Theranostics Centre" (*1*). The guide provided valuable information to enable interested stakeholders to safely initiate and operate theranostics centers. The article defined the theranostics concept as "using the same target for both imaging and therapy." That is also how we define the theranostics concept as Nuclear Medicine Technologists (NMTs) and SNMMI-Technologist Section (SNMMI-TS) Advocacy governance.

SNMMI-TS Advocacy Committee would now like to expand on that article to answer the following questions and cast a level of opinion on: What training does an NMT need to participate and complete theranostics? What does the SNMMI-TS Advocacy Committee feel are important initiatives to have NMTs fully engaged in theranostics today and in the long-term?

We hope the following article will serve as a springboard for theranostics considerations from the perspective of the NMT.

NMT THERANOSTICS TRAINING

What training does a nuclear medicine technologist need to have to administer and safely treat patients with theranostics?

The SNMMI-TS Advocacy Committee supports best practices in evidence-based science that promote the highest quality in patient care and safety by supporting standards for education and training for NMTs as defined by the Joint Review Committee on Educational Programs in Nuclear Medicine (JRCNMT). Currently, the NMT is initially trained to get into the field by way of college, graduate school, or certificate curriculum, to gain their certification. After obtaining certification, the NMT must participate in continuing education annually to maintain their NMTCB (Nuclear Medicine Technology Certification Board) or ARRT (The American Registry of Radiologic Technologists) certification. That education is thorough and encompasses radionuclide therapy, including the handling of radiopharmaceuticals, adjunctive medications to support clinical nuclear medicine, and patient care management through capturing patient vitals, monitoring, and observing patients before and after procedures.

Most accredited programs are at the baccalaureate level, and some are converting to a master's level due to the complexity of the field and the volume of material that must be taught to perform nuclear medicine technology. Educational programs require extensive didactic education in the fundamentals of nuclear medicine, radiation biology, radiopharmaceuticals, and radiation physics. Additionally, clinical competency requirements must be successfully completed under the direct supervision of a qualified and certified practicing NMT. It would be extremely challenging to meet all these educational requirements via an apprenticeship model. As a point of reference in 2021, Arizona enacted a law (*2*) that would allow some junior college programs to offer baccalaureate degrees due to the academic rigor and the number of required hours that a student must take (120 h). Nuclear Medicine Technology was one such program, and as such students who graduate from a Nuclear Medicine associate's program in Arizona are now awarded a baccalaureate degree.

Although current NMT training is inclusive of most of the components that go into the theranostics *therapy* component of patient care, more training and competency would be helpful to be more competent to access patients' chest vascular ports, lead pre- and postpatient therapy management, and administer therapy-related adjunctive medications such as amino acids.

Why is radiation safety training so important, particularly in the context of theranostics?

With new technology and evolving radiotherapeutic therapies, it is important for medical professionals to continue

Received Jun. 25, 2022; revision accepted Jul. 13, 2022.
For correspondence or reprints, contact Dmitry D. Beyder (dbeyder@gmail.com).
Published online Jul. 26, 2022.

DOI: 10.2967/jnmt.122.264565

to develop a comprehensive knowledge and understanding of radiation biology and safety. The misuse, overuse, or inappropriate handling of radiologic technology can be detrimental to both the patient and the NMT. Improper use of equipment can result in faulty images, which in turn can lead to a misdiagnosis or false interpretation of patient conditions. To prepare knowledgeable, competent, and qualified professionals, the educational content and course competencies are expanding and becoming increasingly complex. Currently, SNMMI is in the process of publishing the sixth edition of the *Nuclear Medicine Technology Competency-Based Curriculum Guide* that outlines the radiation safety knowledge, skills, and experience necessary for NMTs and students to complete a JRCNMT-certified program and be ready for the evolving theranostics field. The curriculum guide develops a competency-based education model that is necessary for students to demonstrate understanding of theranostics radiation safety. NMTs must be able to demonstrate and understand the safe handling of radiopharmaceuticals, practice aseptic technique, and understand the selection and use of proper radiation shielding devices.

The SNMMI is currently working on theranostics-based badges that will be purchasable in 2023. The Molecular & Therapy Task force is heading the efforts to develop the theranostics badges, which includes Xofigo, Lutathera, Azedra, and more. The plan is also to have the badges be CEU (continuing education units) based for NMT formal training. These badges do not take the place of certification but are more so a way to promote the field and the work NMTs do.

Radiation safety training plays an integral aspect of administering theranostics to ensure safety to the occupational workers, NMT, and patient. The NMT must understand the radiation emission of the isotopes used in theranostics to select the correct means of following ALARA (as low as reasonably achievable). Selecting the correct shielding, means of delivery, and proper distance from the patient are all considerations that come from proper training. In some theranostics administrations, proper preparation is key to minimize residual radioactivity exposure and contamination, that is, prepping the bathroom on Lutathera administrations. For the NMT and ancillary staff, training from the vendor-specifics to the therapy and the knowledge acquired during school training are essential to ensuring the safety of all involved. In regard to Lutathera and even high-dose ^{131}I administrations, knowing how to handle emesis during and after administration is also essential in conducting successful radiotherapy.

THE THERANOSTICS CARE TEAM

Now is the time most critical to make sure that the nursing and NMT groups work together to ensure that we have enough health-care providers to serve the growing population of patients who are going to require theranostics treatments. The list of available theranostics today includes thyroid cancer, neuroendocrine tumors, and prostate cancer, and this list will grow significantly with time, as other imaging therapy radionuclide packages come to market. Just recently, an analysis from McKinsey and co. found a potential shortage of 200,000–450,000 nurses not available for patient care in the short-term (*3*). The same analysis mentioned that by 2025, there could be a shortage of nurses of half a million throughout the United States.

Today, our nursing partners play a pivotal collaborative role in the provision of theranostics therapy, where much of the patient management and appropriate adjunctive medications for therapy are administered by nurses. The shortfall of nurses puts a larger strain on our health-care system and the provision of theranostics, as nurses may not be available to support the NMTs and authorized users to provide patients with this incredibly important therapy. Therefore, the SNMMI-TS Advocacy Committee feels that a focus on NMT training and further evaluation and possible expansion of the NMT curriculum to include all components of theranostics are crucial. Furthermore, developing a collaborative training process with the nursing professionals is essential to make sure that theranostics will have enough health-care personnel to provide this essential patient therapy and that NMTs can safely and effectively participate in all components of theranostics care delivery.

Another important member of the nuclear medicine care team is the Nuclear Medicine Advanced Associate (NMAA). The NMAA is a master's level and board-certified professional who serves as a physician extender or midlevel provider with specialization in all areas of nuclear medicine. The NMAA performs duties and responsibilities in a manner consistent with our mission, values, guiding principles, and American Heart Association/NMTCB service standards within the scope of an NMAA practice (*4*). In the theranostics setting (as in diagnostics), NMAAs work under the supervision of a licensed physician and serve as an adjunct between the physician and other health-care professionals (including NMTs) to enhance patient care.

SNMMI-TS ADVOCACY THERANOSTICS FUTURE PLANS

Engagement with the U.S. Nuclear Regulatory Commission (NRC) and The Joint Commission (TJC)

It is immensely important to SNMMI-TS and the nuclear medicine community that our regulators are aware of what theranostics is. For this reason, in the fall of 2021, the SNMMI-TS Advocacy Committee met with the U.S. Nuclear Regulatory Commission staff to refine language on the NRC webpage of what "nuclear medicine is and is not." On that same page, we proposed that the NRC include the following, under common nuclear medicine procedures: "Theranostics for targeted radioactive imaging and therapy for various cancers and diseases. Theranostics uses targeted imaging to tailor patient treatment."

Additionally, the SNMMI-TS Advocacy Committee embarked on a multiyear effort to oppose the further dilution of the training and experience (T&E) requirements for

unsealed byproduct materials (10 CFR part 35). In 2020, NRC staff recommended that the Commission pursue regulatory changes to the T&E requirements for radiopharmaceuticals, moving to using solely board certification for determining and obtaining authorized user status. Specifically, NRC staff indicated they planned to modify the board certification criteria to allow for additional medical specialty boards, beyond nuclear medicine and radiation oncology, to qualify for meeting the T&E requirements. In practice, this would necessitate weakening the already robust, yet flexible, board recognition criteria. Thankfully in January 2022, the Commission disapproved of their staff's recommendations, preserving the T&E status quo (*5*).

In the last year, NRC has been busy supporting novel positron emission tomography (PET) diagnostic radiopharmaceuticals and will play a direct role in creating regulations involving proposed rules on ^{82}Rb generators and other new emerging medical technologies (EMTs). The Commission approved of their staff proceeding with rulemaking in January 2022 due to the anticipated increase in the number of EMTs licensed by the NRC (*6*). As the use of medical applications of radioisotopes continues to increase and new advancements in medical technologies are expected, we anticipate that the NRC will continue to be busy in this segment of radiopharmaceuticals. Proactively, to address these challenges, the NRC staff recommended updating part 35 to establish generally applicable, performance-based requirements for EMTs that would focus on the essential, safety-related elements necessary to ensure radiation safety for workers, patients, and the general public. The revised regulation would also include performance-based requirements for ^{82}Rb generators, gamma stereotactic radiosurgery units, and ^{90}Y microspheres (*7*).

In the staff's rule-making plan (*7*), "'radiotheranostics' that merge molecular-targeted diagnostic imaging agents with molecular-targeted radiopharmaceutical therapy" is an example of new EMTs that currently would require licensing under 10 CFR 35.1000. SNMMI and the SNMMI-TS Advocacy will engage in providing comment to the proposed rule, along with participating in stakeholder calls, during the 90-d comment period in March 2023.

The support of not only the NRC, but also the Joint Commission (TJC), a national accrediting body, is essential in having NMTs fully participate in the delivery of theranostics. There are currently regulations within the NRC that allow the NMT to perform all actions of therapeutic radiopharmaceutical administration under the guidance of the authorized user (*8*). The SNMMI-TS Scope of Practice and Performance Standards (SOP) updated in 2022, as written, allows the NMT to perform and participate in all elements of theranostics care delivery (*9*). The SNMMI-TS Advocacy Committee understands and further welcomes guidance or rulemaking on the various NMT roles in radiopharmaceutical therapies, in order for the technologist to be properly supported, licensed, and prepared to safely deliver all components of such therapies. Adjustment of policies and standards are common when you evaluate the history of NRC and TJC, and over the next 3–5 y it is reasonable to see these changes happen with the support and collaboration between these and other appropriate accrediting and governing groups.

State and Local Collaboration

SNMMI-TS Advocacy plays a significant role to ensure that state rules and health-care facility policies allow NMTs to practice to their standardized scope, practice standards, and training. This oversight is pivotal in NMTs playing a fully encompassing role in theranostics therapy. The SNMMI-Technologist Advocacy Group Committee (TAG) has been effectively collaborating throughout most of the states in the United States (in addition to the District of Columbia and Puerto Rico) to ensure that NMTs are properly licensed to deliver all components of nuclear medicine in their published SOP. Although this is an ongoing effort, today almost 80% of our states license NMTs to practice to their training in their respective states. As NMT roles expand with theranostics, licensure will need to keep up with curriculum and scope of practice changes. These changes will need to evolve and be incorporated into state regulations to have NMTs participate and lead in all aspects of theranostics therapy. This is a tall task and one that will require consistent work by the TAG and state governments, working together. The Advocacy Committee will continue to use the SNMMI Model Practice Act (MPA) to equip states with legislative support and a thorough understanding of the NMT scope, so proper licensure and regulation are in place to support the evolving skills needed to provide safe handling and administration of radiopharmaceuticals used for theranostics. Furthermore, the SNMMI-TS Advocacy Committee is currently considering creating one MPA for the field by collaborating with organizations such as the Conference of Radiation Control Program Directors (CRCPD) and the Organization of Agreement States (OAS).

Like the evolution of the NMT SOP, health-care facilities themselves will also need to adjust their practices and determine what components of care they can transition from licensed nurses to NMTs. Hospitals have policies in place for patient monitoring, patient management, and medication administration. These are policies that will need to be evaluated, reevaluated, and updated to allow NMTs to provide full care to radiopharmaceutical *therapy* patients. Some of this training will be done by continuing education units (CEU), on the job training, and supplementary material from certification boards and badging options described earlier. The relationship and collaboration between nurses and NMTs are essential to make sure that the technologists can learn and practice in the safest and most patient-responsible way. The action of training Radiology Technologists from other health-care providers like nurses has historically been successful in various scopes in thousands of hospitals and clinics throughout the United States, and the transition to NMTs performing all aspects of theranostics therapy under

proper guidance and policy management will be no different. With expected severe nursing shortages, the sharing and training is of utmost importance now, to ensure that access to theranostics for patients is not compromised. The Advocacy Committee plans to continue to engage with hospitals and other health-care facilities to further the field of nuclear medicine and NMTs to support the continued growth of theranostics. This continued work and attention to licensure and regulation should allow the NMT to stay front-and-center in theranostics delivery and further create pathways for new NMTs to get into the field and be available to support our patients as the demand grows.

Incorporation of Theranostics into the Scope of Practice

Immediate recommended actions of the SNMMI-TS Advocacy Committee include the continuous evaluation of the SNMMI-TS NMT SOP, to be amended and revised to cover all components of therapy. Some considerations that the advocacy team are considering are adding the term *theranostics* to the *Technologist Qualified to Perform Nuclear Medicine Procedures* section (*9*).

1. Under the supervision of an authorized user, the nuclear medicine technologist is responsible for the safe use of ionizing and nonionizing radiation and molecular imaging for diagnostic, therapeutic, [*theranostics*,] and research purposes.
2. A certified nuclear medicine technologist is qualified to perform general nuclear medicine procedures, nuclear medicine therapy, [*theranostics*,] nuclear cardiology procedures, nuclear breast procedures, PET procedures, and CT attenuation correction and localization, and administer radioactive, adjunctive, and imaging medication at entry-level.

Adding *theranostics* into the SOP achieves the goal of exposing the NMT profession and scope to the rapidly emerging field and places the practice standards and scope at the forefront of the NMT's ability to have a fully inclusive role in this therapy delivery. As NMT curricula expand and training increases to fully encompass all components of the delivery of theranostics by the NMT, the SOP will continue to expand and become more specific to each element.

The Advocacy Committee is also looking to amend the MPA for nuclear medicine technology and to add the *theranostics* definition to the document to start exposing states to the NMT role in these therapies. As NMT education and training expand, so will the MPA, referencing all tasks that the NMT should be allowed to conduct while providing theranostics therapy care to patients.

CONCLUSION

The NMT profession is evolving at a rapid pace. How will current nuclear medicine technologists prepare for these new roles? Because of their position, their education, and the respect they have earned, NMTs are well-positioned to take an active lead in theranostics growth and advancement.

NMTs need to initiate the conversation for policy and process changes locally, with their clinic leaders and the local governments, so they can start building a stake in this exciting emerging therapy available to our patients in the United States. NMTs leading and being fully contributing members to the interdisciplinary theranostics teams may require some NMTs to step out of their comfort zone and gain more training, but this effort will not only allow the NMT scope and profession to expand but also lead to a significant improvement in patient access for these integral therapies.

The work by SNMMI and SNMMI-TS over the next several years will be to continue to build on and further launch a comprehensive theranostics awareness campaign to highlight its importance as a professional growth pathway and encourage NMTs to be front-line health-care providers in the delivery of all radiopharmaceutical therapies. These steps forward will require collaborative work among health-care professionals and various departments in health care and will ultimately help patients have better access to the care that they require to live better and longer lives.

DISCLOSURE

No potential conflict of interest relevant to this article was reported.

REFERENCES

1. Herrmann K, Giovanella L, Santos A, et al. Joint EANM, SNMMI and IAEA enabling guide: how to set up a theranostics centre. *J Nucl Med.* April 21, 2022 [Epub ahead of print].
2. Arizona Senate Bill 1453 (enacted May 4, 2021), amended Arizona Revised Statutes § 15-1401, 15-1444, 15-1444.01, 15-1469.
3. Beals M. Nurse shortfall could approach half million in three years: research. The Hill website. https://thehill-com.cdn.ampproject.org/c/s/thehill.com/policy/healthcare/3485931-nurse-shortfall-could-approach-half-million-in-three-years-research/amp/. Published May 21, 2022. Accessed July 27, 2022.
4. Scope of practice for the nuclear medicine advanced associate 2009. NMTCB website. https://www.nmtcb.org/documents/resources/NMAA_Scope_of_Practice_2010_SNMMI.pdf. 2010. Accessed July 27, 2022.
5. VR-SECY-20-0005: rulemaking plan for training and experience requirements for unsealed byproduct material (10 CFR Part 35). Nuclear Regulatory Commission website. https://www.nrc.gov/docs/ML2202/ML22020A073.html. Released January 27, 2022. Accessed July 27, 2022.
6. VR-SECY-21-0013: rulemaking plan to establish requirements for rubidium-82 generators and emerging medical technologies. Nuclear Regulatory Commission website. https://www.nrc.gov/docs/ML2200/ML22007A160.html. Released January 13, 2022. Accessed July 27, 2022.
7. SECY-21-0013: rulemaking plan to establish requirements for rubidium-82 generators and emerging medical technologies. U.S. Nuclear Regulatory Commission website. https://www.nrc.gov/docs/ML2026/ML20261H562.pdf. February 9, 2021. Accessed August 18, 2022.
8. Supervision. 10 CFR §35.27 (2022).
9. SNMMI-TS. SNMMI nuclear medicine technologist scope of practice and performance standards, 2nd ed. amazonaws website. s3.amazonaws.com/rdcms-snmmi/files/production/public/NMT%20Scope%20of%20Practice%20and%20Performance%20Standards%202nd%20Ed%2D2022%20Complete%2DApproved%5F6%2D9%2D22.pdf. Approved June 9, 2022. Accessed July 27, 2022.

Radioiodine Therapy in Patient with Differentiated Thyroid Cancer and End-Stage Renal Disease on Maintenance Hemodialysis: Case Report with Review of Literature

Munish Kumar[1], Karthikeyan Subramanian[1], Karan Singh Tanwar[1], Arun Prabhahar[2], Smita Divyaveer[2], Ashwani Sood[1], Bhagwant Rai Mittal[1], and Apurva Sood[1]

[1]*Department of Nuclear Medicine, Post Graduate Institute of Medical Education and Research, Chandigarh, India; and* [2]*Department of Nephrology, Post Graduate Institute of Medical Education and Research, Chandigarh, India*

Surgical resection followed by radioactive iodine (^{131}I) therapy constitutes a standard treatment for differentiated thyroid cancer. ^{131}I is normally excreted through the kidneys, and treatment of patients with end-stage renal disease on hemodialysis requires special attention to the dose of ^{131}I, the timing of dialysis, and radiation safety. We present a case of end-stage renal disease in a postthyroidectomy patient on hemodialysis who required radioactive iodine ablation, and we review the literature.

Key Words: radioiodine therapy; ESRD; thyroid cancer

J Nucl Med Technol 2022; 50:228–232
DOI: 10.2967/jnmt.121.261979

Thyroid carcinoma is the most common endocrine malignancy, and surgical resection followed by radioactive iodine (^{131}I) administration for ablation or therapy is a standard treatment for differentiated thyroid cancer (DTC) (*1*). ^{131}I is administered to a patient and absorbed by the thyroidal tissue, and most of the remaining circulating ^{131}I is cleared by the kidneys. The clearance of circulating ^{131}I is significantly reduced in patients with chronic kidney disease (CKD), resulting in a prolonged effective half-life and potentially resulting in an increased patient radiation exposure, particularly to the bone marrow (*2*). Clearance of ^{131}I in patients with CKD is achieved via dialysis, which can be either peritoneal dialysis or hemodialysis. But the use of dialysis in a patient administered ^{131}I poses various questions, such as those concerning the dose of ^{131}I, the timing of dialysis, and radiation safety precautions. The literature on the treatment of DTC with ^{131}I in patients with CKD consists of only a few case reports, with no formal guidelines. We present a review of the literature followed by a description of our case.

Received Jan. 20, 2021; revision accepted Oct. 26, 2021.
For correspondence or reprints, contact Apurva Sood (sood.apurva26@gmail.com).
Published online Dec. 6, 2021.

REVIEW OF LITERATURE

The incidence of cancers, including DTC, is relatively higher in patients with end-stage renal disease than in patients with normal renal function. A few of the postulated reasons are the increasing use of neck ultrasonography for parathyroid imaging, the higher prevalence of DTC in patients with high parathyroid hormone levels, and the higher survival rate of end-stage renal disease patients undergoing hemodialysis (*3–5*).

CKD causes prolonged excretion of ^{131}I, resulting in comparatively higher side effects such as sialadenitis, xerostomia, and marrow depression (*6*). Therefore, the hemodialysis session needs to be adjusted to ensure maximal thyroidal uptake and a minimal extrathyroidal concentration, thereby maximizing the therapeutic effect and minimizing the short- and long-term radiation effects.

DOSE OF ^{131}I

Two general approaches to determining the dose of ^{131}I in patients with thyroid cancer are either to give the empiric dose or to perform dosimetry. Individual dosimetry for calculation of the maximum tolerable dose of ^{131}I takes into consideration a patient's variables such as the volume of the thyroid remnant, metastases, renal dysfunction, TSH levels, and the dialysis schedule. But the process is cumbersome, and one needs to ensure that no changes in variables occur between dosimetry and therapy.

The American Thyroid Association guidelines recommend use of ^{131}I in patients with intermediate- and high-risk DTC with the intent of ablative treatment, adjuvant treatment, and treatment of metastatic disease (*7*). Howard et al. calculated that the effective half-life of ^{131}I was 4.5 times higher in patients on hemodialysis than in patients with normal renal function, and the investigators reduced the dose of ^{131}I (*8*). This finding was supported by other

investigators too (*9–11*). However, some other investigators recommended increasing the ^{131}I dose, as they found faster clearance of ^{131}I in CKD patients during dialysis sessions and reduced effectiveness of a lower dose (*12,13*).

Another factor important for effective treatment with ^{131}I is the prior stimulation of thyroid cancer cells with raised levels of thyrotropin (thyroid-stimulating hormone [TSH]), which can be achieved either via withdrawal of thyroxine supplementation for 3–4 wk or via intramuscular injection of recombinant human TSH. Vermandel et al., in their study of 6 DTC patients with end-stage renal disease, gave a single 0.9-mg dose of recombinant human TSH 48 h before ^{131}I administration to avoid prolonged and excessive TSH levels instead of giving the standard 2 doses (*10*). Both thyroxine withdrawal and recombinant human TSH are efficient in increasing TSH levels in patients with end-stage renal disease and have no major side effects. Unfortunately, the data are insufficient to comment on whether one method is to be preferred over another.

DIALYSIS

Inorganic iodine is cleared via the kidneys, and in CKD, the ^{131}I excretion is further hampered by increased levels of stable iodine in the body. Clearance of ^{131}I is 4–5 times higher through hemodialysis than renally (*14*), making planning of the dialysis sessions crucial so as to allow ^{131}I to be present in a dose sufficient for it to have a therapeutic effect before it is removed by hemodialysis.

To avoid any emergency need for immediate hemodialysis between the planned timings and to achieve an optimum therapeutic effect for ^{131}I, patients should undergo dialysis immediately before the administration of ^{131}I.

The timing of dialysis after administration of ^{131}I differs in various case reports (Table 1). Ideally, after radioiodine administration, the first dialysis should be done after ^{131}I uptake maximizes in the remnant thyroid tissue or malignant cells. Patients on hemodialysis have shown 6% and 10% uptake of ^{131}I in the thyroid remnant at 24 and 48 h, respectively (*8*). Thus, waiting for 48 h before the first dialysis session seems appropriate, and dialysis before 48 h may lead to undertreatment. However, if the dose is kept the same or increased, the first dialysis session may begin early, which in most case reports is within 24 h after dose administration.

TOXICITY

Vermandel et al. retrospectively calculated the radiation dose to bone marrow in 6 postthyroidectomy patients with renal dysfunction, treated with ^{131}I. The mean estimated dose to the bone marrow was 0.992 Gy for all patients, with no significant hematologic toxicity seen in any of them (*10*). Mello et al. reported a fall in hemoglobin levels after a second treatment of 3,700 MBq (100 mCi) of radioiodine requiring a blood transfusion, though the duration for which the fall in hemoglobin level was seen after ^{131}I was not specified (*12*). Mild sialadenitis and bilateral neck pain below the ears has also been reported after ^{131}I treatment (*9,15*).

RADIATION SAFETY

Hemodialysis can be performed safely after radioiodine administration and should be done with appropriate shielding. In addition to the standard safety precautions that are followed after radioiodine therapy, additional measures were described by other authors, such as providing lead aprons to all personnel attending the patient, maintaining a distance of 2 m between technicians and patients, or having the dialysis technician sit outside the lead-shielded room with the door left ajar (*16,17*). Mello et al. used a lead shield between the patient and the dialysis technician; each member of the technical staff was changed after spending 2 h with the patient (*12*). None of the authors reported any significant exposure to the personnel or contamination of the dialysis machine or room.

Therefore, special precautions should include keeping an adequate distance and shielding between the patient and the technician, providing protective wear to the attending personnel, covering the room with absorbent sheets, and disposing of the dialysate directly into the sewer system. More than one technician and nurse may be used, to reduce the radiation exposure. After 3–4 such dialysis sessions after radioiodine administration, the patient can undergo dialysis in the usual manner.

CONTINUOUS AMBULATORY PERITONEAL DIALYSIS (CAPD)

Experience with using CAPD in such a setting is even more limited. In CAPD, excretion of iodine is a slow, continuous process, at approximately one third the rate of normal renal excretion. Similar to hemodialysis, CAPD requires reduction of the dose of ^{131}I (*18*). Toubert et al. administered 814 MBq (22 mCi) of ^{131}I instead of the usual 3,700-MBq (100 mCi) dose in a patient with follicular thyroid carcinoma (*19*). Wang et al. recommended oral administration of ^{131}I after 1 session of CAPD followed by 3 more courses of CAPD, each performed at an interval of 6 h. The investigators even preferred CAPD to hemodialysis because of the ease with which radiation contamination of the environment could be prevented, as the collected dialysate could be allowed to decay (*20*).

CASE REPORT

The patient was a 35-y-old hypertensive man with CKD secondary to chronic tubulointerstitial nephritis. He had been on alternate-day hemodialysis for the past year and had presented with left-sided neck swelling 6 mo previously. Neck ultrasonography revealed a small, 9 × 7 mm, hypoechoic nodule with microcalcifications in the left lobe of the thyroid gland and multiple enlarged level III and IV cervical lymph nodes on the left side. After inconclusive cytology results for the thyroid nodule, a biopsy sample

TABLE 1
Summary of Literature on Hemodialysis in Patients with CKD After Radioiodine Therapy ($n = 23$)

Study	Age (y)	Cancer	Dose (mCi)*	Time of dialysis	Conclusion of studies
Vermandel (*10*)	67	PTC	60	42, 90 h	Use 30% reduction in dose for ablative and adjuvant treatments; for metastatic disease, dosimetry should be done; first dialysis 42 h after dose
	47	PTC	77, 82		
	63	PTC	61		
	63	PTC	50		
	29	PTC	60		
	71	VC	101		
Daumerie (*11*)	42	PTC	25 in 2 sessions 6 mo apart	2, 5, 7 d	Administer 25% of prescribed activity; first dialysis 24 h after dose
	62	PTC			
	27	PTC			
Jiménez (*16*)	42	PTC	75	Daily for 5 d	Use dosimetry to determine dose; dialysis every day for 5 d
	51	PTC	87		
	34	PTC	120		
Holst (*9*)	40	PTC	98	2, 3, 4 d	Use 21%–28% of dose; dialysis at days 2 and 4
Mello (*12*)	42	PTC	100	41, 98 h	Use dosimetry to determine dose
Sinsakul (*17*)	43	PTC	100	20 or 24 h	Perform dialysis 2–24 h after dose
	56	PTC	157		
Culpepper (*14*)	56	FTC	129	24, 43, 66 h	None
Howard (*8*)	34	PTC	80	—	Administer 22% of empiric dose; dialysis 48 h after dose
Morrish (*13*)	36	PTC	50, 120, 150, 250 over 4 y	24–48 h	Use significantly larger ^{131}I dose; first dialysis 48 h after dose
Magne (*21*)	43	PTC	50	1, 3, 6 d	Increase dose up to 25%
Gallegos-Villalobos (*22*)	51	PTC	100	1, 2 d; administer same dose with normal renal function	Administer same dose with normal renal function; use 2 subsequent dialysis sessions daily
	52	PTC	100		
Bhat (*23*)	49	PTC	50	15, 27, 43 h	None

*1 mCi = 37 MBq.
PTC = papillary thyroid carcinoma; VC = vesicular carcinoma; FTC = follicular thyroid carcinoma.

from the left cervical lymph node revealed metastatic papillary carcinoma of the thyroid. Within 1 mo, he underwent total thyroidectomy with central and lateral neck dissection. Histopathologic examination revealed a multifocal papillary carcinoma of the thyroid (maximum tumor dimension, ~2.3 cm), with lymphovascular invasion and without extrathyroidal extension. Twenty-six of the 42 lymph nodes dissected were positive for metastatic disease (T2 N2b Mx), putting him in an intermediate risk category according to the American Thyroid Association (*7*).

For preparation, the patient was asked to withhold the thyroxine supplementation for 4 wk. His TSH level rose to 50 μIU/mL, and his stimulated thyroglobulin level was 132 ng/mL, with normal antithyroglobulin levels. A low-dose whole-body ^{131}I scan done with 44.4 MBq (1.2 mCi) showed that the thyroid bed tracer uptake was likely a thyroid remnant (Supplemental Fig. 1; supplemental materials are available at http://jnmt.snmjournals.org).

A patient with normal renal function in an intermediate risk category would have received a dose of 3,700 MBq (100 mCi) of ^{131}I for ablation of the thyroid remnant and as adjuvant treatment. For our patient, after a literature review and a discussion by the tumor board, the dose of ^{131}I was reduced to 50% (1,850 MBq [50 mCi]) to maximize the effect and reduce the radiation exposure to normal tissues.

On the day of therapy, the patient underwent dialysis in the morning and received a ^{131}I dose of 1,850 MBq (50 mCi) after 2 h (day 0). This was followed by dialysis at 48, 72, and 96 h. The whole-body radioactivity was measured at the stomach level with the patient standing, using an ionization chamber-based gun monitor (Ram Ion; Rotem Industries) at a distance of 1 m. The whole-body radioactivity was measured at various time intervals and after each session of dialysis (Supplemental Fig. 2). A reduction in whole-body radioactivity by 69% was achieved after the first dialysis session. The findings were consistent with the literature, which showed clearance in the range of 50%–80% (*9,16*).

A posttherapy whole-body iodine scan after 5 d showed tracer uptake in the thyroid bed region—the same region as seen on the low-dose diagnostic scan. The patient was discharged 4 d after radioiodine administration, with an exposure rate of about 3 μSv/h measured at the stomach level at a distance of 1 m. The patient remained asymptomatic on follow-up; at 6 wk after ^{131}I therapy, there was no change from baseline in his white blood cell count (5,300 vs. 5,240 cells/mm^3) or hemoglobin level (8.2 vs. 8.4 g/dL).

Under the supervision of a radiation safety officer, the patient underwent dialysis in the nephrology department at the end of the day when there were no other patients in the room, because our hospital did not have a portable dialysis facility or a separate dialysis room with shielding. (Under normal conditions, more than 4 patients at a time undergo dialysis in the same room.) Care was taken to avoid any blood or fluid spills and contamination. The floor near the patient bed was covered with absorbent sheets. During the 4-h hemodialysis procedure, the technician wore all the necessary protective clothing (shoe covers, gloves, face mask, and lead apron). All personnel attending the patient, including the dialysis technician, were given a pocket dosimeter (Rad-60S; Rados; Mirion Technology) for real-time monitoring of the exposure rate. The dialyzer, blood lines, absorbent sheets, and linen used during the procedure were collected in polyethylene sheets and allowed to decay in the radioactive waste storage room of the isolated ^{131}I therapy ward. The dialysate drain line was connected to the sewer system. After the dialysis, the hemodialysis machine was put on rinsing mode to eliminate any ^{131}I contamination, though no contamination was observed in the hemodialysis machine when checked with a Geiger–Müller counter (Ram Gene-1; Rotem Industries). The total dose received by the patient's attendant and dialysis technician was 37 and 16 μSv, respectively—far below the permissible levels.

The patient showed a decline in stimulated serum thyroglobulin level to 5 ng/mL, with a TSH level of 60 μIU/mL, after 6 mo of follow-up. The low-dose ^{131}I scan showed resolution of the previous tracer uptake in the thyroid bed (Supplemental Fig. 3), and the patient was followed on suppressive thyroxine doses, with a target TSH level of 0.1–0.5 IU/mL.

CONCLUSION

Treatment of thyroid cancer with radioiodine therapy in patients with renal dysfunction on maintenance hemodialysis can be performed safely by following a standardized radiation safety protocol and with the combined efforts and coordination of the nuclear medicine physician, nephrologist, radiation safety officer, and dialysis team. The literature on the treatment of DTC with ^{131}I in patients with CKD consists of only a few case reports with variable experiences and recommendations. Therefore, more literature and systematic prospective studies are required to formulate standard procedure guidelines.

DISCLOSURE

No potential conflict of interest relevant to this article was reported.

KEY POINTS

QUESTION: What parameters can be suggested for dose requirements, timing of dialysis, and special radiation safety protocols in CKD patients requiring radioactive iodine?

PERTINENT FINDINGS: A multidisciplinary approach involving the endocrinologist, nuclear medicine physician, nephrologist, radiation safety team, and dialysis team is required for management of these cases.

IMPLICATIONS FOR PATIENT CARE: Fifty percent of an empiric ^{131}I dose followed by dialysis at 48, 72, and 96 h was used in our intermediate-risk DTC patient on maintenance hemodialysis.

REFERENCES

1. DeGroot LJ, Kaplan EL, McCormick M, et al. Natural history, treatment, and course of papillary thyroid carcinoma. *J Clin Endocrinol Metab.* 1990;71:414–424.
2. Cavalieri RR. Iodine metabolism and thyroid physiology: current concepts. *Thyroid.* 1997;7:177–181.
3. Maisonneuve P, Agodoa L, Gellert R, et al. Cancer in patients on dialysis for end-stage renal disease: an international collaborative study. *Lancet.* 1999;354:93–99.
4. Stengel B. Chronic kidney disease and cancer: a troubling connection. *J Nephrol.* 2010;23:253–262.
5. Tarrass F, Daki S, Benjelloun M, et al. Synchronous papillary thyroid carcinoma and secondary hyperparathyroidism: report of cases and review of the literature. *Oral Oncol Extra.* 2005;41:74–76.
6. Luster M, Clarke SE, Dietlein M, et al. Guidelines for radioiodine therapy of differentiated thyroid cancer. *Eur J Nucl Med Mol Imaging.* 2008;35:1941–1959.
7. Haugen BR, Alexander EK, Bible KC, et al. 2015 American Thyroid Association management guidelines for adult patients with thyroid nodules and differentiated thyroid cancer: the American Thyroid Association Guidelines task force on thyroid nodules and differentiated thyroid cancer. *Thyroid.* 2016;26:1–133.
8. Howard N, Glasser M. Iodine 131 ablation therapy for a patient on maintenance haemodialysis. *Br J Radiol.* 1981;54:259.
9. Holst JP, Burman KD, Atkins F, et al. Radioiodine therapy for thyroid cancer and hyperthyroidism in patients with end-stage renal disease on hemodialysis. *Thyroid.* 2005;15:1321–1331.
10. Vermandel M, Debruyne P, Beron A, et al. Management of patients with renal failure undergoing dialysis during ^{131}I therapy for thyroid cancer. *J Nucl Med.* 2020;61:1161–1170.
11. Daumerie C, Vynckier S, Caussin J, et al. Radioiodine treatment of thyroid carcinoma in patients on maintenance hemodialysis. *Thyroid.* 1996;6:301–304.

12. Mello AM, Isaacs R, Petersen J, et al. Management of thyroid papillary carcinoma with radioiodine in a patient with end stage renal disease on hemodialysis. *Clin Nucl Med.* 1994;19:776–781.
13. Morrish DW, Filipow LJ, McEwan AJ, et al. ^{131}I treatment of thyroid papillary carcinoma in a patient with renal failure. *Cancer.* 1990;66:2509–2513.
14. Culpepper RM, Hirsch JI, Fratkin MJ. Clearance of ^{131}I by hemodialysis. *Clin Nephrol.* 1992;38:110–114.
15. Yeyin N, Cavdar I, Uslu L, et al. Effects of hemodialysis on iodine-131 biokinetics in thyroid carcinoma patients with end-stage chronic renal failure. *Nucl Med Commun.* 2016;37:283–287.
16. Jiménez RG, Moreno AS, Gonzalez EN, et al. Iodine-131 treatment of thyroid papillary carcinoma in patients undergoing dialysis for chronic renal failure: a dosimetric method. *Thyroid.* 2001;11:1031–1034.
17. Sinsakul M, Ali A. Radioactive ^{131}I use in end-stage renal disease: nightmare or nuisance? *Semin Dial.* 2004;17:53–56.
18. Kaptein EM, Levenson H, Siegel ME, et al. Radioiodine dosimetry in patients with end-stage renal disease receiving continuous ambulatory peritoneal dialysis therapy. *J Clin Endocrinol Metab.* 2000;85:3058–3064.
19. Toubert ME, Michel C, Metivier F, et al. Iodine-131 ablation therapy for a patient receiving peritoneal dialysis. *Clin Nucl Med.* 2001;26:302–305.
20. Wang TH, Lee CH, Tseng LM, et al. The management of well-differentiated thyroid cancer with end-stage renal disease. *Endocrine.* 2003;21:227–231.
21. Magné N, Magné J, Bracco J, et al. Disposition of radioiodine ^{131}I therapy for thyroid carcinoma in a patient with severely impaired renal function on chronic dialysis: a case report. *Jpn J Clin Oncol.* 2002;32:202–205.
22. Gallegos-Villalobos A, García-López F, Escalada C, et al. Use of radioactive iodine ^{131}I and monitoring of radioactivity in patients with chronic kidney disease on haemodialysis. *Nefrologia.* 2014;34:317–322.
23. Bhat M, Mozzor M, Chugh S, et al. Dosing of radioactive iodine in end-stage renal disease patient with thyroid cancer. *Endocrinol Diabetes Metab Case Rep.* 2017;2017:17–0111.

Analysis of Residence Time, Effective Half-Life, and Internal Dosimetry Before Radioiodine Therapy

Caio Vinicius Oliveira, Tatiane Sabriela Cagol Camozzato, Patricia Fernanda Dorow, and Jéssica Pasqueta

Federal Institute of Education, Science, and Technology of Santa Catarina, Florianópolis, Santa Catarina, Brazil

Radioiodine therapy has been widely used for ablation of remnant tissue after surgical treatment of differentiated thyroid carcinoma (DTC). Internal dosimetry provides a new approach to choosing the administered activity—an approach that considers the distribution and retention of ^{131}I individually per patient. This study used clinical techniques of internal dosimetry to assess the accumulated activity, internal bone marrow dosimetry, and effective half-life in patients undergoing treatment for DTC. **Methods:** This was a quantitative, retrospective study analyzing diagnostic documents and images. The internal dosimetry method calculated the dose absorbed by the bone marrow per administered activity of ^{131}I. Calculation of the absorbed dose took into account the accumulated activity, which was obtained through measurements of whole-body images acquired at 4 intervals over 5 d. **Results:** The median dose absorbed by the bone marrow per administered activity was 0.117 mGy/MBq (range, 0.043–0.152 mGy/MBq). The median whole-body residence time was 22.0 h (range, 12.6–39.4 h). The median effective half-life was 15.6 h (range, 7.6–28.2 h). **Conclusion:** Internal dosimetry provides information relevant to safe dose limits for DTC radioiodine therapy, especially in advanced cases of the disease for which greater activities may be necessary.

Key Words: nuclear medicine; dosimetry; radiometry; thyroid gland neoplasms; iodine radioisotopes

J Nucl Med Technol 2022; 50:233–239
DOI: 10.2967/jnmt.121.263502

Thyroid cancer is the most common cancer of the head and neck region and affects 3 times as many women as men. The most indicated treatment for differentiated thyroid carcinoma (DTC) is partial or total thyroidectomy, complemented by radioactive iodine therapy (*1*). This treatment is indicated because DTC and its metastases maintain the biologic characteristics of a healthy thyroid, including the expression of sodium iodide transport protein, the main cell responsible for specific iodine uptake (*2*). Thus, radioiodine therapy is indicated for ablation of remaining tissue that is not resected or is incompletely resected. For thyroid disease, ^{131}I-NaI is currently the most common radionuclide treatment (*3*).

Received Nov. 30, 2021; revision accepted Jun. 8, 2022.
For correspondence or reprints, contact Tatiane Sabriela Cagol Camozzato (tatiane@ifsc.edu.br).
Published online Jun. 14, 2022.

In ablation of remnant thyroid tissue after surgery, the activity of ^{131}I-NaI usually prescribed is between 1 and 5 GBq in a single administration and may be higher in more advanced cases of the disease (*2*). These amounts of activity have been selected empirically, with no consensus, varying between authors and nuclear medicine centers that perform this therapeutic procedure (*4*).

When fixed activities are considered, the accumulated activity, and hence the absorbed dose, is not thought to change considerably from patient to patient. The characteristics that alter iodine distribution are age, sex, renal function, and injury extent, among others (*5*). The administered activity is individualized through therapeutic planning using dosimetric procedures. Internal dosimetry provides information on the distribution of iodine in a patient's body, allowing estimation of the activity to be used and preventing the biologic effects of ionizing radiation (*6*).

This study assessed accumulated activity, internal bone marrow dosimetry, and effective half-life using clinical internal dosimetry techniques in patients undergoing treatment for DTC.

MATERIALS AND METHODS

The study retrospectively assessed pretherapeutic internal dosimetry in 5 patients who were diagnosed with DTC and were undergoing total or quasi-total thyroidectomy. Dosimetry was used as a strategy to plan radioiodine therapy for ablation of remnant tissue and metastases. The study was conducted in a private nuclear medicine service in southern Brazil. The research was submitted to a Brazilian ethics committee for evaluation, receiving approval 3.988.505. Written informed consent was obtained from each patient before participation in the study. Three internal dosimetry techniques were available for radioiodine therapy, one or all of which could be chosen, depending on the indication: bone marrow–based dosimetry, lung-based dosimetry, or organ-based dosimetry. All used diagnostic images to determine the accumulated activity.

Preparation of patients for dosimetry reproduced preparation for therapy: restriction of foods that contain iodine, and suspension of medications and preparations that contain iodine (up to 4 wk). In 4 cases, hormonal suspension was performed, and in one case, recombinant human thyroid-stimulating hormone was used. A choice between the 2 methods was needed because of the need to reproduce the anticipated therapy method. Some authors have shown that residence time can be different between hormone withdrawal and the use of recombinant human thyroid-stimulating hormone (*7,8*).

Acquisition of Whole-Body Images

An oral ^{131}I-NaI solution with 74 MBq of activity was administered. The activity was measured with a CRC-15R radioisotope dose calibrator (Capintec, Inc.). Afterward, whole-body conjugate images were acquired using a Symbia T2 SPECT/CT γ-camera (Siemens). The equipment has 2 detectors with a 15.875-mm (5/8 in) NaI:Tl crystal and is equipped with high-energy collimators, which are required because of the photon energy of ^{131}I (364 keV). The acquisition mode was a whole-body scan, and the table speed was 12 cm/min.

Four images were acquired, one each at 2, 6, 48, and 120 h after tracer administration, with the patient not emptying the bladder before the first image. Thus, the whole-body count of the 2-h image was considered to be 100% of the administered activity.

For image acquisition, the triple-energy-window method was used to correct the scatter due to ^{131}I γ-radiation energy and use of a high-energy collimator (*9,10*). With 3 energy windows simultaneously, the 15% main window was centered on the 364-keV (range, 336.7–391.3 keV) photopeak and 2 windows of 6%, one below and one above the main window, at 314.9–336.7 keV and 391.3–413.1 keV, respectively.

Data Processing

The acquired images were exported in DICOM format and assessed in ImageJ processing software (National Institutes of Health). Each acquired image series, per interval, consisted of 6 images: anterior and posterior, scattering in the inferior anterior and posterior windows, and scattering in the superior anterior and posterior windows. In each image, a region of interest was drawn outlining the patient's whole body. For the region of interest, the total counts were measured and the values were recorded as $C_{pp,ant,}$ $C_{pp,post,}$ $C_{ls,ant,}$ $C_{ls,post,}$ $C_{us,ant,}$ and $C_{us,post}$ (where C is total counts, *ant* is anterior, *post* is posterior, *pp* is photopeak, *ls* is lower scatter window, and *us* is upper scatter window) as shown in Figure 1.

The triple-energy-window scatter fraction determination is described in Equation 1, considering the measured counts for images with the energy window shifted below (C_{ls}) and above (C_{us}) (*9*):

$$C_{\text{scatter}} = \left(\frac{C_{ls}}{w_{ls}} + \frac{C_{us}}{w_{us}}\right)\frac{W_{pp}}{2}, \qquad \text{Eq. 1}$$

where W_{pp} is the width centered on the photopeak window, W_{us} is the width of the lower window, and W_{up} is the width of the upper window.

The total count is the result for the image counts, with the main energy window (C_{pp}) subtracted from the total scattering (C_{scatter}) (*2*). Both counts are the geometric mean of the anterior and posterior projections:

$$C_{\text{total}} = \sqrt{C_{pp,\,ant}\cdot C_{pp,\,post}} - \sqrt{C_{\text{scatter},\,ant}\cdot C_{\text{scatter},\,post}}\,. \qquad \text{Eq. 2}$$

Accumulated Activity Determination

The total counts for each image set (at 2, 6, 48, and 120 h) were plotted on a chart, and the time–activity curve was determined. The curve adjustment results in an equation of the double-exponential format:

$$\text{Activity}(t) = Ae^{-at} + Be^{-bt}, \qquad \text{Eq. 3}$$

where *A, B, a,* and *b* are curve adjustment coefficients; *t* is time; and e is Euler's number (a numerical constant).

The accumulated activity ($\tilde{A}$) is the total number of disintegrations over a period and is determined by activity integration by time (Eq. 4). In the activity chart by time, the accumulated activity is determined by the area below the curve:

$$\tilde{A} = \int_0^\infty A(t)\,dt = \int_0^\infty Ae^{-at} + Be^{-bt}\,dt. \qquad \text{Eq. 4}$$

Alternatively, the concept of residence time can be used, as well as the accumulated activity per administered activity.

Absorbed Dose Estimation

The absorbed dose to the bone marrow is calculated by an adaptation of the European Association of Nuclear Medicine protocol (*11*) in which a sample of blood is not used. The assessed compartment is blood, considering that the activity concentration in blood and bone marrow is similar (*12*). For this symmetric approach, 2 components are assessed: blood self-irradiation and blood irradiation by ^{131}I concentration in the whole body. The absorbed dose to the bone marrow per unit of activity administered is defined by the sum of these 2 components:

$$\frac{D_{\text{blood}}}{A_0} = S_{\text{blood}\leftarrow\text{blood}}\cdot\tau_{\text{blood}}(\text{h}) + S_{\text{blood}\leftarrow\text{body}}\cdot\tau_{\text{body}}(\text{h}), \qquad \text{Eq. 5}$$

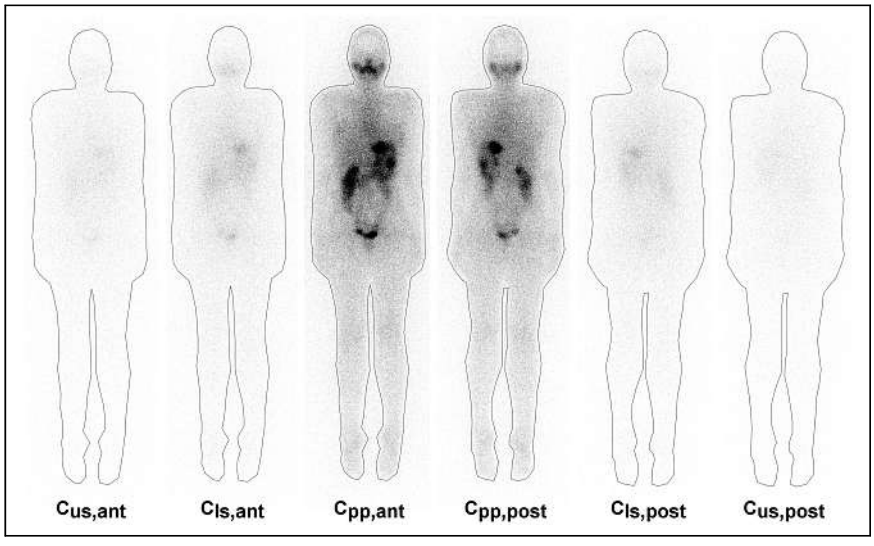

FIGURE 1. Measurement of regions of interest of set of anterior and posterior conjugate images and their respective images for scattered radiation correction.

where D is the absorbed dose, A_0 is the administered activity, S is the mean absorbed dose per unit of accumulated activity, and τ is residence time. The $S_{\text{blood}\leftarrow\text{blood}}$ value, using β-radiation decay, is 108 Gy·mL/GBq·h. The component for the dose coming from the whole body, $S_{\text{blood}\leftarrow\text{body}}$, is $0.0188\cdot m^{-2/3}$ Gy/GBq·h, which depends on the body mass (m) (*11*). S values replaced in Equation 5 are described in Equation 6:

$$\frac{D_{\text{blood}}}{A_0}\left(\frac{\text{Gy}}{\text{GBq}}\right) = 108\left(\frac{\text{Gy}}{\text{GBq}\cdot\text{h}}\right)\cdot\tau_{\text{mL blood}}(\text{h}) + \frac{0.0188\left(\frac{\text{Gy}\cdot\text{kg}}{\text{GBq}\cdot\text{h}}\right)}{m^{2/3}\,(\text{kg})}\cdot\tau_{\text{body}}(\text{h}). \qquad \text{Eq. 6}$$

The first component, $D_{\text{blood}\leftarrow\text{blood}}$, is traditionally measured by the blood sample

density counts over time (*11*). In 2009, Hänscheid et al. (*13*), through the considerations initially made by Thomas et al. in 1993 (*14*), proposed determination of $D_{\text{blood}\leftarrow\text{blood}}$ exclusively through analysis of body residence time, that is, blood residence time is determined indirectly. In their studies, blood residence time represents 14% ± 3% of body residence time. Therefore, the proposed relationship can be expressed as follows:

$$\tau_{\text{ml blood}}(\text{h}) = \frac{0.14}{BV\ (\text{mL})} \cdot \tau_{\text{body}}(\text{h}), \qquad \text{Eq. 7}$$

BV, the blood volume in milliliters, is expressed in Equation 8 for men and in Equation 9 for women (*15*):

$$BV = 31.9 \cdot h + 26.3 \cdot m - 2,402 \qquad \text{Eq. 8}$$

$$BV = 56.9 \cdot h + 14.1 \cdot m - 6,460, \qquad \text{Eq. 9}$$

where h is height in centimeters and m is mass in kilograms.

Equations 6 and 7 can be combined and expressed as Equation 10, which was used to determine the total absorbed blood dose:

$$\frac{D_{\text{blood}}}{A_0}\left(\frac{\text{Gy}}{\text{GBq}}\right) = \left[\frac{15.12\ \left(\frac{\text{Gy}\cdot\text{mL}}{\text{GBq}\cdot\text{h}}\right)}{BV\ (\text{mL})} + \frac{0.0188\ \left(\frac{\text{Gy}\cdot\text{kg}}{\text{GBq}\cdot\text{h}}\right)}{m^{2/3}\ (\text{kg})}\right] \cdot \tau_{\text{body}}(\text{h}). \qquad \text{Eq. 10}$$

Comparatively, D_{blood}/A_0 (dose in blood per administered activity) was calculated using OLINDA/EXM, version 1.0 (Vanderbilt University). In the software, ^{131}I was selected as the radionuclide, and the phantom was chosen between a woman and a man. In biokinetic data entry, body residence time was used for the whole body (total body/remainder of body), and blood residence time was used for the bone marrow (red marrow); however, because blood residence time was calculated to 1 mL, it was necessary for it to be multiplied by the organ mass. For the phantom used, the bone marrow mass was 1,300 and 1,120 g for women and men, respectively.

Maximum Activity

Bone Marrow. The maximum activity is determined by Equation 11. A maximum dose of 2 Gy was used, considering the bone marrow as the target organ. Bone marrow is the critical organ in radionuclide therapy. In dosimetry studies, alterations in the hematopoietic system have been observed in a subgroup that received doses higher than 2 Gy to the bone marrow (*16*).

$$A_{\max}(\text{GBq}) = \frac{2\ (\text{Gy})}{D\ (\text{Gy/GBq})}. \qquad \text{Eq. 11}$$

The maximum activity was also evaluated for a maximum dose of 1.3 Gy, considering the uncertainties in the measurement method without the use of a blood sample (*13*).

Lung. When there was diffuse pulmonary metastasis, the maximum administered activity was determined with consideration that lung activity after 48 h is not higher than 2.96 GBq (*17–19*). A region of interest was drawn for the lungs, and count density was measured in the conjugated images and applied to the scattering correction as the whole-body region of interest. Count density in the lungs after 48 h ($C_{\text{lung,48 h}}$) was compared with the whole-body density counts of the 2-h image ($C_{\text{total,2 h}}$):

$$C_{\text{lung, relative}} = \frac{C_{\text{lung,48 h}}}{C_{\text{total,2 h}}}. \qquad \text{Eq. 12}$$

The maximum activity of administered ^{131}I-NaI to prevent radiation effects is determined as follows:

$$A_{\max}(\text{GBq}) = \frac{2.96\ (\text{GBq})}{C_{\text{lung,relative}}}. \qquad \text{Eq. 13}$$

Effective Half-Life

The activity concentration in a patient's body depends on the physical and biologic half-life of ^{131}I. The physical half-life is 8.02 d, whereas the biologic half-life varies with the individual, depending on multiple variables. Through analysis of accumulated activity, the activity curve as a function of time was calculated for each patient.

Organ-Based Dosimetry

To compare the bone marrow toxicity limit with the activity needed to treat a thyroid remnant, one patient was selected for dosimetry based on the injury. The absorbed dose in the organ was compared with the administered activity using the total-volume dosimetry method (*20,21*).

The SPECT/CT acquisition for dosimetry used 60 projections (30/detector), 6 steps, 60 s, a 128 × 128 matrix, and a triple-energy window. Iterative ordered-subsets expectation maximization was used for reconstruction, with 10 iterations and 5 subsets.

Partial-volume effect correction was experimentally determined using an image-quality International Electrotechnical Commission 61675-1 simulator. Spheres that were 28.7, 16.8, 8.6, 3.6, 2.1, and 1.1 mL in volume were filled with a constant ^{131}I concentration, and the recovery coefficient was projected. The recovery coefficient determines the correlation between differences in the actual and measured values of both activity and volume:

$$RC = \frac{[A]_{\text{measured}}}{[A]_{\text{actual}}} = \frac{v_0}{v_a} = \frac{c_m}{c_0}, \qquad \text{Eq. 14}$$

where RC = recovery coefficient, $[A]_{\text{measured}}$ is the measured activity concentration, $[A]_{\text{actual}}$ is the actual activity concentration, v_0 is the object's actual volume, v_a is the apparent volume, c_m is the measured count density, and c_0 is the actual count density. The apparent volume was measured in the image, with a volume of interest positioned on the structure with a threshold of 5%, and determined as follows:

$$v_a = v_{vx}\ \frac{C}{c_{\max}}, \qquad \text{Eq. 15}$$

TABLE 1
Variables for Internal Dosimetry Cases

Patient no.	Sex	Age (y)	Height (cm)	Weight (kg)	Body mass index	Blood volume (mL)	Residence time per mL of blood (h)	
							Body	Blood
1	F	50	161	59	22.8	3,532.8	22.1	0.00088
2	M	71	182	76	22.9	5,402.6	39.4	0.00102
3	M	36	187	95	27.2	6,061.8	12.6	0.00029
4	M	28	178	82	25.9	5,432.8	19.3	0.00050
5	F	29	165	57	20.9	3,732.2	22.0	0.00083

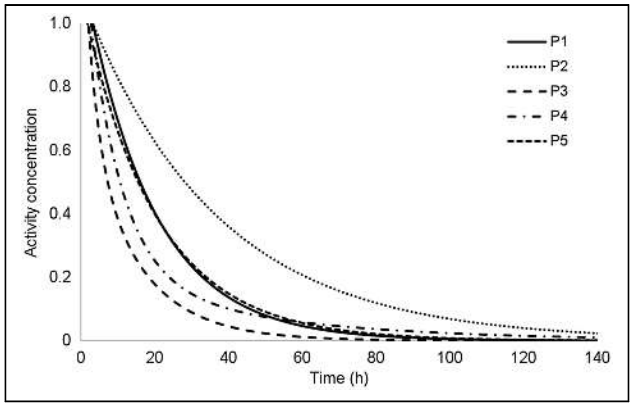

FIGURE 2. Time–activity fitted curves for assessed patients. P1–P5 = patients 1–5.

where v_{vx} is the voxel volume, C is the count density measured in volume of interest, and C_{max} is the highest-intensity voxel count density.

The accumulated activity is determined by assessing the ^{131}I concentration over time by means of a sequence of SPECT images used in bone marrow dosimetry. The activity for each image series is determined as follows:

$$A_i = \frac{C_{30}}{\varepsilon f_{30}}, \quad \text{Eq. 16}$$

where A_i is the activity measured for each interval, C is the total count with a threshold of 30% of the image, f_{30} is the measurement correction factor in a threshold of 30% to 5%, and ε is the activity calibration factor per count (MBq/count) experimentally determined for imaging equipment with a volume with known activity. f_{30} is needed to use a 30% threshold for target area measurement, avoiding the interference of background radiation in the target volume.

Equation 17 describes the absorbed dose in the sphere, as determined by the product sphere residence time. S value is calculated for the actual sphere volume corrected by tissue density: $S = 0.110 \cdot v_{\text{sphere}}^{-0.974}$ Gy/MBq·h and $\rho = 1.05$ g/cm^3 (*20*).

$$\frac{D}{A_0} = \tau_{\text{sphere}} \cdot S_{\text{sphere}\leftarrow\text{sphere}}(v_{\text{sphere}})/\rho_{\text{thyroid}} \quad \text{Eq. 17}$$

$$v_{\text{sphere}} = RC_{v_a} \cdot v_a. \quad \text{Eq. 18}$$

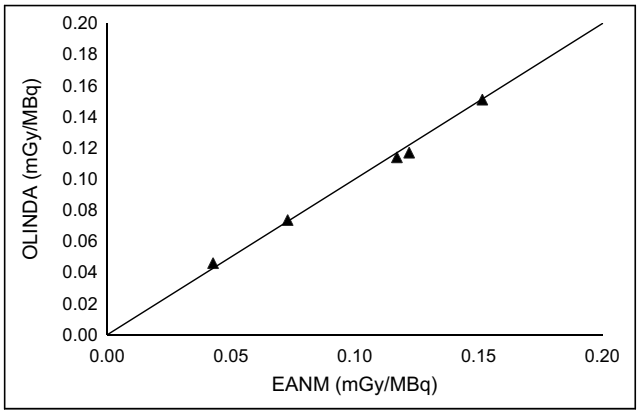

FIGURE 3. Comparison of absorbed dose by activity calculated by OLINDA/EXM and EANM.

TABLE 2
Maximum Activity for Assessed Case Group

Patient no.	Dose in blood per administered activity (mGy/MBq)	Maximum activity (GBq)	
		Limit, 2 Gy	Limit, 1.3 Gy
1	0.122	16.39	10.66
2	0.152	13.20	8.58
3	0.043	46.72	30.37
4	0.073	27.42	17.82
5	0.117	17.09	11.11

RESULTS

Internal dosimetry had, as an indication, cases of advanced disease and cases in retreatment with suspicion or confirmation of metastases. Table 1 lists the sex, age, height, mass, body mass index, and estimated body blood volume of the assessed group, as well as total-body residence time and blood residence time. The residence time for the whole body was a median of 22.0 h.

Count density behavior over time is illustrated in Figure 1. Figure 2 illustrates the time–activity curve of the assessed group. Curve adjustment coefficients were obtained through the fit-data application of OLINDA/EXM.

Bone Marrow–Based Dosimetry

Dose in blood per administered activity was determined with body residence time and blood residence time using an adaptation of the European Association of Nuclear Medicine protocol without blood sampling (Eq. 10) and OLINDA/EXM. The methods did not significantly differ when analyzed by a paired *t* test ($P = 0.564$).

Figure 3 compares OLINDA/EXM and the European Association of Nuclear Medicine protocol. The individual and maximum doses in blood per administered activity, considering red bone marrow toxicity of 2 Gy and 1.3 Gy, are expressed in Table 2.

Table 3 presents the time required for decay of half or a quarter of the initial activity, both effective and biologic. The median time of the first effective half-life was 15.6 h (range, 7.6–28.2 h), and the second half-life was 12.8 h (range,

TABLE 3
Effective and Biologic Times for Half and Quarter of Initial Activity of ^{131}I

Patient no.	Effective (h)		Biologic (h)	
	Half	Quarter	Half	Quarter
1	16.1	28.9	17.6	31.3
2	28.2	53.1	33	61.6
3	7.6	13.1	7.9	13.6
4	12.5	23.2	13.3	24.7
5	15.6	29.5	16.9	32

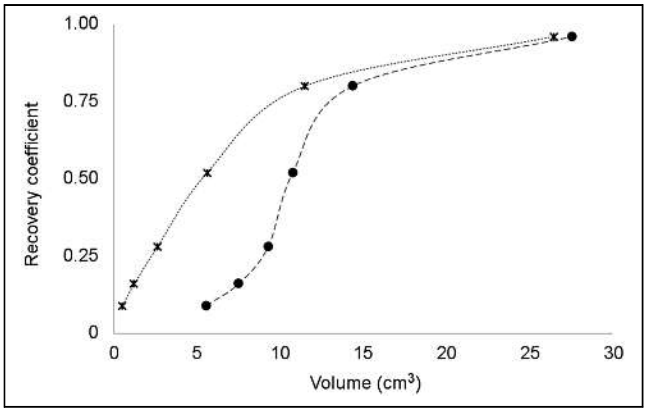

FIGURE 4. Recovery coefficient of definitive experiment. ● = apparent volume; × = true sphere volume.

5.5–24.9 h). Patient 3 was prepared with recombinant human thyroid-stimulating hormone.

Lung Dosimetry

One patient had pulmonary metastasis. Relative count density in the lungs was 0.0246; that is, after 48 h, 2.46% of the iodine concentration was retained in the lung compared with the whole-body measurement measured in the 2-h image. Therefore, the maximum calculated activity was 120.5 GBq. Maximum activity based on dose limits in bone marrow and lung were compared, with the lowest prevailing. The dosimetry for this case, considering the dose limit of 2 Gy in the bone marrow, determined the maximum activity of 27.4 GBq. Thus, the limit for the bone marrow was prioritized.

Organ-Based Dosimetry

The activity ratio measured by the actual activity designated as recovery coefficient is expressed in Figure 4.

The dosimetry for one patient (patient 5) in the studied group was assessed. The injury was characterized as remaining tissue in the thyroid bed, illustrated in Figure 5A. The volume was estimated at 1.9 cm^3. Factor f_{30} was determined at 0.59 for a point source illustrated in Figure 5A, and the equipment ε calibration factor was calculated at 15,604 counts/MBq. The residence time was calculated at 0.995 h; the time–activity curve is expressed in Figure 5B. Through residence time, volume, and S value, the dose absorbed by the organ per unit of ^{131}I administered was 0.0584 Gy/MBq, calculated by Equation 17. Considering the dose of 300 Gy necessary to ablate the remaining thyroid tissue, proposed by Maxon et al. (*22*), the administered activity required to reach this dose threshold would be 4.89 GBq. The maximum ^{131}I activity to prevent bone marrow toxicity in this patient was 11.11 GBq (Table 3).

Determination of small volumes is limited by the spatial resolution of the system. The spatial resolution at full width at half maximum was 13.6 mm, obtained by axial reconstruction of a point source of ^{131}I. Figure 6 shows the result from the acquisition of a cylinder with a volume of 22 mL and 0.74 MBq of ^{131}I with the described protocol. The apparent volume was 23.47 mL, with a difference of 6.3% from the actual volume. In Figure 6, the smallest volume of interest (VOI) represents the actual volume, and central VOI and biggest VOI are the apparent volumes measured with thresholds of 5% and 30%, respectively.

DISCUSSION

Preparation for dosimetry should be the same as for therapy to ensure reproducibility of ^{131}I-NaI distribution (*11*). The patient must not have undergone imaging examinations with the use of iodinated contrast for a period of 6–8 wk (*23*). The patient's metabolic status must be the same for dosimetry as for therapy, as metabolic status affects renal function and, thus, clearance rate and residence time (*19,24*).

The activity for dosimetry is small in comparison with the activity for therapy and must not be enough to alter the tumor's ability to capture and retain iodine, called stunning. Studies show that even small activities can induce stunning (*25*). Activity should be limited to 4 Gy in the remaining thyroid tissue to avoid this effect. The ^{131}I activity for the recommended diagnostic imaging is 10–20 MBq (*19,26*). The activity in this study was 74 MBq. Activity can be reduced to prevent stunning; however, it is necessary to reduce the image scanning speed so that the counting rate is not reduced, making quantification impossible.

When acquiring the 4 series of whole-body images, it is necessary to guarantee the same geometry in each series as in the previous series. The table elevation and detector distance must be maintained in each series. Patient positioning should be as identical as possible between series, and the patient's whole body must be in the detector field of view (*11*). The automatic contouring systems of the equipment must be deactivated. Use of auxiliary straps to immobilize the arms close to the body is important to prevent undesirable movements.

Intervals between acquisitions must be consistent with the physical and biologic half-lives of iodine. The activity concentration in the image at 2 h is considered the maximum (100%) and is used as a reference for other measurements (*6*). Therefore, the patient should not urinate from the time

FIGURE 5. (A) From left to right: axial, sagittal, and coronal SPECT/CT reconstruction of remaining thyroid tissue (arrows). (B) Activity concentration function in organ target.

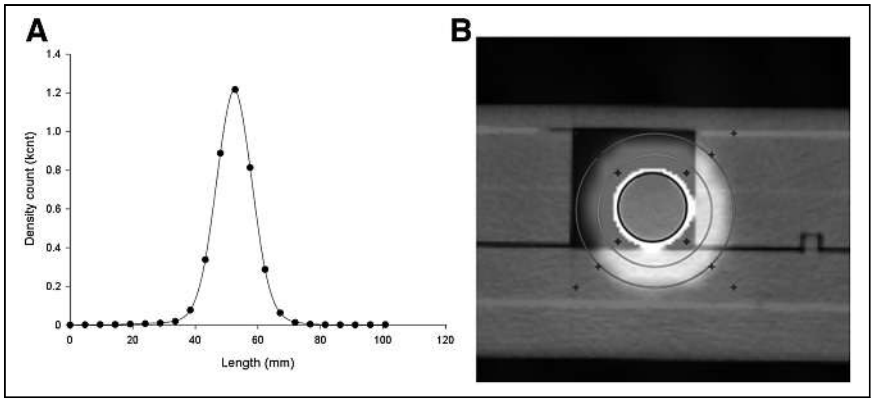

FIGURE 6. (A) Scattering-point function of SPECT of a cylinder of 22 mL filled with ^{131}I. (B) Comparison of apparent and actual volume. kcnt = kilocount.

of iodine administration until the end of this 2-h acquisition. From the samples assessed, significant radioactive material was found to be eliminated in the first hours. The mean activity concentration at 6 h was 78% ± 15%.

Tissue avid for ^{131}I retained considerable iodine at 48 h, whereas the other tissues had almost completely eliminated the iodine. This difference provides contrast between these tissues, with better visualization of the structures. Acquisition at this interval allows assessment of pulmonary metastasis. The delayed image at 120 h contributed to adjustment of the accumulated activity curve. This image commonly shows accumulation of less than 2% of the initial activity. This interval can be adopted with 96-h imaging; however, if the accumulation is higher than 5%, 144-h imaging must be performed (*11*).

When there is diffuse pulmonary metastasis, the absorbed dose in the lung should be assessed. Pulmonary dosimetry plays an important role in preventing pulmonary fibrosis (*19*). On lung dosimetry studies, the ^{131}I activity in the lung should be less than 2.96 GBq after 48 h. Higher activities can result in lung doses that exceed the limit for radiotoxicity effects (*17–19*). Thus, the image previously acquired within 48 h is used to calculate the maximum activity and maintain the dose limits in the lungs.

Because blood residence time is estimated through whole-body residence time, for which blood samples are not analyzed, it is necessary to consider the uncertainties in the calculations. Hänscheid et al. (*13*) proposed a conservative approach to estimating maximum activity. Blood residence time represents 14% ± 3% of body residence time (range, 8%–24%). Considering Equations 16 and 19 in cases in which blood residence time is greater than 14% of body residence time, the absorbed dose per activity can change considerably between the estimation and reality. Therefore, Hänscheid et al. propose a limit of 1.3 Gy, instead of 2 Gy, for absorbed dose in the marrow. In this way, even in cases of extreme variation between the real and measured values, the radiotoxicity limit in the hematopoietic system will not be exceeded. The data published by Willegaignon et al. (*27,28*) indicated that blood residence time was 10.3% ± 4% of body residence time (range, 2%–18%). In that work, if blood residence time had not been measured directly, adoption of a 1.3-Gy limit would have prevented dose limit extrapolation.

The half-life concept is applied to decay portrayed by an exponential function with a single term. Therefore, the time for decay of half the initial activity will not necessarily be the same as the second half-life, that is, a quarter of the initial activity. Compared with recent studies, there is agreement between the results. Barros, in 2019 (*29*), measured the dose rate of 98 hospitalized patients after a therapeutic dose of iodine for DTC therapy and found a mean effective half-life of 10.7 ± 4.5 h. For only the subgroup that was prepared with hormone suspension—that is, not using recombinant human thyroid-stimulating hormone—the mean was 12.5 ± 5 h. Barros also reported that patients older than 65 y had a mean effective half-life of 13.3 ± 4.7 h, approximately 30% higher than in middle-aged patients (10.3 ± 4.6 h).

The influence of spatial resolution on image quantification error is described as the partial-volume effect. As the size of a structure decreases, the measured concentration is reduced and the apparent volume is increased relative to the actual value (*30*). Organ-based dosimetry estimates the tumor-absorbed dose by targeting, to calculate the ^{131}I activity to reach therapeutic levels. Organ dosimetry depends on tissue volume. For DTC, this process becomes even more challenging because the tissue is a remnant or, in some cases, micrometastases (*20*).

Cervical uptake examinations and whole-body research before therapy with low doses of radioiodine are provided for in the "Clinical Protocol and Therapeutic Guidelines for Differentiated Thyroid Carcinoma," approved by the Brazilian Ministry of Health (*31*). The objectives were to estimate the volume of remaining tissue or metastatic disease and the iodine avidity of these tissues. However, the ordinance concludes that patients considered at low and intermediate risk because of a low potential for distant metastasis may not need to undergo whole-body imaging. This measure also aims to prevent the stunning effect, which may harm the therapy.

CONCLUSION

Internal dosimetry takes into account physiologic characteristics in an individualized way, patient by patient, providing important data on ^{131}I absorption and retention. The dosimetric techniques in this study could determine the maximum ^{131}I activity to administer, considering the limits of radiotoxicity to the bone marrow and lungs as described in the literature. In severe cases of DTC, in which patients are classified as being at high risk, the organ-based dosimetry approach enables assessment of larger administered

activities allowing elimination of the disease with a single dose. The dosimetric technique methodology was described in detail, allowing the reproduction of therapy planning as an individualized approach.

DISCLOSURE

No potential conflict of interest relevant to this article was reported.

KEY POINTS

QUESTION: What is the application of internal dosimetry in the care of patients undergoing radioiodine therapy for differentiated thyroid carcinoma?

PERTINENT FINDINGS: Through different techniques, a wide variation of retention time for ^{131}I was obtained. The median dose absorbed by the bone marrow was 0.117 mGy/MBq and median whole-body residence time was 22.0 h, with an effective half-life of 15.6 h.

IMPLICATIONS FOR PATIENT CARE: Internal dosimetry provides information relevant to safe dose limits for application to DTC radioiodine therapy, especially in advanced cases of the disease for which the use of greater activities may be necessary.

REFERENCES

1. Câncer de tireoide. gov.br website. https://www.inca.gov.br/tipos-de-cancer/cancer-de-tireoide. Published June 4, 2022. Accessed August 1, 2022.
2. Luster M, Clarke SE, Dietlein M, et al. Guidelines for radioiodine therapy of differentiated thyroid cancer. *Eur J Nucl Med Mol Imaging.* 2008;35:1941–1959.
3. Sapienza MT, Willegaignon J. Radionuclide therapy: current status and prospects for internal dosimetry in individualized therapeutic planning. *Clinics (Sao Paulo).* 2019;74:e835.
4. Hackshaw A, Harmer C, Mallick U, Haq M, Franklyn JA. ^{131}I activity for remnant ablation in patients with differentiated thyroid cancer: a systematic review. *J Clin Endocrinol Metab.* 2007;92:28–38.
5. Tuttle RM, Leboeuf R, Robbins RJ, et al. Empiric radioactive iodine dosing regimens frequently exceed maximum tolerated activity levels in elderly patients with thyroid cancer. *J Nucl Med.* 2006;47:1587–1591.
6. Smilgys B. Radioiodine therapy of differentiated thyroid cancer with simplified personalized dosimetry [in Portuguese] [master's dissertation]. State University of Campinas; 2018.
7. Luster M, Sherman SI, Skarulis MC, et al. Comparison of radioiodine biokinetics following the administration of recombinant human thyroid stimulating hormone and after thyroid hormone withdrawal in thyroid carcinoma. *Eur J Nucl Med Mol Imaging.* 2003;30:1371–1377
8. Plyku D, Hobbs RF, Huang K, et al. Recombinant human thyroid-stimulating hormone versus thyroid hormone withdrawal in ^{124}I PET/CT-based dosimetry for ^{131}I therapy of metastatic differentiated thyroid cancer. *J Nucl Med.* 2017; 58:1146–1154.
9. Dewaraja YK, Li J, Koral K. Quantitative ^{131}I SPECT with triple energy window Compton scatter correction. *IEEE Trans Nucl Sci.* 1998;45:3109–3114.
10. Dewaraja YK, Ljungberg M, Green AJ, et al. MIRD pamphlet no. 24: guidelines for quantitative ^{131}I SPECT in dosimetry applications. *J Nucl Med.* 2013; 54:2182–2188.
11. Lassmann M, Hänscheid H, Chiesa C, et al.; EANM Dosimetry Committee. EANM Dosimetry Committee series on standard operational procedures for pre-therapeutic dosimetry I: blood and bone marrow dosimetry in differentiated thyroid cancer therapy. *Eur J Nucl Med Mol Imaging.* 2008;35:1405–1412.
12. Sgouros G. Blood and bone marrow dosimetry in radioiodine therapy of thyroid cancer. *J Nucl Med.* 2005;46:899–900.
13. Hänscheid H, Lassmann M, Luster M, Kloos RT, Reiners C. Blood dosimetry from a single measurement of the whole body radioiodine retention in patients with differentiated thyroid carcinoma. *Endocr Relat Cancer.* 2009;16:1283–1289.
14. Thomas SR, Samaratunga RC, Sperling M, Maxon HR III. Predictive estimate of blood dose from external counting data preceding radioiodine therapy for thyroid cancer. *Nucl Med Biol.* 1993;20:157–162.
15. Retzlaff JA, Tauxe WN, Kiely JM, Stroebel CF. Erythrocyte volume, plasma volume, and lean body mass in adult men and women. *Blood.* 1969;33:649–661.
16. Benua RS, Cicale NR, Sonenberg M, Rawson RW. The relation of radioiodine dosimetry to results and complications in the treatment of metastatic thyroid cancer. *AJR.* 1962;87:171–182.
17. Song H, He B, Prideaux A, et al. Lung dosimetry for radioiodine treatment planning in the case of diffuse lung metastases. *J Nucl Med.* 2006;47:1985–1994.
18. Sgouros G, Song H, Ladenson PW, Wahl RL. Lung toxicity in radioiodine therapy of thyroid carcinoma: development of a dose-rate method and dosimetric implications of the 80-mCi rule. *J Nucl Med.* 2006;47:1977–1984.
19. Luster M, Pfestroff A, Hänscheid H, Verburg FA. Radioiodine therapy. Sem Nucl Med. 2017;47:126–134.
20. Mínguez P, Flux G, Genollá J, Delgado A, Rodeño E, Sjögreen Gleisner K. Whole-remnant and maximum-voxel SPECT/CT dosimetry in ^{131}I-NaI treatments of differentiated thyroid cancer. *Med Phys.* 2016;43:5279.
21. Mínguez P, Rodeño E, Genollá J, Domínguez M, Expósito A, Sjögreen Gleisner K. Analysis of activity uptake, effective half-life and time-integrated activity for low- and high-risk papillary thyroid cancer patients treated with 1.11 GBq and 3.7 GBq of ^{131}I-NaI respectively. *Phys Med.* 2019;65:143–149.
22. Maxon HR III, Englaro EE, Thomas SR, et al. Radioiodine-131 therapy for well-differentiated thyroid cancer: a quantitative radiation dosimetric approach: outcome and validation in 85 patients. *J Nucl Med.* 1992;33:1132–1136.
23. Silberstein EB, Alavi A, Balon HR, et al. The SNMMI practice guideline for therapy of thyroid disease with ^{131}I 3.0. *J Nucl Med.* 2012;53:1633–1651.
24. Bhat M, Mozzor M, Chugh S, Buddharaju V, Schwarcz M, Valiquette G. Dosing of radioactive iodine in end-stage renal disease patient with thyroid cancer. *Endocrinol Diabetes Metab Case Rep.* 2017;2017:17-0111.
25. Lassmann M, Luster M, Hänscheid H, Reiners C. Impact of ^{131}I diagnostic activities on the biokinetics of thyroid remnants. *J Nucl Med.* 2004;45:619–625.
26. Medvedec M. Thyroid stunning in vivo and in vitro. *Nucl Med Commun.* 2005;26: 731–735.
27. Willegaignon J, Pelissoni RA, Lima BC, et al. Estimating ^{131}I biokinetics and radiation doses to the red marrow and whole body in thyroid cancer patients: probe detection versus image quantification. *Radiol Bras.* 2016;49:150–157.
28. Willegaignon J, Pelissoni RA, Lima BC, Sapienza MT, Coura-Filho GB, Buchpiguel CA. Prediction of iodine-131 biokinetics and radiation doses from therapy on the basis of tracer studies: an important question for therapy planning in nuclear medicine. *Nucl Med Commun.* 2016;37:473–479.
29. de Barros PP. Análise da radiometria realizada em pacientes submetidos àradioiodoterapia [dissertation]. Curso de Pós-Graduação Strictu Sensu em Proteção Radiológica, Instituto Federal de Educação, Ciência e Tecnologia de Santa Catarina, Florianópolis, 2019.
30. Krempser AR, Velasques de Oliveira SM, de Almeida SA. Evaluation of the effect of partial volume in the quantification of activity in PET/CT images [in Portuguese]. *Revista Brasileira de Física Médica.* 2012;6:35–40.
31. Aprova o protocolo clínico e diretrizes terapêutica do carcinoma diferenciado da tireoide. gov.br website. https://www.gov.br/saude/pt-br/assuntos/pcdt/arquivos/2014/carcinoma-diferenciado-da-tireoide-pcdt.pdf. Published January 3, 2014. Accessed August 2, 2022.

Indirect Lung Absorbed Dose Verification by ^{90}Y PET/CT and Complete Lung Protection by Hepatic Vein Balloon Occlusion: Proof of Concept

Yung Hsiang Kao[1], Calvin Gan[2], Alicia Corlett[1], Alexander Rhodes[2], Dinesh Sivaratnam[1], and Beng Ghee Lim[2]

[1]*Department of Nuclear Medicine, Royal Melbourne Hospital, Parkville, Victoria, Australia; and* [2]*Department of Radiology, Royal Melbourne Hospital, Parkville, Victoria, Australia*

Postradioembolization lung absorbed dose verification was historically problematic and impractical in clinical practice. We devised an indirect method using ^{90}Y PET/CT. **Methods:** Conceptually, true lung activity is simply the difference between the total prepared activity minus all activity below the diaphragm and residual activity within delivery apparatus. Patient-specific lung mass is measured by CT densitovolumetry. True lung mean absorbed dose is calculated by MIRD macrodosimetry. **Results:** Proof of concept is shown in a hepatocellular carcinoma patient with a high lung shunt fraction of 26%, where evidence of technically successful hepatic vein balloon occlusion for radioembolization lung protection was required. Indirect lung activity quantification showed the postradioembolization lung shunt fraction to be reduced to approximately 1% with a true lung mean absorbed dose of approximately 1 Gy, suggesting complete lung protection by hepatic vein balloon occlusion. **Conclusion:** We discuss possible clinical applications such as lung absorbed dose verification, refining the limits of lung tolerance, and the concept of massive activity radioembolization.

Key Words: radioembolization; selective internal radiation therapy; lung shunt fraction; ^{90}Y PET/CT; hepatic vein balloon occlusion

J Nucl Med Technol 2022; 50:240–243
DOI: 10.2967/jnmt.121.263422

Despite decades of radioembolization, the true tolerance limit of the lung to radioembolization has not yet been properly defined and to date has only been estimated by ^{99m}Tc-macroaggregated albumin (^{99m}Tc-MAA) or extrapolated from the experiences of external-beam radiotherapy (*1*). This problem is compounded by different methods of imaging and calculating the lung shunt fraction, lung mass, and radiobiologically distinct microsphere devices (*1*).

In the past decade, ^{90}Y PET with contemporaneous CT (^{90}Y PET/CT) has rapidly evolved to become the current standard of care in postradioembolization verification of tumor and nontumorous liver absorbed doses and in detection of nontarget abdominal activity (*2,3*). However, direct lung ^{90}Y PET/CT is much more problematic. First, lung radioconcentration within a PET field of view is usually low because the prescribed lung mean absorbed dose is limited to less than 20–25 Gy, resulting in noisy, quantitatively inaccurate lung scans (*1,2,4*). Second, increasing lung scan time to improve count statistics is impractical. Abdominal ^{90}Y PET/CT of 1–2 bed positions requires 20–40 min. Doubling lung scan time over 2 bed positions could take 40–80 min just for lungs alone, intolerable for any patient. Third, dedicating 60–120 min of scanner time for a single patient costs the throughput equivalent of approximately 3–6 oncology PET patients, which is difficult to justify financially.

MATERIALS AND METHODS

Dosimetric Concept

Conceptually, the true lung activity is simply the difference between the total prepared activity minus all activity below the diaphragm and residual activity within the delivery apparatus (*5*). Here, true lung activity is expressed as an equation, where radiomicrospheres are permanent implants within a closed system where all injected activity is conserved and activity leeching is negligible:

$$A_{Total} = A_{Lung} + A_{PTV} + A_{Nontarget} + A_{Residual}$$
$$\text{i.e.,}\ A_{Lung} = A_{Total} - (A_{PTV} + A_{Nontarget} + A_{Residual}),$$

where A_{Total} is total prepared activity, A_{Lung} is lung activity, A_{PTV} is activity within all planning target volumes, $A_{Nontarget}$ is abdominal nontarget activity (if any), and $A_{Residual}$ is residual activity within the delivery apparatus. The term *planning target volume* refers to all targeted arterial territories encompassing tumor and nontumorous liver (*6*). All measured activities are decay-corrected to the time of radioembolization. The lung mean absorbed dose is calculated by MIRD macrodosimetry assuming uniform activity biodistribution, using the ^{90}Y absorbed dose coefficient 50 Gy per GBq/kg (*2,6*):

$$D_{Lung} = 50 \times (A_{Lung}/M_{Lung})$$

where D_{Lung} is true lung mean absorbed dose (Gy), A_{Lung} is lung activity (GBq), and M_{Lung} is patient-specific lung mass (kg) measured by CT densitovolumetry (*7*).

Clinical Proof of Concept

We demonstrated clinical proof of concept in a hepatocellular carcinoma patient with high lung shunt fraction, where we implemented lung protection during radioembolization by hepatic vein balloon occlusion but required objective proof of technical success. This success was eventually proven by the indirect method described

Received Oct 21, 2021; revision accepted Mar. 7, 2022.
For correspondence or reprints, contact Yung Hsiang Kao (yung.kao@mh.org.au).
Published online Apr. 19, 2022.

here. We considered lung protection to be complete if the extent of hepatopulmonary shunting was reduced to a clinically negligible level (i.e., ~1%). This report has been approved by the institutional review board. The patient consented to the radioembolization planning, treatment, and this publication.

An 82-y-old man with a large, inoperable 12-cm hepatocellular carcinoma occupying segments 4 and 8 (Fig. 1A) was referred for ^{90}Y resin microsphere radioembolization (SIR-Spheres; Sirtex Medical Limited). Exploratory hepatic angiography with radiomicrosphere simulation confirmed hypervascularity with good tumoral ^{99m}Tc-MAA implantation. However, planar liver–lung scintigraphy showed a high lung shunt of 26% (Fig. 1B). We proceeded with radioembolization by implementing 2 methods of lung protection. First, activity prescription was limited to a lung safety tolerance of 20 Gy, planned by the MIRD method (i.e., partition model) (*4,6*). Second, hepatic vein occlusion of the right and middle hepatic veins was performed before radiomicrosphere infusion to minimize hepatopulmonary shunting; this method has the additional benefit of improving the tumor mean absorbed dose by retaining radiomicrospheres within tumor instead of radiomicrospheres being shunted to the lung (*8*).

For hepatic vein balloon occlusion, LeMaitre 6F Over-the-Wire Embolectomy Catheters (LeMaitre Vascular) were placed in the right and middle hepatic veins (catheter length, 80 cm; guidewire, 0.088 cm) under fluoroscopic guidance via the right internal jugular vein (*8*). Balloons were inflated before radiomicrosphere infusion, with complete occlusion of the right and middle hepatic veins visually confirmed with contrast injection (Fig. 1C). Total balloon inflation time was approximately 20 min during radioembolization (Fig. 1D). Despite visual confirmation of balloon occlusion, there remains the possibility of an unknown and invisible amount of in-transit venous radiomicrospheres temporarily suspended proximal to the inflated balloons, potential for radiomicrosphere dislodgment from tumor into the lungs after balloon deflation, and unknown lung shunt contribution by the patent left hepatic vein. All of these uncertainties require postradioembolization confirmation of the true lung activity to ensure patient safety.

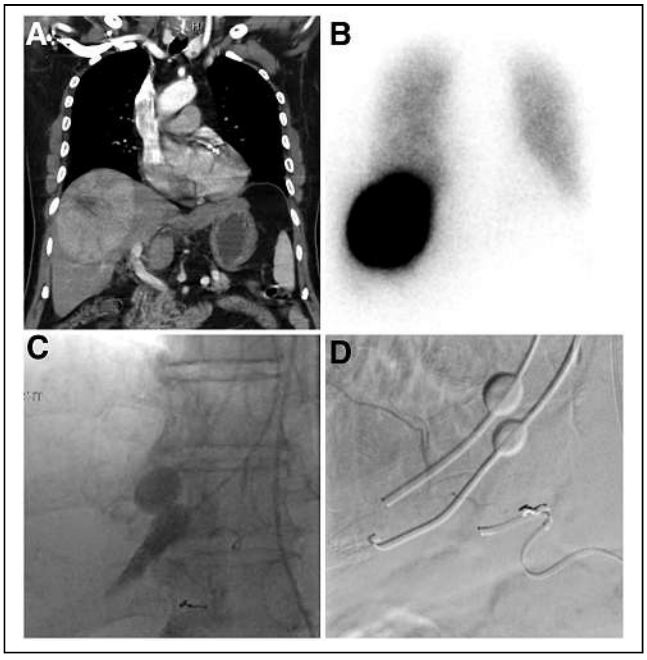

FIGURE 1. (A) CT coronal view shows a large inoperable hepatocellular carcinoma. (B) Planar liver–lung imaging showed a high lung shunt fraction of 26% estimated by ^{99m}Tc-MAA. (C) Fluoroscopy of right and middle hepatic vein balloon occlusion depicts contrast injection within the middle hepatic vein to visually confirm complete occlusion. (D) Fluoroscopy of hepatic vein occlusion balloons in their final inflated positions prior to radiomicrosphere infusion.

Postradioembolization bremsstrahlung planar imaging did not show any visually significant lung activity, a qualitative indication of successful lung protection (Fig. 2A). ^{90}Y PET/CT of the abdomen and delivery apparatus (including catheters, occlusion balloons, and drapes) was performed separately, using the Biograph Horizon (Siemens), as a gradual sweep over 20 min to image the whole liver and delivery apparatus (*2,5*). ^{90}Y PET images were reconstructed using the TrueX time-of-flight iterative algorithm (Siemens), 3 iterations and 10 subsets, a gaussian filter of 5 mm in full width at half maximum, and a 180 × 180 matrix. Low-dose CT was performed for localization, attenuation correction, and scatter correction. Images were displayed in 3-mm slice thickness and analyzed using SyngoVia software (Siemens).

RESULTS

A_{PTV} was quantified by a large volume of interest encompassing all planning target volumes and by setting the PET isocontour threshold to 2% by visual assessment to obtain 1.234 GBq, after decay correction (Fig. 2B). A few small foci of noise artifacts were deemed negligible. $A_{Residual}$ in the delivery apparatus was similarly quantified by setting the PET isocontour threshold to 1% (Fig.2C) to obtain 0.015 GBq, after decay correction (*5*). $A_{Nontarget}$ was undetectable, taken to be zero. A_{Total} was 1.266 GBq measured by a dose calibrator during radiomicrosphere v-vial preparation, after decay correction.

A_{Lung} was therefore $1.266 - (1.234 + 0.015) = 0.017$GBq. Therefore, the true lung shunt fraction was $(0.017/1.266) \times 100$ = approximately 1%. This result was consistent with qualitative bremsstrahlung lung findings and was a vast improvement from the original 26%, objectively affirming technical success and complete lung protection by hepatic vein balloon occlusion. The patient's lung mass, measured by CT densitovolumetry, was 0.85 kg (*7*). D_{Lung} was therefore $50 \times (0.017/0.85)$ = approximately 1 Gy. Clinically, the patient did not develop any respiratory symptoms, and a follow-up MRI scan 2 mo later did not show any evidence of pneumonitis on the routinely acquired high resolution gradient-recalled echo (GRE) T1 and half Fourier single-shot turbo spin-echo (HASTE) T2 sequences, clinically validating our lung protection methods and calculations. Hepatic vein balloon occlusion had also improved the tumor mean absorbed dose from an initial 88 Gy simulated by ^{99m}Tc-MAA predictive dosimetry to a final 101 Gy verified by ^{90}Y PET/CT (Fig. 2D) (*6*). Four-month follow-up MRI showed a mild size reduction of the tumor mass, clinically consistent with the ^{90}Y PET/CT absorbed dose verification.

DISCUSSION

This technical report demonstrates 2 concepts: first, the true lung absorbed dose may be indirectly quantified by ^{90}Y PET/CT, and second, complete lung protection by hepatic vein balloon

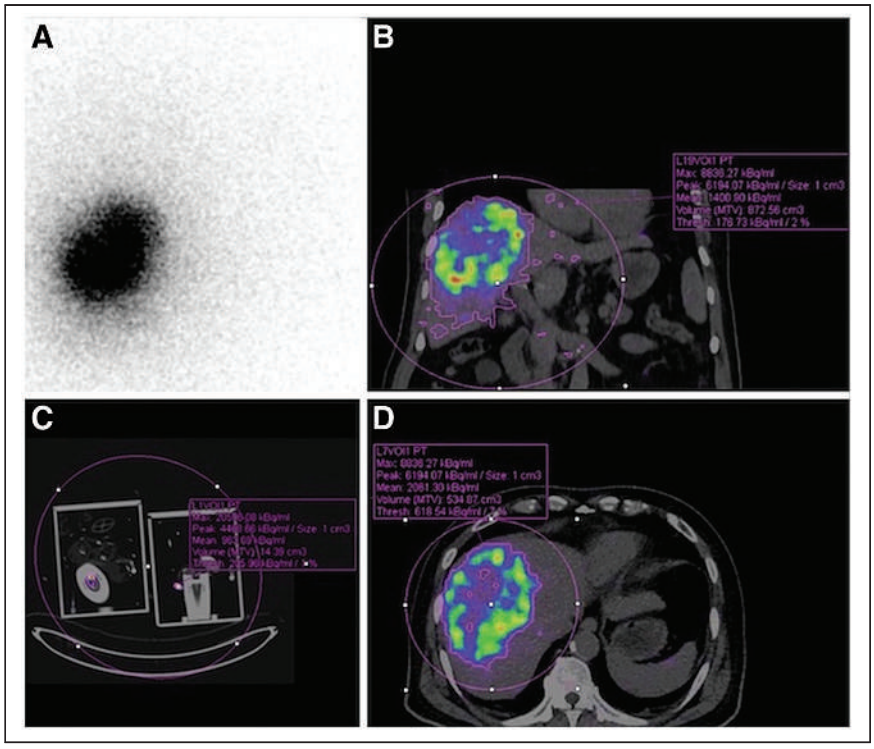

FIGURE 2. (A) Bremsstrahlung planar scintigraphy does not show any visually significant lung activity, a qualitative indication of successful lung protection. (B) ^{90}Y PET/CT with PET isocontour threshold 2% to encompass all activity within planning target volumes. Lungs were outside the PET field of view. Left liver lobe was spared from radioembolization. (C) ^{90}Y PET/CT of delivery apparatus with PET isocontour threshold 1% to encompass all residual activity. (D) ^{90}Y PET/CT with PET isocontour threshold 7% to quantify tumor activity.

occlusion is possible. A recent comprehensive review by Kappadath et al. highlighted the historical pitfalls and limitations in our current methods of lung radiation planning for radioembolization (*1*). These problems with lung dosimetry are attributable to a lack of standardized methods for calculating the lung shunt fraction and lung dosimetry and our incomplete radiobiologic understanding of the true lung tolerance to radiomicrospheres (*1*). Furthermore, our current understanding of an approximately 20- to 25-Gy lung tolerance for ^{90}Y resin microspheres is not wholly applicable to ^{90}Y glass microspheres due to differences in specific activity and tissue biodistribution. As we gradually gain clarity on the true limits of lung tolerance, we will further improve lung predictive dosimetry using normal tissue complication probability (*4*).

In clinical practice, accurate lung dosimetry is important for both preradioembolization predictive dosimetry and also postradioembolization absorbed dose verification. During preradioembolization predictive dosimetry, a common strategy to overcome tumor absorbed dose heterogeneity is to deliberately escalate the prescribed activity up to the limits of normal tissue safety tolerance (*9*). The lung is often the activity-limiting critical organ, and therefore clear knowledge of the true lung tolerance limit is vital to avoid significant radiomicrosphere pneumonitis (*4*). Our method of indirect lung absorbed dose verification could enable us to describe the true lung shunt fraction of different tumor types and establish the true limits of lung tolerance for radiobiologically distinct radiomicrosphere devices.

After radioembolization, lung absorbed dose verification may be clinically important depending on the treatment strategy. Our case of lung protection by hepatic vein balloon occlusion proved to be technically successful; therefore, no further action was required. However, if the lung absorbed dose was unexpectedly found to be dangerously high, immediate action can be initiated to mitigate the risk of developing severe pneumonitis in the ensuing weeks. Such mitigative measures may include corticosteroids, advice on respiratory symptoms, and close outpatient respiratory surveillance in the weeks after radioembolization.

Hepatic vein balloon occlusion is an established technique that may be deployed in situations of high lung shunting (*8*). However, objective proof of technically successful hepatic vein balloon occlusion expressed in terms of a measured absolute reduction in lung activity, lung shunt fraction, or lung absorbed dose has not been described. This report shows that complete lung protection is possible by hepatic vein balloon occlusion, meaning that nearly all injected radiomicrospheres can be retained within the liver to maximize the tumor absorbed dose and avoid unnecessary lung irradiation. This is especially important for hepatocellular carcinoma where the

KEY POINTS

QUESTION: How do we verify the true lung absorbed dose after radioembolization?

PERTINENT FINDINGS: We devised a simple method to indirectly calculate the true lung absorbed dose using postradioembolization ^{90}Y PET/CT. By this method, we showed that hepatic vein balloon occlusion could achieve complete lung protection from hepatopulmonary shunting of radiomicrospheres.

IMPLICATIONS FOR PATIENT CARE: Postradioembolization indirect lung absorbed dose verification is feasible and may benefit patients in terms of mitigating lung radiotoxicity, safety of repeated radioembolization, and research to better define the true limits of lung radiomicrosphere tolerance. By proving that complete lung protection was possible using hepatic vein balloon occlusion, we suggest a possible new paradigm of massive activity radioembolization to benefit radiomicrosphere lobectomy and segmentectomy.

lung shunt fraction is typically higher than liver metastases, which may preclude safe or effective radioembolization. Complete lung protection renders the lung shunt fraction less relevant, allowing massive activities to be infused for radiomicrosphere lobectomy or segmentectomy. With complete lung protection, repeated radioembolization would also be safer because the cumulative lung absorbed dose would be low.

The main dosimetric limitation of our method of indirect quantification is that it can obtain only the true lung mean absorbed dose, to be superseded in the future by lung dose–volume histograms (*4,9*). However, the true lung dose–volume histogram will remain elusive until ^{90}Y PET/CT further improves in acquisition speed, field of view (e.g., total-body PET scanners), and quantitative accuracy to permit direct lung imaging in the routine clinical setting. There were also several technical assumptions in this work. First, we assumed ^{90}Y PET to be quantitatively accurate. Second, we assumed that our visual method of PET isocontour thresholding was reliable to encompass all true ^{90}Y activity, and that all excluded activity was negligible. Third, we assumed that background noise artifacts had negligible effect on clinical dosimetry. However, we felt that these assumptions were reasonable given our prior validation work and years of experience with ^{90}Y PET (*2,3,5*).

CONCLUSION

Indirect lung absorbed dose verification by ^{90}Y PET/CT is feasible and could improve clinical management and our knowledge of lung safety thresholds. Complete lung protection by hepatic vein balloon occlusion is possible, suggesting a new paradigm where the lung shunt fraction is less relevant and permits massive activity radioembolization for radiomicrosphere lobectomy or segmentectomy. Further research is needed to explore these new concepts.

DISCLOSURE

No potential conflict of interest relevant to this article was reported.

REFERENCES

1. Kappadath SC, Lopez BP, Salem R, Lam MGEH. Reassessment of the lung dose limits for radioembolization. *Nucl Med Commun.* 2021;42:1064–1075.
2. Kao YH, Steinberg JD, Tay YS, et al. Post-radioembolization yttrium-90 PET/CT: part 2—dose-response and tumor predictive dosimetry for resin microspheres. *EJNMMI Res.* 2013;3:57.
3. Kao YH, Tan AEH, Lo RHG, et al. Non-target activity detection by post-radioembolization yttrium-90 PET/CT: image assessment technique and case examples. *Front Oncol.* 2014;4:11.
4. Kao YH. Dose-response for yttrium-90 resin microsphere radioembolisation. *Nucl Med Commun.* 2021;42:345–347.
5. Kao YH, Corlett A, Jorna K, Rhodes A, Sivaratnam D. ^{90}Y PET for qualitative and quantitative assessment of residual activity in delivery apparatus after radioembolization. *J Nucl Med Technol.* 2021;49:178–179.
6. Kao YH, Tan AEH, Burgmans MC, et al. Image-guided personalized predictive dosimetry by artery-specific SPECT/CT partition modeling for safe and effective ^{90}Y radioembolization. *J Nucl Med.* 2012;53:559–566.
7. Kao YH, Magsombol BM, Toh Y, et al. Personalized predictive lung dosimetry by technetium-99m macroaggregated albumin SPECT/CT for yttrium-90 radioembolization. *EJNMMI Res.* 2014;4:33.
8. Schiro BJ, Amour ES, Harnain C, Gandhi RT. Management of high hepatopulmonary shunts in the setting of Y90 radioembolization. *Tech Vasc Interv Radiol.* 2019; 22:58–62.
9. Kao YH. Yes, the Holy Gray exists. Learn from modern radioembolisation. *Eur J Nucl Med Mol Imaging.* 2021;48:4115–4117.

Stability Matters: Radiochemical Stability of Therapeutic Radiopharmaceutical ^{177}Lu-PSMA I&T

Madhusudan Vyas[1,2], Remy Lim[1], Jessica Fagan[1], and Rudresh Chandrashekar[1]

[1]*Department of Nuclear Medicine and PET-CT, Mercy Radiology, Auckland, New Zealand; and* [2]*School of Healthcare and Social Practice, Unitec Institute of Technology, Auckland, New Zealand*

Labeling radiopharmaceuticals and testing the quality of the labeled product before injecting it into patients are standard operating procedures in the nuclear medicine department. There is a different shelf life for each labeled product, which determines how long a product can maintain in vitro stability before it needs to be discarded. ^{177}Lu is a radioactive isotope that is increasingly being accepted into the treatment paradigm for palliation of advanced-stage tumors, including metastatic castration-resistant prostate cancer (mCRPC) and neuroendocrine tumors (NETs). In our institution, synthesis of ^{177}Lu with prostate-specific membrane antigen imaging and therapy (PSMA I&T) for palliation of mCRPC is performed on an automated synthesis system. **Methods:** After each synthesis, the final product quality was evaluated by high-performance liquid chromatography (HPLC) and instant thin-layer chromatography (ITLC) at 3 different time points: 0, 24, and 48 h. Between February 2020 and October 2020, the quality of 35 batches of ^{177}Lu-PSMA I&T was evaluated. **Results:** The average radiochemical purity of ITLC-silica gel was found to be greater than 99% (99.70% ± 0.05%), and HPLC was greater than 98% (98.60% ± 0.05%). **Conclusion:** Our findings demonstrate that synthesis of ^{177}Lu-PSMA I&T with an automated synthesis system can remain stable for 48 h after labeling.

Key Words: quality assurance; radiochemistry; radionuclide therapy; high-performance liquid chromatography (HPLC); instant thin-layer chromatography (ITLC); lutetium-177 (Lu177); prostate-specific membrane antigen image and therapy (PSMA)

J Nucl Med Technol 2022; 50:244–247
DOI: 10.2967/jnmt.121.262423

Patients with metastatic castration-resistant prostate cancer have disease progression despite using maximum androgen blockade, as evidenced by a low testosterone level (*1*). It is therefore an advanced, and usually end-stage, form of prostate cancer. Prostate-specific membrane antigen (PSMA) is a type II transmembrane glycoprotein with enzymatic properties that is anchored in the cell membrane of prostate epithelial cells and is overexpressed by prostate cancer cells (*2*). As a result, PSMA can be used as a biomarker for prostate cancer. For peptide receptor radionuclide therapy, PSMA peptides can be radiolabeled with the β-emitter radioisotopes ^{90}Y and ^{177}Lu (PRRT). PSMA I&T, PSMA-617, and J591 are 3 analogs frequently used in therapy (*2*). Because of its favorable physical characteristics (half-life [t1/2] = 6.73 d; mean energy of β-particle [Emax] = 0.497 MeV), ^{177}Lu has been identified as one of the most promising radionuclides for therapeutic applications (*3*). The β-particle emitted by ^{177}Lu has a short pathlength of 1.5 mm, allowing it to deliver effective tumor radiation while causing minimal damage to surrounding normal tissues. The use of the 2 primary γ-energies of 113 and 208 keV, respectively, allows for the use of SPECT imaging after treatment (*4*). The aim of this work was to evaluate the stability of ^{177}Lu-PSMA I&T using the high-performance liquid chromatography (HPLC) and instant thin-layer chromatography (ITLC) methods. This evaluation will assist in the understanding of the shelf life of the labeled product, which might be helpful for logistic purposes.

MATERIALS AND METHODS

The labeling of lutetium trichloride ($177LuCl_3$) and peptide (PSMA I&T; 40 mg of ascorbic acid and 10 mg of sodium hydroxide) was prepared with a fully automated radiopharmaceutical synthesis device using Modular-Lab Pharm Tracer (Eckert & Ziegler). PSMA I&T was labeled with ^{177}Lu using good manufacturing practice–grade disposable cassettes and reagent kits supplied by ABX Advanced Biochemical Compounds (Fig. 1). Labeling of ^{177}Lu-PSMA I&T was performed per the ABX and Eckert & Ziegler synthesis instructions, with the help of a pressure-based cassette (Eckert & Ziegler). The non–carrier-added $177Lucl_3$ was supplied by ANSTO and ITG (Isotope Technologies Garching GmbH). Radiation quantity was procured on the basis of the number of patients treated per cycle. The required dose for 1 patient was usually 7 GBq, based on the estimated synthesis yield of 80%. ABX supplied the accessory chemical, including sodium hydroxide–ascorbic acid and 50 mL of sodium chloride (saline) along with 0.55 μmol filters, long needles, and vent needles. PSMA I&T was supplied by Huwai Chem in a 1-mg vial, which was fractionated into 200 μg and stored in the freezer. The required amount of PSMA I&T (200 μg/5 GBq) was reconstituted with 1.5 mL of sodium ascorbate (0.57 M) to adjust the pH to 4.5 ± 0.1. Labeling was performed using a computer-based automated system (Modular-Lab Eazy; Eckert & Ziegler). All production cassettes were supplied by vendors and were made for a single use only.

The shelf life of prepared ^{177}Lu-PSMA I&T was established on the basis of the evaluation of radiochemical purity (RCP) by HPLC and ITLC-silica gel (ITLC-SG) (*5*).

Received Dec. 10, 2021; revision accepted Apr. 8, 2022.
For correspondence or reprints, contact Rudresh Chandershekar (rchandrashekar@radiology.co.nz).
Published online Jun. 14, 2022.

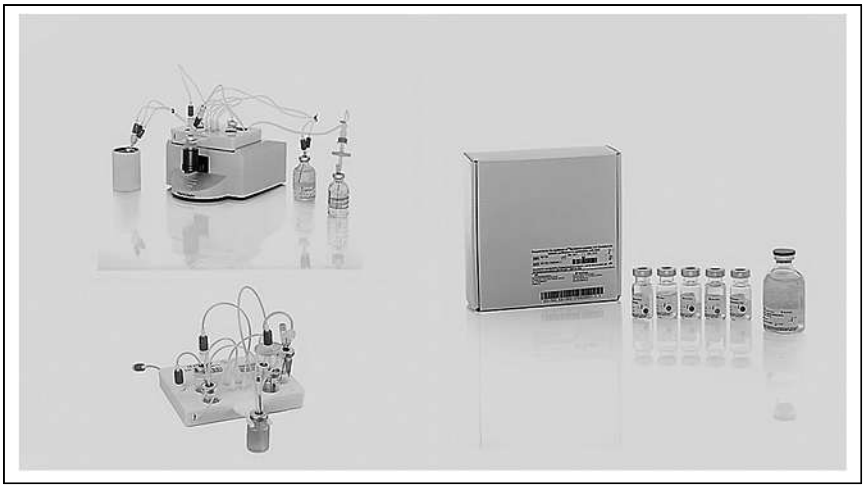

FIGURE 1. Modular-Lab Pharm cassettes supplied by Eckert and Ziegler.

HPLC was used for radiochemical analyses and purification of the ^{177}Lu-labeled PSMA I&T conjugates. A dual-pump HPLC unit with a C18 reversed-phase column (25 × 0.46 cm) (Knauer) purified the labeled conjugates. Mixtures of 1% trifluoroacetic acid, Ultrapure (Sigma-Aldrich) water (solvent A) and and 0.1% trifluoroacetic acid and acetonitrile (solvent B) were used as the mobile phase (*6*). The following gradient elution technique was adopted for the separation: 0–3 min—A, 100% and B, 0%; 3–10 min—A, 50% and B, 50%; 10–15 min—A, 0% and B, 100%. HPLC analysis showed that the fast eluting compound was hydrophilic ^{177}Lu cation (1.0 min), whereas ^{177}Lu-PSMA I&T with a high molecular weight was eluted after

TABLE 1
HPLC Results at Various Times

Batch no.	HPLC purity result at 0 h	HPLC purity result at 24 h	HPLC purity result at 48 h
1	99.78	99.7	99.7
2	99.75	99.87	99.75
3	99.56	99.5	99.65
4	99.89	99.8	99.89
5	99.91	99.91	99.95
6	99.92	99.92	99.92
7	99.98	99.98	99.98
8	99.87	99.87	99.87
9	99.76	99.76	99.76
10	99.56	99.56	99.56
11	99.6	99.6	99.75
12	99.76	99.76	99.76
13	99.8	99.8	99.8
14	99.45	99.45	99.45
15	99.13	99.13	99.13
16	99.35	99.35	99.35
17	99.56	99.56	99.56
18	99.87	99.87	99.87
19	99.74	99.74	99.74
20	99.15	99.15	99.15
21	99.3	99.3	99.3
22	98.9	98.9	98.9
23	99.56	99.56	99.56
24	99.45	99.45	99.45
25	99.57	99.57	99.6
26	99.45	99.45	99.55
27	99.87	99.87	99.77
28	99.67	99.7	99.67
29	99.78	99.78	99.78
30	99.55	99.55	99.55
31	99.65	99.65	99.75
32	99.15	99.2	99.15
33	99.45	99.45	99.45
34	99.5	99.65	99.5
35	99.75	99.75	99.7

TABLE 2
ITLC-SG Results at Various Times

Batch no.	TLC purity result at 0 h	TLLC purity result at 24 h	TLC purity result at 48 h
1	99.70	99.7	99.7
2	99.65	99.87	99.75
3	99.76	99.5	99.65
4	99.95	99.8	99.89
5	99.97	99.91	99.95
6	99.95	99.92	99.92
7	99.98	99.98	99.98
8	99.97	99.87	99.87
9	99.98	99.76	99.76
10	99.66	99.56	99.56
11	99.60	99.6	99.75
12	99.76	99.76	99.76
13	99.80	99.8	99.8
14	98.67	99.45	99.45
15	98.76	99.13	99.13
16	99.76	99.35	99.35
17	99.56	99.56	99.56
18	99.87	99.87	99.87
19	99.65	99.74	99.74
20	99.15	99.15	99.15
21	99.35	99.3	99.3
22	98.91	98.9	98.9
23	99.65	99.56	99.56
24	99.45	99.45	99.45
25	99.57	99.57	99.6
26	99.45	99.45	99.55
27	99.77	99.87	99.77
28	99.67	99.7	99.67
29	99.78	99.78	99.77
30	99.55	99.55	99.55
31	99.65	99.65	99.75
32	99.25	99.2	99.45
33	99.45	99.45	99.45
34	99.65	99.65	99.55
35	99.75	99.75	99.67

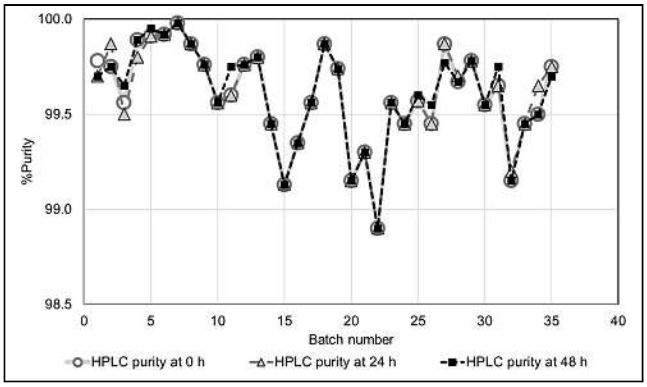

FIGURE 2. A line graph showing HPLC quality control result comparison at 0, 24, and 48 h.

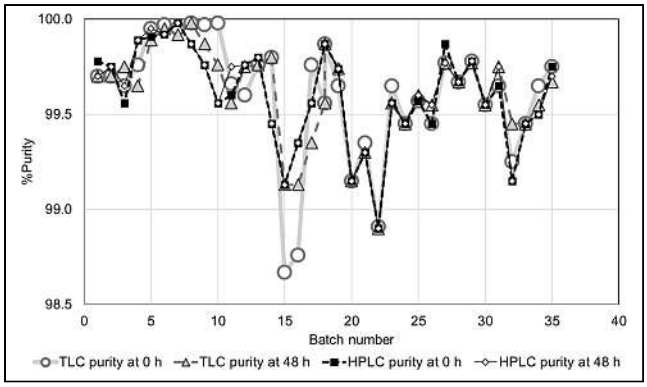

FIGURE 4. A line graph showing result of HPLC and ITLC-SG at 0 and 48 h.

8 min. The typical retention time of radiolabeled PSMA under the above conditions is approximately 500 s (8–10 min).

The ITLC-SG method was applied to check the RCP of the radiolabeled complex. The principle of the ITLC-SG analytic method is that a mobile phase moves along a stationary phase due to capillary forces. Therefore, depending on the distribution of components between the stationary and mobile phase, a radioactive sample spotted in the adsorbent will migrate with different velocities, and thus impurities are separated. The study was performed using a 10-cm-long Whatman 3MM chromatography paper's stationary phase. For this study, 5 μL of the test solution was spotted at 1.5 cm from the lower end of the paper strips, developed in 10% ammonium acetate in methanol as mobile phases (30:70 vol/vol). After each synthesis, the given amount of radiolabeled complex (∼10 MBq) was kept at room temperature for 48 h while being checked by HPLC and ITLC-SG at specified time intervals of 0, 24, and 48 h after preparation (Tables 1 and 2).

RESULTS

Thirty-five batches of ^{177}Lu-labeled PSMA I&T were completed between February 2020 and October 2020. The average RCP of ITLC-SG was greater than 99 percent (99.70 ± 0.05 percent), and HPLC was greater than 98% ($98.60\% \pm 0.05\%$) at room temperature at both 24 and 48 h after synthesis, which was consistent with the various concentrations of the ^{177}Lu-PSMA I&T (Supplemental Table 1 [available at http://jnm.snmjournals.org]; Figs. 2–4).

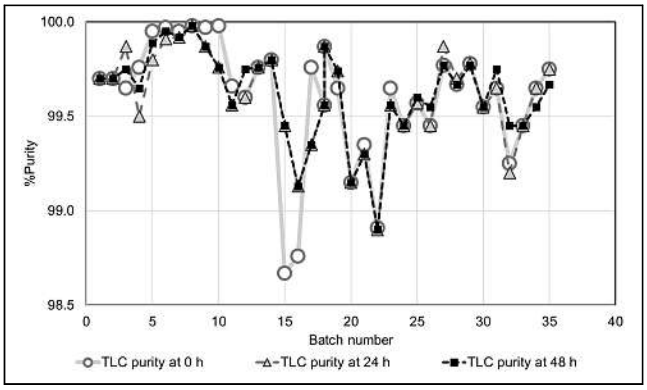

FIGURE 3. A line graph showing ITLC-SG quality control result comparison at 0, 24, and 48 h.

DISCUSSION

Radiopharmaceuticals used for diagnosis and therapeutic purposes are required to have an RCP of greater than 95%, and the length of time a radiopharmaceutical remains at this RCP demonstrates the shelf life of the product. Longer stability allows the radiopharmaceutical to be transportable to distant places, especially in the current COVID-19 environment where traveling is a complex procedure for the patients. The current study found that labeled ^{177}Lu-PSMA I&T stays stable for up to 48 h, which justifies the manufactured product and the influential role of applied quenchers. Both HPLC and ITLC-SG were found to agree with final product stability. In our formulation, we applied sodium ascorbate as a quencher with a concentration of 2 mg/mL. All the results have been evaluated following the suggested methods by Eckert & Ziegler Eurotope's Modular-Lab Pharm Tracer.

CONCLUSION

Our study demonstrates that ^{177}Lu-PSMA I&T, using the automated synthesis of Eckert & Ziegler Eurotope's Modular-Lab Pharm Tracer, can remain stable for 48 h. This longer stability suggests it is feasible for prelabeled ^{177}Lu-PSMA I&T to be supplied from a source location to distant satellite clinics, potentially improving access to PSMA-directed radioligand therapy for palliation treatment metastatic castration-resistant prostate cancer.

DISCLOSURE

No potential conflict of interest relevant to this article was reported.

KEY POINTS

QUESTION: Is the ^{177}Lu-PSMA I&T stable enough to allow it to be transported?

PERTINENT FINDINGS: ^{177}Lu labeled with PSMA I&T was found to be stable for up to 48 h in our study. This finding is encouraging because it suggests that labeled products can be transported from one location to another.

IMPLICATIONS FOR PATIENT CARE: The current finding is encouraging because it suggests that the ^{177}Lu-PSMA I&T has a long enough shelf life. In addition, it opens the door to the possibility of patients receiving treatment without having to travel away from their home locations.

REFERENCES

1. Calopedos RJS, Chalasani V, Asher R, Emmett L, Woo HH. Lutetium-177-labelled anti-prostate-specific membrane antigen antibody and ligands for the treatment of metastatic castrate-resistant prostate cancer: a systematic review and meta-analysis. *Prostate Cancer Prostatic Dis.* 2017;20:352–360.
2. von Eyben FE, Roviello G, Kiljunen T, et al. Third-line treatment and ^{177}Lu-PSMA radioligand therapy of metastatic castration-resistant prostate cancer: a systematic review. *Eur J Nucl Med Mol Imaging.* 2018;45:496–508.
3. Yadav MP, Ballal S, Sahoo RK, Dwivedi SN, Bal C. Radioligand therapy with ^{177}Lu-PSMA for metastatic castration-resistant prostate cancer: a systematic review and meta-analysis. *AJR.* 2019;213:275–285.
4. Afshar-Oromieh A, Babich JW, Kratochwil C, et al. The rise of PSMA ligands for diagnosis and therapy of prostate cancer. *J Nucl Med.* 2016;57(suppl 3):79S–89S.
5. Hofman MS, Violet J, Hicks RJ, et al. [^{177}Lu]-PSMA-617 radionuclide treatment in patients with metastatic castration-resistant prostate cancer (LuPSMA trial): a single-centre, single-arm, phase 2 study. *Lancet Oncol.* 2018;19:825–833.
6. UĞur A, ElÇİ ŞG, YÜksel D. Validation of HPLC method for the determination of chemical and radiochemical purity of a ^{68}Ga-labelled EuK-Sub-kf-(3-iodo-y-) DOTAGA. *Turk J Chem.* 2021;45:26–34.

Discordance Between Histopathologic Grading and Dual-Tracer PET/CT Findings in Metastatic NETs and Outcome of ^{177}Lu-DOTATATE PRRT: Does In Vivo Molecular PET Perform Better from the Viewpoint of Prediction of Tumor Biology?

Aadil Adnan[1,2] and Sandip Basu[1,2]

[1]*Radiation Medicine Centre, Bhabha Atomic Research Centre, Tata Memorial Hospital, Mumbai, India; and* [2]*Homi Bhabha National Institute, Mumbai, India*

Discordance between histopathologic grading and dual-tracer PET/CT (^{68}Ga-DOTATATE and ^{18}F-FDG) findings in neuroendocrine tumors (NETs), though not typical, can be encountered in real-world scenarios. The aim of this study was to assess patients with discordance between World Health Organization (WHO) 2017 grade–predicted molecular PET/CT imaging and the actual dual-tracer PET/CT findings (by exploring their histopathologic, immunohistochemical, and molecular imaging characteristics), with a view toward identifying the prognostic determinants affecting outcome in a peptide receptor radionuclide therapy setup. **Methods:** Thirty-six patients with histopathologically proven inoperable, locally advanced or metastatic NETs, referred for peptide receptor radionuclide therapy, were included in this study. The cohort was divided into 2 broad population groups: those with discordance (between WHO 2017 grade–predicted molecular imaging and the dual-tracer PET/CT findings) and control (showing both ^{18}F-FDG and ^{68}Ga-DOTATATE uptake). The cohort was divided on the basis of dual-tracer PET/CT into 3 groups: metabolically inactive (non–^{18}F-FDG-avid) and somatostatin receptor (SSTR)–expressing tumors, metabolically active (^{18}F-FDG-avid) and non–^{68}Ga-DOTATATE-concentrating (non–SSTR-expressing) tumors, and matched imaging characteristics with the WHO 2017 grading system (showing both ^{18}F-FDG– and ^{68}Ga-DOTATATE–concentrating disease) for statistical analysis. Descriptive statistics were used to analyze categoric data; multivariate analysis was used to assess the correlation between different variables with progression-free survival (PFS) and overall survival (OS). Kaplan–Meier curves were used for survival analysis to calculate median survival and to analyze survival on the basis of WHO 2017 grading and dual-tracer PET. Cox proportional hazards regression analysis was used to determine predictors of survival (OS and PFS). **Results:** Of the 36-patient cohort, 24 (66.7%) showed discordance and 12 (33.3%) were in the control group. Among those showing discordance: 14 (38.9%) had metabolically inactive and SSTR-expressing disease and the remaining 10 (27.8%) had ^{18}F-FDG–concentrating and non–SSTR-expressing disease. Among those in the control group, 12 (33.3%) had intermediate-grade NETs and showed matched (^{68}Ga-DOTATATE– and ^{18}F-FDG–concentrating lesions) disease. Multivariate analysis in patients with discordant findings showed a significant correlation of dual-tracer PET with OS, whereas no significant correlation could be established between WHO grade and OS in the discordant subgroups. No significant correlation could be appreciated between PFS and either dual-tracer PET or WHO grading. The Kaplan–Meier analysis and Cox analysis showed dual-tracer PET/CT imaging to be a significant prognostic determinant and predictor of outcome, respectively. **Conclusion:** In NET patients with discordance between the 2 parameters, dual-tracer PET/CT with ^{18}F-FDG and ^{68}Ga-DOTATATE performed better than WHO grading, differentiation status, and immunohistochemistry in prognosticating and predicting outcome.

Key Words: neuroendocrine neoplasm; histopathologic grading; dual-tracer PET/CT; ^{68}Ga-DOTATATE; ^{177}Lu-DOTATATE; peptide receptor radionuclide therapy

J Nucl Med Technol 2022; 50:248–255
DOI: 10.2967/jnmt.121.261998

Neuroendocrine neoplasms (NENs) are a heterogeneous group of widely distributed tumors comprising both neural and endocrine components (*1*). The neural component is based on identification of dense core granules, and the endocrine component refers to synthesis and secretion of monoamines. Histopathologic grading is considered to be the most important prognostic factor so far and helps in devising tailored therapeutic strategies for patients. However, confusion and enigma have always surrounded this approach, as outliers are quite noticeable in the day-to-day scenario.

Controversy has surrounded the entity since as early as the time that the term *carcinoid* (carcinoma-like) (*2*) was introduced by Oberndorfer at the start of the 20th century, because of the benign behavior of small-bowel tumors comprising argentaffin-positive argyrophilic cells (*3*). This term was criticized because of confusion regarding it and diagnostic irregularities and was regarded to be a misnomer, as these tumors displayed varying degrees of malignant potential (*4–6*). Later, a plethora of terms referring to neuroendocrine tumors (NETs)

Received Jan. 23, 2021; revision accepted Aug. 5, 2021.
For correspondence or reprints, contact Sandip Basu (drsanb@yahoo.com).
Published online Dec. 7, 2021.

was used, such as APUDoma, argentaffinoma, enteroendocrine tumors, tumors of diffuse endocrine system, and argyrophilic cell carcinoma. (*7*). In 1928, Masson characterized carcinoids as NETs on the basis of amine uptake and decarboxylation properties (*8*), whereas in 1963, Williams and Sandler classified them according to embryonic divisions of the digestive tract (*5*), and in 1972, Arrigoni et al. introduced the concept of typical and atypical based on histopathologic characteristics (*9*). In 1980, the World Health Organization (WHO) applied the term *carcinoid* to describe all NETs except pulmonary NETs (*10*); however, this usage led to more discord between pathologists and clinicians (*11,12*). In 1999, the Travis–WHO classification divided pulmonary and thymic NETs into typical carcinoid, atypical carcinoid, and large cell and small cell neuroendocrine carcinomas (NECs) (*13–16*). In 2000 and 2004, WHO revised the definition of gastroenteropancreatic and pulmonary/mediastinal NETs to reflect differentiation and mitotic index/necrosis, respectively (*15,16*). The WHO 2010 classification redefined the entire group of tumors as NENs and subdivided them according to proliferative index (Ki-67/MIB-1) and mitotic counts (*17,18*).

The 2010 WHO classification categorized NENs into 3 grades, with grades 1 and 2 referring to well-differentiated NETs and grade 3 (G3) referring to poorly differentiated NECs (*17,18*). In general, a well-differentiated NEN comprises cells showing minimal to moderate atypia, lacks necrosis, and expresses general markers of neuroendocrine differentiation (diffuse and intense synaptophysin and chromogranin A), whereas a poorly differentiated NEN comprises highly atypical small or large cells expressing faint neuroendocrine differentiation markers. In cases of discordance between differentiation and the proliferative index or when tumors do not concur with the predicted course, the National Comprehensive Cancer Network recommends that clinical judgment should trump the grading system (*19*). In cases of discrepancy between the proliferative and mitotic indices, the higher grade should prevail.

The 2010 WHO grading system was flawed in addressing the contrast between grade and differentiation. Although grade refers to the aggressiveness of tumor cells in terms of their potential for rapid growth and spread, differentiation is the morphologic resemblance of tumor cells to the islets of Langerhans (*20,21*). Hence, it was possible that well-differentiated NETs could be technically graded as G3 but might not be sensitive to the chemotherapy regimen used in poorly differentiated NECs (G3 NEC) (*21*). These well-differentiated NETs, which are technically classified as G3 NEC (on the basis of the proliferation index [WHO 2010]), may not be sensitive to the chemotherapy regimen indicated for G3 NECs. Interestingly, if an adequate number of pathologic specimens is available for an accurate mitotic count, most G3 NETs contain a proportion of cells with a mitotic rate of fewer than 20 per 10 high-power fields, and regions of a still lower grade may be present elsewhere in the tumor focus (*20*), hence rendering proliferation index and mitotic counts to be focal rather than reflective of the overall tumor composition. Furthermore, the genomic composition of G3 NET resembles that of low-grade NET (i.e., MEN1, DAXX, and ATRX mutation) and differs distinctly from that of poorly differentiated NEC (i.e., p53 and RB1 mutation) (*22*). All these issues led to a revised WHO classification of NETs in 2017, which, along with its comparison to the 2010 WHO classification system, is detailed in Table 1 (*23*).

Furthermore, studies evaluating PET using ^{18}F-FDG and ^{68}Ga-DOTATATE showed a relatively lower ^{18}F-FDG concentration than did ^{68}Ga-DOTATATE in patients with G3 NEC—a finding contrary to that theoretically anticipated for G3 NEC on the basis of WHO 2010 (*24*). Receptor-targeted molecular imaging with PET/CT using ^{18}F-FDG and ^{68}Ga-DOTATATE provides an overall, semiquantitative assessment of tumor biology and burden. Hence, this use of dual tracers may potentially score over current conventional classification and grading systems, which rely mainly on focal needle sampling of the most accessible lesion (primary or metastatic) to guide the management strategy. The present study tried to evaluate the plausibility of this dual-tracer concept.

MATERIALS AND METHODS

Thirty-six patients (24 men [66.7%] and 12 women [33.3%]) with histopathologically proven NETs who had undergone peptide receptor radionuclide therapy (PRRT) at our center were retrospectively included in the study and their records analyzed. The median age for the cohort was 50 y (range, 25–66 y). The referral for PRRT was due to metastatic or inoperable locally advanced disease progressing on prior therapy (octreotide therapy or chemotherapy). Table 2 provides an overview of patient demographics.

The study was approved by our institutional scientific and medical ethics committee. The requirement to obtain informed consent was

TABLE 1
WHO NET Classification: 2010 vs. 2017 (*23*)

WHO classification	Ki-67 index	Mitoses/ 10 HPFs
2010		
Well-differentiated NENs		
NET G1	<3	<2
NET G2	3–20	2–20
Poorly differentiated NENs		
NEC G3 (small cell or large cell)	>20	>20
MANEC		
2017		
Well-differentiated NENs		
NET G1	<3	<2
NET G2	3–20	2–20
NET G3	>20	>20
Poorly differentiated NENs		
NEC G3	>20	>20
Small cell type		
Large cell type		
MiNEN		

HPF = high-power field.

TABLE 2
Patient Demographics

Demographic	Data
Total patients	36 (100%)
Sex	
Male	24 (67%)
Female	12 (33%)
Age (y)	
Median	50
Range	25–66
Site of primary	
Pancreas	12 (33.3%)
Unknown	7 (19.4%)
Rectum	5 (13.9%)
Small bowel	4 (11.1%)
Lung	3 (8.3%)
Mediastinum	2 (5.6%)
Stomach	1 (2.8%)
Gallbladder	1 (2.8%)
Skin appendages (Merkel cell carcinoma)	1 (2.8%)
WHO grade (2017 classification)	
G1 NET	7 (19.4%)
G2 NET	15 (41.7%)
G3 NET	7 (19.4%)
G3 NEC	7 (19.4%)
Differentiation status	
Well-differentiated	27 (75.0%)
Poorly differentiated	7 (19.4%)
Not known	2 (5.6%)

Data are number and percentage, except for age.

waived because these patients were referred for PRRT, and the ^{18}F-FDG and ^{68}Ga-DOTATATE scans were done as a part of the routine pretherapy workup. The patients were categorized on the basis of the current 2017 WHO classification. The cohort was divided into 2 broad groups: those with discordance (between WHO 2017 grade–predicted dual-tracer PET/CT findings and the actual dual-tracer PET/CT findings) and a control group (showing both ^{18}F-FDG and ^{68}Ga-DOTATATE uptake). The cohort was divided on the basis of dual-tracer PET into metabolically inactive (non–^{18}F-FDG-avid) and somatostatin receptor (SSTR)–expressing, metabolically active (^{18}F-FDG–avid) and non–SSTR-expressing, and matched (showing both metabolic activity and SSTR expression) and according to the WHO 2017 grading system for statistical analysis. An SUV_{max} of 2.5 on ^{18}F-FDG PET/CT was standardized to an SUV_{max} of 9.0 on ^{68}Ga-DOTATATE PET/CT. The inclusion criteria were histopathologically proven NET/NEC and discordance between histopathologic (WHO 2017) grade–predicted dual-tracer PET and actual dual-tracer PET findings.

All statistical analyses were performed by SPSS software, version 23.0 (SPSS Inc.). Descriptive statistics were used to analyze categoric data. Multivariate analysis was used to evaluate the correlation of different variables with progression-free survival (PFS) and overall survival (OS). The Kaplan–Meier product limit method was used to calculate median survival and to analyze survival on the basis of WHO 2017 grade and dual-tracer PET. The variables dual-tracer PET and WHO 2017 grade determining OS and PFS were compared using the log-rank test. Cox proportional hazards regression analysis was used to identify predictors of OS and PFS. Patients who were alive or with nonprogressive disease (for OS and PFS, respectively) at the time of analysis or last contact were censored. A 2-tailed P value of less than 0.05 was considered statistically significant, and hazard ratios with 95% CIs were determined.

RESULTS

The pancreas was the most commonly involved primary site (12 patients, 33.3%), followed by unknown primary (7 patients, 19.4%), rectum (5 patients, 13.9%), small bowel (4 patients, 11.1%), lungs (3 patients, 8.3%), mediastinum (2 patients, 5.6%), and stomach, gallbladder, and skin appendages (Merkel cell carcinoma), each with a single patient (2.8%). According to the 2017 WHO grading, 15 patients (41.7%) had grade 2 (G2) NET, followed by 7 patients (19.4%) each with grade 1 (G1) NET, G3 NET, and G3 NEC. Twenty-four patients (66.7%) were in the discordance group, and 12 (33.3%) were in the control group. In the discordance group, 14 patients (38.9%) had metabolically inactive and SSTR-expressing disease, and the remaining 10 (27.8%) had metabolically active and non–SSTR-expressing disease. In the control group, all 12 patients (33.3%) and intermediate-grade NETs and showed matched (metabolically active and SSTR-expressing) disease.

Twenty-seven patients (75%) had a well-differentiated histology, 7 (19.4%) had a poorly differentiated histology, and in 2 (5.6%) the histology was not available. Thirty patients (83.3%) were synaptophysin-positive, and in remaining 6 (16.7%) the data were unavailable. Twenty-six patients (72.2%) were positive for chromogranin A, 3 were negative (8.3%), and in remaining 7 (19.4%) the data were unavailable. However, no definitive pattern could be established in chromogranin A–negative patients. Similarly, no definitive trend or pattern was appreciated between epithelial or other immunohistochemistry (IHC) markers and other variables, as possibly could be due in part to inconsistent selection of IHC markers in patients and hence lack of uniformity (Table 3).

TABLE 3
Histopathologic Characteristics

Characteristic	Data
Synaptophysin (IHC)	
Positive	30 (83.3%)
Negative	6 (16.7%)
Chromogranin A (IHC)	
Positive	26 (72.2%)
Negative	3 (8.3%)
Not known	7 (19.4%)
Epithelial markers (AE1/AE3; IHC)	
Positive	11 (30.6%)
Negative	2 (5.6%)
Not known	23 (63.9%)
Other IHC markers (ATRX, cytokeratin, CD56, CK7, CK19, CK20, and CDX2)	
Positive	10 (27.8%)
Not known	26 (72.2%)

Data are number and percentage.

Of the 24 patients with discordant NET (in terms of WHO grade–predicted and actual dual-tracer PET findings), 7 (~30%) progressed (2/14 [14.3%] with metabolically inactive and SSTR-expressing disease and 5/10 [50%] with metabolically active and non–SSTR-expressing disease) and 8 (~33.3%) succumbed to the disease (1/14 [7.1%] with metabolically inactive and SSTR-expressing disease and 7/10 [70%] with metabolically active and non–SSTR-expressing disease). Of the 12 control patients with matched disease, 3 (25%) progressed and 5 (41.7%) died. In the entire cohort, the median cumulative PFS was 83 mo (82.9 mo for metabolically inactive and SSTR-expressing and 49.8 mo for metabolically active and non–SSTR-expressing) and OS was 118 mo (90 mo for metabolically inactive and SSTR-expressing and 61.2 mo for metabolically active and non–SSTR-expressing). Categorization based on WHO 2017 grading did not yield such trends and results (Figs. 1 and 2). The dual-tracer PET/CT characteristics of the patient population has been detailed in Table 4.

On multivariate analysis, the only significant correlation was between dual-tracer PET and OS ($P = 0.01$); however, no significant correlation was flagged between any of the variables and PFS in this study.

For PFS and OS, dual-tracer PET and WHO 2017 grading were compared by Kaplan–Meier analysis and plots (Figs. 1 and 2). A significant difference was noticed between the Kaplan–Meier plots when categorization was based on dual-tracer PET ($P = 0.05$ for PFS and $P = 0.02$ for OS; log rank test) versus WHO 2017 grading ($P = 0.39$ for PFS and 0.67 for OS; log rank test). Cox analysis was used to analyze dual-tracer PET versus WHO 2017 grading as a predictor of PFS and OS and showed dual-tracer imaging to be an independent predictive prognostic variable (PFS: hazard ratio, 0.23 [95% CI, 0.31–1.67; $P = 0.03$]; OS: hazard ratio, 0.027 [95% CI, 0.002–0.35; $P = 0.005$]). No significant statistics could be achieved for WHO 2017 grading (PFS: hazard ratio, 0.49 [95% CI, 0.061–3.861; $P = 0.5$]; OS: hazard ratio, 0.301 [95% CI, 0.3–3.013; $P = 0.31$]).

A smaller substudy was done categorizing patients on the basis of ^{68}Ga-DOTATATE uptake (Krenning score). Two patients ($n = 2$) with a Krenning score of 1 were denied PRRT. Of 5 patients with a Krenning score of 2, 2 received a single cycle of PRRT and the remaining 3 received 2–3 cycles (with the first cycle given mainly on trial or compassionate-use grounds because there were few available alternatives). Additional PRRT cycles in Krenning 2 patients were administered either because of some initial symptomatic benefit or as part of a combined chemo-PRRT trial, which in almost all cases showed—after a third cycle of PRRT—disease progression, which was followed by withholding of further PRRT. Of 7 patients with a Krenning score of 1 or 2, 5 (71.4%) progressed and all 7 (100%) succumbed to disease with an adverse clinical outcome (marked by a relatively brief OS and PFS). The cohort with a Krenning score of 3 or 4 comprised 29 patients (80.6%), of whom 10 (27.8%) and 19 (52.8%) had a Krenning score of 3 and 4, respectively. Of these 29 patients, 5 (17.2%) progressed and 6 (20.7%) died. Hence, a higher SSTR expression was associated with a favorable outcome and vice versa.

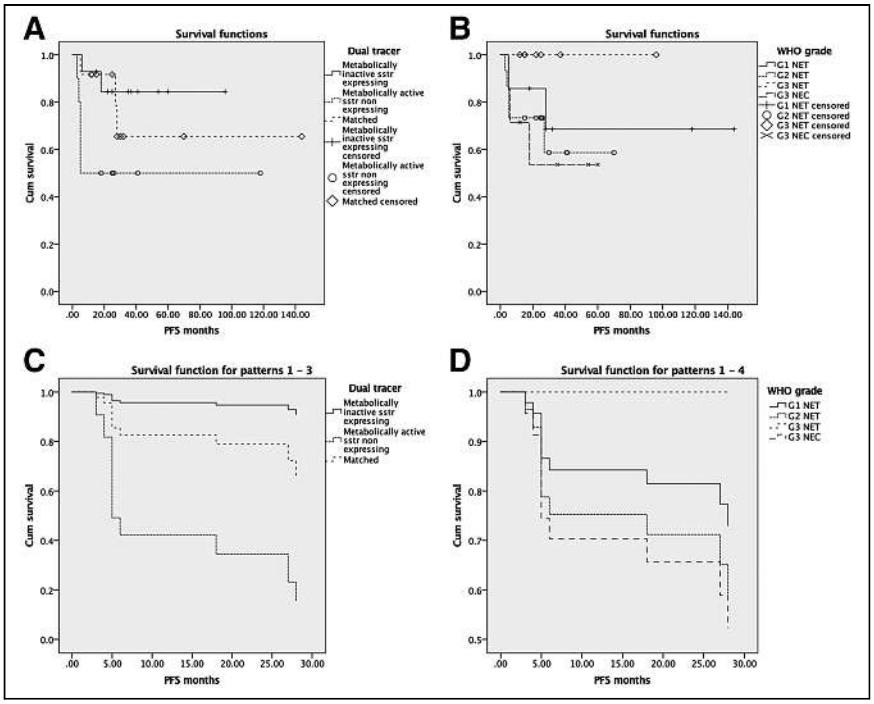

FIGURE 1. (A) Kaplan–Meier curves for PFS on basis of dual-tracer PET. (B) Kaplan–Meier curves for PFS on basis of 2017 WHO grading system. (C) Cox proportional hazards survival curves for PFS on basis of dual-tracer PET. (D) Cox proportional hazards survival curves for PFS on basis of 2017 WHO grading system. Kaplan–Meier and Cox curves showed significantly better PFS for metabolically inactive and SSTR-expressing group than for metabolically active and non–SSTR-expressing group when cohort was analyzed on basis of dual-tracer PET. Analysis based on 2017 WHO grading system did not yield any significant difference. Cum = cumulative.

DISCUSSION

The WHO 2010 grading system was revised in 2017 to classify NETs with a Ki-67 of more than 20% as well differentiated and NECs with a Ki-67 of more than 20% as poorly differentiated. (Earlier in 2010 grading, all NETs with Ki-67 > 20% were considered NEC.) Ideally, grade I NETs should have high ^{68}Ga-DOTATATE uptake and low ^{18}F-FDG uptake, and grade III NETs and NECs should have low

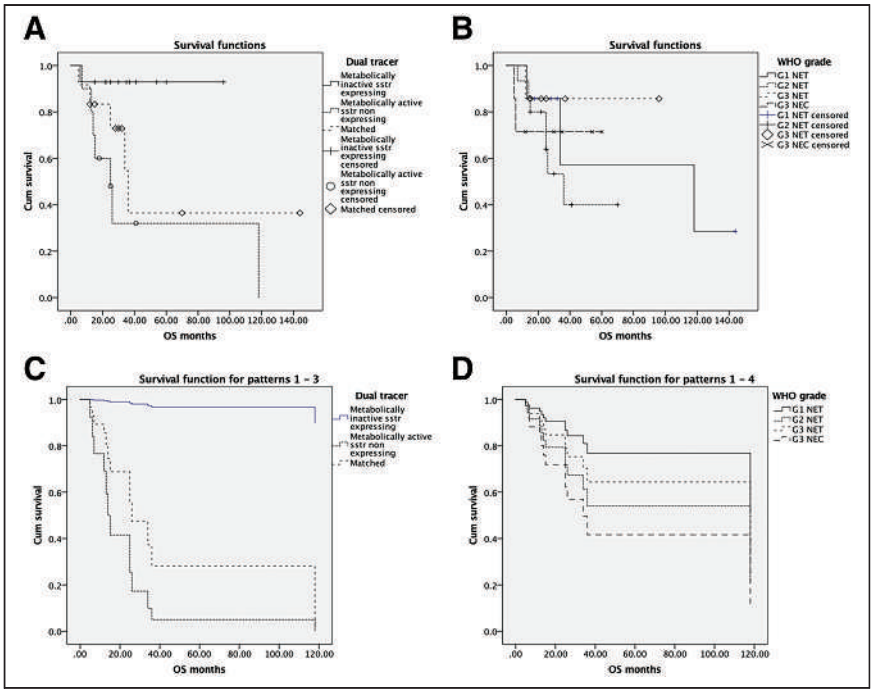

FIGURE 2. (A) Kaplan–Meier curves for OS on basis of dual-tracer PET. (B) Kaplan–Meier curves for OS on basis of 2017 WHO grading system. (C) Cox proportional hazards survival curves for OS on basis of dual-tracer PET. (D) Cox proportional hazards survival curves for OS on basis of 2017 WHO grading system. Kaplan–Meier and Cox curves showed significantly better OS for metabolically inactive and SSTR-expressing group than for metabolically active and non–SSTR-expressing group when cohort was analyzed on basis of dual-tracer PET. Analysis based on 2017 WHO grading system did not yield any significant difference. Cum = cumulative.

^{68}Ga-DOTATATE uptake and high ^{18}F-FDG uptake. But our clinical experience has shown obvious outliers with high ^{18}F-FDG uptake and low ^{68}Ga-DOTATATE uptake in grade I NETs and vice versa (high ^{68}Ga-DOTATATE uptake and low ^{18}F-FDG uptake in grade III NETs and NECs). Grade II NETs have shown mixed uptake. Usually, histopathologic grading serves as an excellent prognostic marker, and in most cases, the functional imaging findings are in concordance with it. But when there is discordance, histopathologic grading may not reflect the exact, overall tumor biology, as clinically observed and affirmed by this study.

Here, we specifically evaluated NETs showing discordance between actual functional imaging findings (^{68}Ga-DOTATATE and ^{18}F-FDG) and imaging findings predicted by 2017 WHO grade. These entities, although not regularly encountered in normal clinical scenarios, do exist. The study group comprised patients with contradictory imaging findings (e.g., ^{68}Ga-DOTATATE–negative and ^{18}F-FDG–positive findings in grade I well-differentiated tumors and vice versa). We tried to evaluate and explain this paradoxic behavior of some NETs and whether dual-tracer PET/CT can aid in therapeutic decision making and predict the outcome of treatment, especially PRRT. The main objective of this study was to evaluate the validity of dual-tracer PET/CT as a prognostic marker in comparison to other available determinants (e.g., histopathology), especially in deciding whether PRRT is a therapeutic option and in predicting its outcome. This concept resonated with the WHO's approach in classifying G3 NETs as well differentiated (G3 NET) or poorly differentiated (G3 NEC), exhibiting a stark contrast in their biologic behavior and response to treatment (particularly chemotherapy) and ultimately culminating in the current 2017 WHO NET grading system.

TABLE 4
Dual-Tracer PET Characteristics

Characteristic	Data
Baseline ^{18}F-FDG uptake (SUV_{max})	
<5	14 (38.9%)
5–10	5 (13.9%)
10–20	10 (27.8%)
>20	7 (19.4%)
Baseline DOTATATE uptake	
Krenning 1	2 (5.6%)
Krenning 2	5 (13.9%)
Krenning 3	10 (27.8%)
Krenning 4	19 (52.8%)
Dual-tracer PET	
Metabolically inactive and SSTR-expressing	14 (38.9%)
Metabolically active and non–SSTR-expressing	10 (27.8%)
Matched (metabolically active and SSTR-expressing)	12 (33.3%)

Data are number and percentage.

This nuanced difference from the usual and predicted course may be secondary to high-grade transformation of original low-grade disease, as well as to overestimation and generalization of histopathologic and IHC findings as representative of the tumor or the overall disease burden, whereas such findings essentially are—in most if not all cases—a localized and focal representation covering the extent of only the sampling needle tip or the tissue specimen biopsied. Vis-à-vis discordant NETs, the current database of available articles is relatively deficient, with only occasional reports, and these are both nascent and ambiguous in their understanding of the entity. Tang et al., in their study of the histopathologic, IHC, and genetic constitution of well-differentiated NETs (*25*), deduced that mixed grades do exist within the population of well-differentiated NETs and are distinguishable from poorly differentiated NECs by their

unique phenotype, proliferative indices, and genotype, either at the time of diagnosis or afterward at both primary and metastatic sites. Nuñez-Valdovinos et al., in a study using the large Spanish tumor registry (RGETNE [Registro del Grupo Español de Tumores Neuroendocrinos]) (*26*), inferred that substantial clinical heterogeneity is observed for both G2 and G3 NENs and that analysis of the tumor registry suggested tumor morphology to be a valuable aid in addition to the proliferation index, to further stratify the clinical outcome and prognosis in patients with gastroenteropancreatic NENs. Choe et al., in their review article (*22*), highlighted that functional imaging—specifically, SSTR scintigraphy (SRS with ^{68}Ga-DOTATATE) and ^{18}F-FDG—may be helpful in distinguishing well-differentiated NETs from poorly differentiated NECs (*27*), especially in challenging situations with a discrepancy between imaging features and histology. In the context of NECs, which do not always show positive IHC markers (*28*), or when a tissue sample may not be representative of the entire tumor or disease burden, functional imaging with dual-tracer PET has a particularly important role to play (*29*). Basu et al. (*24*) also concluded that even in the presence of different proliferative indices, an inverse correlation in uptake on ^{68}Ga-DOTATATE and ^{18}F-FDG PET is propitious in 3 instances: cases requiring in vivo depiction of the overall tumor phenotype resulting from multiple putative and unknown interactions at the cellular level; cases involving interlesional and intralesional heterogeneity, rendering histopathology and IHC subject to possible sampling errors and underrepresentation; and cases requiring assessment of tumor biology using intermediate grading indices. Thapa et al. (*30*) and Zhang et al. (*31*) showed that high ^{18}F-FDG uptake was associated with poorer outcomes in NETs treated with PRRT. However, symptomatic improvement was observed in most cases irrespective of grade and ^{18}F-FDG uptake. High pretherapy ^{18}F-FDG uptake in both low-grade and high-grade NETs predicted an inferior outcome and was associated with disease progression. Although these studies emphasize the prognostic implication of ^{18}F-FDG uptake, the study by Thapa et al. used the WHO 2010 NET grading system and did not take into account the value of dual-tracer PET, and neither study evaluated the discordance between actual functional imaging findings and histopathologic grade–predicted dual-tracer functional PET findings. The literature data make clear that both ^{18}F-FDG and ^{68}Ga-DOTATATE uptake would form determinants of response and that their relative concentrations on PET/CT imaging would be an important molecular imaging parameter for such predictions (*32–35*). In a previously published study from our center (*36*), Sampathirao et al. investigated the potential role of dual-tracer PET/CT in detection of the primary site in carcinoma of unknown primary, and the findings on PET/CT usually correlated well with the tumor proliferation index; however, a few outliers were noticed. Some of these outliers may have been included in the present study, which looked primarily into their outcome viewpoint (clinical response to PRRT/chemotherapy).

For such clinical situations, imaging using dual tracers has proved useful, as individual sampling of all lesions will be almost impossible for obvious practical and ethical reasons. Dual-tracer ^{68}Ga-DOTATATE and ^{18}F-FDG imaging seems potentially advantageous and pragmatic for several reasons: it can provide a noninterventional representation of whole-body disease burden; it shows relative tracer uptake reflective of differentiation status and lesion aggressiveness; it can direct the appropriate treatment strategy; it is effective in evaluating responses and determining prognoses; and, to a lesser extent, it can guide toward the diagnosis (Figs. 3 and 4). The present study was unique in that it evaluated a small and specified entity: discordance between WHO 2017 grade–predicted dual-tracer PET/CT findings and the actual dual-tracer PET/CT findings. There were encouraging results supporting the role of dual-tracer functional imaging in solving the conundrum surrounding management and prognosis, and the study was imperative in its concept and approach. The PFS and OS of the patients with discordance correlated more closely with the dual-tracer PET findings as opposed to the 2017 WHO grading system. Furthermore, dual-tracer PET (as opposed to the 2017 WHO grading) was found to be an independent prognostic factor for PFS and OS.

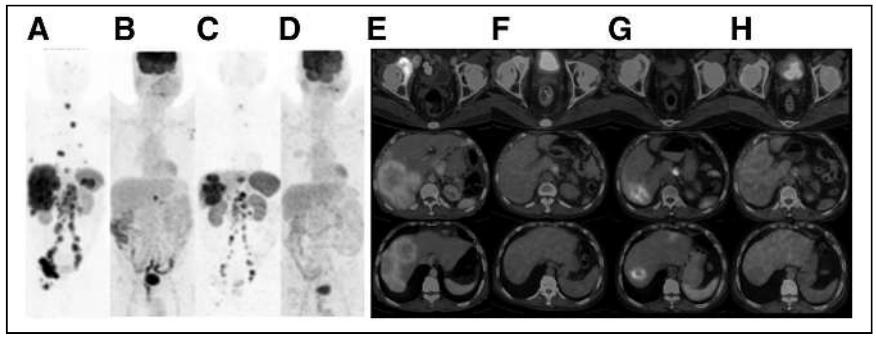

FIGURE 3. A 61-y-old man with NET metastatic to liver, mediastinal and abdominal nodes, and multiple skeletal sites, with unknown primary. Histopathology revealed poorly differentiated NEC, positive for synaptophysin and chromogranin, and CK19-positive on IHC. Despite high proliferative index of 25%, ^{68}Ga-DOTATATE PET/CT at baseline revealed intense SSTR expression in hepatic and skeletal lesions and in mediastinal, abdominal, and pelvic nodes, whereas ^{18}F-FDG PET/CT showed single metabolically active pariceliac node. Follow-up ^{68}Ga-DOTATATE PET/CT revealed partial response, with decrease in size and SSTR expression in almost all lesions, whereas ^{18}F-FDG PET/CT did not show any abnormal uptake, suggesting complete metabolic resolution. Despite poorly differentiated G3 NEC (WHO 2017), dual-tracer PET/CT studies suggested favorable tumor biology, which was adequately clinically translated. After third PRRT, patient is doing fine, with significant symptomatic and morphologic improvement.

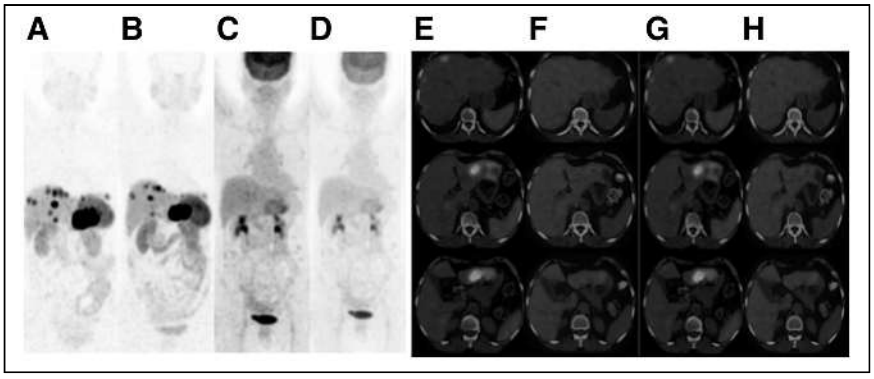

FIGURE 4. A 64-y-old woman with NET metastatic to liver and skeletal sites, with unknown primary. Patient presented with pain in abdomen and weight loss and was referred for PRRT in view of SSTR-expressing metastatic NET. Histopathology of liver lesion revealed metastatic, well-differentiated NET with MIB-1 index of 24%, positive for synaptophysin and chromogranin, and CDX2-negative on IHC. Baseline ^{68}Ga-DOTATATE PET/CT revealed multiple areas of increased tracer uptake (SSTR expression) in both lobes of liver (bilobar hepatic metastases, which is not amenable to surgical resection) and skeletal sites, with no abnormal hypermetabolism evident on baseline ^{18}F-FDG PET/CT. Follow-up dual-tracer PET/CT after 4 PRRTs showed decrease in number of smaller hepatic metastases, with mild interval decrease in size of larger hepatic lesion in left lobe (overall partial response). Dual-tracer PET/CT appeared to agree with histopathologic finding of well-differentiated G3 NET (WHO 2017), and findings were adequately clinically translated.

The major limitations of the study were its retrospective design, its lack of a homogeneous histopathology protocol (especially with respect to IHC markers), and its lack of a standardized approach to tumor marker evaluation among the referring institutions and hospitals. Another possible limitation was that the cohort lacked uniformity in disease burden and general condition, which could affect the duration of OS and PFS in these heavily pretreated patients, who had been referred for PRRT at various disease stages. The fact that genetic mutations and pathways were not studied might represent a major pitfall that we believe could be pivotal to discordance. An understanding of such mutations and pathways could potentially lead to a paradigm shift in our present management of discordant NETs. However, this study did have some important findings. In evaluating the novel concept of discordance between WHO 2017 grade–predicted molecular imaging and actual dual-tracer PET/CT findings, it showed encouraging results in favor of dual-tracer PET. It highlighted possible pitfalls in histopathologic grading and its reliability in devising a personalized treatment strategy. It revealed the need for a well-structured prospective study recruiting a homogeneous patient cohort. Finally, it showed that the greatest need in deciphering this medical conundrum is to perform studies encompassing all possible determinants, including genomic and proteomic analyses.

CONCLUSION

Dual-tracer PET using ^{18}F-FDG and ^{68}Ga-DOTATATE is a promising entity in NET management and may perform better than histopathology in evaluating overall tumor burden and biology, especially in making clinical decisions and selecting patients who will benefit from PRRT. The present work indicated that histologic classification alone is not sufficient. On the one hand, a focal high MIB-1 index should not preclude a patient from PRRT (if SSTR PET imaging reveals high receptor expression), and on the other hand, a low tumor proliferation rate at initial diagnosis does not clearly predict concordant biology in all lesions. Because a temporal change in tumor grade (dedifferentiation) is possible, a workup that includes the dual-tracer PET/CT features would be useful and add a scientific basis to the management strategy. Discordance in NETs can be multifaceted and complex, for which a continued multidisciplinary approach is the key to gaining greater insight.

DISCLOSURE

No potential conflict of interest relevant to this article was reported.

KEY POINTS

QUESTION: How does the issue of discordance between histopathologic grading and dual-tracer PET/CT (^{68}Ga-DOTATATE and ^{18}F-FDG) findings in metastatic NENs affect routine clinical practice?

PERTINENT FINDINGS: Dual-tracer PET/CT imaging was shown to be a significant prognostic determinant and predictor of outcome.

IMPLICATIONS FOR PATIENT CARE: A multifaceted workup encompassing dual-tracer PET/CT features along with histopathology would be greatly useful and add scientific basis to the management strategy.

REFERENCES

1. Basu B, Sirohi B, Corrie P. Systemic therapy for neuroendocrine tumours of gastroenteropancreatic origin. *Endocr Relat Cancer.* 2010;17:R75–R90.
2. Modlin IM, Shapiro MD, Kidd M. Siegfried Oberndorfer: origins and perspectives of carcinoid tumors. *Hum Pathol.* 2004;35:1440–1451.
3. Rosai J. The origin of neuroendocrine tumors and the neural crest saga. *Mod Pathol.* 2011;24(suppl):S53–S57.
4. Modlin IM, Sandor A. An analysis of 8305 cases of carcinoid tumors. *Cancer.* 1997;79:813–829.
5. Williams ED, Sandler M. The classification of carcinoid tumours. *Lancet.* 1963;1:238–239.
6. Soga J. The term "carcinoid" is a misnomer: the evidence based on local invasion. *J Exp Clin Cancer Res.* 2009;28:15.
7. Hajdu SI, Tang P. A note from history: the saga of carcinoid and oat-cell carcinoma. *Ann Clin Lab Sci.* 2008;38:414–417.
8. Masson P. Carcinoids (argentaffin-cell tumors) and nerve hyperplasia of appendicular mucosa. *Am J Pathol.* 1928;4:181–212.
9. Arrigoni MG, Woolner LB, Bernatz PE. Atypical carcinoid tumors of the lung. *J Thorac Cardiovasc Surg.* 1972;64:413–421.
10. Williams ED. *Histological Typing of Endocrine Tumours.* Geneva: Springer; 1980.
11. Chang S, Choi D, Lee SJ, et al. Neuroendocrine neoplasms of the gastrointestinal tract: classification, pathologic basis, and imaging features. *Radiographics.* 2007;27:1667–1679.

12. Vinik A, Hughes MS, Feliberti E, et al. Carcinoid tumors. National Center for Biotechnology Information website. http://www.ncbi.nlm.nih.gov/books/NBK279162/. Updated February 5, 2018. Accessed March 25, 2022.
13. Pusceddu S, Catena L, Valente M, et al. Long-term follow up of patients affected by pulmonary carcinoid at the Istituto Nazionale Tumori of Milan: a retrospective analysis. *J Thorac Dis.* 2010;2:16–20.
14. Axiotis CA. The neuroendocrine lung. In: Li Volsi V, Asa SL, eds. *Endocrine Pathology.* Churchill Livingstone; 2002:261–296.
15. Klöppel G. Classification and pathology of gastroenteropancreatic neuroendocrine neoplasms. *Endocr Relat Cancer.* 2011;18(suppl 1):S1–S16.
16. Travis WD. The concept of pulmonary neuroendocrine tumours. In: Travis WD, Brambilla E, Muller-Hermelink HK, Harris CC, eds. *Pathology and Genetics of Tumours of the Lung, Pleura, Thymus and Heart.* IARC Press; 2004:59–64.
17. Farrell JM, Pang JC, Kim GE, Tabatabai ZL. Pancreatic neuroendocrine tumors: accurate grading with Ki-67 index on fine-needle aspiration specimens using the WHO 2010/ENETS criteria. *Cancer Cytopathol.* 2014;122:770–778.
18. Bosman FT, Carneiro F, Hruban RH, Theise ND. *WHO Classification of Tumours of the Digestive System.* 4th ed. International Agency for Research on Cancer; 2010.
19. Neuroendocrine tumors guidelines. Medscape website. http://emedicine.medscape.com/article/2500010-overview. Updated July 27, 2020. Accessed March 25, 2022.
20. Singhi AD, Klimstra DS. Well-differentiated pancreatic neuroendocrine tumours (PanNETs) and poorly differentiated pancreatic neuroendocrine carcinomas (PanNECs): concepts, issues and a practical diagnostic approach to high-grade (G3) cases. *Histopathology.* 2018;72:168–177.
21. Klimstra DS, Modlin IR, Coppola D, Lloyd RV, Suster S. The pathologic classification of neuroendocrine tumors: a review of nomenclature, grading, and staging systems. *Pancreas.* 2010;39:707–712.
22. Choe J, Kim KW, Kim HJ, et al. What is new in the 2017 World Health Organization classification and 8th American Joint Committee on Cancer staging system for pancreatic neuroendocrine neoplasms? *Korean J Radiol.* 2019;20:5–17.
23. Lloyd RV, Osamura RY, Klöppel G, Rosai J. *WHO Classification of Tumours of Endocrine Organs.* 4th ed. International Agency for Research on Cancer; 2017: 209–240.
24. Basu S, Ranade R, Thapa P. Correlation and discordance of tumour proliferation index and molecular imaging characteristics and their implications for treatment decisions and outcome pertaining to peptide receptor radionuclide therapy in patients with advanced neuroendocrine tumour. *Nucl Med Commun.* 2015;36:766–774.
25. Tang LH, Untch BR, Reidy DL, et al. Well-differentiated neuroendocrine tumors with amorphologically apparent high-grade component: a pathway distinct from poorly differentiated neuroendocrine carcinomas. *Clin Cancer Res.* 2016;22:1011–1017.
26. Nuñez-Valdovinos B, Carmona-Bayonas A, Jimenez-Fonseca P, et al. Neuroendocrine tumor heterogeneity adds uncertainty to the World Health Organization 2010 classification: real-world data from the Spanish tumor registry (R-GETNE). *Oncologist.* 2018;23:422–432.
27. Rust E, Hubele F, Marzano E, et al. Nuclear medicine imaging of gastro-entero-pancreatic neuroendocrine tumors: the key role of cellular differentiation and tumor grade—from theory to clinical practice. *Cancer Imaging.* 2012;12:173–184.
28. Lam KY, Lo CY. Pancreatic endocrine tumour: a 22-year clinico-pathological experience with morphological, immunohistochemical observation and a review of the literature. *Eur J Surg Oncol.* 1997;23:36–42.
29. Volante M, Righi L, Berruti A, Rindi G, Papotti M. The pathological diagnosis of neuroendocrine tumors: common questions and tentative answers. *Virchows Arch.* 2011;458:393–402.
30. Thapa P, Ranade R, Ostwal V, Shrikhande SV, Goel M, Basu S. Performance of ^{177}Lu-DOTATATE-based peptide receptor radionuclide therapy in metastatic gastroenteropancreatic neuroendocrine tumor: a multiparametric response evaluation correlating with primary tumor site, tumor proliferation index, and dual tracer imaging characteristics. *Nucl Med Commun.* 2016;37:1030–1037.
31. Zhang J, Liu Q, Singh A, Schuchardt C, Kulkarni HR, Baum RP. Prognostic value of ^{18}F-FDG PET/CT in a large cohort of patients with advanced metastatic neuroendocrine neoplasms treated with peptide receptor radionuclide therapy. *J Nucl Med.* 2020;61:1560–1569.
32. Basu S, Chakraborty S, Parghane RV. et al. One decade of 'bench-to-bedside' peptide receptor radionuclide therapy with indigenous [^{177}Lu]Lu-DOTATATE obtained through 'direct' neutron activation route: lessons learnt including practice evolution in an Indian setting. *Am J Nucl Med Mol Imaging.* 2020;10:178–211.
33. Basu S, Parghane RV, Kamaldeep CS. Peptide receptor radionuclide therapy of neuroendocrine tumors. *Semin Nucl Med.* 2020;50:447–464.
34. Sitani K, Parghane RV, Talole S, Basu S. Long-term outcome of indigenous ^{177}Lu-DOTATATE PRRT in patients with metastatic advanced neuroendocrine tumours: a single institutional observation in a large tertiary care setting. *Br J Radiol.* 2021;94:20201041.
35. Adnan A, Sampathirao N, Basu S. Implications of fluorodeoxyglucose uptake in low-intermediate grade metastatic neuroendocrine tumors from peptide receptor radionuclide therapy outcome viewpoint: a semi-quantitative standardized uptake value-based analysis. *World J Nucl Med.* 2019;18:389–395.
36. Sampathirao N, Basu S. MIB-1 index-stratified assessment of dual-tracer PET/CT with ^{68}Ga-DOTATATE and ^{18}F-FDG and multimodality anatomic imaging in metastatic neuroendocrine tumors of unknown primary in a PRRT workup setting. *J Nucl Med Technol.* 2017;45:34–41.

Validation of Convolutional Neural Networks for Fast Determination of Whole-Body Metabolic Tumor Burden in Pediatric Lymphoma

Elba Etchebehere[1,2], Rebeca Andrade[1], Mariana Camacho[2], Mariana Lima[1,2], Anita Brink[3], Juliano Cerci[4], Helen Nadel[5], Chandrasekhar Bal[6], Venkatesh Rangarajan[7], Thomas Pfluger[8], Olga Kagna[9], Omar Alonso[10], Fatima K. Begum[11], Kahkashan Bashir Mir[12], Vincent Peter Magboo[13], Leon J. Menezes[14], Diana Paez*[15], and Thomas NB Pascual*[15]

[1]University of Campinas, Campinas, Brazil; [2]Medicina Nuclear de Campinas, Campinas, Brazil; [3]University of Cape Town, Cape Town, South Africa; [4]QUANTA Diagnóstico e Terapia, Curitiba, Brazil; [5]University of British Columbia, Vancouver, British Columbia, Canada; [6]All India Institute of Medical Sciences, New Delhi, India; [7]Tata Memorial Centre, Mumbai, India; [8]Ludwig-Maximillian University of Munich, Munich, Germany; [9]Rambam Health Care Campus, Haifa, Israel; [10]Centro Uruguayo de Imagenología Molecular, Montevideo, Uruguay; [11]National Institute of Nuclear Medicine and Allied Sciences, Dhaka, Bangladesh; [12]Nuclear Medicine, Oncology and Radiotherapy Institute, Islamabad, Pakistan; [13]University of the Philippines, Manila, Philippines; [14]Institute of Nuclear Medicine, London, United Kingdom; and [15]Nuclear Medicine and Diagnostic Imaging Section, Division of Human Health, International Atomic Energy Agency, Vienna, Austria

^{18}F-FDG PET/CT quantification of whole-body tumor burden in lymphoma is not routinely performed because of the lack of fast methods. Although the semiautomatic method is fast, it is not fast enough to quantify tumor burden in daily clinical practice. Our purpose was to evaluate the performance of convolutional neural network (CNN) software in localizing neoplastic lesions in whole-body ^{18}F-FDG PET/CT images of pediatric lymphoma patients. **Methods:** The retrospective image dataset, derived from the data pool of the International Atomic Energy Agency (coordinated research project E12017), included 102 baseline staging ^{18}F-FDG PET/CT studies of pediatric lymphoma patients (mean age, 11 y). The images were quantified to determine the whole-body tumor burden (whole-body metabolic tumor volume [wbMTV] and whole-body total lesion glycolysis [wbTLG]) using semiautomatic software and CNN-based software. Both were displayed as semiautomatic wbMTV and wbTLG and as CNN wbMTV and wbTLG. The intraclass correlation coefficient (ICC) was applied to evaluate concordance between the CNN-based software and the semiautomatic software. **Results:** Twenty-six patients were excluded from the analysis because the software was unable to perform calculations for them. In the remaining 76 patients, CNN and semiautomatic wbMTV tumor burden metrics correlated strongly (ICC, 0.993; 95% CI, 0.989 − 0.996; $P < 0.0001$), as did CNN and semiautomatic wbTLG (ICC, 0.999; 95% CI, 0.998–0.999; $P < 0.0001$). However, the time spent calculating these metrics was significantly (<0.0001) less by CNN (mean, 19 s; range, 11–50 s) than by the semiautomatic method (mean, 21.6 min; range, 3.2–62.1 min), especially in patients with advanced disease. **Conclusion:** Determining whole-body tumor burden in pediatric lymphoma patients using CNN is fast and feasible in clinical practice.

Key Words: ^{18}F-FDG PET/CT; whole-body tumor burden; pediatric; lymphoma

Received Jul. 14, 2021; revision accepted Feb. 10, 2022.

For correspondence or reprints, contact Elba Etchebehere (elba@hc.unicamp.br).

*Contributed equally to this work.

Published online Apr. 19, 2022.

J Nucl Med Technol 2022; 50:256–262
DOI: 10.2967/jnmt.121.262900

For pediatric staging and treatment response evaluation of Hodgkin and non-Hodgkin lymphoma, ^{18}F-FDG PET/CT is an invaluable tool and an established modality (*1–7*). Visual interpretation of ^{18}F-FDG PET/CT studies to assess the extent of disease can be subjective; therefore, qualitative interpretation is necessary to provide additional insight, reducing the subjectivity of visual interpretation (*8,9*). ^{18}F-FDG PET/CT whole-body metabolic tumor burden parameters such as metabolic tumor volume (MTV) and total lesion glycolysis (TLG) bear a high prognostic value in lymphoma patients, much greater than SUVs (*10–13*). However, the prognostic determination, although easily measured in primary solid tumors (*14–17*), has not been applied in daily clinical practice to patients with widespread lymphoma disease because calculations are extremely time-consuming.

There is a wide variety of methods to quantify MTV and TLG, using threshold-based or algorithm-based methods. Specifically relating to the threshold-based methods, the most commonly applied is the volume-of-interest (VOI) isocontour method (*15,17,18*). Automatic multifocal segmentation quantification in patients with lymphoma uses VOI isocontour and has been validated before and proven to be quite fast (*19*). Depending on patient tumor burden, the time spent calculating MTV and TLG could be impractical and still not feasible in daily clinical practice. The extraction and processing of imaging features from radiologic data, also known as radiomics, may also link imaging features with patient outcome. However, radiomics also requires precise tumor ROI delineation, which is also time-consuming, with delineation variabilities between observers.

Computer deep learning and functioning as a neural network have evolved substantially, achieving remarkable success in tumor segmentation and diagnosis and ultimately transforming and optimizing clinical practice (*18,20–23*), providing objective and accurate diagnoses in medicine by building diagnostic models. For example, software for multimodality imaging using deep convolutional neural networks (CNNs) automatically localizes and delineates metastases in whole-body ^{18}F-FDG PET/CT scans. Deep CNN seems capable of correctly localizing and classifying uptake patterns in ^{18}F-FDG PET/CT images into foci suggestive and nonsuggestive of cancer. These extracted features help the semantic interpretation and may simplify the PET workflow with a 1-click calculation of whole-body tumor burden (*24–26*). However, the clinical applicability of this software has not yet been fully tested, and unusual features may be identified if unsupervised by a physician (*27,28*).

The purpose of this study was to evaluate the performance of the recently developed CNN software in a clinical setting in pediatric lymphoma patients.

MATERIALS AND METHODS

This dataset, retrospectively studied, is derived from a subset of 102 baseline staging ^{18}F-FDG PET/CT studies of pediatric lymphoma patient images from the data pool of the prospective multicenter research project coordinated by the International Atomic Energy Agency (coordinated research project E12017).

Research Regulation and Data Protection

The study protocol was approved by each center's Institutional Review Board. A signed parental consent form was an inclusion criterion for recruitment, and all subjects gave such consent. Cases and forms were anonymized to ensure confidentiality while sharing data internationally.

Patients

The eligibility criteria consisted of pediatric patients (age $<$ 18 y) with newly diagnosed Hodgkin lymphoma or non-Hodgkin lymphoma who underwent a staging ^{18}F-FDG PET/CT scan. According to the World Health Organization classification criteria, the diagnosis was based on biopsy with immunohistochemistry (*29*). Exclusion criteria consisted of prior radiation therapy and chemotherapy and concurrent HIV infection.

The patient's clinical characteristics and tumor stage were evaluated, such as the age at diagnosis, the final clinical stage, spleen disease, additional nodal sites, disease volume, B symptoms, lactate dehydrogenase level, leukocytosis, erythrocyte sedimentation rate, anemia, albumin level, bone marrow ^{18}F-FDG uptake, Deauville score, MTV, and TLG.

^{18}F-FDG PET/CT Imaging and Quantification

All patients underwent staging whole-body ^{18}F-FDG PET/CT, from the top of the skull to the toes. All scans were obtained according to standard Society of Nuclear Medicine and Molecular Imaging or European Association of Nuclear Medicine procedure guidelines (*30*).

The whole-body MTV (wbMTV) and whole-body TLG (wbTLG) metrics were calculated using semiautomatic and CNN software. All images on both types of software were processed by 2 observers. Differences in the wbMTV and wbTLG metrics (if any) were recalculated to reach consensus. The semiautomatic software was used as the reference standard to evaluate the CNN software's performance.

Semiautomatic Quantification of Whole-Body Tumor Burden. The wbMTV and wbTLG metrics were calculated using semiautomatic multifocal segmentation software (Syngovia VB20; Siemens Medical Solutions), previously validated for clinical use (*19*) using a fixed threshold.

With this software, the whole-body tumor burden metrics (semiautomatic wbMTV and wbTLG) were obtained. The semiautomatic whole-body tumor burden was obtained by choosing the multifocal segmentation tool that automatically draws a rectangular VOI around the patient's entire body on the coronal axis. If necessary, the VOI is adjusted in the axial and sagittal planes. The liver is set as the background reference, and then volumes of interest are automatically determined surrounding each lymphoma lesion with uptake higher than the SUV_{mean} of the liver. A VOI threshold of 41% of the SUV_{max} using isocontour drawings was applied for all automatically delineated lesions. The image and VOIs were then reviewed to exclude physiologic areas incorrectly

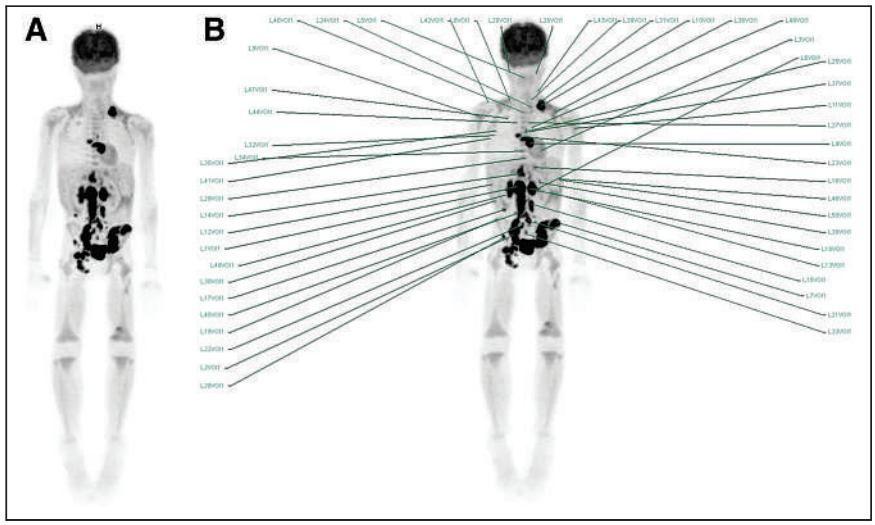

FIGURE 1. Whole-body tumor burden quantification on baseline staging ^{18}F-FDG PET/CT using semiautomatic software on patient with non-Hodgkin lymphoma. (A) Maximum-intensity projection shows hypermetabolic lymphoma infiltration in left supraclavicular and cervical lymph nodes, mediastinal lymph nodes, and extensively in abdominopelvic lymph nodes; lung nodules; and bone infiltration. (B) For calculation, liver is set as background reference, and VOIs automatically surround each lymphoma lesion with uptake higher than SUV_{mean} of liver. VOIs also include physiologic areas incorrectly selected as cancer to include metastatic foci with relatively low uptake, such as lung nodule metastasis with mild ^{18}F-FDG uptake in right upper lobe.

selected as cancer (such as brain, kidneys, bladder, and ureters) and include metastatic foci with relatively low uptake that were missed by the software (e.g., small lymph nodes). Afterward, whole-body MTV and TLG calculations were readily available and displayed as semiautomatic wbMTV and wbTLG (Fig. 1).

CNN Quantification of Whole-Body Tumor Burden. The wbMTV and wbTLG metrics were calculated using software based on deep CNN (Syngovia VB50; Siemens Healthineers). With this software, the whole-body tumor burden metrics (CNN wbMTV and wbTLG) were obtained.

Computation of the whole-body tumor burden on the CNN software was automatically performed by the deep CNN method as described by Sibille et al. (*24*). Unlike the semiautomatic software, the CNN software does not require an initial positioning of a VOI surrounding the body. The CNN automatically computes the maximum-intensity-projection ^{18}F-FDG PET image and integrates the anatomic CT image using an intuitive interface. Afterward, the software automatically detects ^{18}F-FDG–avid anatomic landmarks and discriminates hypermetabolic areas related to the physiologic activity that will be automatically excluded (Fig. 2) from cancer. Briefly, the PET VOIs are segmented using a fixed threshold algorithm and evaluated by the deep CNN. Whole-body CT examinations are aligned to an anatomic atlas. Finally, a maximum-intensity projection of the whole-body ^{18}F-FDG PET/CT is reconstructed, and the lesions are classified. The deep CNN uses a combination of multiplanar reconstructions of PET and CT, ^{18}F-FDG PET maximum-intensity projections, and anatomic atlases to predict the anatomic localization of ^{18}F-FDG foci and determine whether a focus was suggestive (or not) for malignancy. The advantage of the CNN algorithm is that it does not require the initial positioning of a VOI. This specific CNN software is not yet validated for pediatric patients.

Two forms of analyses were undertaken on the CNN software: the observer method, in which all VOIs automatically generated by the multifocal segmentation tool were reviewed (in a masked manner) by both observers to determine whether the VOIs were wrongly included or excluded from the results (afterward, values were calculated and displayed as CNN + observer wbMTV and wbTLG), and the no-observer method, in which the VOIs automatically obtained were accepted and did not undergo a masked review by each of the observers. The calculations were readily available and displayed as CNN wbMTV and wbTLG.

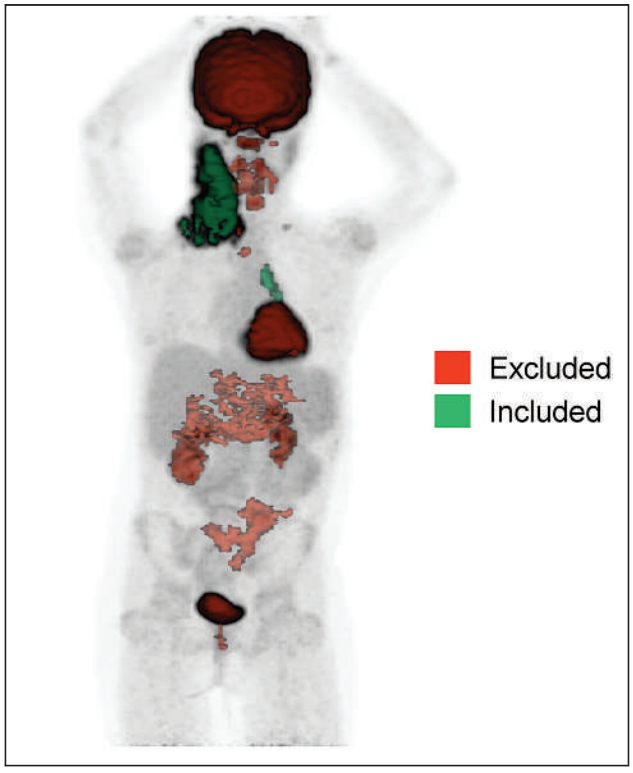

FIGURE 2. Whole-body tumor burden quantification on staging ^{18}F-FDG PET/CT using CNN. Displayed in red are regions that software excluded from analysis (regions related to physiologic uptake: brain, head and neck, heart, intestines, kidneys, and bladder), and displayed in green are regions that software included in calculation of whole-body tumor burden. In this patient, extensive cervical lymph node bulky mass and mediastinal lymph nodes were included.

Statistical Analysis

The sample was characterized by descriptive analysis, performed using frequency tables for categoric variables and measures of position and dispersion for continuous variables (mean, SD, median, minimum and maximum).

TABLE 1
Clinical Characteristics of Patients (n = 102)

Parameter	Variable	Number	Percentage
Sex	Female	32	31.4%
	Male	70	68.6%
Lymphoma type	Hodgkin	80	78.4%
	Non-Hodgkin	22	21.6%
Clinical final stage	1	8	7.8%
	2	34	33.3%
	3	34	33.3%
	4	26	25.5%
Spleen	Yes	29	28.4%
Disease	No	73	71.6%
Extranodal sites	0	67	65.7%
	1	15	14.7%
	≥2	20	19.6%
Disease bulk	Bulky	63	61.8%
	Nonbulky	39	38.2%
B symptoms	Yes	43	43.0%
	No	57	57.0%
LDH	High	47	52.8%
	Normal	42	47.2%
Leukocytosis	Yes	32	31.7%
	No	69	68.3%
Erythrocyte sedimentation rate	Normal	34	52.3%
	Elevated	31	47.7%
Anemia	Yes	47	47.5%
	No	52	52.5%
Albumin	Yes	27	37.0%
	No	46	63.0%
Bone marrow	Diffuse	12	11.9%
^{18}F-FDG	Focal	16	15.8%
Uptake	Negative	73	72.3%
Event	Yes	10	9.8%
	No	92	90.2%
Status	Alive	101	99.0%
	Dead	1	1.0%

The χ^2 test or Fisher exact test was used to check associations or compare proportions, and the Mann–Whitney test was used to compare continuous or orderable measurements between the 2 groups. Risk factors associated with the event were identified with univariate and multiple Cox regression analyses. The variable selection process used was stepwise.

To verify the relationship between continuous measurements, the Spearman correlation coefficient was used ranging from −1 to 1.

To assess agreement between the semiautomatic and CNN software, the intraclass correlation coefficient (ICC) was used (values above 0.7 were considered to indicate substantial agreement). The Friedman test and the Wilcoxon test for related samples were used to compare the times. The time was defined as the moment that the physician began focusing on the task until the moment that the whole-body tumor burden calculation was completed. The level of significance was 0.05.

RESULTS

The whole-body tumor burden was quantified using both types of software in 102 ^{18}F-FDG PET/CT baseline scans of pediatric lymphoma patients. There were 32 (31.4%) girls and 70 (68.6%) boys. The mean age at lymphoma diagnosis was 11.1 ± 4.3 y (range, 4.0–18.0 y). Among these, 80 (78.4%) patients had Hodgkin lymphoma, and 22 (21.6%) had non-Hodgkin lymphoma. Table 1 displays the clinical characteristics.

Semiautomatic Calculation of Whole-Body Tumor Burden

The semiautomatic wbMTV and wbTLG were calculated in all 102 patients. The average time spent on this calculation was 21.6 min, ranging from 3.2 to 62.1 min. Notably, in patients with widespread lesions in multiple organs or confluent with areas of physiologic excretion, the software took longer to identify and delineate abnormal areas.

CNN-Based Calculation of Tumor Burden

The CNN + observer wbMTV and wbTLG were also calculated in all 102 patients. The average time spent on this calculation, with the CNN software having the observers evaluate the images before calculation, was 3.8 min, ranging from 0.5 to 19.6 min.

On the other hand, CNN wbMTV and wbTLG (i.e., without any observer evaluating the CNN software's performance before calculation) were calculated in 76 of the 102 patients. Twenty-six patients were excluded from the analyses because the software could not perform calculations because of patient movement or misregistration (n = 6), because the software could not recognize small lymph nodes as diseased (n = 8), or because there was widespread brown fat (n = 3), diffuse bone infiltration (n = 5), diffuse homogeneous mild infiltration of the spleen (n = 2), or subcutaneous infiltration of ^{18}F-FDG at the injection site (n = 2) (Fig. 3).

Impressively, the average total time spent calculating CNN wbMTV and wbTLG was 19 s, ranging from 11 to 50 s. This total time begins when the physician begins focusing on the task and ends at completion of the whole-body tumor burden calculation. Thus, the times spent calculating CNN, CNN + observer, and semiautomatic wbMTV metrics in 76 paired patients were significantly different (P < 0.0001). The CNN software alone was much faster and more precise than either the semiautomatic or the CNN + observer method (Table 2).

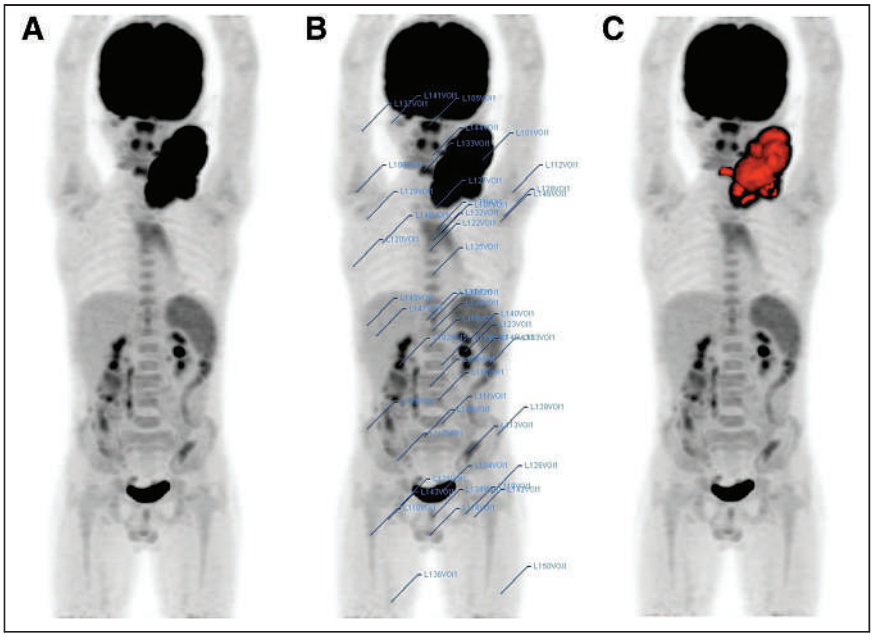

FIGURE 3. Baseline staging ^{18}F-FDG PET/CT of patient with Hodgkin lymphoma. (A) Maximum-intensity projection reveals cervical hypermetabolic bulky mass. (B) Image displayed with different whole-body tumor burden quantification methods shows that using semiautomatic method, VOIs are delineated in cancer lesions and also in physiologic regions not related to cancer; these regions must be deleted before quantification. Whole-body tumor burden calculation showed semiautomatic wbMTV of 104 and TLG of 1,663; time spent calculating these metrics was 5 min. (C) CNN whole-body tumor burden quantification does not delineate regions nonrelated to cancer and demonstrates similar metrics: CNN + observer wbMTV of 105 and CNN + observer wbTLG of 1,671. Time spent calculating was significantly less (13 s) even though CNN software failed to delineate spleen, which had to be performed manually.

Comparison of Semiautomatic and CNN Tumor Burden Measurements

The CNN + observer and semiautomatic wbMTV metrics calculated on the 102 patients correlated strongly (ICC, 0.993; 95% CI, 0.989–0.996; P < 0.0001), as did the CNN + observer and semiautomatic wbTLG metrics (ICC, 0.999; 95% CI, 0.998–0.999; P < 0.0001). Among the 76 ^{18}F-

TABLE 2
Time Spent Quantifying Whole-Body Tumor Burden Metrics on Semiautomatic Software and CNN Software With and Without Observer Input

		Time (s)					
Variable	*n*	Mean	SD	Minimum	Median	Maximum	*P*
Semiautomatic	76	1,301.3	863.5	198.0	1,107.0	3,724.0	<0.0001
CNN + observer	76	221.1	204.4	31.0	155.0	1,176.0	
CNN	76	19.6	8.0	11.0	17.0	50.0	

FDG PET/CT studies in which the fully automatic CNN was performed, the CNN + observer, CNN, and semiautomatic wbMTV metrics also correlated strongly, as did the CNN + observer, CNN, and semiautomatic wbTLG metrics (Table 3).

Impressively, the correlation between CNN and semiautomatic wbMTV was significantly high (ICC, 0.950; 95% CI, 0.922–0.968; $P < 0.0001$), as was CNN and semiautomatic wbTLG (ICC, 0.947; 95% CI, 0.917–0.966; $P < 0.0001$). Therefore, the CNN software performed equally well, similar to the semiautomatic tool in which an experienced observer evaluated the images.

More impressive, however, was the fact that the correlation between CNN + observer and CNN wbMTV was significantly high (ICC, 0.946; 95% CI, 0.912–0.966; $P < 0.0001$), as was CNN + observer and CNN wbTLG (ICC, 0.952; 95% CI, 0.925–0.969; $P < 0.0001$). Consequently, the CNN software performance did not require an observer to evaluate the images and validate all VOIs.

DISCUSSION

To our knowledge, this was the first study to quantify the whole-body tumor burden of pediatric lymphoma patients using CNN and deep learning. Despite the difference in ^{18}F-FDG biodistribution between children and adults, the CNN-based software accurately delineated abnormal regions. The CNN-based software optimized the working time, was extremely fast, and performed better than the semiquantitative software in calculating whole-body tumor burden.

The CNN-based software allows a review of the VOIs provided automatically (i.e., VOIs can be added manually or incorrect ones deleted). Ultimately comparison of the CNN-based software with and without the observer's review of the VOIs rendered the same metrics. However, the time spent determining the whole-body tumor burden metrics by the semiautomatic software was longer, because it depends primarily on the extent of the disease. The semiautomatic quantification does not allow preselection of VOIs by the operator before creating the definitive findings and thus does not distinguish diseased areas from physiologic areas, creating many VOIs that overload the program.

On the other hand, quantifying the whole-body tumor burden through CNN-based software was significantly faster, with and without the observer reviewing the VOIs. Impressively, when we compared quantification of the whole-body tumor burden on the CNN-based software (without observer interference) with the semiautomatic software and CNN-based software with observer interference, CNN-based software without the interference of the observer was significantly faster and just as precise. CNN-based software took as little as 20 s to calculate the patient's entire tumor burden, without the need to review the VOIs (Figs. 4 and 5).

However, there were some limitations. It was not possible to show whether the measurements predicted by the CNN-based software could be applied to our patient cohort to predict prognosis and response evaluation. Most (78.4%) of the patients had Hodgkin lymphoma, and there were only 2 deaths; therefore, it was not possible to determine overall survival. A

TABLE 3
Correlation of Whole-Body Tumor Burden Metrics on Semiautomatic Software and CNN-Based Software With and Without Observer Input in 76 Patients

Variable	Mean	SD	Min	Median	Max	ICC	95% CI	*P*
MTV						0.960	0.942–0.974	<0.0001
Semiautomatic	242.8	205.9	4.6	149.0	772.6			
CNN + observer	254.8	212.8	4.1	178.3	778.3			
CNN	234.8	206.9	11.7	147.6	784.4			
TLG						0.963	0.947–0.975	<0.0001
Semiautomatic	1,626.4	1,674.6	50.0	894.7	6,963.1			
CNN + observer	1,647.3	1,685.8	50.1	902.1	5,963.4			
CNN	1,647.7	1,811.2	31.0	871.3	8,218.6			

Min = minimum; Max = maximum; ICC = intraclass correlation coefficient.

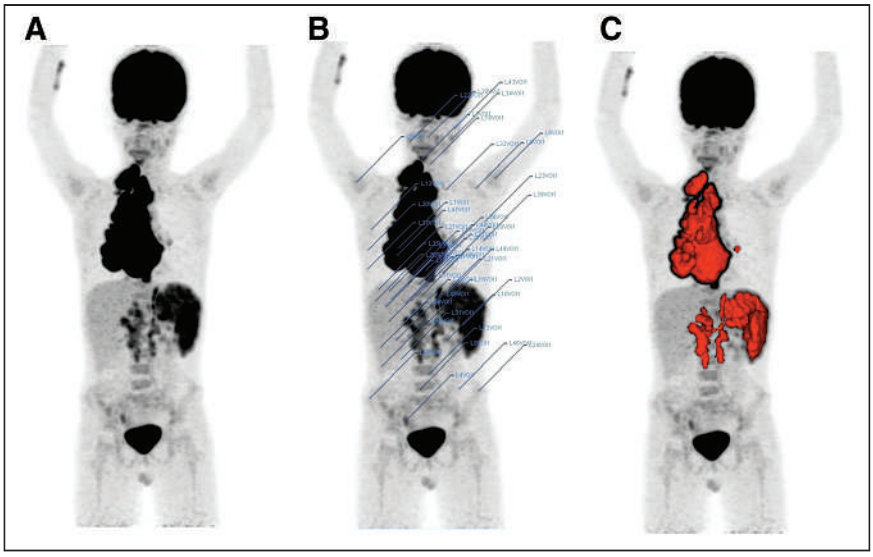

FIGURE 4. Baseline staging ^{18}F-FDG PET/CT of Hodgkin lymphoma. (A) Maximum-intensity projection reveals mediastinal hypermetabolic bulky mass and extensive infiltration of cervical lymph nodes, abdominal lymph nodes, and spleen. (B) Semiautomatic quantification reveals semiautomatic wbMTV of 548 and semiautomatic wbTLG of 5,238; time spent calculating was 15 min. (C) CNN whole-body tumor burden quantification demonstrates similar metrics: CNN wbMTV of 570 and CNN wbTLG of 5,213, but time spent calculating was significantly less (14 s). CNN software excludes focal areas of physiologic uptake such as right ureter and includes areas of mild uptake such as left hilar lymph node.

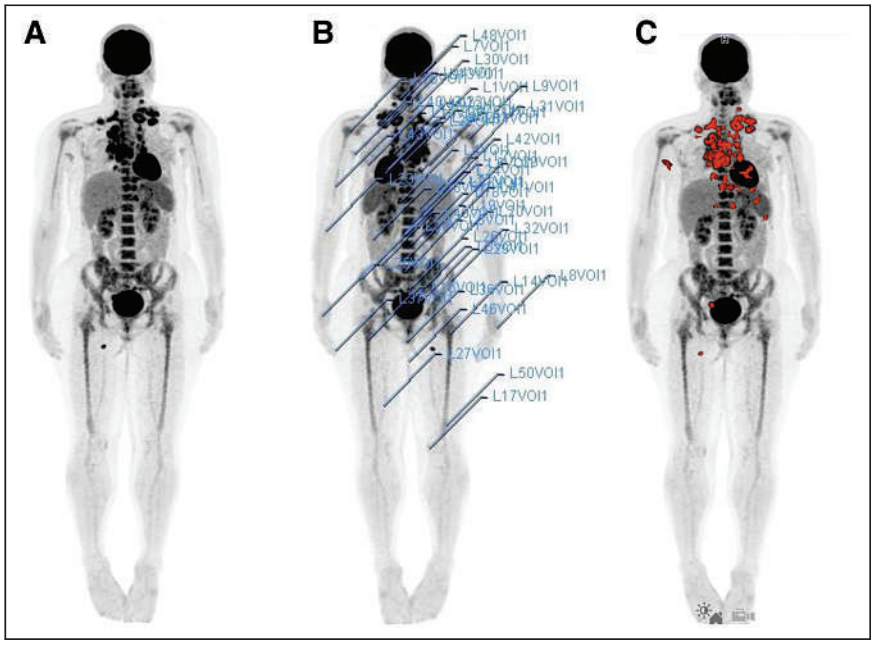

FIGURE 5. ^{18}F-FDG PET/CT of patient with Hodgkin lymphoma. (A) Maximum-intensity projection reveals mediastinal hypermetabolic bulky mass and cervical, axillary, and inguinal nodes. (B) Semiautomatic VB20 whole-body tumor burden quantification reveals MTV of 194 and TLG of 1,007; time spent calculating these metrics was 30 min because of extent of lesions and need to exclude multiple areas of physiologic uptake. (C) CNN whole-body tumor burden quantification demonstrates similar metrics: MTV of 200 and TLG of 968. However, time spent calculating was significantly less (36 s). CNN software excludes physiologic areas with high uptake such as heart and includes lymph nodes with less uptake adjacent to heart.

larger number of patients with events are required to determine whether the measurements predicted by CNN-based software can predict prognosis. Another limitation is that 25% of the patients were excluded from analyses because the CNN-based software could not recognize areas of metabolically active disease and could not perform calculation. In such situations, these patients had to be excluded because there was no ability to compare CNN quantification with manual or semiautomatic quantification. The CNN software we tested was not initially designed or validated to quantify specifically pediatric patients but, even so, performed quite well. These exclusions were caused by either the wrong lesion being segmented or lesions being missed. For example, small lymph nodes with mild ^{18}F-FDG uptake were excluded; extensive brown fat was erroneously included as lymphomatous infiltration; extensive diffuse bone marrow infiltration (5/12 patients) was missed; and radiopharmaceutical extravasation sites and bladder catheter were erroneously included. Most likely, with further CNN and deep-learning development and specific training in pediatric patients regarding differentiation of normal biodistribution from cancer tissue, failure rates will decrease.

CNN-based software with CNN and deep learning still requires the input of the observer (*26–28*). In 25% of the patients, CNN could not depict the correct neoplastic tissue or added nonneoplastic tissue; thus, quantification had to be excluded because the software was not performing the calculations. Therefore, errors and failure to detect proper tissue will occur even in CNN and DL software, arguing in favor of the observer input. Most likely, the largest errors may be associated with unsupervised quantification.

CONCLUSION

CNN-based quantification of whole-body tumor burden in pediatric lymphoma patients is an emerging field. Determination of whole-body tumor

burden using CNN-based software is extremely fast and feasible in clinical practice in pediatric lymphoma patients. CNN-based software requires CNN and deep-learning development and specific training in pediatric patients, as well as the input of the observer to minimize failure rates. Tumor burden should be evaluated in most if not all tumors and age groups for therapy purposes.

DISCLOSURE

The whole-body metrics were calculated using a loaned Siemens device equipped with a software based on deep CNN (Syngovia VB50).

ACKNOWLEDGMENT

We thank Cleide Silva from the Statistics Research Department of the University of Campinas for her invaluable help.

KEY POINTS

QUESTION: Will the use of CNN promote fast and reliable quantification data regarding whole-body metabolic tumor burden in ^{18}F-FDG PET/CT pediatric lymphoma patients?

PERTINENT FINDINGS: Quantification of whole-body metabolic tumor burden using CNN correlates strongly with semiautomatic quantification (ICC, 0.993; 95% CI, 0.989 − 0.996; $P < 0.0001$).

IMPLICATIONS FOR PATIENT CARE: In addition to reliable data, implementation of CNN quantification tools in clinical practice may be able to quickly and accurately deliver prognostic information for better patient management.

REFERENCES

1. Ansell SM, Armitage JO. Positron emission tomographic scans in lymphoma: convention and controversy. *Mayo Clin Proc.* 2012;87:571–580.
2. Cheson BD. PET/CT in lymphoma: current overview and future directions. *Semin Nucl Med.* 2018;48:76–81.
3. Kobe C, Dietlein M, Hellwig D. PET/CT for lymphoma post-therapy response assessment in Hodgkin lymphoma and diffuse large B-cell lymphoma. *Semin Nucl Med.* 2018;48:28–36.
4. Gillman J, States LJ, Servaes S. PET in pediatric lymphoma. *PET Clin.* 2020;15:299–307.
5. D'souza MM, Jaimini A, Bansal A, et al. FDG-PET/CT in lymphoma. *Indian J Radiol Imaging.* 2013;23:354–365.
6. Cronin CG, Swords R, Truong MT, et al. Clinical utility of PET/CT in lymphoma. *AJR.* 2010;194:W91–W103.
7. London K, Cross S, Onikul E, Dalla-Pozza L, Howman-Giles R. ^{18}F-FDG PET/CT in paediatric lymphoma: comparison with conventional imaging. *Eur J Nucl Med Mol Imaging.* 2011;38:274–284.
8. Lin C, Itti E, Haioun C, et al. Early ^{18}F-FDG PET for prediction of prognosis in patients with diffuse large b-cell lymphoma: SUV-based assessment versus visual analysis. *J Nucl Med.* 2007;48:1626–1632.
9. Jhanwar YS, Straus DJ. The role of PET in lymphoma. *J Nucl Med.* 2006;47:1326–1334.
10. Yang J, Zhu S, Pang F, et al. Functional parameters of ^{18}F-FDG PET/CT in patients with primary testicular diffuse large B-cell lymphoma. *Contrast Media Mol Imaging.* 2018;2018:8659826.
11. Jung S-H, Ahn J-S, Kim Y-K, et al. Prognostic significance of interim PET/CT based on visual, SUV-based, and MTV-based assessment in the treatment of peripheral T-cell lymphoma. *BMC Cancer.* 2015;15:198.
12. Albano D, Camoni L, Giubbini R, Bertagna F. Prognostic value of ^{18}F-FDG PET/CT metabolic parameters in splenic marginal zone lymphoma. *Clin Lymphoma Myeloma Leuk.* 2020;20:e897–e904.
13. Wang X-Y, Zhao Y-F, Liu Y, Yang Y-K, Wu N. Prognostic value of metabolic variables of ^{18}F-FDG PET/CT in surgically resected stage I lung adenocarcinoma. *Medicine (Baltimore).* 2017;96:e7941.
14. Salavati A, Duan F, Snyder BS, et al. Optimal FDG PET/CT volumetric parameters for risk stratification in patients with locally advanced non-small cell lung cancer: results from the ACRIN 6668/RTOG 0235 trial. *Eur J Nucl Med Mol Imaging.* 2017;44:1969–1983.
15. Wang L, Bai J, Duan P. Prognostic value of ^{18}F-FDG PET/CT functional parameters in patients with head and neck cancer: a meta-analysis. *Nucl Med Commun.* 2019;40:361–369.
16. Brito AE, Mourato F, Santos A, Mosci C, Ramos C, Etchebehere E. Validation of the semiautomatic quantification of ^{18}F-fluoride PET/CT whole-body skeletal tumor burden. *J Nucl Med Technol.* 2018;46:378–383.
17. Im H-J, Bradshaw T, Solaiyappan M, Cho SY. Current methods to define metabolic tumor volume in positron emission tomography: which one is better? *Nucl Med Mol Imaging.* 2018;52:5–15.
18. Han D, Bayouth J, Song Q, et al. Globally optimal tumor segmentation in PET-CT images: a graph-based co-segmentation method. *Inf Process Med Imaging.* 2011;22:245–256.
19. Camacho MR, Etchebehere E, Tardelli N, et al. Validation of a multifocal segmentation method for measuring metabolic tumor volume in Hodgkin lymphoma. *J Nucl Med Technol.* 2020;48:30–35.
20. Davenport T, Kalakota R. The potential for artificial intelligence in healthcare. *Future Healthc J.* 2019;6:94–98.
21. Deo RC. Machine learning in medicine. *Circulation.* 2015;132:1920–1930.
22. Shaw J, Rudzicz F, Jamieson T, Goldfarb A. Artificial intelligence and the implementation challenge. *J Med Internet Res.* 2019;21:e13659.
23. Recht MP, Dewey M, Dreyer K, et al. Integrating artificial intelligence into the clinical practice of radiology: challenges and recommendations. *Eur Radiol.* 2020;30:3576–3584.
24. Sibille L, Seifert R, Avramovic N, et al. ^{18}F-FDG PET/CT uptake classification in lymphoma and lung cancer by using deep convolutional neural networks. *Radiology.* 2020;294:445–452.
25. Froelich JW, Salavati A. Artificial intelligence in PET/CT is about to make whole-body tumor burden measurements a clinical reality. *Radiology.* 2020;294:453–454.
26. Currie G, Hawk EK, Rohren E, Vial A, Klein R. Machine learning and deep learning in medical imaging: intelligent imaging. *J Med Imaging Radiat Sci.* 2019;50:477–487.
27. Currie G. Intelligent imaging: anatomy of machine learning. *J Nucl Med Technol.* 2019;47:273–281.
28. Currie G, Rohren E. Intelligent imaging in nuclear medicine: the principles of artificial intelligence, machine learning and deep learning. *Semin Nucl Med.* 2021;51:102–111.
29. Jaffe ES, Barr PM, Smith SM. Understanding the new WHO classification of lymphoid malignancies: why it's important and how it will affect practice. *Am Soc Clin Oncol Educ Book.* 2017;37:535–546.
30. Boellaard R, Delgado-Bolton R, Oyen WJG, et al. FDG PET/CT: EANM procedure guidelines for tumour imaging—version 2.0. *Eur J Nucl Med Mol Imaging.* 2015;42:328–354.

Reducing Radiation Exposure from PET Patients

Shorouk F. Dannoon[1,2], Saud Alenezi[1,3], Naheel Alnafisi[1,2], Samar Almutairi[1], Fatma Dashti[3], Medhat M. Osman[4], and Abdelhamid Elgazzar[1,2]

[1]Nuclear Medicine Department, Faculty of Medicine, Kuwait University, Jabryia, Kuwait; [2]Nuclear Medicine Department, Mubarak Hospital, Ministry of Health, Jabryia, Kuwait; [3]Nuclear Medicine Department, Farwania Hospital, Ministry of Health, Farwania, Kuwait; and [4]Department of Radiology, Division of Nuclear Medicine, St. Louis University, St. Louis, Missouri

This study measured the typical emitted radiation rate from the urinary bladder of PET patients after their scan and investigated simple methods for reducing the emitted radiation before discharge. **Methods:** The study included 83 patients (63 ^{18}F-FDG and 20 ^{18}F-NaF patients). Emitted radiation from the patients' urinary bladder was measured with an ionization survey meter at a 1-m distance, presuming the urinary bladder to be the primary source of radiation. The measurements were taken at different time points after PET image acquisition: immediate (prevoid 1), voided (postvoid 1), after waiting 30 min in the uptake room while drinking 500 mL of water (prevoid 2), and voided again (postvoid 2). **Results:** For ^{18}F-FDG patients, the reduction of emitted radiation due to drinking water and voiding alone from prevoid 1 to decay-corrected postvoid 2 was an average of 22.49% ± 7.48% (13.65 ± 3.42 μSv/h to 10.48 ± 2.37 μSv/h, $P < 0.001$). For ^{18}F-NaF patients, the reduction was an average of 25.80% ± 10.03% (9.83 ± 2.01 μSv/h to 7.23 ± 1.49 μSv/h, $P < 0.001$). **Conclusion:** In addition to the physical decay of the radiotracers, using the biologic clearance properties resulted in a significant decrease of the emitted radiation in this study. Implementing additional water consumption to facilitate voiding with 30 min of wait time before discharging certain ^{18}F-FDG and ^{18}F-NaF patients who need to be in close contact with others, such as elderly, caregivers, and inpatients, might facilitate lowering their emitted radiation by an average of 22%–25% due to voiding, not counting in the physical decay that should add an additional 17% reduction.

Key Words: PET/CT; public safety; radiation exposure; ALARA

J Nucl Med Technol 2022; 50:263–268
DOI: 10.2967/jnmt.121.263223

PET imaging procedures have increased in the past few decades. The increased use of PET is attributed to multiple factors, including awareness of referring physicians and the emergence of a variety of tracers with numerous clinical applications (*1*). Further, the clinical indications of PET have expanded beyond oncology to include infection, inflammation, cardiovascular, brain and skeletal imaging. The first approved PET radiotracers by the U.S. Food and Drug Administration (FDA) and most widely used were ^{18}F-FDG (^{18}F-FDG) and ^{18}F-sodium fluoride (^{18}F-NaF) (*2*). Recently, the FDA has approved more PET radiotracers that are being used in clinical practice: ^{13}N-ammonia in 2007, ^{18}F-florbetapir in 2012, ^{18}F-flutemetamol in 2013, ^{18}F-florbetaben in 2014, ^{18}F-fluciclovine in 2016, ^{68}Ga-DOTATATE in 2016, ^{68}Ga-DOTATOC in 2019, ^{18}F-fluorodopa in 2019, ^{64}Cu-DOTATATE in 2020, ^{18}F-fluoroestradiol in 2020, and ^{68}Ga-PSMA in 2020. Currently, there are additional PET radiotracers that are being evaluated in clinical trials and as investigational new drugs.

With the recent development of these PET radiotracers, there has been more attention given to the radiation exposure from PET patients after being discharged. Although radiation from medical use and nuclear medicine is overall safe (*3,4*), lowering radiation exposure from the patients to their caregivers or contacts is desirable. This is particularly important in special patient groups such as inpatients, who immediately return to their wards after imaging, and also for patients who require special assistance from a caregiver. There are a couple of studies that measured the emitted radiation from patients undergoing ^{68}Ga-DOTATOC, ^{18}F-fluorodopa, ^{18}F-FDG, and ^{18}F-fluciclovine scans (*3,5*).

Because most diagnostic studies before PET popularity were performed using ^{99m}Tc-labeled radiotracers, the discharge criteria for these studies are well-defined as there is minimal radiation exposure from the patients due to the 140 keV γ-emission and a 6-h half-life of a ^{99m}Tc radionuclide. On the other hand, PET radionuclides emit two 511-keV photons simultaneously, which are capable of more ionizing damage to their surroundings in comparison to ^{99m}Tc radionuclides. Therefore, both types of radiotracers cannot be treated equally and separate guidelines should be implemented for PET radiotracers. To date, however, there are no mandated release criteria for discharge of PET patients after completion of their scan.

Published articles have stated that most of the patients who underwent ^{18}F-FDG scanning had emitted radiation exceeding or close to 20 μSv/h at the time of discharge (*3–7*). Muzaffar et al. stated that 97% of these patients had dropped the radiation exposure to below 20 μSv/h using simple interventions such as waiting half an hour after scanning and voiding before being discharged (*5*). This was, however, not the case with ^{18}F-fluciclovine patients: only 25% of the patients had a drop of radiation exposure below 20 μSv/h after the same interventions.

Received Oct. 2, 2021; revision accepted Mar. 21, 2022.
For correspondence or reprints, contact Shorouk Faleh Dannoon (sdannoon@hsc.edu.kw).
Published online Apr. 19, 2022.

This observation is mainly because the imaging protocol and the biodistribution of ^{18}F-fluciclovine are significantly different from those of ^{18}F-FDG (*5*).

The objectives of this project were to determine the typical emitted radiation rate from the urinary bladder region of PET patients after the completion of ^{18}F-FDG or ^{18}F-NaF PET scans and to further investigate and validate the importance of simple interventions in an attempt to reduce the emitted radiation. These simple interventions may help in lowering the potential radiation exposure to close contacts without compromising the quality of images and at no additional cost.

MATERIALS AND METHODS

Patients undergoing PET scans in the nuclear medicine department for various clinical indications were asked to volunteer for this study. The study protocol was approved by the Kuwait University, Faculty of Medicine Ethical Review Committee as well as the Ministry of Health Ethical Review Committee. All the subjects signed a written informed consent form to participate in this study.

A total of 83 eligible patients consented to participate in the study. The study included patients undergoing PET scans using ^{18}F-FDG or ^{18}F-NaF. Patients who were bedridden, on kidney dialysis, with urine catheters, and under the age of 18 y were excluded from the study.

There were 63 patients (35 men and 28 women; mean age, 54.27 ± 15.14 y) who received a weight-based ^{18}F-FDG dose of 5.18 MBq/kg ([0.14 mCi/kg]; range, 185–352 MBq [5–9.5 mCi]) (Table 1). After injection, the patients had an approximately 60-min uptake time followed by a whole-body PET/CT acquisition of about 15–20 min (Gemini TF 64 slice PET/CT; Philips). Each patient's equivalent dose rate was then measured with an ionization survey meter (GM Detector, model IA-V2; International Medcom) at 1 m immediately after the completion of the PET scan. On the basis of the institutional guidelines, the ionization survey meter is calibrated every 6 mo. For distance consistency, 2 tape marks were placed on the floor of the uptake rooms at a 1-m distance. Patients were asked to stand by one of the tape marks on the floor with the technologist on the other tape mark. Presuming the urinary bladder is the primary source of activity emitted from the patient, the radiation emissions from the urinary bladder were recorded. The bladder was assumed to be in its normal location in the pelvis. The survey meter was held by the technologist at the height of the patient's urinary bladder. The measurements were recorded after the radiation reading became steady on the ionization survey meter. After the initial radiation measurement (prevoid 1), the patients were then asked to void, and another measurement (postvoid 1) was recorded. Then the patients were given 500 mL of water to drink while waiting for 30 min in the uptake room and instructed not to void during this period. As per the study protocol, the patients waited in their individual uptake rooms and did not come into contact with anyone during this time. Additional measurements were recorded after the 30-min wait (prevoid 2), and finally, the patients were asked to void again for a last measurement (postvoid 2) before being discharged from the department. The average stay of the patients in the department during this study was 139 ± 16 min (range, 86–177 min) from the time of ^{18}F-FDG administration until the time of the postvoid 2 measurement.

For ^{18}F-NaF, 20 patients (8 men and 12 women; mean age, 57.55 ± 18.69 y) were eligible and agreed to participate in this study (Table 1). These patients received a weight-based dose of 5.18 MBq/kg ([0.14 mCi/kg] range, 186–376 MBq [5.02–10.17 mCi]). The emitted radiation was measured in a manner similar to that for ^{18}F-FDG patients. The average stay of the patients in the department during this study was 168 ± 15 min (range, 140–191 min) from the time of ^{18}F-NaF administration until the time of the postvoid 2 measurement.

Statistical Analysis

The IBM Statistical Package for Social Sciences (version 23; SPSS-Inc.) was used to perform all statistical analyses. Group statistics, providing basic information about group comparisons, including the sample size (*n*), mean, and SD, were calculated and presented as mean ± SD. The independent-samples *t* test was conducted to compare the means between groups to determine statistical significance.

The data were analyzed on the basis of different categories, including sex, body mass index (BMI), and age. In the sex category, there were 35 men and 28 women for the ^{18}F-FDG group and 8 men and 12 women in the ^{18}F-NaF group. In the BMI category, the patients were grouped according to World Health Organization classifications: a normal group, from 18.5 to 24.9; an overweight group, from 25 to 29.9; and an obese group, with a BMI of 30.0 and higher (*8*). There were 13 normal, 22 overweight, and 28 obese ^{18}F-FDG patients, and there were 5 normal, 5 overweight, and 10 obese ^{18}F-NaF patients. The age category included

TABLE 1
Patient Demographic Data

Tracer	Study group	No. of patients	Age (y)	BMI	Dose (MBq)
^{18}F-FDG	Male	35	Range, 27–77	Range, 19.31–43.04	Range, 188–337
			Mean, 54.63 ± 14.95	Mean, 28.99 ± 5.39	Mean, 284 ± 35
	Female	28	Range, 21–81	Range, 17.58–39.91	Range, 185–352
			Mean, 53.82 ± 15.37	Mean, 29.80 ± 4.86	Mean, 278 ± 77
	All	63	Range, 21–81	Range, 17.58–43.04	Range, 185–352
			Mean, 54.27 ± 15.14	Mean, 29.33 ± 5.19	Mean, 281 ± 37
^{18}F-NaF	Male	8	Range, 22–81	Range, 21.55–34.55	Range, 224–376
			Mean, 63 ± 20.84	Mean, 28.34 ± 4.87	Mean, 289 ± 50
	Female	12	Range, 23–78	Range, 20.09–39.84	Range, 186–369
			Mean, 53.92 ± 16.11	Mean, 29.66 ± 5.39	Mean, 261 ± 51
	All	20	Range, 22–81	Range, 20.09–39.84	Range, 186–376
			Mean, 57.55 ± 18.69	Mean, 29.25 ± 5.26	Mean, 272 ± 53

a youth group of 18–24 y old, an adult group of 25–64 y old, and a senior group of 65 y and older. For the ^{18}F-FDG patients, there were 2 in the youth group, 41 in the adult group, and 20 in the senior group. For the ^{18}F-NaF patients, there were 2 in the youth group, 8 in the adult group, and 10 in the senior group.

RESULTS

^{18}F-FDG Patients

For ^{18}F-FDG patients, the average decrease of emitted radiation rate from prevoid 1 to postvoid 1 was 10.05% ± 6.54% (13.69 ± 3.42 μSv/h to 12.16 ± 2.74 μSv/h, P = 0.008) as illustrated in Figure 1. The average decrease from prevoid 2 to postvoid 2 was 12.08% ± 6.02% (9.87 ± 2.18 μSv/h to 8.67 ± 1.96 μSv/h, P = 0.001). The average reduction of emitted radiation due to drinking water and voiding from prevoid 1 to decay-corrected postvoid 2 was 22.49% ± 7.48% (13.65 ± 3.42 μSv/h to 10.48 ± 2.37 μSv/h, $P < 0.001$).

In the sex category, the difference in the overall reduction of the emitted radiation between the men and women was not statistically significant (Fig. 2). In the BMI category, the difference in an overall reduction of the emitted radiation between the normal, overweight, and obese patient groups was not statistically significant (Fig. 2). For the grouping based on age, the difference in overall reduction of the emitted radiation between the youth, adult, and senior groups was not statistically significant (Fig. 2).

^{18}F-NaF Patients

For ^{18}F-NaF patients, the average decrease of emitted radiation rate from prevoid 1 to postvoid 1 was 13.33% ± 11.26% (9.83 ± 2.01 μSv/h to 8.32 ± 1.63 μSv/h, P = 0.011) as illustrated in Figure 3. The average decrease from prevoid 2 to postvoid 2 was 15.64% ± 8.17% (7.08 ± 1.58 μSv/h to 5.98 ± 1.24 μSv/h, P = 0.012). The average reduction of emitted radiation rate due to drinking water and voiding from prevoid 1 to decay-corrected postvoid 2 was 25.80% ± 10.03% (9.83 ± 2.01 μSv/h to 7.23 ± 1.49 μSv/h, $P < 0.001$).

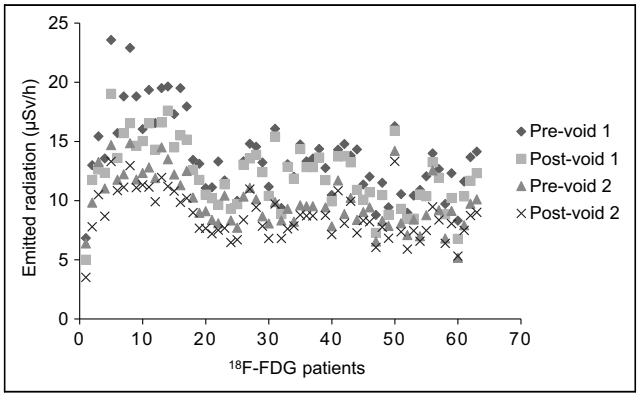

FIGURE 1. Exposure rates (μSv/h at 1 m) from ^{18}F-FDG patients (n = 63) at different time points.

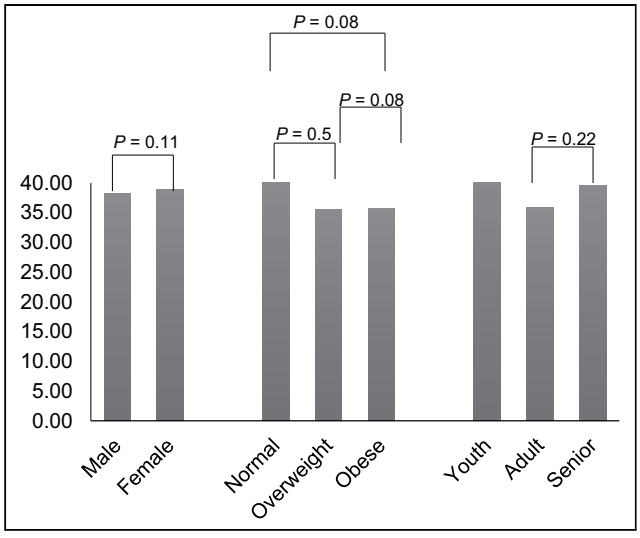

FIGURE 2. Comparison of overall reduction of emitted radiation from voiding after decay correction of categorized ^{18}F-FDG patients with corresponding P values. P values indicate no statistical significance between different patient categories regarding effect of decay-corrected void. Youth group has only 2 patients, therefore, P value of this group was not calculated.

In the sex category, the difference in the overall reduction of the emitted radiation between the men and women was not statistically significant (Fig. 4). In the BMI category, the difference in an overall reduction of the emitted radiation between the normal, overweight, and obese patient groups was not statistically significant (Fig. 4). For the category based on age, the overall reduction in the emitted radiation between the youth, adult, and senior patient groups was not statistically significant (Fig. 4).

DISCUSSION

Nuclear medicine departments routinely perform both diagnostic and therapeutic procedures using a variety of radionuclides with different types and energies of emitted radiations. Most performed procedures in nuclear medicine are diagnostic radionuclide imaging. Extensive work has been undertaken for the reduction of radiation exposure to patients and nuclear

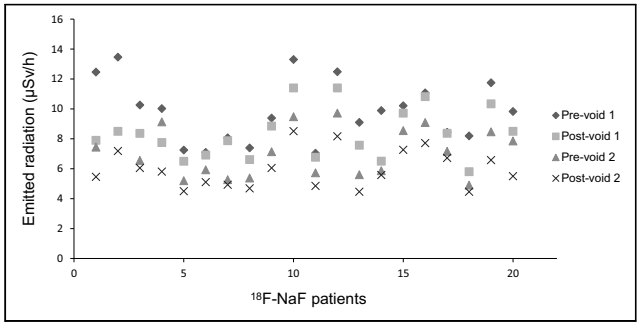

FIGURE 3. Exposure rates (μSv/h at 1 m) from ^{18}F-NaF patients (n = 20) at different time points.

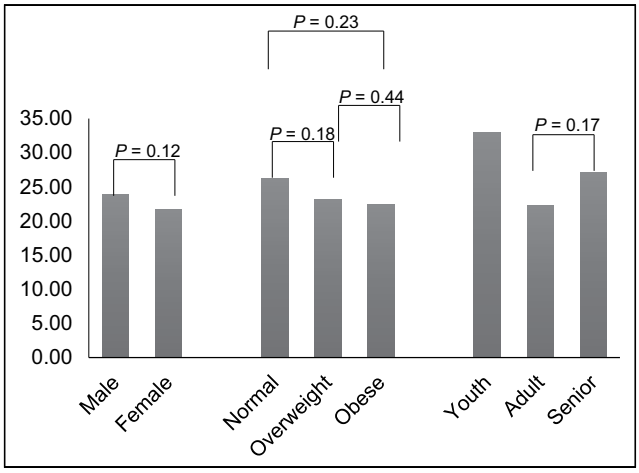

FIGURE 4. Comparison of overall reduction of emitted radiation from voiding after decay correction of categorized ^{18}F-NaF patients with corresponding *P* values. *P* values demonstrate that there was no statistical significance between different categories regarding effect of decay-corrected void. Youth group has only 2 patients, therefore, *P* value of this group was not calculated.

medicine staff (*9–13*). It has been well reported that patient radiation exposure from nuclear medicine is overall safe and might be beneficial in some cases (*3,4*). Consequently, nuclear medicine practice incorporates important principles for the reduction of the radiation dose, such as As Low As Reasonably Achievable (ALARA) principle. The nuclear medicine staff are trained to handle all types of radioactivity, keeping in mind the time, distance, and shielding principles to minimize radiation exposure. In addition, the radiation exposure of the nuclear medicine staff is continuously monitored to ensure that the allowed radiation dose limits are not exceeded.

Unlike the radiation exposure to patients and nuclear medicine staff, the radiation exposure from the PET patients at the time of discharge has not been extensively addressed. The goal of our study was to determine the typical emitted radiation rate from the urinary bladder region of patients after the completion of ^{18}F-FDG or ^{18}F-NaF PET scans and to evaluate simple, noninvasive interventions aimed at reducing radiation exposure to close contacts and caregivers from the discharged PET patients using both the physical half-life and the biologic half-life. The physical half-life is the time during which an initial activity of a radionuclide is reduced to one half by physical decay (*14*). Biologic half-life is the time by which one half of the administered dose is eliminated via biologic processes such as urinary and fecal excretion (*14*). Effective half-life is calculated on the basis of both the physical half-life and the biologic half-life for each radiotracer. It is defined as the time required for an initial administered dose to be reduced to one half due to both the physical decay and the biologic elimination of the radiotracer (*14*).

The 2 PET tracers investigated in this study are eliminated via the kidneys, with the urinary bladder being the organ with the highest radiation-absorbed dose (*15–19*). However, each radiotracer has a different biologic half-life. About 21% of ^{18}F-FDG is cleared in urine approximately 2 h after administration (*15*). For ^{18}F-NaF, about 20% is cleared in urine within the first 2 h (*16,17*). Both ^{18}F-FDG and ^{18}F-NaF are labeled with the same radionuclide, that is, ^{18}F, which has a physical half-life of 110 min. The shorter physical and biologic half-lives of PET radiotracers allow for faster elimination, and hence presumably implementing simple interventions based on these properties before patient discharge may be potentially advantageous. Having the patient wait for a certain period of time before being discharged is based on the decay property of the radionuclide. As for voiding, the concept of biologic half-life is important, and this is achieved by ensuring that the patient is well hydrated during the uptake time and before discharge.

Our data show that a simple precautionary measure of making the patients void before discharge reduces the emitted radiation by a mean of about 10% for ^{18}F-FDG and 13% for ^{18}F-NaF. Waiting an additional 30 min while drinking water resulted in an additional reduction of the emitted radiation by 12% and 16% for ^{18}F-FDG and ^{18}F-NaF, respectively, because of revoiding. From another perspective, a 30-min exposure dose at a 1-m distance would be around 6.83 and 4.92 μSv from ^{18}F-FDG and ^{18}F-NaF patients, respectively, at the standard time of discharge. This radiation exposure dose would drop to 4.33 and 2.99 μSv from ^{18}F-FDG and ^{18}F-NaF patients, respectively, after the simple steps outlined in this study. This decrease might be of benefit in patients who need to be in close contact with a caregiver. These include elderly patients and young patients as well as their mothers, particularly mothers who are nursing or have young children who would not comply with the instruction to maintain a safe distance. Also, there are other patients who do not have the luxury of separate rooms or bathrooms in their homes, and they may benefit from the extra time in the department before discharge. This might also be beneficial for inpatients who will be returning back to the ward immediately after completing the scan and potentially exposing other patients and nursing staff to unnecessary radiation.

A previously published article by Muzaffar et al. aimed at introducing simple methods to reduce radiation exposure rates to the public from ^{18}F-FDG PET/CT patients (*5*). They used ^{18}F-FDG doses of 370–740 MBq (10–20 mCi), and our patients were injected with ^{18}F-FDG doses of 185–352 MBq (5–9.5 mCi). Muzaffar et al. reported that about 75% of their patients leave the imaging facility with emitted radiation exceeding 20 μSv/h (2 mR/h) (*3*). Only 3% of our patients would have left the department with emitted radiation exceeding 20 μSv/h because they were injected with lower doses than the patients in the study by Muzaffar et al. Our data also showed that the overall emitted radiation reduction from both ^{18}F-FDG and ^{18}F-NaF was not affected by the patients' sex, BMI or age, as the *P* values showed no statistical significance.

Patient preparation before the scan may play an important role in decreasing the radiation dose. Good hydration and voiding have always been advised and recommended before, during, and after the scan in the patients' instructions but are not usually reenforced (*20–23*). This is mainly recommended to accelerate the clearance of the background blood-pool activity to improve the image quality and decrease the radiation dose to the patient (*20–23*). In addition to these benefits, based on our decay-corrected data, the biologic clearance permitted the decrease of emitted radiation of an average of 22.49% for ^{18}F-FDG, which is equivalent to 40 min of ^{18}F decay time, and 25.80% for ^{18}F-NaF, which is equivalent to 47 min of ^{18}F decay time. Therefore, good hydration assisted in significantly decreasing the emitted radiation from the patients to their close contacts.

The decay property of ^{18}F will always result in a reduction of 17% of the emitted radiation from the patients when they wait 30 min. However, the drop of radiation due to decay cannot be measured accurately from our collected data because the radiotracer is continuously circulating in the patients' body between postvoid 1 and prevoid 2 measurements as accumulation of the radiotracer is taking place in the urinary bladder. Therefore, this value was not calculated from our data as it is not feasible.

During this study, none of the staff was exposed to additional radiation since the department has shielded uptake rooms in the PET suite. Each patient stayed comfortably in their individual uptake room without exposing any of the nuclear medicine staff to additional radiation. We can accommodate the use of these rooms even if there is a busy schedule. However, the logistics vary from one hospital to another and this is outside the scope of this article.

The lower-than-expected number of patients was a limitation, as most of the eligible patients did not consent to be a part of this study. In addition, the renal function tests of most patients were not available due to logistical issues. Therefore, it was not feasible to study the relationship between renal function and its effect on emitted radiation rates. Also, using a whole-body radiation counter would have provided a more accurate measurement, but unfortunately, this was not available in our institution. However, on the basis of the collected data from the 2 different PET tracers, it was obvious that using both physical decay and biologic elimination properties had a significant impact on lowering the emitted radiation from the patients. There should not be major logistical issues to implement these steps at the nuclear medicine department since it will be based on individual cases.

CONCLUSION

With the increasing use of PET in clinical practice and the approval of new PET radiotracers, the emitted radiation from the discharged PET patients has been of interest. Use of the biologic half-life properties of radiotracers demonstrated a significant impact on lowering the emitted radiation rate from PET patients. Requesting the patient to consume additional water after the completion of the scan will facilitate voiding with 30 min of wait time before being discharged, which will be of benefit to certain PET patients such as the elderly, caregivers, and inpatients who need to be in close contact with others. In addition to the possible reduction of emitted radiation rates an average of 22%–25% due to voiding, there is an additional 17% reduction due to decay of the radioactivity during this time.

DISCLOSURE

No potential conflict of interest relevant to this article was reported.

KEY POINTS

QUESTION: Will undertaking simple steps with the PET patients before their discharge from the department significantly reduce the emitted radiation to their close contacts?

PERTINENT FINDINGS: In a prospective study of patients undergoing PET scans, the emitted radiation from their urinary bladders were measured after completing the exam (prevoid 1), voiding (postvoid 1), waiting 30 min while drinking water (prevoid 2), and voiding again (postvoid 2). Overall, voiding in this study resulted in an average decrease of emitted radiation rate of 22.49% for ^{18}F-FDG and 25.80% for ^{18}F-NaF, in addition to a fixed 17% decrease from the physical decay of ^{18}F radiotracers after 30 min of wait time.

IMPLICATIONS FOR PATIENT CARE: Following simple steps after the completion of the PET scan will significantly decrease the emitted radiation from the PET patients to their close contacts.

REFERENCES

1. Hillner BE, Tosteson A, Song Y, et al. Growth in use of positron emission tomography for six cancer types after coverage by Medicare: additive or replacement? *J Am Coll Radiol.* 2012;9:33–41.
2. Bural G, Torigian D, Houseni M, Alavi A. PET radiotracers in oncology other than ^{18}F-FDG [abstract]. *J Nucl Med.* 2020;61(suppl 1):1177.
3. Zhang-Yin J, Dirand AS, Sasanelli M, et al. Equivalent dose rate 1 meter from neuroendocrine tumor patients exiting the nuclear medicine department after undergoing imaging. *J Nucl Med.* 2017;58:1230–1235.
4. Siegel JA, Pennington CW, Sacks B. Subjecting radiologic imaging to the linear no-threshold hypothesis: a non sequitur of non-trivial proportion. *J Nucl Med.* 2017;58:1–6.
5. Muzaffar R, Koester E, Frye S, Alenezi S, Sterkel B, Osman M. Development of simple methods to reduce the exposure of the public to radiation from patients who have undergone 18F-FDG PET/CT. *J Nucl Med Technol.* 2020;48:63–67.
6. Howe DB, Beardsly M, Basksh S. Consolidated guidance about materials licenses: program-specific guidance about medical use licenses final report. U.S. Nuclear Regulatory Commission; 2008. NUREG-1556. Vol. 9, Rev.2.

7. Güneş B, Erez Ö, Gündoğan C, Ergül N. The evaluation of external dose rate measurements of patients during and after F-18 FDG PET/CT imaging and appropriate discharge time from PET/CT department. *İstanbul Med J.* 2019;20: 188–192.
8. Lim JU, Lee J, Kim J, et al. Comparison of World Health Organization and Asia-Pacific body mass index classifications in COPD patients. *Int J Chron Obstruct Pulmon Dis.* 2017;12:2465–2475.
9. Madsen MT, Anderson JA, Halama JR, et al. AAPM task group 108: PET and PET/CT shielding requirements. *Med Phys.* 2006;33:4–15.
10. Al-Aamria M, Al-Balushia N, Bailey D. Estimation of radiation exposure to workers during ^{18}F-FDG PET/CT procedures at molecular imaging center, Oman. *J Med Imaging Radiat Sci.* 2019;50:565–570.
11. Costa PF, Reinhardt M, Poppe B. Occupational exposure from F-18-FDG PET/CT: implementation to routine clinical practice. *Radiat Prot Dosimetry.* 2018;179:291–298.
12. Leide-Svegborn S. Radiation exposure of patients and personnel from a PET/CT procedure with ^{18}F-FDG. *Radiat Prot Dosimetry.* 2010;139:208–213.
13. Brix G, Lechel U, Glatting G, et al. Radiation exposure of patients undergoing whole-body dual-modality ^{18}F-FDG PET/CT examinations. *J Nucl Med.* 2005;46: 608–613.
14. Saha GB. *Fundamentals of Nuclear Pharmacy.* 5th ed. Springer; 2004:358–359.
15. Fludeoxyglucose. rxlist website. https://www.rxlist.com/fludeoxyglucose-drug.htm. Accessed August 1, 2022.
16. Li Y, Schiepers C, Lake R, Dadparvar S, Berenji G. Clinical utility of ^{18}F-fluoride PET/CT in benign and malignant bone diseases. *Bone.* 2012;50:128–139.
17. Czernin J, Satyamurthy N, Schiepers C. Molecular mechanisms of bone ^{18}F-NaF deposition. *J Nucl Med.* 2010;51:1826–1829.
18. Pauwels E, Cleeren F, Bormans G, Deroose C. Somatostatin receptor PET ligands: the next generation for clinical practice. *Am J Nucl Med Mol Imaging.* 2018;8: 311–331.
19. Hartmann H, Zöphel K, Freudenberg R, et al. Radiation exposure of patients during ^{68}Ga-DOTATOC PET/CT examinations. *Nuklearmedizin.* 2009;48:201–207.
20. Jadvar H, Colletti PM, Delgado-Bolton R, et al. Appropriate use criteria for ^{18}F-FDG PET/CT in restaging and treatment response assessment of malignant disease. *J Nucl Med.* 2017;58:2026–2037.
21. Boellaard R, Delgado-Bolton R, Oyen WJ, et al. FDG PET/CT: EANM procedure guidelines for tumour imaging: version 2.0. *Eur J Nucl Med Mol Imaging.* 2015; 42:328–354.
22. American College of Radiology. ACR–SPR practice parameter for performing FDG-PET/CT in oncology. ACR website. https://www.acr.org/-/media/ACR/Files/Practice-Parameters/fdg-pet-ct.pdf. Revised 2021. Accessed August 1, 2022.
23. Bayram T, Yilmaz AH, Demir M, Bircan S. Radiation dose to technologists per nuclear medicine examination and estimation of annual dose. *J Nucl Med Technol.* 2011;39:55–59.

Radiation Dose to Medical Staff from Administering ^{177}Lu-PSMA-DKFZ-617 Therapy

Elahe Mahmoudi[1], Elahe Pirayesh[2], Mohammad Reza Deevband[1], Mahasti Amoui[2], Mohammadali Ghodsi Rad[2], Mehrdad Ghorbani Rad[3], and Mahdi Ghorbani[1]

[1]Biomedical Engineering and Medical Physics Department, School of Medicine, Shahid Beheshti University of Medical Sciences, Tehran, Iran; [2]Nuclear Medicine Department, Shohadaye Tajrish Hospital, School of Medicine, Shahid Beheshti University of Medical Sciences, Tehran, Iran; and [3]Nuclear Medicine Department, Shohadaye Tajrish Hospital, Tehran, Iran

The number of radioligand therapy applications for metastatic castration-resistant prostate cancer has been continuously rising in most nuclear medicine departments in Iran, but to our knowledge, no one has studied the dose to staff who perform treatment procedures. The current study aimed to determine the external radiation dose received by staff who, using or not using a lead shield, treat patients with ^{177}Lu-prostate-specific membrane antigen therapy. **Methods:** This study used a personal thermoluminescent digital survey meter to measure dose rates to staff at various distances from patients and determined the average time spent by staff at these distances. The deep-dose equivalent to staff was obtained. **Results:** The measured deep-dose equivalent to staff per patient was within the range of 1.8–5.2 mSv using a 2-mm lead shield and 3.3–8.1 mSv not using the shield. The shield markedly reduced the external dose to staff. **Conclusion:** The skill and accuracy of staff, and the speed with which they act, can directly affect their received dose.

Key Words: nuclear medicine; ^{177}Lu-PSMA-DKFZ-617; dose rate; prostate cancer; mean doses

J Nucl Med Technol 2022; 50:269–273
DOI: 10.2967/jnmt.121.263135

Recently, radioligand therapy targeted at the prostate-specific membrane antigen (PSMA) was introduced, and such therapy with ^{177}Lu-PSMA-DKFZ-617 has shown promise for castration-resistant prostate cancer. The physical half-life of ^{177}Lu is estimated at 6.73 d. ^{177}Lu emits 2 types of radiation, namely β-rays (maximum energy, 0.498 MeV) and γ-rays (113 keV with 6% abundance and 208 keV with 11% abundance) (*1–3*). These γ-rays allow scintigraphy and subsequent dosimetry to be performed with the same therapeutic compounds. Because of the γ-rays of ^{177}Lu, radiation protection can become an issue (*4*).

The aim of radionuclide therapy is to deliver an effective absorbed dose to tumor cells while protecting critical organs from an excessive radiation dose. Meanwhile, unnecessary radiation doses to family members, the medical team, and the general public must be avoided. In particular, nuclear medicine technologists come into close proximity to radiation sources when targeted therapy such as ^{177}Lu-PSMA-DKFZ-617 is used, receiving radiation doses while preparing and administering the radioligand, positioning the treated patient on the scanner bed, controlling the patient during data acquisition, transferring the patient from the bed, and escorting the patient to the department (*5*). Thus, nuclear medicine societies have introduced several protective recommendations for targeted therapy, and various reports on methods of reducing the dose received by patients and staff have been published in some national and international journals (*6*).

Many investigators have measured the average external dose rates to staff, using pocket electronic and thermoluminescent dosimeters to record the total dose per study (*7,8*). There are two ways to directly determine the external radiation dose to staff per procedure: the first is based on accurate measurement of the dose rate at set distances from the patient and less accurate evaluation of the time spent by the operator at these distances, and the second is based on direct reading of an electronic dosimeter used by the staff during the procedure. The first tactic is a rough approximation of dose rate measurements but is more general and directly compares dose rates between different sets of published data (*9*).

The primary aim of this study was to determine the mean external dose to staff administering ^{177}Lu-PSMA-DKFZ-617 therapy while using or not using a lead shield and while at different distances from the patient. A secondary aim was to determine the annual dose to staff administering this therapy.

MATERIALS AND METHODS

The study was authorized by the hospital ethics committee and was performed in accordance with the Declaration of Helsinki. All patients gave written informed consent. The inclusion criteria were an age of more than 55 y, the presence of metastatic castration-resistant prostate cancer, and treatment with ^{177}Lu-PSMA-DKFZ-617. In total, 45 patients were enrolled from March 2019 to March 2020 (mean age, 66.2 y; range, 55–80 y) and were admitted to the Nuclear Medicine Department of Shohadaye Tajrish Hospital in Tehran, Iran. Demographic information on the staff is presented in Table 1.

Received Aug. 29, 2021; revision accepted Oct. 22, 2021.
For correspondence or reprints, contact Mohammad Reza Deevband (mdeevband@sbmu.ac.ir).
Published online Dec. 6, 2021.

TABLE 1
Demographic Information on Staff

Staff	Female (*n*)	Male (*n*)	Distance
Technologist in charge of injection	4	4	0 m (injecting radiopharmaceutical)
Technologist in charge of imaging	4	4	0.25 m (positioning patient);1 m (presenting information to patient)
Nurse	2	2	2 m (monitoring treatment process)
Physicist	2	2	2 m (providing protection guidelines)
Physician	3	1	0.25 m (checking patient's vital signs)

Four patients were treated on each therapy day in a 4-bed isolation room in the hospital's day-procedure unit. The beds were located in the 4 corners of the room, which had an area of about 30 m^2 and was shielded with lead (1.6 cm thick and 2 m high in the walls; 0.8 cm thick in the door) so that the patients could be isolated after the administration. The distance between beds was 2 m, and a mobile lead shield (2 mm thick) was placed between beds. The injection was prepared in a separate dedicated room. All patients were separately measured for dose rate in the lead-shielded room at specified intervals.

The study was performed using a digital survey meter (FH 40G-L10; Thermo Fisher), which was calibrated by a secondary standard dosimetry laboratory. This type of personal thermoluminescent dosimeter was chosen because it is capable of measuring photons in the range of 10 nSv/h–100 mSv/h and has a range of energy response of 30 keV–4.4 MeV; the dosimeters were dedicated to the ^{177}Lu-PSMA-DKFZ-617 therapy procedures.

The patients were treated with a mean of 5.5 ± 1.1 GBq (range, 3.7–7.4 GBq) of ^{177}Lu-PSMA-DKFZ-617. The dose rate at chest level was then measured at distances of 0, 0.25, 0.5, 1, and 2 m from the patients (*10*), once with and once without a 2-mm lead shield, after 0, 1, 2, 3, 4, 5, 6, 18, 24, and 36 h. The staff also recorded the mean time spent at each distance. Doses were measured as μSv/h and were converted to μSv/GBq·h according to the amount of radiopharmaceutical injected. Time (seconds) and relative dose rates were multiplied by each other. Finally, the mean (±SD) external doses to staff were calculated.

We routinely administer ^{177}Lu-PSMA-DKFZ-617 treatment on an outpatient basis. The dose limit recommended by European guidelines for the discharge of patients after ^{131}I therapy and by African guidelines on ^{177}Lu-PSMA-DKFZ-617 was set as the basis for discharge (20 μSv/h within 1 m) (*11–15*). From Equation 1, one can estimate the cumulative dose, *E,* to a caregiver standing a specified distance away from the patient for an unlimited time (*t*), assuming that only physical decay occurs. We assumed a distance, D_0, of 1 m and set an initial dose rate reading of 20 μSv/h at this distance. The half-life, $t_{1/2}$, of ^{177}Lu is 6.7 d. The calculation found *E* to be 4.6 mSv (*16*):

$$E = \int_0^\infty D_0 \times e^{-\ln(2)\times\frac{t}{t_{1/2}}}\,\mathrm{dt}. \qquad \text{Eq. 1}$$

Data processing, data fitting, and the statistical analysis were performed using Excel (Microsoft Office Professional Plus, version 2013) and SPSS (version 16.0, IBM Corp.). The Kolmogorov–Smirnov method was used to investigate the normal distribution of data. A *P* value of 0.05 or less was assumed to indicate statistical significance. Data are presented as the mean and SD unless stated otherwise.

RESULTS

The mean dose rates at various distances and time intervals are presented in Table 2. The dose rate gradually decreased as activity was excreted from the body. Differences in injectable activity, tumor uptake, and renal function had a great impact on the rate of clearance. Because most patients did not start to urinate until about 1 h after infusion, the initial readings were the highest: 47.5 ± 2.0 μSv/(h·GBq) (range, 40.0–58.0 μSv/[h·GBq]) at 0.25 m, 21.5 ± 1.2 μSv/(h·GBq) (range, 18.5–24.5 μSv/[h·GBq]) at 0.5 m, and 7.1 ± 0.3 μSv/(h·GBq) (range, 5.5–8.3 μSv/[h·GBq]) at 1 m. The dose rate 1 m from the patient decreased exponentially with time after infusion. The

TABLE 2
Mean Dose Rates (μSv/[h·GBq]) and Related SDs at Various Distances from Patient and Various Times

	Distance (m)				
Time (h)	0	0.25	0.5	1	2
0	78.6 ± 5.0 (72.7–87.5)	47.5 ± 2.0 (40.0–58.0)	21.5 ± 1.2 (18.5–24.5)	7.1 ± 0.3 (5.5–8.3)	5.4 ± 0.5 (4.4–7.2)
1	70.3 ± 3.0 (63.6–78.1)	36.3 ± 3.1 (32.0–44.6)	19.1 ± 1.5 (16.8–21.3)	6.0 ± 0.5 (4.4–6.6)	3.6 ± 0.4 (2.8–4.5)
2	53.0 ± 3.4 (55.0–44.9)	32.3 ± 1.1 (24.3–34.4)	16.5 ± 1.1 (12.4–18.4)	5.1 ± 0.6 (3.4–5.5)	2.6 ± 0.3 (2.0–3.1)
3	44.5 ± 3.0 (35.7–47.3)	24.3 ± 1.2 (18.8–27.9)	12.6 ± 1.3 (7.7–14.4)	4.2 ± 0.2 (2.7–4.7)	2.3 ± 0.2 (1.6–2.7)
4	34.4 ± 1.5 (29.9–39.5)	17.2 ± 1.6 (14.6–19.7)	8.5 ± 1.7 (6.5–10.8)	3.2 ± 0.3 (2.4–3.9)	1.8 ± 0.2 (1.4–2.4)
5	24.2 ± 1.5 (19.0–27.3)	13.3 ± 0.9 (10.9–14.9)	6.1 ± 0.3 (5.5–7.6)	2.8 ± 0.2 (1.9–3.2)	1.3 ± 0.3 (0.8–1.8)
6	22.2 ± 1.3 (17.0–25.5)	11.5 ± 0.5 (8.8–14.0)	5.5 ± 0.2 (5.0–7.0)	2.2 ± 0.3 (1.2–3.0)	1.0 ± 0.5 (0.5–1.5)
18	17.5 ± 1.1 (15.2–20.4)	10.5 ± 0.7 (7.9–11.9)	5.0 ± 0.4 (3.7–5.9)	1.4 ± 0.3 (0.9–1.7)	0.8 ± 0.2 (0.3–1.0)
24	13.5 ± 1.3 (12.4–16.2)	6.5 ± 1.1 (5.9–8.0)	3.1 ± 0.2 (2.9–3.5)	1.0 ± 0.04 (0.5–1.4)	0.5 ± 0.02 (0.3–0.8)
36	10.0 ± 1.1 (8.4–13.3)	4.5 ± 1.0 (3.8–6.0)	2.3 ± 0.3 (1.8–3.0)	0.6 ± 0.03 (0.3–1.0)	0.3 ± 0.03 (0.1–0.8)

Data are mean ± SD.

TABLE 3
Total Dose to Staff per Patient

Staff	Without lead shield			With lead shield			
	Minimum per patient (μSv)	Maximum per patient (μSv)	Mean ± SD	Minimum per patient (μSv)	Maximum per patient (μSv)	Mean ± SD	*P*
Technologist in charge of injection	6.5	8.6	7.6 ± 1.1	4.0	5.2	4.8 ± 0.9	≤0.05
Technologist in charge of imaging	3.7	5.0	4.0 ± 0.5	2.1	3.0	2.4 ± 0.3	≤0.05
Physician	3.0	3.6	3.3 ± 0.3	1.6	2.1	1.8 ± 0.4	<0.05
Physicist	3.2	4.2	3.5 ± 0.5	1.7	2.5	2.2 ± 0.3	<0.05
Nurse	7.4	9.2	8.1 ± 0.8	4.2	5.7	5.2 ± 0.3	≤0.05

average dose rate at this distance at 4–5 h was considered safe, as it was below the release limit required by our department (20 μSv/h).

Table 3 shows the per-patient dose to staff while using or not using the lead shield, and Table 4 shows the estimated mean annual dose to staff while using or not using the lead shield. The mean annual dose was calculated both for patients included in the study and for patients excluded and was determined using the data in Table 3 and the annual numbers of cases in the nuclear medicine laboratory. Table 5 shows the mean annual dose to staff as measured using the personal thermoluminescent dosimeters. The calculations are based on the number of treatment sessions in a year, with the assumption that nuclear medicine staff participated in all such sessions.

Annual mean doses differed among staff in different job positions, with nurses receiving the highest minimum dose, at 3.8 mSv (Table 5), and a dose of 2.3 mSv (Table 4) while shielded. Technologists in charge of the injection and in charge of imaging received doses of 2.2 and 1.5 mSv, respectively, while shielded and 3.4 and 2.6 mSv, respectively, while not shielded (Table 4). Physicians and physicists received the lowest doses: 1.0 and 1.2 mSv, respectively, while shielded and 1.8 and 2.1 mSv, respectively, while not shielded (Table 4).

TABLE 4
Estimated Mean Annual Dose to Staff With and Without Shielding

Staff	With lead shield (mSv)	Without lead shield (mSv)
Technologist in charge of injection	2.2	3.4
Technologist in charge of imaging	1.5	2.6
Physician	1.0	1.8
Physicist	1.2	2.1
Nurse	2.3	3.8

DISCUSSION

^{177}Lu-PSMA-DKFZ-617 therapy of castration-resistant prostate cancer has been practiced at a few specialized centers around the world. Essential criteria for incorporating any new cancer therapy, including targeted therapy, are safety, efficacy, regularity, practicality, and affordability (*7,8*). If such therapy requires an extended stay in the hospital, patients may have extra costs to bear and face the possibility of acquiring a nosocomial infection. Also, patients may experience emotional disturbance due to the isolation such therapy requires. Our findings demonstrated that ^{177}Lu-PSMA-DKFZ-617 is safe to apply as an outpatient protocol, since the external dose rate decreases below the 20 μSv/h threshold after approximately 4–5 h.

In a study by Demir et al. (*7*), patients could be discharged from the hospital when the dose rate fell below the determined threshold of 30 μSv/h after approximately 4–5 h. A similar study was performed by Calais et al. (*17*); patients reached the 1-m release limit of 25 μSv/h at a mean of 2.3 h, and all were released within 6 h. Differences in results among various studies may be due to differences in injected activity, biologic uptake, and radiopharmaceutical clearance.

In our study, the highest dose was received by nurses (without shielding, 8.1 μSv per patient), who routinely entered the isolation room at the beginning of infusion to meet the patients' needs and observe them. The ^{177}Lu-PSMA-DKFZ-617 therapy was scheduled for the same time each day, with the same nurse generally being present. Our department performs around 300 sessions of ^{177}Lu-PSMA-DKFZ-617 therapy per year (45 patients treated 3–6 times at an interval of 8–12 wk).

In comparison to physicists and physicians, technologists in charge of injection received a high radiation dose (7.6 μSv per patient), as predicted, because they spend long hours preparing the ^{177}Lu-PSMA-DKFZ-617 activity and stay close to the bedside during the infusion. Technologists in charge of imaging also received a considerable total dose (4 mSv per patient), because they accompany patients to the scintigraphy room, position them on the bed, and thus also spend significant time near them. Because technologists in charge of injection received a higher dose than those in charge of imaging,

TABLE 5
Mean Annual Dose to Staff as Measured with Thermoluminescent Dosimeters

Staff	Maximum (mSv)	Minimum (mSv)	Mean without lead shield (mSv)
Technologist in charge of injection	4.9	3.6	4.6
Technologist in charge of imaging	3.5	2.4	3.1
Physician	1.8	1.3	1.6
Physicist	2.2	1.6	1.9
Nurse	4.8	3.8	4.3

rotation of these two type of duties is recommended. Unlike nurses and technologists, physicians had a confined role during the therapy; their role in medical supervision required only sporadic attendance in the treatment room, resulting in a total dose of 3.3 μSv per patient. Lastly, physicists received a relatively low dose of 3.5 μSv per patient, resulting from their entering the isolation room to measure the dose rate.

Generally, our results were close to those of Demir et al. (*7*), who showed that the mean radiation doses to nurses and radiopharmacists were 6.0 and 4.0 μSv/patient, respectively, whereas physicists and physicians received 2.0 μSv/patient. That work analyzed the dose rate for 23 patients treated with 7,400 MBq of ^{177}Lu-PSMA-DKFZ-617, and the total dose to the medical team was estimated by an electronic personal dosimeter. The estimated values from the study of Demir et al. are presented in Table 6 for comparison to our study. Differences in the results may be due to differences in experience, skill, time between examination and injection, and promptness of staff.

Some treatment centers may choose to hospitalize patients to monitor their condition or facilitate further medical examinations. If 4 patients were treated on each therapy day in the 4-bed isolation room, the nurse, who spent up to 4 h attending the 4 patients after infusion, received a mean dose of 26–53 μSv. This wide range reflects differences in nursing requirements, tumor burden in each patient group, and behavior of the individual nurse. Although patient privacy may be somewhat compromised in this situation, the ability of both patients and their caregivers (usually a family member or friend) to talk to fellow patients, share their individual experiences, and gain mutual support is, in itself, a valuable therapy for this rare disease, for which authoritative, first-hand patient information is relatively scarce.

Although no measured radiation dose to medical staff exceeded the allowed limit (20 mSv/y), it is recommended that a protocol be proposed to minimize staff exposure. This protocol would include improving work procedures, minimizing close contact with patients, and using equipment and shielding when contact is unavoidable. Table 3 indicates that a 2-mm lead shield decreased the dose to physicists, physicians, nurses, and nuclear medicine technologists significantly—by approximately 2 times. Tables 3 and 4 show that even without a rotation of the workforce, and even with a significant increase in the number of patients, the annual dose to individual staff would not reach the annual limit (20 mSv/y) defined by the International Commission on Radiological Protection. Annual doses as indicated by thermoluminescent dosimeters agreed with the estimated mean annual doses, except for technologists in charge of injection. The lack of agreement regarding the injecting technologists may have occurred because, in the same shift, these staff administered both therapeutic ^{177}Lu-PSMA-DKFZ-617 and diagnostic radiopharmaceuticals. The doses may therefore have appeared lower than they really were.

Various studies have determined the dose reductions to nuclear medicine staff when lead shields and aprons are worn (*18–20*). He et al. (*21*) studied the effect of lead aprons on reducing the dose from ^{57}Co, ^{33}Ba, ^{137}Cs, ^{99m}Tc, and ^{131}I radionuclides and found that the effect was greatest for radiopharmaceuticals that emit γ-rays of less than 140 keV. Furthermore, Bayram et al. (*10*) showed that a 2-mm lead shield could reduce the external radiation dose to staff performing various diagnostic tests. If a shield thicker than 2 mm were to be used, the dose could be lowered even further. We emphasize that regardless of job position, staff should consider the use of protective equipment. Additionally, reducing the exposure time and increasing the distance from the radiation source

TABLE 6
Comparison of Mean Dose (μSv per patient) from Current Study and from Another International Study

Staff	Demire et al. (*7*)	Current study without lead shield	Current study with lead shield
Radiopharmacist	4.0	7.6 ± 1.1	4.8 ± 0.9
Physicist	2.0	4.0 ± 0.5	2.4 ± 0.3
Physician	2.0	3.3 ± 0.3	1.8 ± 0.4
Technologist	3.0	3.5 ± 0.5	2.2 ± 0.3
Nurse	6.0	8.1 ± 0.8	5.2 ± 0.3

±SD is also shown for current study.

are advisable when working with positron nuclides and other high-energy γ-ray sources.

One limitation of this study was the low number of patients, and another is that we did not use lead shielding of varying thicknesses (<2 mm or >2 mm). In addition, the sensitivity of measurement and imaging devices decreases over time; therefore, a larger quantity of radioactive material must be administered to obtain sufficient counts for a quality image. Because administering a larger quantity to patients also increases the dose to staff, the devices must be subjected to a regular quality control program. Provided that such safety precautions are undertaken, our data showed that ^{177}Lu-PSMA-DKFZ-617 therapy for prostate cancer is safe and tolerable and that external radiation doses to medical staff were within the allowable limits.

CONCLUSION

A 2-mm lead barrier reduced the dose to staff for the therapeutic procedures performed in this study. Thus, it is recommended that this protective device be used at all treatment stages. No measured radiation doses to staff exceeded the annual limit of 20 mSv/y.

DISCLOSURE

No potential conflict of interest relevant to this article was reported.

ACKNOWLEDGMENT

This article was extracted from the thesis of Elahe Mahmoudi, School of Medicine, Sahid Beheshti University of Medical Sciences, Tehran, Iran (project 410, 9,139).

KEY POINTS

QUESTION: What is the radiation dose to staff from administering radioligand therapy for metastatic castration-resistant prostate cancer?

PERTINENT FINDINGS: The amount of radiation dose to staff from treatment of patients with ^{177}Lu-PSMA-DKFZ-617 was within the allowable range. The results were statistically significant.

IMPLICATIONS FOR PATIENT CARE: Lead protection can reduce the radiation dose to staff. This finding underscores the need for staff to consider use of shielding.

REFERENCES

1. Bodei L, Mueller-Brand J, Baum RP, et al. The joint IAEA, EANM, and SNMMI practical guidance on peptide receptor radionuclide therapy (PRRNT) in neuroendocrine tumors. *Eur J Nucl Med Mol Imaging.* 2013;40:800–816.
2. Mair C, Warwitz B, Fink K, et al. IJ. Radiation exposure after ^{177}Lu-DOTATATE and ^{177}Lu-PSMA-617 therapy. *Ann Nucl Med.* 2018;32:499–502.
3. Parkin DM, Bray F, Ferlay J, Pisani P. Global cancer statistics. *CA Cancer J Clin.* 2005;55:74–108.
4. Chakraborty S, Das T, Sarma HD, Venkatesh M, Banerjee S. Preparation and preliminary studies on ^{177}Lu-labeled hydroxyapatite particles for possible use in the therapy of liver cancer. *Nucl Med Biol.* 2008;35:589–597.
5. Seierstad T, Stranden E, Bjering K, et al. Doses to nuclear technicians in a dedicated PET/CT centre utilising ^{18}F fluorodeoxyglucose (FDG). *Radiat Prot Dosimetry.* 2007;123:246–249.
6. Archer BR. Recent history of the shielding of medical x-ray imaging facilities. *Health Phys.* 2005;88:579–586.
7. Demir M, Abuqbeitah M, Uslu-Besli L, et al. Evaluation of radiation safety in ^{177}Lu-PSMA therapy and development of outpatient treatment protocol. *J Radiol Prot.* 2016;36:269–278.
8. Abuqbeitah M, Demir M, Lebriz Uslu B, Nami Y, Sonmezoğlu K. Blood clearance and occupational exposure for ^{177}Lu-DOTATATE compared to ^{177}Lu-PSMA radionuclide therapy. *Radiat Environ Biophys.* 2018;57:55–61.
9. Chiesa C, De Sanctis V, Crippa F, et al. Radiation dose to technicians per nuclear medicine procedure: comparison between technetium-99m, gallium-67, and iodine-131 radiotracers and fluorine-18 fluorodeoxyglucose. *Eur J Nucl Med.* 1997;24:1380–1389.
10. Bayram T, Yilmaz AH, Demir M, Sonmez B. Radiation dose to technologists per nuclear medicine examination and estimation of annual dose. *J Nucl Med Technol.* 2011;39:55–59.
11. Steyn PF, Uhrig J. The role of protective lead clothing in reducing radiation exposure rates to personnel during equine bone scintigraphy. *Vet Radiol Ultrasound.* 2005;46:529–532.
12. Culver CM, Dworkin H. Comparison of personnel radiation dosimetry from myocardial perfusion scintigraphy: technetium-99m-sestamibi versus thallium-201. *J Nucl Med.* 1993;34:1210–1213.
13. Murphy PH, Wu Y, Glaze S. Attenuation properties of lead composite aprons. *Radiology.* 1993;186:269–272.
14. Gomez-Palacios M, Terron J, Dominguez P, Vera DR, Osuna RF. Radiation doses in the surroundings of patients undergoing nuclear medicine diagnostic studies. *Health Phys.* 2005;89(suppl):S27–S34.
15. Ahmadi Jeshvaghane N, Paydar R, Fasaei B, et al. Criteria for patient release according to external dose rate and residual activity in patients treated with ^{131}I-sodium iodide in Iran. *Radiat Prot Dosimetry.* 2011;147:264–266.
16. Olmstead C, Cruz K, Stodilka R, Zabel P, Wolfson R. Quantifying public radiation exposure related to ^{177}lutetium octreotate therapy for the development of a safe outpatient treatment protocol. *Nucl Med Commun.* 2015;36:129–134.
17. Calais PJ, Turner JH. Radiation safety of outpatient ^{177}Lu-octreotate radiopeptide therapy of neuroendocrine tumors. *Ann Nucl Med.* 2014;28:531–539.
18. Warren-Forward H, Cardew P, Smith B, et al. A comparison of dose savings of lead and lightweight aprons for shielding of 99m-technetium radiation. *Radiat Prot Dosimetry.* 2007;124:89–96.
19. Bauman T, Carey A, Zimmer A, Spies S. Evaluation of the effectiveness of a front shielding lead skirt apron for pregnant radiation workers [abstract]. *J Nucl Med.* 2006;47(suppl 1):539P.
20. Huda W, Boutcher SH. Should nuclear medicine technologists wear lead aprons? *J Nucl Med Technol.* 1989;17:6–11.
21. He X, Zhao R, Rong L, Yao K, Chen S, Wei B. Answers to if the lead aprons are really helpful in nuclear medicine from the perspective of spectroscopy. *Radiat Prot Dosimetry.* 2017;174:558–564.

Risk of Radiation Exposure to Clinical Staff from Paracenteses of Large-Volume Chylous Ascites After ^{177}Lu-DOTATATE Infusion

Sameer Tipnis, William J. Rieter, Vladimir Henderson-Suite, and Leonie Gordon

Department of Radiology, Medical University of South Carolina, Charleston, South Carolina

^{177}Lu-DOTATATE has gained wide clinical acceptance for the treatment of advanced gastroenteropancreatic neuroendocrine tumors; however, little is known regarding its accumulation in ascites. As such, clinical staff performing paracenteses shortly after a treatment dose may be concerned about their potential radiation exposure or the risk of contamination. **Methods:** In this report, therapeutic paracenteses were performed on a patient with metastatic intestinal carcinoid complicated by recurrent chylous ascites at various time intervals after a standard 7.4 GBq dose of ^{177}Lu-DOTATATE. Samples of the fluid were analyzed in a scintillation counter to estimate the concentration of radioactivity. **Results:** The concentration of activity in the ascitic fluid obtained 3 d after an infusion was exceptionally low (175.3 ± 25.9 Bq/mL). **Conclusion:** Our findings suggest that paracenteses conducted as soon as 3 d after a standard dose of ^{177}Lu-DOTATATE pose little to no risk in terms of radiation safety to staff performing the procedure.

Key Words: ^{177}Lu-DOTATATE; Lutathera; ascites; paracentesis; radiation safety

J Nucl Med Technol 2022; 50:274–277
DOI: 10.2967/jnmt.121.262820

Gastroenteropancreatic neuroendocrine tumors (GEP-NETs) are generally considered an indolent class of neoplasms and tend to present in advanced stages of disease that respond poorly to conventional chemotherapies (*1*). Many GEP-NETs are initially diagnosed after nonspecific signs or symptoms related to tumor mass effect, invasion, or distant metastases present themselves. Several of the most common signs and symptoms include abdominal pain, weight loss, bloating, nausea, diarrhea, and jaundice. In rare incidences, patients with GEP-NETs may develop chylous ascites, which can occur either as a result of the obstruction of a lymph node by tumor invasion or fibrosis or by the impaired flow of lymph due to fibrosis of the lymphatic ducts in the surrounding tissues (*2–5*). Regardless of the cause, chylous ascites has been associated with more aggressive forms of the disease, as well as poorer outcomes, and often leads to additional challenges related to patient management (*2,3*).

Since its approval by the Food and Drug Administration in January 2018, ^{177}Lu-DOTATATE has become a popular second-line treatment option in the management of advanced, well-differentiated somatostatin receptor–positive GEP-NETs that have progressed on conventional octreotide therapy (*6,7*). The typical therapeutic regimen includes 4 7.4-GBq doses of ^{177}Lu-DOTATATE administered via infusion 8 wk apart. As is the case with most nuclear medicine procedures, clinical staff may be apprehensive about conducting interventional procedures shortly after the administration of ^{177}Lu-DOTATATE because of fear of radiation exposure or contamination. This is particularly true of invasive procedures, such as paracenteses or thoracenteses, for which the potential of contamination is increased. Staff concern is complicated given that little is known about how much radioactive material accumulates within these fluids. Herein, we report on our experience performing paracenteses in a patient with metastatic ileocecal carcinoid complicated by recurrent chylous ascites after the standard 7.4-GBq treatment dose of ^{177}Lu-DOTATATE as well as provide estimates of the concentration of radioactivity in the fluid. These data should serve to reassure clinical staff performing paracenteses of the extremely low radiation exposure during the procedure.

MATERIALS AND METHODS

Case History

A 59 y old with a history of an ileocecal carcinoid tumor status after resection with metastatic somatostatin receptor–positive mesenteric and retroperitoneal adenopathy was referred to our nuclear medicine department for ^{177}Lu-DOTATATE therapy (Fig. 1). The patient was previously treated with long-acting octreotide, and subsequently everolimus, both of which were terminated due to associated side effects and progression of disease. Several weeks before initiating therapy with ^{177}Lu-DOTATATE, the patient began developing recurrent chylous ascites that required the therapeutic drainage of greater than 7 L of fluid every 3–4 d. A multidisciplinary team consisting of oncology, nuclear medicine, medical physics, and radiology staff performing the paracenteses discussed the case and agreed to proceed with the treatment as well as the as-needed therapeutic paracenteses, out of medical necessity. Although attempts were made to postpone the routine scheduled paracentesis immediately after

Received Jun. 30, 2021; revision accepted Nov. 30, 2021.
For correspondence or reprints, contact William J. Rieter (rieter@musc.edu).
Published online Dec. 21, 2021.

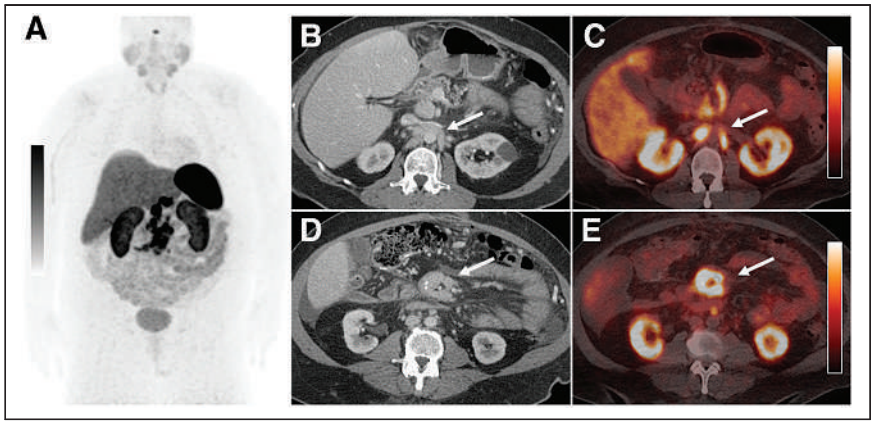

FIGURE 1. A 59 y old with metastatic ileocecal carcinoid tumor. (A) Anterior ^{68}Ga-DOTATATE PET maximum-intensity-projection image showing intense somatostatin receptor avidity greater than that of the liver within a conglomerate of central abdominal lymph nodes. Axial contrast-enhanced CT images of abdomen with fused PET/CT images at same level illustrating examples of retroperitoneal (B and C) and central mesenteric lymph nodes (D and E) (arrows) that showed somatostatin receptor positivity on PET/CT. Scale bars = SUV_{max} = 14.

the ^{177}Lu-DOTATATE infusion, the patient required it after 3 d because of worsening abdominal discomfort. This occurrence prompted us to investigate the potential risk of radiation exposure to the clinical staff performing the procedure. Because of the limited number of subjects, our institutional review board deemed it unnecessary to submit this case for approval, and the requirement for informed consent was waived.

Infusion Protocol

^{177}Lu-DOTATATE was administered using the standard infusion protocol (*6,7*). Briefly, the patient was premedicated with an antiemetic 30 min before initiating the infusion of an amino acid solution containing L-arginine and L-lysine. The amino acid infusion was started 30 min before, and continued during and 3 h after the ^{177}Lu-DOTATATE infusion, and was infused at a rate of 250 mL/h. The 7.4-GBq dose of ^{177}Lu-DOTATATE was infused over 20–30 min. The patient was instructed to void frequently over the course of their treatment to reduce the radiation dose to their kidneys and bladder. Before the patient left the nuclear medicine suite, 30 mg of subcutaneous long-acting octreotide was administered.

Paracentesis and Fluid Analysis

Fluid samples from paracenteses performed at various intervals after each of the first 3 doses of ^{177}Lu-DOTATATE were collected and analyzed using a standard protocol. Samples were always collected during paracenteses performed 3 and 10 d after the treatment doses; however, samples could not always be obtained during paracenteses performed 7, 13, and 20 d after the treatment doses due to logistical factors.

Large-volume paracenteses were performed in the radiology department under ultrasound guidance. A 50-mL sample of the drained fluid was transported to the radiation safety department where it was interrogated with a NaI(Tl)-based survey meter (Exploranium miniSpec GR-130; Exploranium G.S. Limited). The scan revealed 2 peaks, at 208 and 113 keV, matching the expected γ-peaks of ^{177}Lu (Table 1). Subsequently, 0.5-mL aliquots (n = 5 after the first treatment dose and n = 10 after the second and third treatment doses) were drawn and mixed with 7 mL of liquid scintillation cocktail fluid (Insta-fluor Plus; Perkin Elmer) in a standard 20-mL glass vial. A blank sample with no peritoneal fluid was also prepared. All samples were scanned in a liquid scintillation counter (Guardian1414; Perkin Elmer) using an open energy window (channel 5-1024).

RESULTS

Table 2 shows the results of the liquid scintillation counter measurements of the fluid samples obtained at various intervals after the first 3 treatment doses. The mean activity concentration 3 d after a treatment dose was 175.3 ± 25.9 Bq/mL. The maximum activity within a total volume of drained fluid was estimated to be 1.42 MBq in 7.3 L, which was collected on day 3 after the first treatment dose. The residual activity fell rapidly after day 3, as can be seen from the subsequent measurements. Figure 2 is a graphical presentation of the data in Table 2. An exponential curve fit to the data yielded an effective half-life in the fluid of 2.9 d.

DISCUSSION

For patients who must undergo paracentesis within a few days of a ^{177}Lu-DOTATATE infusion, the issue of radiation safety to clinical staff can pose a tricky problem. However, the data presented here suggest that as soon as 3 d after an infusion, the concentration of activity in the peritoneal fluid is exceptionally low, on the order of approximately 175 Bq/mL. Given the low concentration of activity, the drained fluid can be safely disposed of via the usual biowaste channel. Moreover, the estimated activity implies that the associated radiation exposure to the clinical staff is negligible, and they should be able to safely conduct the procedure without the fear of high radiation exposure from the patient or contamination from the fluid. Normal

TABLE 1
Principal Emissions for ^{177}Lu and Their Relative Intensities (Those > 1%)

Radiation	Energy (keV)	I (%)
β^-	176.5	12.2
β^-	384.9	9.1
β^-	497.8	78.6
γ	112.9	6.4
γ	208.4	11.0

I (%) = intensity percentage.
Half-life of ^{177}Lu = 6.7 D.

TABLE 2
Mean Activity Concentration Based on Liquid Scintillation Measurements of Ascitic Fluid Samples Obtained at Various Intervals After Treatment Doses of ^{177}Lu-DOTATATE

	Activity concentration (Bq/mL)			
Postinfusion day	Treatment 1 (n = 5)	Treatment 2 (n = 10)	Treatment 3 (n = 10)	Mean
3	194.3 ± 15.5	190.2 ± 17.8	141.3 ± 10.7	175.3 ± 25.9
7	—	—	59.6 ± 5.6	59.6 ± 5.6
10	22.2 ± 2.2	24.80 ± 3.3	29.6 ± 2.6	25.5 ± 4.8
13	—	11.1 ± 2.6	13.7 ± 1.5	12.4 ± 3.0
20	—	3.0 ± 0.4	—	3.0 ± 0.4

precautions to avoid contamination, such as the use of gloves, gowns, and masks, should be sufficient for protection during the procedure.

The results of this case also suggest that the concentration of activity within the peritoneal fluid may follow a trend similar to that of the terminal blood activity of ^{177}Lu-DOTATATE. Pharmacokinetic analyses have shown that the radiopharmaceutical rapidly clears from circulation with a mean effective half-life in blood of 0.31 ± 0.13 h (*8,9*). After most of the injected activity distributes to somatostatin receptor type 2–expressing cells or undergoes renal excretion, its terminal half-life in blood is estimated to be 71 ± 28 h (*6*). In our case, the concentration of activity within the ascites had an estimated effective half-life of 2.9 d, which is similar to its terminal half-life in blood. These findings suggest there is likely a pseudoequilibrium that exists between the concentration of radiopharmaceutical circulating in the blood pool and the concentration that accumulates in the ascites, which is skewed heavily toward the blood pool. Moreover, biodistribution studies have shown that less than 1 percentage of the injected activity remains in the blood pool after 24 h (*8*), and thus it is expected that minimal activity should be present within the ascites when a paracentesis is performed after 3 d.

Several limitations of this case should be noted. First, the results are based on our experience with a single patient, in part because chylous ascites is an incredibly rare complication of metastatic neuroendocrine tumors, specifically carcinoid. Second, due to the small sample size, we could not assess how the composition of peritoneal fluid or its rate of accumulation might affect the concentration of activity in the fluid. Last, we did not perform direct measurements of the radiation exposure to clinical staff performing the paracenteses. Rather, our inference that the radiation exposure is extremely low so as to be inconsequential is based on the measured radioactivity in the ascitic fluid. To this end, we have shown that minimal activity is present within the fluid even in a case of rapidly accumulating large-volume chylous ascites, which should be applicable to less severe cases of ascites.

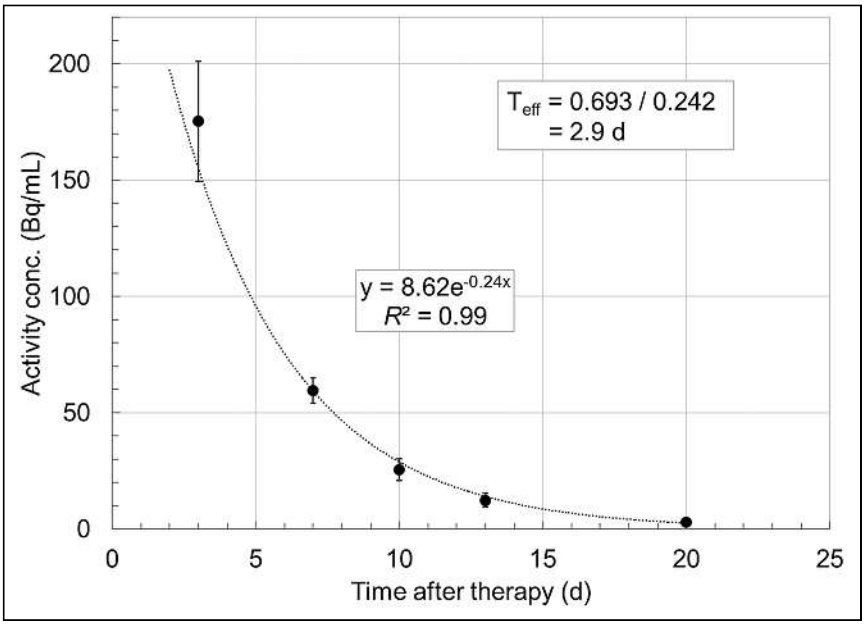

FIGURE 2. Plot of ^{177}Lu activity concentration in ascitic fluid as function of time. Estimated effective half-life in ascitic fluid is 2.9 d.

CONCLUSION

Paracenteses conducted on patients as soon as 3 d after a standard dose of ^{177}Lu-DOTATATE likely pose little to no risk in terms of radiation safety to the staff performing the procedure. The peritoneal fluid likely retains minimal levels of radioactivity and thus can be safely disposed in the usual stream of medical waste.

DISCLOSURE

No potential conflict of interest relevant to this article was reported.

KEY POINTS

QUESTION: What is the risk of radiation exposure to staff from ascitic fluid collected during large-volume paracenteses in a patient who has recently been treated with ^{177}Lu-DOTATATE?

PERTINENT FINDINGS: The results of this single case suggest that the concentration of activity in the ascites as soon as 3 d after a standard dose of ^{177}Lu-DOTATATE is likely negligible at approximately 175 Bq/mL.

IMPLICATIONS FOR PATIENT CARE: Clinical staff performing paracenteses in a patient receiving ^{177}Lu-DOTATATE therapy should feel comfortable knowing that the potential risk of radiation exposure and contamination is likely very low.

REFERENCES

1. Kim KW, Krajewski KM, Nishino M, et al. Update on the management of gastroenteropancreatic neuroendocrine tumors with emphasis on the role of imaging. *AJR.* 2013;201:811–824.
2. Bhardwaj R, Vaziri H, Gautam A, Ballesteros E, Karimeddini D, Wu GY. Chylous ascites: a review of pathogenesis, diagnosis and treatment. *J Clin Transl Hepatol.* 2018;6:105–113.
3. Cárdenas A, Chopra S. Chylous ascites. *Am J Gastroenterol.* 2002;97:1896–1900.
4. Portale TR, Mosca F, Minona E, et al. Gastrointestinal carcinoid tumor and chylous ascites, a rare association with a poor prognosis: a case report. *Tumori.* 2008;94:419–421.
5. Kypson AP, Onaitis MW, Feldman JM, Tyler DS. Carcinoid and chylous ascites: an unusual association. *J Gastrointest Surg.* 2002;6:781–783.
6. Highlights of prescribing information: LUTATHERA®. FDA website. https://www.accessdata.fda.gov/drugsatfda_docs/label/2018/208700s000lbl.pdf. Accessed July 25, 2022.
7. Product monograph: LUTATHERA®. Sam Nordic website. https://www.samnordic.se/wp-content/uploads/2018/05/LUTATHERA-MONOGRAPH-120218.pdf. Accessed July 25, 2022.
8. Abuqbeitah M, Demir M, Uslu-Beşli L, Yeyin N, Sönmezoğlu K. Blood clearance and occupational exposure for ^{177}Lu-DOTATATE compared to ^{177}Lu-PSMA radionuclide therapy. *Radiat Environ Biophys.* 2018;57:55–61.
9. Hennrich U, Kopka K. Lutathera®: the first FDA- and EMA-approved radiopharmaceutical for peptide receptor radionuclide therapy. *Pharmaceuticals (Basel).* 2019;12:114.

^{68}Ga-Pentixafor PET/CT Demonstrating In Vivo CXCR4 Receptor Overexpression in Rare Lung Malignancies: Correlation with Histologic and Histochemical Findings

Ankit Watts[1], Baljinder Singh[1], Harmandeep Singh[1], Harneet Kaur[1], Amanjit Bal[2], Mehak Vohra[3], Sunil K. Arora[3], and D. Behera[4]

[1]Department of Nuclear Medicine, Postgraduate Institute of Medical Education and Research, Chandigarh, India; [2]Department of Histopathology, Postgraduate Institute of Medical Education and Research, Chandigarh, India; [3]Department of Immunopathology, Postgraduate Institute of Medical Education and Research, Chandigarh, India; and [4]Department of Pulmonary Medicine, Postgraduate Institute of Medical Education and Research, Chandigarh, India

^{68}Ga-pentixafor PET/CT imaging allows noninvasive assessment of C-X-C chemokine receptor type 4 (CXCR4) expression in various malignancies, but its use in rare lung cancer variants has not been reported. **Methods:** ^{68}Ga-pentixafor PET/CT imaging was performed on 6 patients (3 men, 3 women; mean age, 57.0 ± 16.8 y) with suspected lung masses. Whole-body PET/CT images were acquired 1 h after intravenous injection of 148.0–185.0 MBq of the tracer. PET/CT images were reconstructed and analyzed. The image findings were correlated with histopathologic and quantitative (CXCR4) fluorescence-activated cell sorting analysis. **Results:** Histopathologic diagnosis of hemangioendothelioma, sarcomatoid carcinoma, and hemangiopericytoma was confirmed in 1 patient each. Lung metastasis was diagnosed in the remaining 3 of 6 patients with primary sarcoma (n = 1), renal cell carcinoma (n = 1), and unknown primary (n = 1). Increased uptake in the primary lung mass, with an SUV_{max} of 3.0, 6.34, and 13.0, was noted in the hemangiopericytoma, sarcomatoid carcinoma and hemangioendothelioma cases, respectively. The mean SUV_{max}, mean fluorescence intensity, and percentage of stained cells were highest in hemangioendothelioma. Among 3 patients with lung metastases, the highest SUV_{max}, 9.5, was in the primary sarcoma patient. **Conclusion:** ^{68}Ga-pentixafor selectively targets the in vivo whole-body disease burden of CXCR4 receptors. This approach thus holds promise for developing suitable radiotheranostics for lung cancers expressing these targets.

Key Words: [^{68}Ga]pentixafor; PET/CT imaging; CXCR4 receptors; lung cancer; rare variants; metastasis

J Nucl Med Technol 2022; 50:278–281
DOI: 10.2967/jnmt.122.264141

Despite ever-evolving research and advances in diagnostic and treatment strategies, lung carcinoma remains the most lethal type of cancer worldwide (*1*). The diagnostic work-up in suspected lung tumors involves tissue diagnosis, including histopathology and immunohistochemistry analysis and imaging. A presumptive differentiation between small cell lung cancer (SCLC) and non–small cell lung cancer (NSCLC) can be made on the basis of clinical presentation and radiologic findings (*2*). Functional tumor imaging using ^{18}F-FDG PET/CT offers complementary information by assessing tumor burden and helps in staging (*3*). However, noninvasive PET/CT imaging of receptor expression and the heterogeneity of specific receptors can provide complementary information (*4*).

There is evidence that SCLC and NSCLC display C-X-C chemokine receptor type 4 (CXCR4) overexpression, which is associated with high tumor aggressiveness, metastasis, and recurrence (*5*). CXCR4 expression is analyzed using immunohistochemistry and fluorescence-activated cell sorting (FACS) analysis of biopsy samples (*6*). Noninvasive imaging using high-throughput PET probes targeting CXCR4 receptors may provide important diagnostic or prognostic information on such patients (*7*).

Few studies have described the feasibility of radiolabeling a cyclic pentapeptide (pentixafor) with ^{68}Ga, and the recent use of ^{68}Ga-pentixafor has yielded encouraging preclinical and clinical results for in vivo imaging of CXCR4 expression in solid tumors as well as in hematologic malignancies (*8–10*). The use of ^{68}Ga-pentixafor PET/CT imaging for selective targeting of CXCR4 receptors has made much progress in hematologic malignancies, whereas its role in solid tumors has been seldom reported (*11–13*).

Because there are more than 30 human malignancies known to overexpress CXCR4 receptors, the imaging applications of ^{68}Ga-pentixafor PET/CT for targeting these receptors are fast expanding in other malignancies. It has recently been reported that ^{68}Ga-pentixafor PET/CT shows high tumor uptake in patients with lung cancer (SCLC and NSCLC), glioblastoma multiforme, and multiple myeloma. This tracer exhibited strong affinity and specificity for the in vivo localization and imaging of CXCR4 receptors in these malignancies (*11,14–16*).

In this study, we investigated—for the first time, to our knowledge—the diagnostic utility of ^{68}Ga-pentixafor PET/CT

Received Mar. 22, 2022; revision accepted Apr. 27, 2022.
For correspondence or reprints, contact Baljinder Singh (drbsingh5144@yahoo.com).
Published online May 24, 2022.

imaging in a few cases of rare lung cancer variants and in lung metastasis cases with distant primaries.

MATERIALS AND METHODS

Six patients (3 men, 3 women; mean age, 57.00 ± 16.80 y; range, 33–73 y) with clinically and radiologically suspected lung cancer were recruited prospectively for the study. Written informed consent was obtained from all participants. The protocol was approved by the Institute Ethics Committee as the doctoral thesis of the first author. All patients underwent ^{68}Ga-pentixafor PET/CT, bronchoscopic or PET/CT-guided lung biopsy, routine histopathology, immunohistochemistry, and quantitative CXCR4 receptor analysis by FACS.

^{68}Ga-Pentixafor PET/CT Data Acquisition and Analysis

Briefly, 148.0–185.0 MBq of ^{68}Ga-pentixafor were injected intravenously. Whole-body PET (Discovery; GE Healthcare) and contrast-enhanced CT (using standard CT acquisition parameters) were performed consecutively 1 h after tracer administration. The PET was performed at a rate of 3 min/frame (7–8 frames) from the base of the skull to the proximal thighs. Attenuation-corrected PET images were reconstructed iteratively using ordered-subset expectation maximization. The reconstructed images were projected in 3 planes (cross-sectional, coronal, and sagittal) and used for visual and quantitative (SUV_{max}) analysis.

FACS Analysis

In FACS analysis, the freshly biopsied lung sample was processed, and 5.0 μL of fluorescein isothiocyanate–labeled CD184 (BD Pharmingen) was used to further label the CXCR4-positive tumor cells in the tissue suspension. A flow cytometer (FACS Calibur; BD) was used to analyze the stained and unstained cell population, and the results were expressed as mean fluorescence intensity (MFI) and percentage of CXCR4-positive stained cells.

The ^{68}Ga-pentixafor PET/CT image findings (SUV_{max}) were compared with histopathology and with the quantitative parameters of the FACS assay—that is, the MFI and the percentage of stained cells.

RESULTS

The results of histopathology, FACS, and ^{68}Ga-pentixafor PET are presented in Table 1. High uptake was noted in all lung lesions. In 3 patients (patients 1–3), rare primary lung pathologies were identified. The highest SUV_{max}, 13.04, with the highest corresponding MFI, 682.0, was noted in the patient (patient 2) with histopathologic evidence of hemangioendothelioma (Fig. 1). The SUV_{max} and MFI were 6.34 and 110.5, respectively, in patient 1 (sarcomatoid carcinoma) and 3.0 and 27.90, respectively, in patient 3 (hemangiopericytoma). The corresponding SUV_{max} and MFI were 9.5 and 191.20, respectively, in a case of secondary lung metastasis from sarcoma (patient 4), 6.0 and 62.0, respectively, in a case of renal cell carcinoma (patient 5), and 7.5 and 216.0, respectively, in a case of unknown primary (patient 6). The results of ^{68}Ga-pentixafor PET/CT, FACS, and histopathologic analysis for patient 4 are presented in Figure 2.

Pearson correlation analysis indicated a significant correlation between SUV_{max} and MFI ($r = 0.90$), between SUV_{max} and percentage of stained cells ($r = 0.79$), and between MFI and percentage of stained cells ($r = 0.72$).

DISCUSSION

In the present study, ^{68}Ga-pentixafor PET/CT imaging demonstrated high uptake (SUV_{max}, 13.0; MFI, 682.0) in hemangioendothelioma. The SUV_{max} in the other 2 pathologies—that is, sarcomatoid carcinoma and hemangiopericytoma—varied as a function of MFI. Interestingly, among the 3 cases of lung metastases, the highest SUV_{max}, 9.5 (MFI, 191.0), was seen in the lung metastasis with sarcoma as the primary disease. These findings presented a positive correlation ($r = 0.90$) between ^{68}Ga-pentixafor uptake and CXCR4 receptor expression and density, which in turn indicated the high specificity of the tracer for these receptors. Likewise, SUV_{max} also correlated ($r = 0.79$) with the percentage of stained cells.

To our knowledge, we were the first to report the normal biodistribution of ^{68}Ga-pentixafor in a healthy volunteer; the highest SUV_{mean} and SUV_{max} were in the urinary bladder (146.0 and 239.0, respectively) and spleen (6.80 and 10.10, respectively), followed by the kidneys (4.99 and 20.55, respectively) (*17*). Variable physiologic uptake of ^{68}Ga-pentixafor was seen in the spleen in different imaging studies and was found to have an association with stage of disease and clinical outcome, as reported in a study on 145 solid-tumor patients (*18*). A positive correlation was found between ^{68}Ga-pentixafor splenic uptake and platelet or leukocyte counts in lung cancer and neuroendocrine tumors, suggesting that splenic uptake might play a role in systemic immunity or inflammation (*18*).

TABLE 1
Findings in 6 Patients with Rare Lung Tumors and Metastatic Lung Disease

Patient no.	Age (y)	Sex	Histopathology	^{68}Ga-pentixafor PET SUV_{max}	FACS analysis	
					MFI	CXCR-positive tumor cells (%)
1	73	F	Sarcomatoid carcinoma (primary tumor)	6.34	110.50	2.70
2	33	F	Hemangioendothelioma (primary tumor)	13.0	682.0	73.60
3	68	M	Hemangiopericytoma (primary tumor)	3.0	27.90	2.50
4	70	F	Lung metastasis (primary sarcoma)	9.5	191.20	45.2
5	40	M	Lung metastasis (primary renal cell carcinoma)	6.0	62.0	47.0
6	58	M	Lung metastasis (unknown primary)	7.5	216.6	59.2

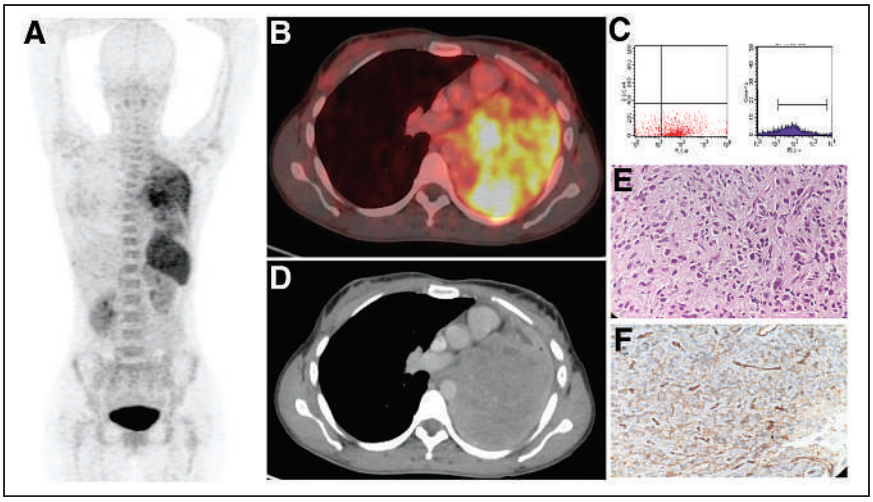

FIGURE 1. A 73-y-old woman (patient 2) with primary lung hemangioendothelioma. (A, B, and D) ^{68}Ga-pentixafor PET/CT maximum-intensity projection (A) and cross-sectional PET/CT image (B) showing increased uptake (SUV_{max}, 13.0), with corresponding CT image (D). (C, E, and F) FACS analysis using CD184-PE showing stained CXCR4-positive tumor cells in scatterplots (C), photomicrograph with histopathologic disease evidence showing epithelioid tumor cells (hematoxylin and eosin, ×40) (E) and immunohistochemistry staining with CD31 showing diffuse membranous positivity (F).

We previously reported that uptake of ^{68}Ga-pentixafor in SCLC patients was higher than in NCSLC and other lung cancer variants and that the uptake varied as a function of CXCR4 receptor density (*11,14*). However, the pattern of uptake and the in vivo evidence of CXCR4 expression in rare lung malignancies have not been studied before.

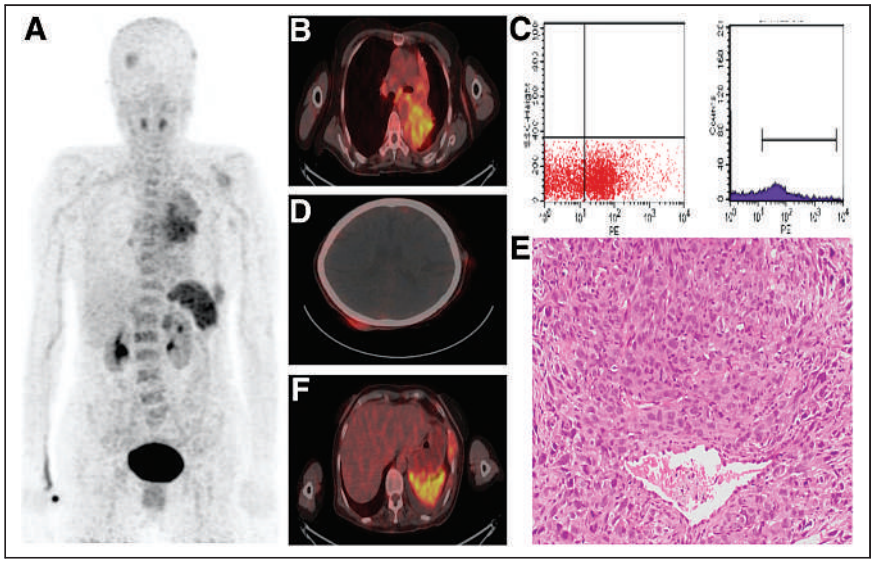

FIGURE 2. A 70-y-old woman (patient 4) with secondary lung cancer disease. (A) ^{68}Ga-pentixafor PET/CT maximum-intensity projection showing increased uptake in lung and in multiple sarcomatoid lesions. (B, D, and F) Cross-sectional PET/CT image showing increased (SUV_{max}, 9.5) uptake in metastatic lung lesion (B), in posterior subcutaneous lesions and left lateral aspect of scalp (SUV_{max}, 4.6) (D), and in lytic expansile lesion with soft-tissue component involving lateral aspect of fifth rib (SUV_{max}, 5.4) (F). (C) FACS analysis using CD184-PE showing stained CXCR4-positive tumor cells in scatterplots. (E) Photomicrograph with histopathologic disease evidence (hematoxylin and eosin, ×40).

^{68}Ga-pentixafor PET tracer was shown to have excellent affinity for CXCR4 receptors in preclinical and clinical studies (*19,20*). According to the available literature, noninvasive imaging of CXCR4 expression in SCLC is feasible, and ^{68}Ga-pentixafor as a novel PET tracer might serve as a readout for confirming the CXCR4 expression (*20*). Watts et al. reported that ^{68}Ga-pentixafor uptake denoting CXCR4 expression is higher in SCLC than NSCLC patients (*11,14*). Evaluation of CXCR4 expression is a prerequisite for potential CXCR4-directed radiotherapies and chemotherapies in lung cancer and especially in SCLC, which has higher CXCR4 expression compared with all other variants of lung cancer.

The reports on CXCR4 expression in rare lung tumors included in this study are not available. However, the role of overexpression of CXCR4 receptors in tumor growth and progression in sarcoma and renal cell carcinoma primaries and in metastasis to lungs has been demonstrated (*21,22*). ^{68}Ga-pentixafor PET imaging may thus be expanded beyond SCLC and NSCLC to unravel the CXCR4 receptor density and to understand the process of metastatic spread and the intra- or interindividual heterogeneity of these tumors (*23*). In a recent study, an urgent clinical need to develop novel therapeutics for devastating NSCLC disease targeting the CXCR4/CXCL12 axis has been advocated (*24*). The study has further stressed that this is the time to move forward and attempt to incorporate CXCR4 inhibitors into novel immune-based therapeutic protocols for lung cancer.

CONCLUSION

^{68}Ga-pentixafor selectively targets and accurately maps the in vivo whole-body disease burden of CXCR4 receptors, a task that is not possible by tissue sampling methods. This technique thus holds great promise for translating this approach by labeling the vector with α- or β-emitters to a therapeutic scenario in such aggressive lung cancer variants having limited treatment options.

DISCLOSURE

Baljinder Singh of the Department of Nuclear Medicine received extramural research funding from the

Department of Science and Technology under the DST-FIST program (grant SR/FST/LSI-548/2012) for the purchase of the automated chemistry module and other chemicals and peptides. No other potential conflict of interest relevant to this article was reported.

KEY POINTS

QUESTION: Can the in vivo expression of CXCR4 receptors be shown in rare lung cancers noninvasively by ^{68}Ga-pentixafor PET/CT?

PERTINENT FINDINGS: ^{68}Ga-pentixafor PET/CT detected the presence of CXCR4 receptors in rare lung cancers and metastases. The uptake varied as a function of receptor density, showing high specificity for in vivo imaging of CXCR4 receptor disease burden in lung cancers.

IMPLICATIONS FOR PATIENT CARE: This technique holds great promise for translating this approach by labeling the vector with α- or β-emitters for therapeutic applications in aggressive lung cancer variants having limited treatment options.

REFERENCES

1. Barta JA, Powell CA, Wisnivesky JP. Global epidemiology of lung cancer. *Ann Glob Health.* 2019;85:8.
2. Silvestri GA, Gonzalez AV, Jantz MA, et al. Methods for staging non-small cell lung cancer: diagnosis and management of lung cancer, 3rd ed: American College of Chest Physicians evidence-based clinical practice guidelines. *Chest.* 2013; 143(suppl):e211S–e250S.
3. Kandathil A, Kay FU, Butt YM, Wachsmann JW, Subramaniam RM. Role of FDG PET/CT in the eighth edition of TNM staging of non-small cell lung cancer. *Radiographics.* 2018;38:2134–2149.
4. George GP, Pisaneschi F, Nguyen QD, Aboagye EO. Positron emission tomographic imaging of CXCR4 in cancer: challenges and promises. *Mol Imaging.* 2014;13:10.2310/7290.2014.00041.
5. Domanska UM, Kruizinga RC, Nagengast WB, et al. A review on CXCR4/CXCL12 axis in oncology: no place to hide. *Eur J Cancer.* 2013;49:219–230.
6. Stankovic B, Bjørhovde HAK, Skarshaug R, et al. Immune cell composition in human non-small cell lung cancer. *Front Immunol.* 2019;9:3101.
7. Demmer O, Gourni E, Schumacher U, Kessler H, Wester HJ. PET imaging of CXCR4 receptors in cancer by a new optimized ligand. *ChemMedChem.* 2011;6: 1789–1791.
8. Shekhawat AS, Singh B, Malhotra P, et al. Imaging CXCR4 receptors expression for staging multiple myeloma by using 68Ga-Pentixafor PET/CT: comparison with 18F-FDG PET/CT. *Br J Radiol.* 2022;95:20211272.
9. Vag T, Gerngross C, Herhaus P, et al. First experience with chemokine receptor CXCR4-targeted PET imaging of patients with solid cancers. *J Nucl Med.* 2016; 57:741–746.
10. Lapa C, Herrmann K, Schirbel A, et al. CXCR4-directed endoradiotherapy induces high response rates in extramedullary relapsed multiple myeloma. *Theranostics.* 2017;7:1589–1597.
11. Watts A, Singh B, Basher R, et al. ^{68}Ga-pentixafor PET/CT demonstrating higher CXCR4 density in small cell lung carcinoma than in non-small cell variant. *Eur J Nucl Med Mol Imaging.* 2017;44:909–910.
12. Wald O. CXCR4 based therapeutics for non-small cell lung cancer (NSCLC). *J Clin Med.* 2018;7:303.
13. Herrmann K, Schottelius M, Lapa C, et al. First-in-human experience of CXCR4-directed endoradiotherapy with ^{177}Lu- and ^{90}Y-labeled pentixather in advanced-stage multiple myeloma with extensive intra- and extramedullary disease. *J Nucl Med.* 2016;57:248–251.
14. Watts A, Singh B, Dhanota N, et al. In vivo imaging and quantification of CXCR4 expression in lung cancer subtypes using ^{68}Ga-pentixafor PET/CT and flow cytometry analysis: a single center and first Asian experience [abstract]. *J Nucl Med.* 2019;60(suppl 1):84.
15. Watts A, Arora D, Kumar N, et al. ^{68}Ga-pentixafor PET/CT offers high contrast image for the detection of CXCR4 expression in recurrent glioma [abstract]. *J Nucl Med.* 2019;60(suppl 1):491
16. Singh B, Shekhawat A, Malhotra P. Comparison of ^{68}Ga-pentixafor PET/CT versus ^{18}F-FDG PET/CT in staging of multiple myeloma [abstract]. *J Nucl Med.* 2020;61(suppl 1):171.
17. Watts A, Chutani S, Arora D, et al. Automated radiosynthesis, quality control, and biodistribution of Ga-68 pentixafor: first Indian experience. *Indian J Nucl Med.* 2021;36:237–244.
18. Lewis R, Habringer S, Kircher M, et al. Investigation of spleen CXCR4 expression by [^{68}Ga]pentixafor PET in a cohort of 145 solid cancer patients. *EJNMMI Res.* 2021;11:77.
19. Knight JC, Wuest FR. Nuclear (PET/SPECT) and optical imaging probes targeting the CXCR4 chemokine receptor. *MedChemComm.* 2012;3:1039–1053.
20. Lapa C, Lückerath K, Rudelius M, et al. [^{68}Ga]pentixafor-PET/CT for imaging of chemokine receptor 4 expression in small cell lung cancer: initial experience. *Oncotarget.* 2016;7:9288–9295.
21. Zhu Y, Tang L, Zhao S, et al. CXCR4-mediated osteosarcoma growth and pulmonary metastasis is suppressed by microRNA-613. *Cancer Sci.* 2018;109: 2412–2422.
22. Floranović MP, Veličković LJ. Effect of CXCL12 and its receptors on unpredictable renal cell carcinoma. *Clin Genitourin Cancer.* 2020;18:e337–e342.
23. Buck AK, Stolzenburg A, Hänscheid H, et al. Chemokine receptor-directed imaging and therapy. *Methods.* 2017;130:63–71.
24. Osl T, Schmidt A, Schwaiger M, Schottelius M, Wester HJ. A new class of PentixaFor- and PentixaTher-based theranostic agents with enhanced CXCR4-targeting efficiency. *Theranostics.* 2020;10:8264–8280.

^{18}F-DCFPyL PET/CT in Metastatic Renal Cell Carcinoma

Geoffrey M. Currie[1], Marko Trifunovic[2], Jui Liu[2], Sang Kim[3], and Howard Gurney[3]

[1]*Faculty of Science, Charles Sturt University, Wagga Wagga, Australia;* [2]*Macquarie Medical Imaging, Macquarie University Hospital, Sydney, Australia; and* [3]*Medical Oncology, Macquarie University, Sydney, Australia*

Targeted molecular imaging with PET uses chemical ligands that are peptides specifically targeting a receptor of interest. Prostate-specific membrane antigen (PSMA) is substantially upregulated in prostate cancer but is also expressed in the neovascular tissue of several malignancies, including renal cell carcinoma (RCC). Radiolabeled peptide targets for PSMA may be helpful in detecting metastatic RCC lesions. We present a case of incidental detection of RCC metastatic disease with PSMA-targeted PET, and we explore potential use for deliberate evaluation of RCC with PSMA-targeted tracers.

Key Words: ^{18}F-PSR; PET/CT; RCC; metastases

J Nucl Med Technol 2022; 50:282–285
DOI: 10.2967/jnmt.121.262799

Targeted molecular imaging has a foundation in the receptor principle. An important cell surface receptor is the class II membrane glycoprotein prostate-specific membrane antigen (PSMA). PSMA is the glutamate carboxypeptidase II enzyme that catalyzes *N*-acetylaspartylglutamate into glutamate and *N*-acetylaspartate. PSMA is weakly expressed on normal prostate cells but substantially upregulated in prostate cancer, particularly those of higher grade (*1,2*). It is well known that PSMA is also expressed in the neovascular tissue of several malignancies, including renal cell carcinoma (RCC) (*1–3*). PSMA is also expressed in a range of normal tissues, including the salivary glands, brain, intestines, and proximal renal tubules (*3*).

For PSMA radiotracers, PSMA itself is the receptor target, not the peptide. Thus, a numeric suffix generally identifies the specific peptide. PSMA-617, PSMA-11, PSMA-1007, and PSMA-I&T are commonly used. These all share the identical Lys-urea-Glu active portion of the peptide that binds to the receptor. ^{68}Ga-PSMA PET/CT imaging provides a high tumor-to-background ratio and so has become increasingly important in the detection and localization of prostate cancer. ^{68}Ga is conveniently available via a ^{68}Ge/^{68}Ga generator, which typically services a department for 6–12 mo before renewal. ^{18}F-PSMA takes advantage of the longer half-life of 110 min and direct labeling (or Al-F chelation). ^{18}F-PSMA is accessible to those without the workload to justify a ^{68}Ga generator and those without an onsite cyclotron. Two versions are most widely reported in the literature: ^{18}F-DCFPyL and ^{18}F-PSMA-1007. ^{18}F-PSMA-1007 has been reported to have less urinary excretion and bladder visualization than ^{68}Ga-PSMA-11 and therefore to be more useful in imaging the prostate bed (*4,5*). 2-(3-{1-carboxy-5-[(6-^{18}F-fluoro-pyridine-3-carbonyl)-amino]-pentyl}-ureido)-pentanedioic acid (^{18}F-DCFPyL), or dichlorofluorescein (DCF) pyrrolysine (PyL), is widely referred to as PSR (prostate-specific radiopharmaceutical). PSR has been reported to have less liver accumulation, which may be helpful in detecting liver metastases, although a higher distribution of dose to the kidneys and lacrimal glands was also noted (*6*). Importantly, ^{18}F-PSR has been reported to have a higher accumulation than other PSMA probes in disease with a lower level of prostate-specific antigen (*6*).

CASE

A 70-y-old woman presented with hematuria. Twenty years previously, she had undergone laparoscopic left nephrectomy for clear cell RCC. She was found to have a bladder mass on imaging. The patient underwent a cystoscopic surgical resection of the bladder mass, and histopathologic examination confirmed metastatic clear cell RCC. The patient was referred for staging ^{18}F-PSR PET/CT. ^{18}F-PSR (275 MBq) was administered intravenously, with whole-body PET (vertex to thighs) and low-dose CT performed 90 min after administration.

The ^{18}F-PSR PET/CT findings revealed no residual disease in the pelvis or abdomen (Fig. 1). However, a focus of uptake (SUV_{max}, 7.0) that exhibited a photopenic core was seen in the left parietal lobe, and a mild focus (SUV_{max}, 2.3) was seen in the right occipital lobe. There was also uptake (SUV_{max}, 6.2) associated with a large (4.2 × 4.7 × 5.7 cm) soft-tissue-density mass extending from the inferior pole of the right thyroid lobe distally into the high mediastinum; uptake associated with the mediastinal lymph nodes, including the right paratracheal (SUV_{max}, 4.9), prevascular (SUV_{max}, 6.7), and subcarinal (SUV_{max}, 5.1) regions; and uptake (SUV_{max}, 6.7) associated with the left hilar node. Physiologic uptake was noted in the left parotid and bilateral submandibular glands, whereas the right parotid gland was absent (confirmed on coregistered CT).

The ^{18}F-PSR PET/CT findings were suggestive of moderately ^{18}F-PSR–avid cerebral metastases involving the left

Received Jun. 25, 2021; revision accepted Sep. 10, 2021.
For correspondence or reprints, contact Geoff Currie (gcurrie@csu.edu.au).
Published online Nov. 8, 2021.

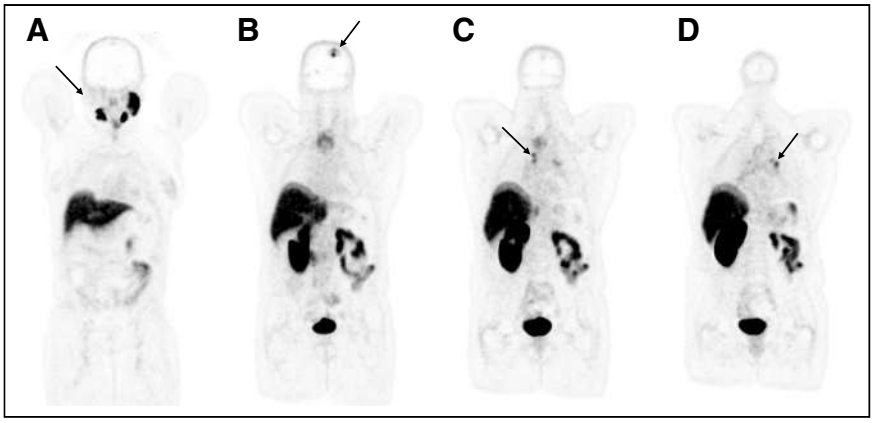

FIGURE 1. Representative coronal slices of ^{18}F-PSR PET scan. (A) Physiologic ^{18}F-PSR uptake in left parotid and bilateral submandibular glands, but absence (arrow) of right parotid gland. (B) Focal accumulation (arrow) of ^{18}F-PSR in left parietal lobe. (C) ^{18}F-PSR uptake (arrow) associated with mediastinal lymph nodes. (D) ^{18}F-PSR uptake (arrow) associated with left hilar node.

parietal and right occipital lobes, as well as of lymph nodal metastases involving the mediastinal and the left hilar nodes (Fig. 2). The moderately ^{18}F-PSR–avid right thyroid mass might have represented thyroid malignancy or further metastatic disease (Fig. 3). The patient had no symptoms of either brain metastases or mediastinal or hilar node metastases. Follow-up MRI confirmed 2 brain metastases correlating with the PET/CT. The patient underwent surgical resection of the brain metastases, and histopathologic examination confirmed metastatic clear cell RCC. She then received stereotactic radiosurgery to the surgery bed. A CT scan 2 mo later showed progression in the mediastinal nodes and thyroid, whereas MRI brain showed resolution of the brain metastases. The patient started receiving systemic therapy using lenvatinib and pembrolizumab plus a CTLA4 antibody, in a clinical trial. The patient recalled undergoing thyroid surgery some 30 years previously for a hemorrhagic cyst, but no details could be provided.

DISCUSSION

RCC is the most common primary malignancy of the kidney, with as many as 35% of patients presenting with metastatic disease at the time of diagnosis (*7*). Clear cell RCC represents 75% of cases and has been targeted with PSMA imaging because of the high level of neovascularity and high degree of PSMA expression (*7*). Anatomic characterization (radiography, CT, and MRI) of metastatic RCC and molecular characterization with ^{18}F-FDG PET are suboptimal because of their nonspecific nature, which has further increased interest in PSMA imaging (*7*). PSMA is particularly helpful in detecting small metastatic lesions, although study sizes have been small. For example, one of the larger studies included 22 RCC patients, 20 with clear cell RCC, and showed that patient management was changed from the initial CT staging in 13 of 20 patients using ^{68}Ga-PSMA (*8*). Using ^{18}F-PSR, Rowe et al. (*9*) evaluated 5 clear cell RCC patients

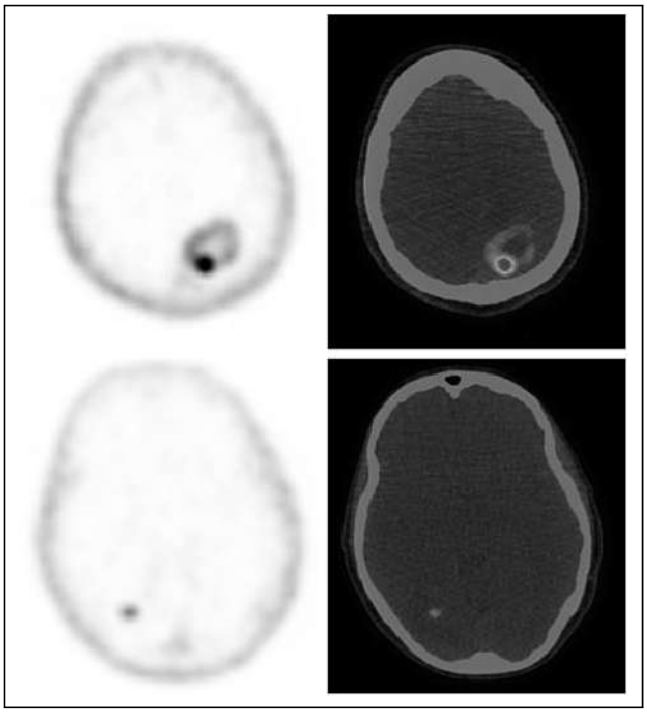

FIGURE 2. ^{18}F-PSR PET scan with transaxial slices through head demonstrating left parietal (top) and right occipital (bottom) cerebral metastases.

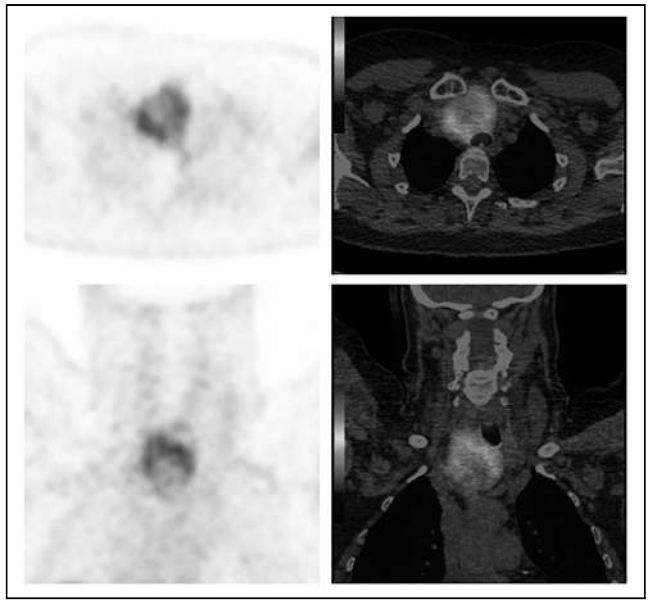

FIGURE 3. Transaxial (top) and coronal (bottom) slices of ^{18}F-PSR PET (left) with low-dose CT coregistration (right) in the right thyroid lesion.

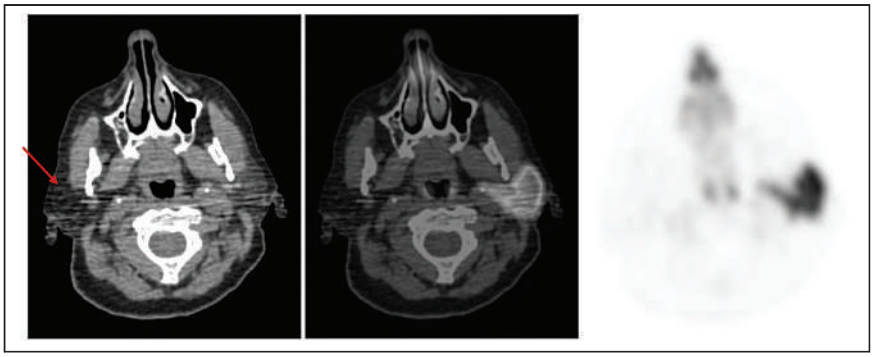

FIGURE 4. Transaxial head slices with CT (left) and ^{18}F-PSR PET (right) with low-dose CT coregistration (middle) indicating the absence of accumulation (arrow) in the right parotid salivary gland.

with 18 lesions characterized by conventional imaging and 28 on ^{18}F-PSR PET.

Brain metastases are present in 6.5% of RCC patients at the time of diagnosis (*10*), although reports range from 4% to 48% (*11*). Brain metastases are asymptomatic in patients with known RCC metastases in as many as 33% of cases (*11*). The presence of brain metastases is an indicator of poor prognosis (*12*). Given PSMA expression in RCC metastases, the detection of brain metastases in this patient was unexpected but not surprising.

Under normal conditions, both the lacrimal glands and the salivary glands accumulate PSMA-targeted radiopharmaceuticals at a high level (*13,14*). Indeed, decreased uptake of PSMA-targeted radiopharmaceuticals is a marker for abnormality, including inflammatory conditions (*14*). In this patient, despite normal ^{18}F-PSR uptake in the salivary glands, the right parotid salivary gland had an absence of uptake. Careful review of the low-dose nondiagnostic CT (Fig. 4) suggests absence of the right parotid gland, with replacement by fat tissue. This may reflect the patient's vague history of previous surgery associated with a hemorrhagic cyst, which was reported by the patient as thyroid gland but may have been salivary gland and mistakenly recalled as thyroid.

Among 12 published articles reporting an incidental accumulation of PSMA-targeted radiopharmaceuticals in the thyroid, 6 of 23 cases were malignant and 17 of 23 were benign (*15*). Sager et al. (*16*) reported 2 incidental cases of ^{68}Ga-PSMA uptake in the thyroid: the first with extensive accumulation associated with follicular thyroid carcinoma and the second with mild focal accumulation in a thyroid nodule. ^{68}Ga-PSMA imaging was suggested to be of potential value in distinguishing follicular thyroid lesions, and at a minimum it is important to be aware of potential thyroid incidentalomas to avoid misinterpretation. Verburg et al. (*17*) and Santhanam et al. (*18*) have suggested—for anti-PSMA and PSR, respectively—that PSMA expression offered a potential novel theranostic pair for advanced differentiated thyroid cancer in patients with negative radioiodine imaging results or ^{131}I resistance.

Although PSMA-targeting PET tracers are well established in prostate cancer, they have recently been reported to change management in 42% of RCC patients (*19*). Physiologic uptake in the parenchyma renders PSMA-targeted tracers less than ideal for primary RCC, yet they may be useful for detecting metastatic disease (*20*).

CONCLUSION

PSMA-targeting PET tracers provide a useful tool for both incidental and deliberate detection of metastatic RCC and may be particularly useful in the evaluation of small lesions and those in the brain. Further clinical evaluation is recommended to explore efficacy and the potential for theranostic-pair approaches to patient management. The availability and affordability of ^{18}F-PSR provide access to PSMA-targeted PET imaging at sites without a ^{68}Ge/^{68}Ga generator or onsite cyclotron.

DISCLOSURE

No potential conflict of interest relevant to this article was reported.

KEY POINTS

QUESTION: Is ^{18}F-PSR useful in the evaluation of RCC metastatic disease?

PERTINENT FINDINGS: The recently Food and Drug Administration–approved ^{18}F-PSR has value for detecting metastatic RCC.

IMPLICATIONS FOR PATIENT CARE: Although ^{18}F-PSR is valuable in the armamentarium for evaluation of prostate cancer, it also has a potential role to play in RCC and other metastatic diseases that exhibit overexpression of prostate-specific antigen.

REFERENCES

1. Bravaccini S, Puccetti M, Bocchini M, et al. PSMA expression: a potential ally for the pathologist in prostate cancer diagnosis. *Sci Rep.* 2018;8:4254.
2. Ha H, Kwon H, Lim T, Jang J, Park SK, Byun Y. Inhibitors of prostate-specific membrane antigen in the diagnosis and therapy of metastatic prostate cancer: a review of patent literature. *Expert Opin Ther Pat.* 2021;31:525–547.
3. Pozzessere C, Bassanelli M, Ceribelli A, et al. Renal cell carcinoma: the oncologist asks, can PSMA PET/CT answer? *Curr Urol Rep.* 2019;20:68.
4. Ilhan H, la Fougère C, Krause BJ. PSMA-based theranostics in prostate cancer. *Urologe A.* 2020;59:617–625.
5. Kesch C, Kratochwil C, Mier W, Klaus K, Giesel FL. Gallium-68 or fluorine-18 for prostate cancer imaging? *J Nucl Med.* 2017;58:687–688.
6. Werner RA, Derlin T, Lapa C, et al. ^{18}F-labeled, PSMA-targeted radiotracers: leveraging the advantages of radiofluorination for prostate cancer molecular imaging. *Theranostics.* 2020;10:1–16.
7. Yin Y, Campbell S, Markowski M, et al. Inconsistent detection of sites of metastatic non-clear cell renal carcinoma with PSMA-targeted ^{18}F-DCFPyL PET/CT. *Mol Imaging Biol.* 2019;21:567–573.

8. Siva S, Callahan J, Pryor D, et al. Utility of ^{68}Ga prostate specific membrane antigen positron emission tomography in diagnosis and response assessment of recurrent renal cell carcinoma. *J Med Imaging Radiat Oncol.* 2017;61:372–378.
9. Rowe SP, Gorin M, Hammers H, et al. Imaging of metastatic clear cell renal carcinoma with PSMA-targeted ^{18}F-DCFPyL PET/CT. *Ann Nucl Med.* 2015;29:877–882.
10. Ke ZB, Chen S, Chen Y, et al. Risk factors for brain metastases in patients with renal cell carcinoma. *BioMed Res Int.* 2020;2020:6836234.
11. Remon J, Lianes P, Martínez S. Brain metastases from renal cell carcinoma: should we change the current standard? *Cancer Treat Rev.* 2012;38:249–257.
12. Dudani S, de Velasco G, Wells JC, et al. Evaluation of clear cell, papillary, and chromophobe renal cell carcinoma sites and association with survival. *JAMA Netw Open.* 2021;4:e2021869.
13. van Kalmthout LW, Lam M, de Keizer B, et al. Impact of external cooling with icepacks on ^{68}Ga-PSMA uptake in salivary glands. *EJNMMI Res.* 2018;8:56.
14. Rupp NJ, Umbricht CA, Pizzuto DA, et al. First clinicopathological evidence of a non PSMA-related uptake mechanism for ^{68}Ga-PSMA-11 in salivary glands. *J Nucl Med.* 2019;60:1270–1276.
15. Bertagna F, Albano D, Giovanella L, et al. ^{68}Ga-PSMA PET thyroid incidentalomas. *Hormones (Athens).* 2019;18:145–149.
16. Sager S, Vatankulu B, Uslu L, Sönmezoglu K. Incidental detection of follicular thyroid carcinoma in ^{68}Ga-PSMA PET/CT imaging. *J Nucl Med Technol.* 2016;44:199–200.
17. Verburg FA, Krohn T, Heinzel A, Mottaghy FM, Behrendt FF. First evidence of PSMA expression in differentiated thyroid cancer using [^{68}Ga]PSMA-HBED-CC PET/CT. *Eur J Nucl Med Mol Imaging.* 2015;42:1622–1623.
18. Santhanam P, Russell J, Rooper LM, et al. The prostate-specific membrane antigen (PSMA)-targeted radiotracer ^{18}F-DCFPyL detects tumor neovasculature in metastatic, advanced, radioiodine-refractory, differentiated thyroid cancer. *Med Oncol.* 2020;37:98.
19. Raveenthiran S, Esler R, Yaxley J, Kyle S. The use of ^{68}Ga-PET/CT PSMA in the staging of primary and suspected recurrent renal cell carcinoma. *Eur J Nucl Med Mol Imaging.* 2019;46:2280–2288.
20. Lindenberg L, Mena E, Choyke P, Bouchelouche K. PET imaging in renal cancer. *Curr Opin Oncol.* 2019;31:216–221.

PET/CT of Delayed Uterine Leiomyoma Metastasizing to Lung and Femur

Kenneth N. Huynh and Ba D. Nguyen

Department of Radiology, Mayo Clinic Arizona

Benign metastasizing leiomyomas are benign disseminated extrauterine tumors in patients with prior history of uterine leiomyomas and may occur years after hysterectomy. The lung is mostly affected, with a less common occurrence in the brain, heart, spine, retroperitoneum, and bone. We present the role of ^{18}F-FDG PET/CT in the metabolic staging and postsurgical monitoring of a patient with lung and femoral involvement.

Key Words: uterine leiomyoma; metastasis; thorax; femur; PET

J Nucl Med Technol 2022; 50:286–287
DOI: 10.2967/jnmt.122.263901

A case of pulmonary and osseous benign metastasizing leiomyoma is presented with ^{18}F-FDG PET/CT imaging.

CASE REPORT

A 76-y-old woman had a 6-mo history of right hip pain with MRI detection of a right femoral diaphyseal intramedullary lesion. Further CT imaging showed a left hemithoracic mass with chest wall and rib invasion. Contemporary ^{18}F-FDG PET/CT (Fig. 1) showed borderline hypermetabolic left lung mass (SUV, 4.2) and right femoral lesion (SUV, 3.4). Subsequent CT-guided biopsy of both lesions showed spindle cell features considered as synchronous metastatic smooth cell neoplasm, with immunostains positive for desmin, estrogen receptor, and progesterone receptor and negative for pancytokeratin, CK5/6, S100, CD117, and CD10. Her clinical history was remarkable for a total abdominal hysterectomy and bilateral salpingo-oophorectomy for uterine leiomyoma 15 y before the present event. These lesions were consistent with benign metastasizing leiomyoma (Fig. 2). The patient underwent the left thoracic and right femoral tumor resection with right hip arthroplasty. No residual or recurrent tumor was detected during the subsequent 6-y PET/CT surveillance.

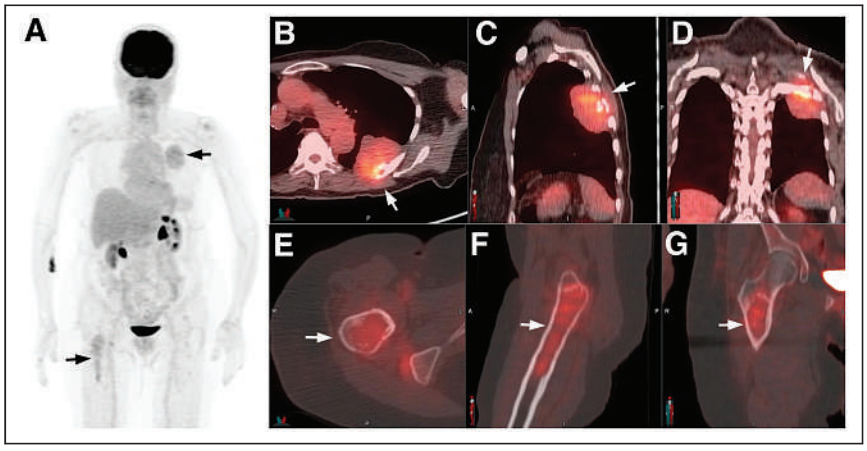

FIGURE 1. Anterior PET maximum-intensity-projection image shows the borderline hypermetabolic lesions of left thorax and right proximal femur (A, arrows). (B–G) Corresponding axial, sagittal, and coronal fused PET/CT of the mass of lung and chest wall (B–D, arrows) and of proximal right femur (E–G, bone window, arrows).

DISCUSSION

Benign metastasizing leiomyoma (BML) is a rare disease characterized by histologically benign extrauterine smooth cell metastatic tumors in patients with prior history of uterine leiomyomas. BML may occur years after hysterectomy for benign uterine leiomyomas; however, few cases have been reported in women without previous uterine surgery (*1*). The lung is the site most affected, with rare involvement of the brain, heart, spine, retroperitoneum, and bone (*1–3*). Although several theories detail the route of metastasis, the etiology and pathogenesis of BML still remain unclear. A few theories suggest a metaplastic process or hematologic spread of uterine leiomyomatous tissue at the time of hysterectomy (*1*). Even though MR and CT depicted well the femoral and chest tumors in our patient, ^{18}F-FDG PET/CT provided the metabolic characteristics of these lesions, the whole-body assessment for potential additional lesions/metastasis, and the postsurgical surveillance of BML. Leiomyosarcomas are ^{18}F-FDG–avid, whereas BML typically lacks tracer

Received Jan. 22, 2022; revision accepted Mar. 14. 2022.
For correspondence or reprints, contact Ba D. Nguyen (Nguyen.ba@mayo.edu).
Published online Jul. 26, 2022.

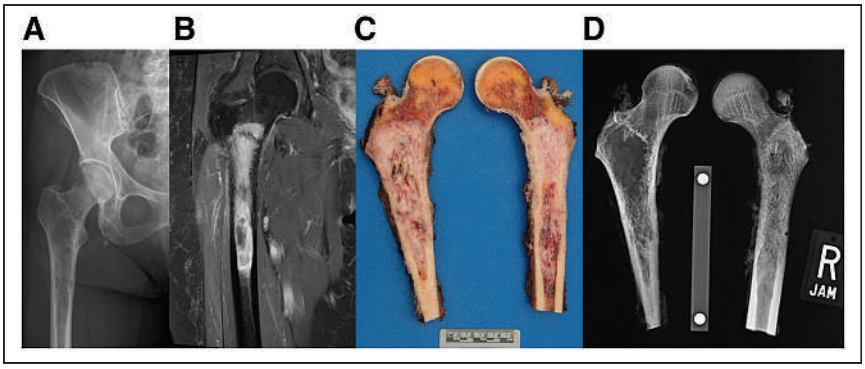

FIGURE 2. Corresponding radiograph of the right femur before resection (A), coronal contrast-enhanced MR image (B), photograph of surgical specimen (C), and radiograph of surgical specimen (D) of proximal femoral lesion.

uptake. However, a small proportion of BML may exhibit mild borderline tracer uptake as seen in our case (*2*). ^{18}F-FES (16α-^{18}F-fluoro-17β-estradiol) PET/CT may provide useful information about BML estrogen receptor expression with an option for antihormonal therapy (*4*). Histologically, the absence of cellular atypia and low mitotic activity favor a diagnosis of BML. However, low-grade and slow-growing leiomyosarcoma cannot be totally excluded from the differential diagnosis even with benign histologic features.

CONCLUSION

BML is of rare occurrence. PET/CT is a useful functional imaging modality for a comprehensive evaluation and post-therapeutic surveillance of this potentially multifocal disease.

DISCLOSURE

No potential conflict of interest relevant to this article was reported.

REFERENCES

1. Barnaś E, Książek M, Raś R, Skręt A, Skręt-Magierło J, Dmoch-Gajzlerska E. Benign metastasizing leiomyoma: a review of current literature in respect to the time and type of previous gynecological surgery. *PLoS One.* 2017;12:e0175875.
2. Sawai Y, Shimizu T, Yamanaka Y, Niki M, Nomura S. Benign metastasizing leiomyoma and 18-FDG-PET/CT: a case report and literature review. *Oncol Lett.* 2017; 14:3641–3646.
3. Pimentel JR, de Almeida ALB, Aymoré IL, Pinto EP, Osthoff L, Smith J. Metastatic skeletal leiomyomatosis (leiomyomatosis ossea). *Skeletal Radiol.* 2002;31:30–34.
4. Has Simsek D, Kuyumcu S, Sanli Y, et al. Demonstration of in vivo estrogen receptor status with 16α- [^{18}F] fluoro-17β-oestradiol (FES) PET/CT in a rare case of benign metastasizing leiomyoma. *Eur J Nucl Med Mol Imaging.* 2021;48:4101–4102.

SNMMI TECHNOLOGIST SECTION PRESENTS AWARDS, ELECTS NEW OFFICERS AT 2022 ANNUAL MEETING

More than 6,700 physicians, technologists, physicists, scientists, and exhibitors gathered at the Society of Nuclear Medicine and Molecular Imaging (SNMMI) 2022 Annual Meeting, held June 11–14 in Vancouver, British Columbia, Canada. The meeting had more than 130 continuing education and scientific sessions and more than 1,000 posters, as well as sessions on new tracers and applications, emerging technologies, theranostics and nuclear medicine and molecular imaging in the post-COVID world.

During the meeting, SNMMI Technologist Section (SNMMI-TS) inducted new officers, who will serve through June 2023. A number of technologists were also recognized for their outstanding contributions to nuclear medicine, molecular imaging, and the society.

2022–2023 SNMMI-TS OFFICERS


Krystle W. Glasgow

SNMMI-TS introduced a new slate of officers during the Annual Meeting. **Krystle W. Glasgow, MIS, CNMT, NMTCB(CT), NMAA, FSNMMI-TS**, has been elected as the 2022–23 president for the SNMMI-TS. Glasgow is a teacher and clinical coordinator at the University of Alabama at Birmingham (UAB) in Birmingham, Alabama, and is currently pursuing her doctorate degree in health services administration with a concentration in health informatics at UAB. "We have had great momentum in the past year in bringing in more members to our great society," said Glasgow. "As president, I will continue working to engage with technologists and build excitement for our field."


Dmitry Beyder

During the meeting, SNMMI-TS also announced, **Dmitry Beyder, CNMT, MPA**, as president-elect. As SNMMI-TS president-elect, Beyder will focus on guiding technologists and the Technologist Section out of the COVID-19 pandemic. He will also work on strengthening the nuclear medicine technologist workforce and professional pipeline, as well as growing the role of nuclear medicine technologists in therapeutics, especially as theranostics continues to advance.

Other elected individuals include:

- Secretary: Amy B. Brady, MAEd, CNMT
- Finance Committee: Lance Burrell, MS, CNMT, PET, RT(CT)
- Nominating Committee:
  - Chair: Dusty York, CNMT, PET, RT(N)(CT)
  - Mario DiDea, MS, RT(N)
  - Sarah Frye, MBA, CNMT, PET, CCRP
  - Rebecca Gallagher, CNMT
  - Kathleen Krisak, BS, CNMT, FSNMMI-TS
- Delegate-at-Large:
  - Sarah Gibbons, MBA, CNMT, NMTCB(CT)
  - Duane Hollier, CNMT, ARRT(N), BS
  - Shannon Youngblood, EdD, MSRS, CNMT
- Director-at-Large: Matt McMahon, MS, CNMT, RT(CT)
- Member-at-Large: Meg Keefe, MSA, CNMT
- Specialty Area Representatives
  - Cardiology: Jamie Warren, EdD, MBA, BHS, CNMT, NCT
  - Education: Julie Bolin, MS, CNMT
  - Emerging Technologies: Lisa Patrick, RT(N), NCT, CT, PET
  - Student: Leila Alsarag

SNMMI-TS FELLOWS

The following four individuals were named SNMMI-TS Fellows. These are members of SNMMI-TS who have demonstrated leadership and have made a significant contribution to the profession of nuclear medicine technology at the national level. SNMMI-TS selects Fellows based on exemplary contributions in the following areas: participation in professional activities, education, professional experience, professional contributions, and civic activities. New SNMMI-TS Fellows receive a memorial plaque and pin signifying their Fellow status.

- **L. David Wells, CNMT**
  JNMT Editor (1974–1977)
- **Patricia Weigand, CNMT**
  JNMT Editor (1978–1982)
- **Susan Gilbert, CNMT**
  JNMT Editor (1995–2000)
- **Beth A. Harkness, MS**
  JNMT Editor (2001–2006)

OUTSTANDING JNMT ARTICLES

The Editor's Choice Awards for the best *JNMT* articles published in 2021 were selected by JNMT editor Kathy S. Thomas, MHA, CNMT, PET, FSNMMI-TS, and the journal's editorial board. Awards include:

- **Editors' Choice Award – 1st Place:** Shannon N. Youngblood, University of Arkansas for Medical Sciences, Little Rock, Arkansas, and Ochsner Medical Center, Baton Rouge, Louisiana, for "Bullying in the Nuclear Medicine Department and During Clinical Nuclear Medicine Education." *J Nucl. Med. Technol*. 2021; 49:156–163.

Outstanding JNMT award winners, from left: Shannon Youngblood, Kyohei Okuda, Pietro Paolo de Barros, Julie Bolin, George Patchoros, and Grace Wenzler.

- **Editors' Choice Award – 2nd Place:** Kyohei Okuda, Daisuke Hasegawa, Takashi Kamiya, Hajime Ichikawa, Takuro Umeda, Takushi Ohkubo, and Kenta Miwa, Department of Clinical Radiology, Tottori University Hospital, Yonago, Japan, for "Multicenter Study of Quantitative SPECT: Reproducibility of ^{99m}Tc Quantitation Using a Conjugated-Gradient Minimization Reconstruction Algorithm." *J Nucl. Med. Technol.* 2021; 49:138–142.
- **Editors' Choice Award – 3rd Place:** Pietro Paolo de Barros, Tatiane Sabriela Cagol Camozzato, Tiago Jahn, Flávio Augusto Penna Soares, Letícia Machado da Silva, Jacqueline de Aguiar Soares, and Marco Antonio Neiva Koslosky, Federal Institute of Education, Science, and Technology of Santa Catarina–IFSC, Florianópolis, Santa Catarina, Brazil, for "Analysis of Radiometry on Patients Undergoing Radioactive Iodine Therapy." *J Nucl. Med. Technol*. 2021; 49:75–81.
- **Editors' Choice Award – Best Continuing Education Article:** Julie Bolin, Nuclear Medicine Technology Program, GateWay Community College, Phoenix, Arizona, for "Thyroid Follicular Epithelial Cell–Derived Cancer: New Approaches and Treatment Strategies." *J Nucl. Med. Technol*. 2021; 49:199–208.
- **Editors' Choice Award — Best Educator's Forum Article:** George Patchoros and Grace Wenzler, Department of Engineering, Physics, and Technology, Bronx Community College, Bronx, New York, for "Satisfying Program-Level Outcomes by Integrating Primary Literature into the Online Classroom." *J Nucl. Med. Technol.* 2021; 49:170–174.

SNMMI-TS OUTSTANDING TECHNOLOGIST AWARD

Chloee Wendorf, MHA, CNMT, NMTCB (CT), PET, NCT, manager of nuclear medicine and PET/CT at the University of California – San Diego Health, received the 2022 SNMMI-TS Outstanding Technologist award. The award recognizes SNMMI-TS members who have demonstrated outstanding service and dedication to the field of nuclear medicine technology.

SNMMI-TS KATHY E. THOMPSON-HUNT OUTSTANDING EDUCATOR AWARD

Crystal Botkin, PhD, MPH, CNMT, PET, FSNMMI-TS, was awarded the 2022 SNMMI-TS Kathy E. Thompson-Hunt Outstanding Educator Award. The award is presented to members who have exhibited commitment to advancing the field in their workplace and through their involvement with the society.

Chloee Wendorf (right) receives Outstanding Technologist Award from 2021–2022 SNMMI-TS President Dusty York.

Crystal Botkin (right) receives Kathy E. Thompson-Hunt Outstanding Educator Award from 2021–2022 SNMMI-TS President Dusty York.

SNMMI-TS ADVOCATE(S)-OF-THE-YEAR AWARD

The 2022 SNMMI-TS Advocate(s)-of-the-Year Award was presented to **Melissa M. Snody, BS, CNMT**, nuclear

medicine PET/CT technologist at Beaumont Health, in Royal Oak, Michigan, and **Janice D. Van Dolsen, BHS, RT(N), CNMT**, manager of nuclear medicine and diagnostic imaging at Doylestown Health in Doylestown, Pennsylvania. This award recognizes an individual or individuals who have made significant contributions to advancing advocacy efforts at the state and federal level.

SNMMI-TS LIFETIME ACHIEVEMENT AWARD

Sal Martino

Jerry Reid

The 2022 SNMMI-TS Lifetime Achievement Award was presented to **Sal Martino, EdD, RT(R), FASRT, CAE**, CEO and executive director of the American Society of Radiologic Technologists in Albuquerque, New Mexico, and **Jerry Reid, PhD**, CEO of The American Registry of Radiologic Technologists, based in St. Paul, Minnesota. This award is reserved for individuals who have made significant contributions to the field of nuclear medicine and the SNMMI-TS and its chapters.

SNMMI-TS PRESIDENTIAL DISTINGUISHED SERVICE AWARDS

The 2022 Presidential Distinguished Service Award is given to individuals who made a significant impact during the presidential tenure of Dusty York, CNMT, PET, RT(N)(CT). The individuals being recognized for this award have shown exceptional leadership and have provided strategic guidance in the areas of education and research. The SNMMI-TS Presidential Distinguished Service Award was presented to:

- **C. David Gilmore, EdD, CNMT, FSNMMI-TS,** associate professor and program director for nuclear medicine at Massachusetts College of Pharmacy and Health Sciences, for his outstanding leadership and strategic vision with the NMT Entry Level Curriculum Revisions.
- **Crystal Botkin, PhD, MPH, CNMT, PET, FSNMMI-TS,** associate professor of clinical health sciences at St. Louis University for her outstanding leadership and strategic vision with the NMT Entry Level Curriculum Revisions.
- **Mary Beth Farrell, EdD, CNMT, FSNMMI-TS,** director of research for the Intersocietal Accreditation Commission, for outstanding contributions to the PET/CT Oncology Mini-Books.
- **Kathy S. Thomas, MHA, CNMT, PET, FSNMMI-TS,** for outstanding contributions to the PET/CT Oncology Mini-Books.
- **Art Maune, MEd, CNMT,** assistant professor at University of Arkansas Medical Sciences, for outstanding contributions to the Nuclear Medicine Student Registry Review Course.
- **Leesa Ann Ross, MA, CNMT, PET, RT(N), FSNMMI-TS,** for leadership and support in her role as the nuclear medicine program director at Chattanooga State Community College.
- **Tina Buehner, PhD, CNMT, FSNMMI-TS,** medical science liaison – oncology for GE Healthcare, for outstanding leadership to the SNMMI-TS and mentorship as immediate past president.
- **Cheryl Rickley, CNMT, FSNMMI-TS,** nuclear medicine technologist for TTG Imaging Solutions, for outstanding contributions to the SNMMI-TS as the chair of the State TAGs.
- **Nikki Wenzel, MBA, CAE,** senior director and SNMMI-TS administrator, for her outstanding contributions on the SNMMI-TS.
- **Rebecca Maxey**, SNMMI communications director, for outstanding contributions to the PET/CT Oncology Mini-Books.

SNMMI-TS PRESIDENT'S PLAQUE

Dusty York, CNMT, PET, RT(N)(CT), was awarded the SNMMI-TS president's plaque and gavel for her service as 2021–2022 SNMMI-TS president. York began her career as a staff technologist at Memorial Hospital in Chattanooga and has been in her current position at Chattanooga State Community College since 2003.

An active member of the SNMMI-TS, York serves on the SNMMI Board of Directors, House of Delegates and Committee on Women in Nuclear Medicine as well as the Technologist Section Executive Board, Educators Committee, Grants and Awards Committee, and Professional Development and Education Fund. In the past she has served on and chaired multiple committees across the organization, including the Nuclear Medicine Week Task Force, the Continuing Education Committee, the International Outreach Task Force, and the local Organization Task Force, among others.

SNMMI-TS/CARDIOVASCULAR COUNCIL BEST ABSTRACT AWARD WINNERS

First Place

Sarah A. Frye, MBA, CNMT, PET, CCRP, Saint Louis University, Saint Louis, Missouri: "Quantitative perfusion SPECT (QPS) analysis using both male and female normal databases in an obese male patient: A case study."

Second Place

Mitsuha Fukami, Kyushu University, Japan: "The application of compressed sensing reconstruction for myocardial perfusion image shortens the acquisition time: A simulation study."

2021–2022 SNMMI-TS President Dusty York (center) receives SNMMI-TS President's Plaque from 2020–2021 SNMMI-TS President Tina Buehner (left) and 2022–2023 SNMMI-TS President Krystle Glasgow (right).

SNMMI-TS/PET CoE Technologist Best PET Abstract Award

Runze Wu, PhD, Tsinghua University, China: "Deep learning denoising technique enables low-injected-dose whole-body 18F-FDG PET/CT on lymphoma patients - A feasibility study."

SNMMI-TS/Therapy CoE Technologist Best Therapy Abstract Award

Crystal Botkin, PhD, MPH, CNMT, PET, FSNMMI-TS, Saint Louis University, Festus, Missouri: "Administration of Lutetium 177 PSMA therapy in an outpatient nuclear medicine department, a technologist's perspective."

SNMMI-TS Technologist Poster Awards

First Place
Yuya Shirakawa, Kyorin University Hospital, Japan: "Digital PET/CT images can be reconstructed more efficiently using a network designed with deep learning."

Second Place
Noritake Matsuda, Tokushima University, Japan: "Quantitative evaluation of cardiac amyloidosis with 99mTc-pyrophosphate scintigraphy."

Third Place
Takayuki Shibutani, Kanazawa University, Japan: "Image characteristics of brain perfusion SPECT/CT using a new multi-focal collimator: Comparison with conventional SPECT with LEHR collimator."

Technologist Student Abstract Award Winners

First Place
Jonathon Garrett, Vanderbilt University Medical Center, Brentwood, Tennessee: "Analysis of prostate cancer imaging agents: F-18 fluciclovine vs. F-18 PSMA."

Second Place
Kimberly Cornejo, Northwestern Memorial Hospital, School of Nuclear Medicine, Chicago, Illinois: "A more clinically relevant assessment of spatial resolution of a PET-CT system."

Third Place
Hayley Bergner, University of Oklahoma Health Sciences Center, Adair, Oklahoma: "Tagging efficiency of radiolabeled eggs with Technetium 99m macroaggregated albumin compared to Technetium 99m sulfur colloid for gastric emptying studies."

Technologist Student Poster Award Winner

Kori Wright, Student (Non-Credit), Shirley, Indiana: "The difference in tagging efficiency of unfiltered Tc99m-sulfur colloid and filtered Tc99m-sulfur colloid to egg beaters."

I. EDITORIAL POLICY

The Journal of Nuclear Medicine Technology (*JNMT*) publishes material of interest to practitioners and scientists in the fields of nuclear medicine and molecular imaging. Proffered articles describing original laboratory or clinical investigations, brief communications, and letters to the editor will be considered for publication. Occasionally, invited articles, editorials, and invited perspectives of selected topics will be published. Manuscripts, including figures and tables, must be original and not under consideration by another publication.

In preparing manuscripts, authors should follow the *Recommendations for the Conduct, Reporting, Editing and Publication of Scholarly Work in Medical Journals* (http://www.icmje.org/recommendations/) of the International Committee of Medical Journal Editors and the specific instructions detailed below. Also, helpful guidance in conforming to the Recommendations may be found in *Medical Style & Format: An International Manual for Authors, Editors, and Publishers* (Philadelphia, PA: Lippincott Williams & Wilkins; 1989) and in the *AMA Manual of Style* (available by subscription at http://www.amamanualofstyle.com/oso/public/index.html).

According to the Recommendations, allegation of scientific misconduct or fraud arises if there is substantial doubt about the honesty or integrity of the work, either submitted or published. In the event of allegations of scientific misconduct or fraud, *JNMT* follows the Recommendations. When appropriate, *JNMT* reserves the right to present the allegations to the author's institution or the agency funding the research.

II. MANUSCRIPT SUBMISSION

New manuscripts should be submitted online at https://submit-jnm.snmjournals.org. For instructions visit https://submit-jnm.snmjournals.org/submission/submissionhelp.

Inquiries regarding manuscript status and preparation can be directed to salexand@snmmi.org.

Correspondence about manuscripts should be sent to the *JNMT* office:

Kathy S. Thomas, MHA, CNMT, PET, FSNMMI-TS
Journal of Nuclear Medicine Technology
Society of Nuclear Medicine and Molecular Imaging
1850 Samuel Morse Drive
Reston, VA 20190-5316
Phone: 703-326-1185
Fax: 703-708-9018

A. Cover Letter

All manuscripts should be accompanied by a cover letter from the author responsible for correspondence about the manuscript. The cover letter should contain a statement that the manuscript has been seen and approved by all authors. If there are more than 10 authors, the specific contribution of each author must be substantiated in the cover letter. The cover letter should inform the editor of potential overlap with other materials already published or submitted for publication and should provide a reference to or a copy of this material. The cover letter should also disclose any conflict of interest—financial or otherwise—that may directly or indirectly influence the content of the manuscript submitted. Finally, the cover letter should provide any additional information that may be helpful to the editor.

B. Authorship, Rights, and Permissions

Each author must have contributed significantly to the submitted work. As recommended by the International Committee of Medical Journal Editors, all authors must have made substantial contributions in all 3 of the following categories:

1. Contributing to conception and design, or acquiring data, or analyzing and interpreting data;
2. Drafting the manuscript, or critically contributing to or revising the manuscript, or enhancing its intellectual content; and
3. Approving the final content of the manuscript.

Simple participation or collection of data alone does not justify authorship but should be mentioned in the acknowledgment section. Changes in authorship after the first review require a written request by the corresponding author and a written authorization from the authors who are to be added or deleted.

If any figures or tables in the manuscript were previously published, this should be acknowledged and written permission from the publisher should be included.

For human studies, approval must be obtained from the institutional review board or equivalent ethics committee and written informed consent must be obtained from research subjects, unless this requirement is waived by the institutional review board or equivalent. For studies in the United States, compliance with the Health Insurance Portability and Accountability Act is also required. Authors must also comply with the clinical trial registration statement from the International Committee of Medical Journal Editors, and the clinical trial registration number must be provided.

For any first-in-human study of a new radiopharmaceutical, the following language should be included in the article to facilitate allowing others to study the drug under the Radioactive Drug Research Committee regulations, rather than having to file additional applications for an investigational new drug or an exploratory investigational new drug: "The mean and standard deviation of the administered mass of [drug] was XX ± YY μg (range, AA–ZZ μg). The mean administered activity was XX ± YY MBq (range, AA–ZZ MBq). There were no adverse or clinically detectable pharmacologic effects in any of the [##] subjects. No significant changes in vital signs or the results of laboratory studies or electrocardiograms were observed [if true]."

For animal studies, approval must be obtained from the appropriate institutional animal care and use committee for compliance with the National Institutes of Health for use of laboratory animals or equivalent.

In compliance with the Copyright Revision Act of 1976, effective January 1, 1978, the following copyright transfer agreement must be faxed, e-mailed, or mailed to the *JNMT* office. (A printable version is available at https://tech.snmjournals.org/site/misc/ifora.xhtml).

> Upon acceptance of the article named above by *JNMT,* all copyright ownership is transferred to the Society of Nuclear Medicine and Molecular Imaging. We, the undersigned coauthors of this article, have contributed to (1) data design, analysis, or interpretation; (2) writing or critiquing drafts of the manuscript; and (3) approval of the final manuscript before publication. We share in the responsibility for the release of any part or all of the material contained within the manuscript. We also affirm that the manuscript has been seen and approved by all authors. The undersigned warrant that the manuscript (or its essential substance) is **new and original**; has not been published other than as an abstract in any language or format; and has not been submitted elsewhere for print or electronic publication consideration.
>
> We warrant that the manuscript does not contain any material the publication of which would violate any copyright or other personal or proprietary right of any person or entity. We will obtain and include with the manuscript written permission from any respective copyright owners for the use of any textual, illustrative, or tabular materials that have been previously published or are otherwise copyrighted and owned by third parties. We agree that it is our responsibility to pay any fees charged for permissions.
>
> We also warrant that **any** human and/or animal studies undertaken as part of the research from which this manuscript was derived are in

compliance with regulations of our institution(s) and with generally accepted guidelines governing such work.

We further warrant that we have herein disclosed any and all financial or other relationships that could be construed as a conflict of interest and that all sources of financial support for the study have been indicated in the disclosure.

1. Copyright transfer: The authors hereby transfer all copyrights in and to the manuscript titled above in all forms and media, now or hereafter known, to the Society of Nuclear Medicine and Molecular Imaging effective if and when the article is accepted for publication in *JNMT*.

2. Permission to reprint: The authors retain the following nonexclusive copyrights, to be exercised only after the article has been published in final format in the print version of *JNMT*.

(a) Reprint the article in print collections of the author's own writing.
(b) Present the article orally in its entirety.
(c) Use the article in theses and/or dissertations.
(d) Reproduce the article for use in courses the author is teaching. (If the author is employed by an academic institution, that institution may also reproduce the article for course teaching.)
(e) Distribute photocopies of the article to colleagues, but only for noncommercial purposes.
(f) Reuse original figures and tables in future works created by the author.
(g) Post a copy of the article on the author's personal website, departmental website, and/or the university's intranet, provided a hyperlink to the article on the *JNMT* website is included.
(h) In all the instances under clauses 2a through 2g above, the author will give proper credit to the original publication in *JNMT* as follows: This research was originally published in *JNMT*. Author(s). Title. *J Nucl Med Technol*. Year;vol:pp–pp. © by the Society of Nuclear Medicine and Molecular Imaging, Inc.

3. Publish Ahead of Print policy: The authors understand that if and when the manuscript is accepted for publication in *JNMT,* it will be pre-published online as a Publish Ahead of Print paper. The authors acknowledge that *JNMT*'s Publish Ahead of Print papers undergo full peer review. Ahead of print articles have not been copyedited, nor have they appeared in a print or online issue of the journal.

Conditions 1–3 in the agreement must be met **by all coauthors,** and the agreement must be signed **by all coauthors.** Designate "first author" and "corresponding author" in parentheses by their signatures.

This copyright transfer requirement does not apply to work prepared by U.S. government employees as part of their official duties. However, the authors of such work are required to complete section B of the copyright transfer agreement found at https://tech.snmjournals.org/site/misc/ifora.xhtml.

III. MANUSCRIPT REVIEW, REVISION, AND RESUBMISSION

Submitted manuscripts are reviewed for originality, significance, adequacy of documentation, composition, and adherence to these guidelines. However, editorial decisions are based not only on the technical merits of the work but also on factors such as priority for publication and relevance to the general readership of *JNMT*. All manuscripts are judged in relation to other submissions currently under consideration.

Two helpful publications to read before writing a manuscript are "The Efficacy of Diagnostic Imaging" by Fryback and Thornbury (*Med Decis Making*. 1991;11:88–94) and "Bias in Research Studies" by Sica (*Radiology*. 2006;238:780–789).

At the discretion of the Editors, the manuscript may be returned rapidly—without external peer review—if deemed not competitive or outside the scope of *JNMT*. Rebuttals to rejected manuscripts are strongly discouraged, and requests for resubmission of rejected manuscripts are generally not granted without significant demonstration of errors in the review or decision process. Most articles are rejected on grounds of insufficient priority or lack of relevance to *JNMT*, not data quality or technical issues.

Manuscripts must be written in English. When necessary, authors should seek the assistance of experienced, English-speaking medical editors before submission. A medical editor should review the final draft of the original and any revisions of the manuscript. Authors will be required to provide revisions of articles written in substandard English before peer review.

Manuscripts considered suitable for review are evaluated by 2 reviewers. The Editors select the reviewers and make the final decision on the manuscript. Authors may suggest reviewers for their manuscripts. Referees who review a manuscript remain unknown to the authors.

It is unusual for a manuscript to be accepted for publication without first undergoing a process of revision. Revised manuscripts are judged on the adequacy of responses to suggestions and criticisms made during the initial review. Revision of a manuscript does not guarantee acceptance. A revision should be accompanied by a point-by-point reply to the reviewers' and editors' critiques in which any changes are briefly described. The authors also should provide justification for not altering the manuscript in response to any reviewer comments believed to be inappropriate. Red font should be used to indicate all changes within the manuscript itself, and a clean version of the manuscript should be provided.

The revised manuscript and accompanying reply must be submitted to *JNMT* via the online submission and review website at https://submit-jnm.snmjournals.org within 30 days of the date of the editorial decision. If circumstances prevent completing the revisions by the deadline, please contact Susan Alexander at 703-326-1185 or at salexand@snmmi.org. If the revisions are not received within 3 months after being requested, the manuscript may be started on a new review cycle and given a new manuscript number.

All accepted manuscripts are subject to editing for accuracy, clarity, and style.

IV. ARTICLE TYPES

Original scientific and methodology articles should contain no more than 6,000 words. This word limit includes all data: title page, abstract, text, disclosure, acknowledgments, key points, references, figure legends, and tables. The goal is to limit original articles to 8 printed pages. A maximum of 7 figures (maximum of 14 parts in total with no more than 4 parts per figure preferred), 7 tables, and 40 references is allowed. Abstracts should be structured (see VI. C. below) and should contain a maximum of 350 words.

Teaching case studies should contain no more than 750 words. This word limit includes all data: title page, abstract, text, disclosure, acknowledgments, references, figure legends, and tables. A maximum of 5 figures and 5 references is allowed, and the maximum number of authors is three. The objective of teaching case studies is to present images that demonstrate key facts or concepts in clinical nuclear medicine and molecular imaging. Emphasis is placed on studies in which imaging has been useful in helping with the diagnosis. Teaching case studies will be accepted for publication in *JNMT* at the discretion of the Editor and may also be posted on the SNMMI website. Submissions not accepted for publication in *JNMT* may be accepted for posting on the SNMMI website only. Teaching case studies should include a brief, unstructured abstract followed by 4 sections: an "Introduction" section briefly describing the point that the article is teaching, explaining the significance of the article, and summarizing its educational value; a "Case Report" section describing relevant medical history, laboratory findings, clinical course, procedures

Category	Article type	Topic	Maximum no. of…				
			Total words*	Words in abstract	References	Figures	Tables
Uninvited	Original research	Clinical or basic science	6,000	350	40	7	7
	Brief communications	Novel data of broad import	2,500	150	20	4	2
	Quality case studies	Quality improvement	3,000	150	20	4	2
	Letters to the editor	*JNMT* articles or general	800	None	10	None	None
Invited	Perspectives	*JNMT* articles	1,600	None	10	None	None
	Editorials	Variable	1,600	None	10	None	None
	Continuing education	Educational reviews	6,000	350	80	7	7
	Teaching case studies	Educational cases	750	150	5	5	0
	Special Contributions	Variable	Variable	Variable	Variable	Variable	Variable

*Includes all data: title page, abstract, text, disclosure, acknowledgments, references, tables, and figure legends.
Tables must fit on 1 page.
Figures cannot have more than 14 parts combined; no more than 4 parts per figure is preferred.
Additional online data supplements are permitted for all types of articles.

performed, and condition at last follow-up; a "Discussion" section describing any findings, differential diagnosis, and final diagnosis; and a "Conclusion" section summarizing the take-home teaching points.

Quality case studies should contain no more than 3,000 words. This word limit includes all data: title page, abstract, text, disclosure, acknowledgments, references, figure legends, and tables. A maximum of 4 figures, 2 tables and 20 references is allowed, and the maximum number of authors is three. The objective of a quality case study is to present a specific event that required an in-depth analysis resulting in an operational assessment, resolution, corrective action, and verification of effectiveness using standard quality assessment tools (e.g., a root cause analysis using Lean or Six Sigma methodology). The quality case study should contain a brief, unstructured abstract followed by 4 sections: an introduction (a description of the event, answering the questions what, how, when, where, and who), a "Quality Analysis" section (repeatedly asking the question why until a solution to the error is found), a "Corrective Action" section, and a "Verification of Effectiveness" section.

Letters should concern previously published material or matters of general interest and should be brief and to the point. Letters should be given a title and should also be accompanied by a copyright transfer agreement as specified above in Manuscript Submission. All material is subject to editing. Letters commenting on previously published articles should be received within 1 year of the date of the referenced article's publication. Letters should contain no more than 800 words; this word limit includes all data: title page, authors and affiliations, the letter itself, and any references. Letters should contain no figures or tables and no more than 10 references.

V. FORMAT REQUIREMENTS

A. General Requirements

Use a type size of at least 10 points, double spacing every line. Use the following order for the sections of the manuscript: title page; abstract; text; financial disclosure; disclaimer, if any; acknowledgments, if any; references; figures with legends; and tables. Number all pages consecutively. Do not use automated word-processing features or embedding for numbering, footnotes, or endnotes.

B. Title Page

The title page of the manuscript should include the following: (1) concise and informative title (fewer than 200 characters); (2) short running title of no more than 40 characters (letters and spaces) placed at the bottom of the title page and identified; (3) complete byline, with first name, middle initial, and last name of each author (a limit of 10 authors is recommended; if there are more than 10 authors, the specific contribution of each author must be substantiated in the cover letter); (4) complete affiliation for each author, with the name of department(s) and institution(s) to which the work should be attributed; (5) disclaimer, if any; (6) name, address, telephone number, fax number, and e-mail address of one author responsible for correspondence about the manuscript and to whom reprint requests should be directed, or statement that reprints are not available; (7) name, address, telephone number, fax number, and e-mail address of the first author, specifying whether this person is currently in training (e.g., fellow, resident, or student); and (8) the word count of the manuscript. Financial support for the work should be noted in a statement on this page as well as in the disclosure (see section V. K. below).

C. Abstract

A structured abstract must be included with each original scientific manuscript, including brief communications. The abstract should contain a maximum of 350 words for original scientific and methodology articles or 150 words for brief communications and include 4 clearly identifiable elements of content: rationale (goals of the investigation), methods (description of study subjects, experiments, and observational and analytic techniques), results (major findings), and principal conclusions. Except for the rationale, these sections should be preceded by headings (i.e., **Methods, Results,** and **Conclusion**). Three to 5 key words should also be submitted with the abstract.

A graphical abstract must also be included with each original scientific manuscript, including brief communications. The graphical abstract, a visual aid to understanding your key findings, is intended to attract the attention of readers and help them find articles that interest them. It should be clear, concise, eye-catching, and easily understood by a typical *JNMT* reader. It will be displayed in the online article and online table of contents and might also be used in promotional media, in the *JNMT* carousel, or on the *JNMT* cover if your article is selected to be featured in that issue. It must comprise a single, simple, original graphic that is not densely packed with information, has no legend, and is not a figure from your article. It cannot be a table, be reprinted from another source, or include any trade names, logos, or images of trademarked items. Text can be used sparingly but must be in Arial font large enough to be legible. For ease of comprehension, it should have a clear start and end, with the information preferably running from top to bottom or left to right. Build the graphical

abstract using the PowerPoint template supplied at http://jnm.snmjournals.org/ authors, and upload it as a single, high-quality, full-color .jpg or .png image file, as well as placing it (labeled as "Graphical Abstract") at the end of the manuscript file.

D. Text

Describe procedures in sufficient detail to allow other investigators to reproduce the results. Do not use hyperbolic terms or phrases in the title, abstract, or body of the text. Qualitative claims as to the superiority (superior, best) or primacy (first, novel, unique) of an idea or instrument are not acceptable. Do not use numbered or bulleted lists. Any brand-name or trademarked instrument, pharmaceutical, or other product mentioned must be followed by the name of the manufacturer, in parentheses. The use of generic names is preferred to the use of brand names or trademarked names. Original scientific and methodology articles are divided into the following sections:

Introduction

This section should be brief and focused. The final paragraph should state the hypothesis investigated.

Materials and Methods

This section should include statements about Institutional Review Board approval, written informed consent, compliance with the Health Insurance Portability and Accountability Act, and animal care committee approval, as appropriate. The standard statement for institutional board approval and consent is the following: "The study has been approved by the institutional review board [or equivalent], and all subjects signed an informed consent form [or the need for written informed consent was waived]." The clinical trial registration number should also be included when appropriate (http://www.clinicaltrials.gov/). For any first-in-human study of a new radiopharmaceutical, the mean, standard deviation, and range of the administered mass of drug and mean administered activity need to be provided, as well as clinically detectable pharmacologic effects. The checklist and flow diagram from one of the following evidencebased statements should be followed as appropriate and submitted as supplemental material: STARD (http://www.stard-statement. org); CONSORT (http://www.consort-statement.org); PRISMA (http://www.prisma-statement.org/statement.htm); REMARK (http://www.nature.com/nrclinonc/journal/v2/n8/full/ncponc0252.html). The number and selection of subjects must be clearly described, as well as the prospective or retrospective nature of the study. Procedures must be described in enough detail to allow reproducibility by others. The last paragraph should describe the statistical methods.

Results

The text of this section should not repeat information presented in the tables and figures. When percentages are given, the ratio of numerator to denominator should be in parentheses.

Discussion

This section should summarize any advances in knowledge provided by the results and then discuss their implications in relation to other studies. Limitations and biases of the study must be addressed. The direction of future research may be mentioned.

Conclusion

This section should be brief, should summarize the key points of the paper, and should not introduce new material or references.

E. References

References (not to exceed 40 in an original scientific or methodology article, 20 in a brief communication, 10 in a letter, or 5 in a teaching case study) should be cited in consecutive numeric order at first mention in the text and designated by reference number italicized, in red font, and in parentheses. References appearing only in a table or figure should be placed at the end of the reference list.

When listing references, follow the *AMA Manual of Style: A Guide for Authors and Editors* (available by subscription at http://www.amamanualofstyle.com/oso/public/index.html). Abbreviate journal names according to the journals database available at PubMed.gov. For journal articles, include the year and volume number in the citation but not the month or issue number. "Unpublished observations" and "personal communications" should not be used as references, although written or oral personal communications may be noted as such in the text. References cited as "in press" must have been accepted for publication and not merely be in preparation or submitted. The author is responsible for the accuracy of all references and must verify them.

List all authors when 6 or fewer; for 7 or more, list the first 3 followed by "et al."

Examples of journal articles:

Alawneh JA, Moustafa RR, Marrapu ST, et al. Diffusion and perfusion correlates of the ^{18}F-MISO PET lesion in acute stroke: pilot study. *Eur J Nucl Med Mol Imaging*. 2014;41:736–744.

Fotos JS, Tulchinsky M. Standing prone positioning in establishing causality between matched ventilation-perfusion defects and pleural effusion. *Clin Nucl Med.* September 22, 2014 [Epub ahead of print].

Huang S, Doke A, Zhang Y, Wang X, DeFilippo F, Heston W. A novel [F-18] aluminum-fluoride labeled PSMA tracer with minimal background uptake [abstract]. *J Nucl Med.* 2014;55(suppl 1):499.

Example of a book and book chapter:

Prakash D. *Nuclear Medicine: A Guide for Healthcare Professionals and Patients. New York, NY: Springer; 2014:118, 147.*

Heiss W-D, Drzezga A. PET/MR in brain imaging. In: Carrio I, Ros P, eds. *PET/MRI: Methodology and Clinical Applications*. New York, NY: Springer; 2014:109–126.

Example of an Internet reference:

Orange book: approved drug products with therapeutic equivalence evaluations. U.S. Food and Drug Administration website. http://www.accessdata.fda.gov/scripts/cder/ob/default.cfm. Updated May 17, 2013. Accessed May 8, 2014.

Example of a package insert:

Cialis [package insert]. Indianapolis, IN: Eli Lilly & Co; 2003.

Authors are encouraged to generate their references using EndNote (Thomson Scientific). The *JNMT* Output Style for EndNote is available at http://endnote.com/downloads/styles.

F. Units of Measurement

All measurements should be listed in Système Internationale (SI) units. Non-SI units may be used after the SI units but should be placed in parentheses. Use becquerels, not curies, as the unit of activity (1 mCi = 37 MBq).

G. Abbreviations and Symbols

With the exception of units of measurement, *JNMT* strongly discourages the use of abbreviations. Whenever possible, terms should be spelled out in full rather than being abbreviated. Every abbreviation, **even those that are well known and in common use,** must be defined the first time it is mentioned in the manuscript; spell out the full term and place the abbreviation, in parentheses, after the full term.

H. Tables

Place tables at the end of the manuscript file; do not submit them as separate files. Do not submit tables as images. Tabbed or space-separated table text is not allowed; tables should be created in Microsoft Word table format or a similar format. The

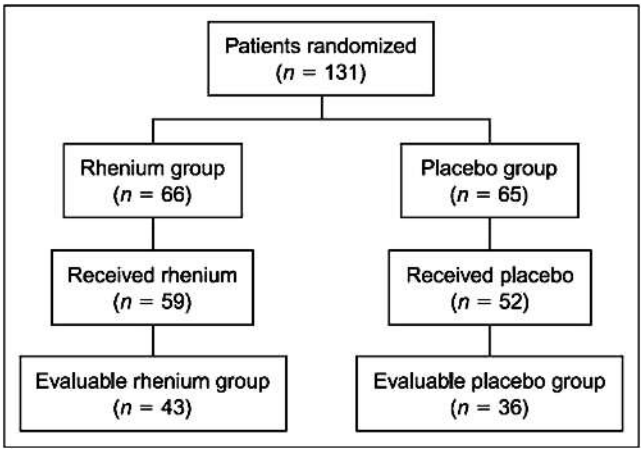

EXAMPLE FIGURE. Flowchart in single-column format. Note the use of Arial font and capitalization of only the first word in each line.

number of tables is limited to 7, except in the case of dosimetry articles, which may exceed that number in lieu of figures. The final typeset table must fit on a single page.

Tables should be self-explanatory and should supplement, not duplicate, the text. Each table must be cited in consecutive numeric order in the text. Number the tables consecutively with an Arabic numeral after the word "TABLE." Titles should be descriptive and brief. Horizontal rules should be placed below the title and column headings and at the end of the table. Do not use vertical rules. Give each column a brief heading.

Place explanatory matter in footnotes, not in the title. Use the following symbols in this sequence: *, †, ‡, §, ‖, ¶, #, **. In a footnote, define all abbreviations in the order in which they appear in the table and identify statistical measures of variations, such as standard deviation and standard error of the mean. If data from another published source are used, obtain written permission from the publisher, cite the original source in the references, and include the following credit line in a footnote: "Reprinted with permission of Ref X." If data from an unpublished source are used, obtain permission from the principal investigator and acknowledge fully.

I. Figures

For online-submission specifications, visit https://submit-jnm.snmjournals.org/submission/submissionhelp.

Figures should clarify and augment the text and should be embedded (with their legends) within the text as well as uploaded as separate files. Because imaging is a major aspect of nuclear medicine, the selection of sharp, high-quality figures is of paramount importance. The author will be required to correct or replace figures of inferior quality. Each submitted figure should clearly identify areas of interest with only enough surrounding area for orientation.

To best convey the quantitative information in nuclear images and to standardize their display, all PET, SPECT and planar nuclear images submitted for publication must provide "as much quantitative information as reasonably achievable" (AQARA) as described in the summary table below. A full description of the requirements is published online at: https://jnm.snmjournals.org/AQARA.

The number of figures submitted should not be excessive for the length of the manuscript and in no case should exceed 7. These 7 figures may consist of up to 14 separate parts. No more than 4 parts per figure is preferred. Each figure must be numbered and cited in consecutive numeric order in the text.

If possible, the figures submitted should be the size in which they will appear when published so that no reduction is necessary. Figures should be either single-column format (published width, 8.5 cm; maximum submitted width, 11 cm), mid-size format (published width, 11.4 cm; maximum submitted width, 14 cm), or double-column format (published width, 17.4 cm; maximum submitted width, 22 cm). The Arial font should be used for all figure text, and the size should be 8–12 points. Composite figures should be preassembled, with each figure part (e.g., A, B, C) lettered in 12-point Helvetica type in the upper left corner. Cover images should have a submitted width of 17 cm, and the submitted depth can be no more than 8.5 cm.

Color figures will be considered for publication if appropriate. Color files should be supplied in RGB color and should have an ICC profile applied.

Acceptable resolution for digital figures is 300 dpi. Internet graphics are not acceptable under most circumstances because the 72-dpi resolution is too low for satisfactory reproduction.

AQARA Requirements for Radionuclide-Based Images

Feature	Specific requirement
Intensity-scale bar	Show for each figure
	Indicate unit and upper and lower window settings
	Prefer absolute units
	Use biologic parameters if available (e.g., rate constants, metabolic rates, binding potential)
	If not, use activity concentration (e.g., SUV, Bq/mL, %IA/cm^3)
	Minimally, include relative units (e.g., percentage of maximum)
Background subtraction	Avoid
	If unavoidable, clearly indicate in scale bar
	Keep bottom of scale bar at "0"
	Set subtracted fraction of scale bar to background color
Image display	Use same window settings for all figures
	Accompany fusion images (SPECT/CT, PET/CT, PET/MR) by corresponding stand-alone SPECT or PET images
	Limit cropping
	If cropping is applied, show corresponding uncropped, full-field-of-view image

%IA/cm^3 = percentage of injected activity per cubic centimeter of tissue.

The file format must be . tiff, .eps, jpeg, .ppt, .doc, .docx, .png, or .pdf. If the .jpeg file format is used, the images must be of medium quality or better (quality setting of at least 6). Each figure, including those in .ppt, .doc, and .pdf formats, must be submitted as a separate file. Each figure must also be included in the manuscript file before its respective legend. Crop and size digital figures to match figure specifications and to minimize total file size.

All submitted illustrations become the property of the Society of Nuclear Medicine and Molecular Imaging.

Videos can be published as supplemental data online.

J. Figure Legends

Legends for figures should be concise and should not repeat the text. Number the legends with an Arabic numeral after the word "FIGURE." If a figure has more than one part, describe each part clearly. Any letter designations or arrows appearing on the figures should be identified and described fully. Abbreviations used in each figure should be defined in the legend in alphabetical order.

Besides being submitted as a separate file, each figure should be inserted before its respective legend in the figure legends section of the manuscript file.

Original (not previously published) figures are preferred for publication in *JNMT*; however, if figures have been published previously, authors are responsible for obtaining written permission from the publisher to reprint. The source of the original material must be cited in the references and the following credit line in parentheses included in the legend: "Reprinted with permission of Ref. X." All permission letters should be submitted online at the time of manuscript submission.

K. Disclosure

A statement of disclosure is required for all submissions. Include in the disclosure any potential conflicts of interest as reported in the disclosure form of the International Committee of Medical Journal Editors. For the work under consideration for publication, these include any payments received from a third party, such as grants, consulting fees, travel fees, or honoraria. Also disclose any relevant financial activities outside the submitted work, such as employment, royalties, stock options, or patents. For industry-sponsored or industry-supported research, authors who are not employees of or consultants to the industrial entity must be specified as having control of any data that might present a conflict of interest for employees or consultants. If no conflicts exist, this should be specified in the statement.

L. Acknowledgments

Individuals whom the authors wish to thank may be listed in the acknowledgments. In addition, persons who have contributed intellectually to the work but do not fulfill conditions 1–3 of the copyright transfer agreement in section II may be listed.

M. Key Points

Original submissions must include 3 key points just before the reference list:

KEY POINTS

QUESTION: A one-sentence focused question based on the study hypothesis or goal.

PERTINENT FINDINGS: One or two sentences on the design (e.g., clinical trial, cohort study, case-control study, meta-analysis), the primary outcome, and the findings (only basic numbers and whether they are statistically significant, but not the results of statistical tests or measures of variance).

IMPLICATIONS FOR PATIENT CARE: One sentence on how the findings might affect patient outcomes or, for basic science, what the translational implications might be.

N. Supplemental Data

All data that are needed to support the central conclusions of the article must be presented in the manuscript itself. Other data (e.g., large-scale tabulations) that are integral to the manuscript and of interest to specialists but not practical to include in the printed journal can be submitted for online-only publication as supplemental data. The data may include images with legends, tables, or videos; supplemental text is discouraged (if some of the methods have been described in a previous publication, the manuscript can reference that publication). Each item of supplemental data should be given a brief descriptive title and should be directly referred to in the manuscript (e.g., Supplemental Table 1). Because supplemental data files are placed online unedited, as submitted by the author, the uploaded files need to be final and ready for publication. Provide original files rather than .pdfs. Do not include a title page.

VI. CHECKLIST FOR NEW SUBMISSIONS

___ Is all text in the manuscript double-spaced, including the references?

___ Does the title page include the title, short running title, and authors' names and complete affiliations; complete address, telephone number, fax number, and e-mail address for the first author, if different from the corresponding author?

___ Does the paper have a structured abstract and key words?

___ Are the references in consecutive numeric order and in the correct style?

___ Have the financial disclosure section and key points been included?

___ Are the figures and tables in consecutive numeric order?

___ Have the figures been included in the manuscript file before their respective legends, as well as being submitted as separate image files of an acceptable format and resolution?

___ Do all PET, SPECT and planar nuclear images follow AQARA requirements (http://jnm.snmjournals.org/site/misc/AQARA.xhtml)?

___ Has permission been obtained from the publisher to reprint previously published figures and tables?

___ Has the copyright transfer agreement been signed by all authors?

___ Was the study approved by an institutional review board or equivalent, and has this approval been mentioned in the "Materials and Methods" section?

___ Did all subjects give written informed consent, or did the institutional review board waive the need to obtain informed consent?

___ Was the study approved by an institutional animal care and use committee or equivalent?

___ Has the clinical trial registration number been provided?

___ Has first-in-human radiopharmaceutical language been included?

___ Did you follow the checklist and flow diagram from one of the following evidence-based statements, and did you submit the checklist as supplemental material: STARD (http://www.stard-statement.org); CONSORT (http://www.consort-statement.org); PRISMA (http://www.prisma-statement.org/statement.htm); REMARK (http://www.nature.com/nrclinonc/journal/v2/n8/full/ncponc0252.html).

SNMMI Designated Radiopharmaceutical Therapy Centers of Excellence

SNMMI designated centers meet strict regulatory, training, qualification, experience, and performance criteria to help assure patients, their families, referring physicians, and payors that rigorous procedures are in place and followed, leading to appropriate patient selection and outcomes from radiopharmaceutical therapy.

THE FOLLOWING SITES HAVE BEEN DESIGNATED AS SNMMI RADIOPHARMACEUTICAL THERAPY CENTERS OF EXCELLENCE:

CLINICAL CENTERS OF EXCELLENCE

- ARA Theranostics Center
- ChristianaCare
- Excel Diagnostics and Nuclear Oncology Center
- Hoag Memorial Hospital Presbyterian
- Kettering Health Main Campus
- Northwestern Memorial Hospital

COMPREHENSIVE CENTERS OF EXCELLENCE

- Ahmanson Translational Theranostics Division, David Geffen School of Medicine at UCLA, UCLA Heath Medical Center
- Dana-Farber /Brigham and Women's Cancer Center
- Duke University Health
- Emory University Hospital
- M Health Fairview University of Minnesota Medical Center - East Bank Hospital
- Mayo Clinic
- MD Anderson Cancer Center
- Memorial Sloan Kettering Cancer Center
- Mount Sinai Health System
- SSM Saint Louis University Hospital
- Stanford University - Stanford HealthCare
- The Ohio State University Wexner Medical Center - The James Hospital and Solove Research Institute
- University of California, San Francisco
- University of Colorado Anschutz Medical Center
- University of Iowa
- University of Pittsburgh Medical Center (UPMC)

SNMMI is currently accepting applications from centers based in the United States (its territories) and Canada.

Visit **www.snmmi.org/RPTCoE** to get started.

SNMMI Value Initiative
SOCIETY OF NUCLEAR MEDICINE & MOLECULAR IMAGING

September Savings Event

Buy any flood source and get...

An "E" vial or "S" vial at 50% off or a free spot marker*

Find a distributor at radqual.com or contact sales@radqual.com

sales@radqual.com · 208.524.5300

RADQUAL
An International Isotopes Co

** Offer available for select products. Contact distributor for details.*

Achieve the True Mark of

Excellence in Patient Care

for Your Facility with IAC

ACCREDITED FACILITY

IAC

INTERSOCIETAL ACCREDITATION COMMISSION

Earning IAC accreditation indicates that your facility is:

Dedicated to Quality and Patient Safety

IAC's seal of approval verifies the quality your patients deserve. By earning IAC accreditation, you are showing referring physicians, patients and insurers that **your facility has undergone a rigorous evaluation, has been found to be in compliance with industry standards and is committed to continuous quality improvement**.

Engaged in Continuous Improvement

The IAC accreditation process is more than an update every three years. Accredited facilities receive a detailed Application Review Findings document as a **tool for improving the overall quality of their facility**. Special topic webinars, a CE finder and the IAC Quality Improvement (QI) Self-Assessment Tool are offered complimentary. Facilities use the QI Tool to assess case studies and final reports and receive a quantitative report targeting opportunities for continuous process improvement.

Complying with Reimbursement and Regulatory Mandates

IAC notifies CMS and third-party payers of the status of accredited facilities to help ensure compliance with related mandates. Physicians may also utilize IAC accreditation to satisfy a component of the Centers for Medicare & Medicaid Services (CMS) MIPS Improvement Activity as part of the MACRA Quality Payment Program. The IAC QI Tool is an independent option that may also be utilized to satisfy the MIPS Improvement Activity and MOC.

Diagnostic Imaging Accreditation

Vascular Testing . Echocardiography
Nuclear/PET . MRI . CT / Dental CT

IAC

Vascular and Cardiac Interventional Accreditation

Carotid Stenting . Cardiac Electrophysiology
Vein Center . Cardiovascular Catheterization

Improving health care through accreditation® | **intersocietal.org** | 800.838.2110

Coming Soon! Deep Venous Intervention . Hemodialysis Access Intervention . Peripheral Arterial Intervention
Perioperative Transesophageal Echocardiography . Adult Congenital Transthoracic Echocardiography